e-ISSN : 2320-0847
p-ISSN : 2320-0936

American Journal of Engineering Research (AJER)

Volume 3 Issue 10– October 2014

www.ajer.org ajer.research@gmail.com

Editorial Board

American Journal of Engineering Research (AJER)

Dr. Moinuddin Sarker,
Qualification :PhD, MCIC, FICER,
MInstP, MRSC (P), VP of R & D
Affiliation : Head of Science / Technology
Team, Corporate Officer (CO)
Natural State Research, Inc.
37 Brown House Road (2nd Floor)
Stamford, CT-06902, USA.

Dr. Jonathan Okeke Chimakonam
Qualification: PHD
Affiliation: University of Calabar
Specialization: Logic, Philosophy of
Maths and African Science,
Country: Nigeria

Dr. ABDUL KAREEM
Qualification: MBBS, DMRD, FCIP, FAGE
Affiliation: UNIVERSITI SAINS Malaysia
Country: Malaysia

Dr. sukhmander singh
Qualification: Phd
Affiliation: Indian Institute Of
Technology, Delhi
Specialization : PLASMA PHYSICS
Country: India

Dr. Nwachukwu Eugene Nnamdi
Qualification: Phd
Affiliation: Michael Okpara University of
Agriculture, Umudike, Nigeria
Specialization: Animal Genetics and
Breeding
Country: Nigeria

Dr. June II A. Kiblasan
Qualification : Phd
Specialization: Management, applied
sciences
Country: PHIILIPPINES

Dr. Narendra Kumar Sharma
Qualification: PHD
Affiliation: Defence Institute of Physiology
and Allied Science, DRDO
Specialization: Proteomics, Molecular
biology, hypoxia
Country: India

Prof. Dr. Shafique Ahmed Arain
Qualification: Postdoc fellow, Phd
Affiliation: Shah abdul Latif University
Khairpur (Mirs),
Specialization: Polymer science
Country: Pakistan

Dr. Alcides Chaux
Qualification: MD
Affiliation: Norte University, Paraguay,
South America
Specialization: Genitourinary Tumors
Country: Paraguay, South America

Dr. Md. Nazrul Islam Mondal
Qualification: Phd
Affiliation: Rajshahi University,
Bangladesh
Specialization: Health and Epidemiology
Country: Bangladesh

AJER

American Journal of Engineering Research

Volume-3 Issue-10

American Journal of Engineering Research (AJER)
e-ISSN : 2320-0847 p-ISSN : 2320-0936
Volume-3, Issue-10, pp-01-06
www.ajer.org

Research Paper Open Access

A Review of the Fatigue Analysis of Heavy Duty Truck Frames

Ahmad O. Moaaz[1], Nouby M. Ghazaly[2]
[1]*Mechanical Engineering Dept., Faculty of Engineering, Beni-Suef University, Beni Suef-62511, Egypt.*
[2]*Mechanical Engineering Dept., Faculty of Engineering, South Valley University, Qena-83523, Egypt.*

ABSTRACT: *Heavy duty vehicle plays a more important role in highway transportation. The major focus in the truck manufacturing industries is design of truck chassis with more pay load capacity and possible less weight. An important aspect of chassis' design and analysis is the stress distribution and fatigue life of prediction process. Fatigue is one of the most important parameters to consider when designing truck components. The components are typically subjected to dynamic loads when in service. In this paper, an effort is made to review the investigations that have been made on the different fatigue analysis techniques of heavy duty truck frames. A number of analytical and numerical techniques are available for the fatigue analysis of the heavy duty truck frames has been reported in literature.*

KEYWORDS *: Heavy duty truck, Chassis frames, Fatigue analysis.*

I. INTRODUCTION

Transportation industry plays a major role in the economy of modern industrialized and developing countries. The early damages caused by heavy load reduce the road service life and ride comfort. Highway maintenance brings huge economic losses, while serious road failure threats traffic safety. Chassis is one of the most significant components in automotive industry and is considered as the bigger parts in the vehicle. The chassis of trucks is tasked with holding all the components systems together; hence it should be rigid enough to withstand the shock, twist, vibration and other stresses. Along with strength, an important consideration in chassis design is to have adequate bending stiffness for better handling characteristics. So, maximum stress, maximum equilateral stress and deflection are important criteria for the design of the chassis. The greater the energy absorbed by the chassis on impact the lower the energy levels transmitted to a vehicles occupants and surroundings, lowering the chances of injury [1]. The chassis of trucks which is the backbone of vehicles that integrates the main truck component systems such as the axles, suspension, power train, cab and trailer etc., is one of the possible candidates for significant weight reduction [2].

In general, the chassis experiences several loading situations that include vertical bending, longitudinal torsion, lateral bending, torsion loading and fatigue loading [3]. In additions, the chassis design includes the selection of suitable shapes and cross-section of chassis-members. Moreover, the design should consider the reinforcement of the chassis side- and cross member joints, and the various methods of fastening them together. There are number of parameters which affect the fatigue life of the structure as listed: cyclic stress state, geometry, surface quality, material type, residual stresses, size and distribution of internal defects, direction of loading & grain size. Many researchers in the automotive industry have taken this opportunity to be involved in the chassis manufacturing technology and development [2].The objective of this review paper is to present the fatigue analysis techniques of heavy duty truck frames. Prevention of fatigue failure is one of the most important parameters to when designing truck components. The components are typically subjected to dynamic loads when in service. A number of analytical, numerical and experimental techniques are considered for the fatigue analysis of the heavy duty truck frames. Conclusion of the fatigue analysis in the vehicle chassis has been reported in literature.

II. ASPECT OF TRUCK CHASSIS FRAME

The common chassis frame consists of two channel shaped side members that are sustained apart by many cross members, as shown in Figure1. The cross members are placed at points of high stress and are joined to side members. The depth of the channel must be enough to reduce the deflection. Since the load at each point of the frame varies, a weight reduction can be achieved by either minimums the depth of the channel, or having a series of holes positioned along the axis in the regions where the load is not so high. On the normal road surfaces, the chassis frame is subjected to both bending and torsional distortion. The open-channel sections exhibit excellent resistance to bending, but have very little resistance to twist. From the global torsion analysis, it has been found that the torsion load is more severe than bending load. In order to overcome this problem, a cross bar and material selection are very important to consider during design stage [4]. Therefore, both side and cross-members of the chassis must be designed to resist torsional distortion along their length.

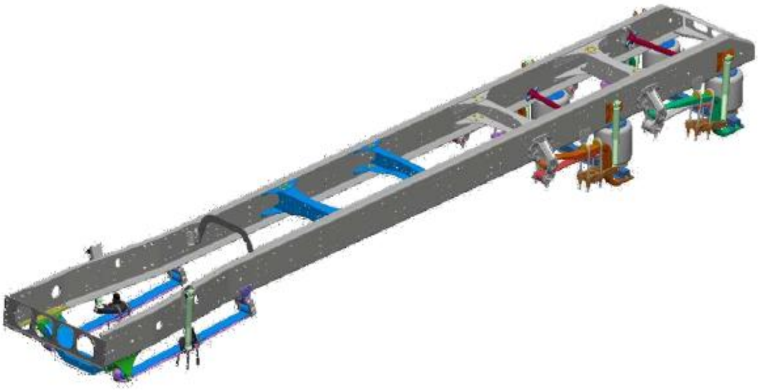

Figure1 Construction of the common chassis frame

Generally for heavy commercial vehicle channel section is preferred over hollow tube due to high torsional stiffness. The chassis frame, however, is not designed for complete rigidity, but for the combination of both strength and flexibility to some degree. The chassis frame supports the various components and the body, and keeps them in correct positions. The frame must be light, but sufficiently strong to withstand the weight and rated load of the vehicle without having appreciable distortion. It must also be rigid enough to safeguard the components against the action of different forces. The chassis design includes the selection of suitable shapes and cross-section of chassis-members. Moreover, the design should consider the reinforcement of the chassis side- and cross member joints, and the various methods of fastening them together [3].

III. FATIGUE ANALYSIS OF TRUCK CHASSIS

Fatigue is the phenomenon in which a repetitively loaded structure fractures at a load level less than its ultimate static strength, as shown in Figure 2. There are many parameters that contribute to fatigue failures namely: number of load cycles experienced, range of stress experienced in each load cycle, mean stress experienced in each load cycle and presence of local stress concentrations [5]. Also, the fatigue analysis refers to one of three methodologies: local strain or strain life, commonly referred to as the crack initiation method, which is concerned only with crack initiation, stress life that commonly referred to as total life and crack growth or damage tolerance analysis that is concerned with the number of cycles until fracture. The main steps for calculating fatigue life is sometimes called the Five Box Trick, including material, loading, geometry inputs, analysis and results.

Figure 2 Fatigue crack of the sub-frame

The stress analysis is important in fatigue study and life prediction of components to determine the highest stress point commonly known as critical point which initiates to probable failure, this critical point is one of the factors that may cause the fatigue failure. The magnitude of the stress can be used to predict the life span of the chassis. The location of critical stress point is thus important so that the mounting of the components like engine, suspension, transmission and more can be determined and optimized. Finite Element Method (FEM) is one of the methods to locate the critical point. Safety factor is used to provide a design margin over the theoretical design capacity. This allows consolidation of uncertainties in the design process [3]. Chetan et al. [5] reviews various factors affecting the fatigue life of a structure like cyclic stress state, geometry, surface quality, material type, residual stresses, size and distribution of internal defects, direction of loading & grain size.

Determining the stresses of a truck chassis before manufacturing is important due to improvement in design. An important aspect of chassis design and analysis is the stress distribution and fatigue life of prediction process. Chassis analysis mainly consists of static analysis to predict stress distribution and subsequently, the fatigue simulation to predict the life of the chassis. Many researchers carried out study on truck body components. Fermer et al. [6] investigated the fatigue life of Volvo S80 Bi-Fuel using MSC/Fatigue. Also, Fermer and Svensson in 2001 [7] studied the mechanical finite element analyses of welded structures performed on a daily basis in the automotive industry. One objective is to estimate the fatigue strength, which is given mainly by the strength of the joints. This article give some insight into the dimensioning process, with special focus on fatigue analysis of spot welds and seam welds in thin-walled car body structures made of steel. Experiences from daily use at Volvo Car Corporation, limitations of methods, future and on-going work are discussed.

Conle and Chu [8] did research about fatigue analysis and the local stress –strain approach in complex vehicular structures. Moreover, Conle and Mousseau in 1991 [9] described an analytical study of the fatigue life of automobile chassis components using automotive proving ground load history results combined with recent computational advances. This work advances knowledge in two ways: a vehicle dynamics model is used to generate the history of the load vectors acting on the components and the element stress equivalency procedure used until now is improved. It can be concluded that the combination of vehicle dynamics modeling, finite-element analysis and fatigue analysis is a viable technique for the design of automotive components. However, before our durability process can be suitable for applied engineering work a number of improvements are required, which has been outlined.Thompson et al. (1998) [10] discussed the design and Analysis of a Winston Cup Stock Car Chassis for Torsional Stiffness using the Finite Element method. Roll stiffness between sprung and unsprung masses. The application of the method is demonstrated using two case studies, namely a road tanker and a load haul dumper. In both cases, it was possible to obtain adequately accurate fatigue life prediction results, using simplified loading, static finite element analyses and a stress-life approach to fatigue damage calculations, with material properties available in design codes.Fatigue life analysis and improvements of the auto body in a sports utility vehicle (SUV) were performed by Zhong and Ping in 2006 [11]. The stress distribution under unit displacement excitation was obtained by the finite element (FE) method. A bilateral track model was adopted to obtain load spectra in accordance with the vehicle reliability test. The total life of the autobody was evaluated by the nominal stress method with the assumption of a uniaxial stress state, and thus the critical regions were determined. The life of components with critical regions was further investigated on the basis of multiaxial fatigue theory. The results show that some components near to the suspension are easy to damage because they are directly subjected to impact loading from the road. It is also indicated that the result from multiaxial fatigue analysis is more reasonable than that from the nominal stress method, which was verified by experimental results. Finally, topological optimization of the spot weld location in the critical region was carried out by the homogenization method to improve its fatigue life. In addition, Hoffmeyer et al. in 2006 [12] discussed some issues in multi axial fatigue and life estimation is presented. While not intended to be comprehensive, these are a relatively broad range of issues which are commonly encountered when dealing with multi axial fatigue. They include damage mechanisms, non-proportional hardening and constitutive behavior, damage parameters and life estimation, variable amplitude loading, cycle counting, damage accumulation, and mixed-mode crack growth. Some simple approximations in capturing some of these effects in multi axial life estimations are also presented.

In 2007, Ye and Moan [13] discussed static and fatigue behavior of three types of aluminum box-stiffener/web connections are investigated in this study. The main purposes are to provide a connection solution that can reduce the fabrication costs by changing the cutting shapes on the web frame and correspondingly the weld process and meanwhile sufficient fatigue strength can be achieved. Finite element analyses (FEA) show the influence of local geometry and weld parameters on the stress gradient near the fatigue cracking area. The influence of the weld parameters on the structural stress concentration factors is also studied. Twelve specimens of every type were tested and the test data are compared both to a nominal stress based design SN curve Eurocode9/31 and a structural stress based design SN curve Eurocode9/44.

RoslanAbd Rahman et al. [14] conducted stress analysis of heavy duty truck chassis by utilizing a commercial finite element package ABAQUS. To determine critical point so that by design modifications the stresses can be reduces to improve the fatigue life of components. During this he uses ASTM low alloy steel a 710 C (Class 3) with 552 MPa of yield strength and 620 MPa of tensile strength for chassis founds the maximum stress 386.9 MPa at critical point occurred at opening of chassis This critical point is located at element 86104 and node 16045, which is in contacted with the bolt from this he concludes that this critical point is an initial to probable failure. Kurdi et al. in 2008, [15] discussed about the one of the most important steps in development of a new truck chassis is the prediction of fatigue life span and durability loading of the chassis frame. The age of many truck chassis in Malaysia are of more than 20 years and there is always a question arising whether the chassis is still safe to use. Thus, fatigue study and life prediction on the chassis is necessary in order to verify the safety of this chassis during its operation. Stress analysis using Finite Element Method (FEM) can be used to locate the critical point which has the highest stress. Critical point is one of the factors that may cause the fatigue failure. The magnitude of the stress can used to predict the life span of the truck chassis.

The stress analysis is accomplished using the commercial finite element packaged ABAQUS by Veloso et al. [16]. They discussed the failure investigation and stress analysis of a longitudinal stringer of an automobile chassis Fiat Automóveis, Rod. Fernão Dias, km 429, Betim, MG, Brazil Pontifical Catholic University of Minas Gerais (PUC Minas), Mechanical Engineering, Belo Horizonte, MG, Brazil A prototype vehicle was submitted to durability test, on road at a proving ground test track. Failures of posterior longitudinal stringers were observed during this test. Cracks were nucleated on these stringers during durability test, before the designed life of these components is reached. These cracks were observed at nearly the bumpers fixation points of the vehicle suspension. Loads are transmitted by wheels to the body of the vehicle through the suspension components. Thus, the longitudinal stringers are subjected to these localized cyclic stresses. Also, Palma et al. in

2009 [17] investigated to analyze the fatigue behavior of an automobile body part, according to the standards of performance. The methodology is based on experiments performed on a rear trailer tow hook pin of a passenger automobile vehicle. Experiments were performed simulating the actual conditions in the customer environment. Stress and strain were experimentally measured by using strain gages, bonded on assembly critical points. Besides, stress analysis was also performed using a finite element program. Fatigue analysis is used to access and to compare the fatigue damage imposed during laboratory experiments.

Recently in 2011, Chen and Zhu [18] studied the YJ3128-type dump truck's sub-frames, for the fatigue crack occurred in the Sub-frame which has worked in bad condition for 3 to 5 months. The sub-frame was analyzed by ANSYS and the reason for the cracking of the frame was found according to the different stress. At last an improvement and optimization to the structures of the frame was provided. Also Hengji et al. in 2012 [19] explained the fatigue life for frame of the 220t mining dump truck, a fatigue life analysis method was presented by integrating multi body dynamic analysis and finite element method. The forces of main joints at frame were measured from the multi body dynamic model, whose road was restructured. The dynamic stress test of the whole truck was implemented to obtain the peak stress of the mainly forced area, which was compared with the simulated stress. It was found out that the error was allowable so that the accuracy of the finite element model was definitely ensured. The quasi-static stress analysis method was employed to acquire stress influence coefficient under unit load, which was associated with load histories of the frame to get the dangerous stress area. The fatigue life of the frame was calculated on the basis of Palmgren–Miner damage theory. It was turned out that the minimum life area of the frame is located at the frame joints of suspension, which matches the practice. More recently, Bhat et al. in 2014 [20], redesigned a modified chassis for tractor trolley. The existing trolley chassis designed by industry uses 'C' Cross section having dimension 200mm x 75mm x 7mm and the material used was mild steel. By keeping the material and dimension similar and using 'I' cross section area instead of 'C' resulted in more safer stresses than 'C' and 31.79kg reduction in weight. They concluded that the Reduction in weight shows that raw material required for manufacturing of the Chassis was reduced. Also, they obtained safer stresses in new suggested design and increase in factor of safety obtained in new suggested design.

IV. CONCLUSION

Fatigue analysis of the track chassis has been the focus of a number of previous works. The review of some of the previously conducted work related to vehicle structural design, analysis and optimization is surveyed. It is found that the chassis analysis mainly consists of stress analysis to predict the weak points and fatigue analysis to predict the life of the chassis. Several state of the art papers and even books on chassis stress analysis have been presented in the recently years. This study makes a case for further investigation on the design of truck chassis using Fatigue analysis.

REFERENCES

[1] S. Monika Agrawal, Md. Razik "Finite Element Analysis of Truck Chassis" International Journal of Engineering Sciences & Research Technology, December, 2013, 2(12).

[2] Nouby M. Ghazaly "Applications of Finite Element Stress Analysis of Heavy Truck Chassis: Survey and Recent Development" Journal of Mechanical Design and Vibration. 2014, 2(3), 69-73. DOI: 10.12691/jmdv-2-3-3.

[3] E. Macha and Nieslony A. Critical plane fatigue life models of materials and structures under multiaxial stationary random loading: The state-of-the-art in Opole Research Centre CESTI and directions of future activities. International Journal of Fatigue. 2012;. 39:95-102.

[4] G. Murail, B. Subramanyam and D. vaveen "Design Improvement of a Truck Chassis based on Thickness" Altair Technology conference , India, 2013.

[5] J. Chetan S., Panchal Khushbu C., Patel Fajalhusen "A Review of the Fatigue Analysis of an Automobile Frames" International Journal of Advanced Computer Research, December-2012, Volume-2 Number-4 Issue-6.

[6] M., Fermer, McInally, G. and Sandin, G. Fatigue Life Analysis of Volvo S80 Bi-Fuel using MSC/Fatigue, Worldwide MSC Automotive Conference, and Germany, 1999.

[7] M., Fermér and Svensson, H. Industrial Experiences of FE-based Fatigue Life Predictions of Welded Automotive Structures, Fatigue & Fracture of Engineering Materials and Structures 24 (7), 2001, 489-500.

[8] F.A. Conle, and Chu, C.C., Fatigue Analysis and the Local Stress-strain Approach in Complex Vehicular Structures, International Journal of Fatigue. 01/1997; DOI: 10.1016/S0142-1123(97)00045-5.

[9] F. A. Conle, Mousseau, C. W. Using vehicle dynamics simulations and finite-element results to generate fatigue life contours for chassis components. International Journal of Fatigue. 13, 3(1991), pp. 195-205.

[10] L. Thompson. Srikanth Raju and E. Harry Law "Design of a Winston Cup Chassis for Torsional Stiffness" SAE, 983053.

[11] DU Zhong-zhe, ZHU Ping,HE Jun, Fatigue lifetime analysis of auto-body structure and spot weld based on finite element method",

Journal of Automotive Engineering, 2006, Vol. 28, pp. 944-947.
[12] J. Hoffmeyer, Doring, R.; Seeger, T.; Vormwald, M.: Deformation behaviour, short crack growth and fatigue lives ¨under multiaxial non proportional loading. Int. J. Fat. , 28, 2006, 508 – 520.
[13] N. Ye, and T. Moan, Static and Fatigue Analysis of Three Types of Aluminium Box-Stiffener/Web Frame Connections, International Journal of Fatigue, 2007, 29: 1426-1433.
[14] R. Abd Rahman, Mohd Nasir Tamin, OjoKurdi “Stress analysis of heavy duty truck chassis as a preliminary data for its fatigue life prediction using FEM” JurnalMekanikal December 2008, No. 26, 76 – 85.
[15] O Kurdi R., Abd-Rahman M N Tamin. “Stress analysis of heavy duty truck chassis using finite element method”, Journal of Mechanical engineering, 2008, Vol. 26, pp. 76-85.
[16] V, VelosoMagalhaes H S, Bicalho G Iand Palma E S “Failure Investigation and Stres Analysis of a Longitudinal Stringer of an Automobile Chasis”, Enginering Failure Analysis, 2009, Vol. 16, pp. 1696-1702.
[17] E.S., Palma, Petracconi, C.L. and Ferreira, S.E. “Fatigue behavior analysis of a rear tow hook pin of a passenger vehicle”, Engineering Failure Analysis, 2009, Vol. 16, pp. 2408 - 2416.
[18] C. Yanhong, Zhu Feng “The Finite Element Analysis and The Optimization Design of the Yj3128-type Dump Truck’s Sub-Frames Based on ANSYS” Procedia Earth and Planetary Science, 2011, 133 – 138.
[19] M. Hengji, ZhengqiGu ,Qingquan Yang, DuzhongNie,. Et al, “Frame fatigue life assessment of a mining dump truck based on finite element method and multi body dynamic analysis”, Engineering Failure Analysis, 2012, Vol. 23 pp. 1-90.
[20] K. Bhat, UntawaleSp, KatoreHv “Failure Analysis and Optimization of Tractor Trolley Chassis: An Approach Using Finite Element Analysis” International Journal of Pure and Applied Research in Engineering and Technology, 2014; volume 2 (12): 71-84.

American Journal of Engineering Research (AJER)
e-ISSN : 2320-0847 p-ISSN : 2320-0936
Volume-3, Issue-10, pp-07-13
www.ajer.org

Research Paper Open Access

COMING SOON!...
*(A New theory on **"j-66 human"**)*

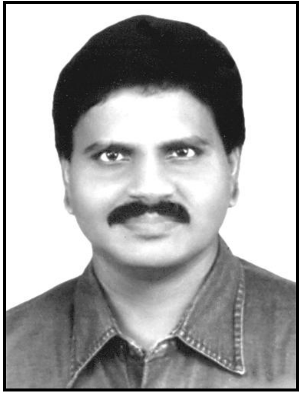

M.Arulmani, B.E.
(Engineer)

V.R.Hema Latha, M.A., M.Sc., M.Phil.
(Biologist)

ABSTRACT: This scientific research article focus that "**COMING SOON**" shall be considered as the **TRANSITION** to New Technology and **NEW LIFE** by overcoming present day **global warming** and to **ADOPT** new conducive environment to face the **FUTURE CHALLENGES** and forecasting **PEACE.** The **j-66 human** shall be considered as origin of new **SUPERHUMAN** due to impact of growth of new environmental radiation called "**j^+-Radiation**" in the expanding universe. The j-66 human populations shall be considered as genetically varied "**Fourth generation**" populations having high level potent called as **virgin population** or **juvenile population.**

Further the **'j-66' populations** shall be considered as having birth of additional blood type say '**j-type**' and could live and promote as a **joint family** without any discrimination of **'caste' 'religion' 'race' and 'language'** in the new Generation.

> ***"Juvenile population** shall mean promoting **PEACE** rather than promoting regeneration and multiplex of population growth"*
>
> ***- Author***

Key Words:
a) Philosophy of '**j-66 human**'?...
b) Philosophy of '**j^+-Radiation**'?...
c) Philosophy of '**j-type blood**'?...
d) Philosophy of '**jail**'?...

I. INTRODUCTION:

Scientists forecast that the present "**Earth Planet**" where we live experiencing consistent **increase in temperature** especially at **higher rate** in the past **100-200 years**. Further they speculate that there is a possibility of increased level of **ozone depletion** which may further melts the ice zone in the Arctic, Antarctic region and there may be chance of increase of "**mean sea level**" and possibility of more destruction and damage to the living organisms on the earth. Because of global warming climatic issue global level advanced research is going on for examining the possibility of human inheritance in future in other plants such as **RED PLANET MARS**, **MOON.**

It is speculated that the present earth **shall not be damaged** for another **1000 years** and the present '**global warming**' shall be **counter balanced** by birth of new radiation '**j^+-radiation**' and '**j-66 human**' populations (Fourth generation populations)

This research article further speculates that the existence of all planets, statelier, asteroids, meteors shall be considered as responsible only for promoting **various environmental conditions** and they **shall not support** for existence and inheritance of future populations **except present earth planet and white mars (prehistoric life existence)**.

This article further emphasize that the present earth planet is capable of supporting and subsistence of future populations also for another **1000 years** without any difficulty due to impact of growth of new radiation called '**j^+-Radiation**'.

II. HYPOTHESIS AND NARRATION

a) Philosophy of Trisomy populations?...

It is hypothesized that **Trisomy** shall be considered as the prehistoric human ancestral populations lived in **WHITE MARS** (also called as white planet) responsible for '**MALE PREGNANCY**' and regenerations by **laying Egg** by **asexual means** due to impact of '**J-Radiation**' (Zero hour radiation) near white hole region which composed of **three-in-one** fundamental ions of **Photon, Electron, Proton** having definite charge, electronic, magnetic, optic properties exist under highly **endothermic environment under Zero gravity or Negligible gravity.**

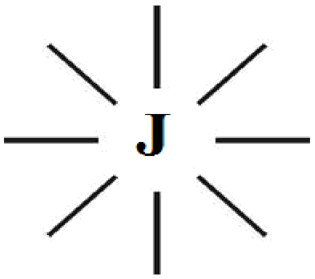

VIRGIN LIGHT
(Zero Hour Radiation)

It is further focused that the philosophy of '**FEMALE PREGNANCY**' shall be considered as the new genetic characteristics inherited only on the **EARTH PLANET** when human population started living on Earth under varied growth of new radiations such as **γ**-family radiation, **β**-family radiation, **α**- family radiation in **three nuclear ages**.

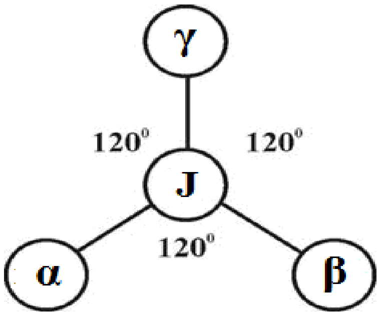

(3G RADIATION)

b) Philosophy of j^+-Radiation?...

It is hypothesized that in the expanding universe **γ, β, α** families of radiation shall be considered as distinguish family of radiation emanated from "**J-Radiation**" in different nuclear age responsible for various **HCNO** based genetically varied atomic matters and responsible for various genetically varied species of human population having distinguished chromosome level of human in different nuclear age. The philosophy of **j^+-Radiation** shall be considered as the new family of radiation say '**fourth generation family**' having distinguished genetic feature of future population. The fourth generation radiation shall be considered having genetically varied charge, Electric, magnetic, optic properties, higher downward gravity compared to Three generation family radiations. It is further hypothesized that the fourth generation radiation shall be considered having ability to overcome the **current global warming issues** and provide pathway for better are conducive environment for **subsistence and sustainability** of human populations on the earth planet for another **1000 years**. The philosophy of distinguished characteristics of **J-Radiation, j^+-Radiation** shall be hypothetically narrated as below.

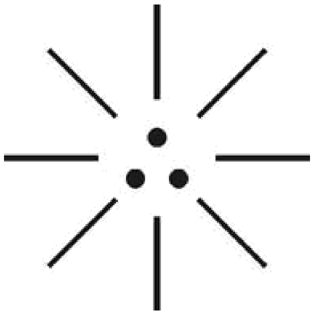

CREATION LOGIC
(Law of Early Universe)

i) **Right dot** – "**Proton**" (like **DNA** responsible for functional property)
ii) **Left dot** – "**Electron**" (like **HORMONE** responsible for structural property)
iii) **Centre dot** – "**Photon**" (like **RNA** responsible for sequence control property)

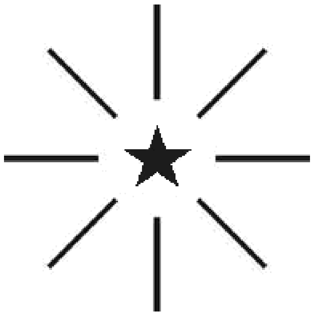

MORNING STAR
(Law of 4th Generation)

c) Philosophy of 'j-66 human'?...

It is hypothesized that in the **expanding universe** the human population shall be considered having different "**Chromosome level**" having different genetic characteristics in **different age** as hypothetically described below. The j-66 human shall also be called as "**JANE DOE**".

e) **White Age** (Human origin) **- Trisomy**
f) **Dark Age** (Plasma age) **- 20**
g) **γ**-age (1st generation) **- 30**
h) **β**-age (2nd generation) **- 40**
i) **α**-age (3rd generation) **- 46**
j) **j-66 human** (4th generation) **- 66**

The philosophy of '**j-66 human**' within "**MOTHERS WOMB**" due to impact of **j$^+$-radiation** shall be described below.

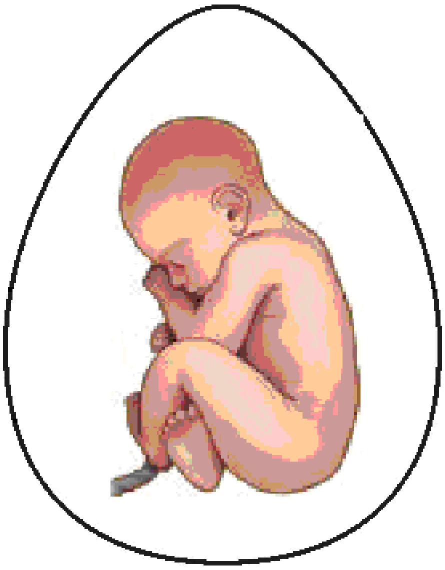

NEW COVENANT
(j-66 Human)

It is further hypothesized that the new **j-66 human** shall be considered as having genetically varied having '**Five chamber heart**' due to growth of additional blood type '**j-type**' due to impact of **j$^+$-radiation** along with conventional four type **A, B, AB, O** already exist.

4th GENERATION
(j-Type Blood)

*"The **mothers womb** shall be considered as **paradox and heaven**. The Philosophy of English word **JAIL** might be derived from the proto Indo-Europe root **CHEI-e ILLAM**. CHEI-e shall mean **INFANT; Illam** shall mean paradox. The mothers womb shall alternatively mean Jail where the law of creation is developed"*

- Author

III. CONCLUSION:

It is focused that there is "**No Worry**"… for the impact of present day **global warming**. The new generation radiation shall promote **immunity** against present day environment and global warming and promote pathway for consistent reduction in global population growth by impact of promoting '**NO PREGNANCY**' by increased level of **virgin and juvenile population** in 4th Generation populations.

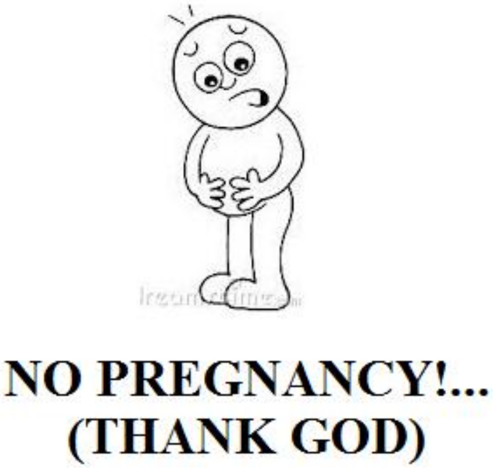

IV. PREVIOUS PUBLICATION:

The philosophy of origin of first life and human, the philosophy of model Cosmo Universe, the philosophy of fundamental neutrino particles have already been published in various international journals mentioned below. Hence this article shall be considered as **extended version** of the previous articles already published by the same author.

[1] Cosmo Super Star – IJSRP, April issue, 2013
[2] Super Scientist of Climate control – IJSER, May issue, 2013
[3] AKKIE MARS CODE – IJSER, June issue, 2013
[4] KARITHIRI (Dark flame) The Centromere of Cosmo Universe – IJIRD, May issue, 2013
[5] MA-AYYAN of MARS – IJIRD, June issue, 2013
[6] MARS TRIBE – IJSER, June issue, 2013
[7] MARS MATHEMATICS – IJERD, June issue, 2013
[8] MARS (EZHEM) The mother of All Planets – IJSER, June issue, 2013
[9] The Mystery of Crop Circle – IJOART, May issue, 2013
[10] Origin of First Language – IJIRD, June issue, 2013
[11] MARS TRISOMY HUMAN – IJOART, June issue, 2013
[12] MARS ANGEL – IJSTR, June issue, 2013
[13] Three principles of Akkie Management (AJIBM, August issue, 2013)
[14] Prehistoric Triphthong Alphabet (IJIRD, July issue, 2013)
[15] Prehistoric Akkie Music (IJST, July issue, 2013)
[16] Barack Obama is Tamil Based Indian? (IJSER, August issue, 2013)
[17] Philosophy of MARS Radiation (IJSER, August 2013)
[18] Etymology of word **“J”** (IJSER, September 2013)
[19] NOAH is Dravidian? (IJOART, August 2013)
[20] Philosophy of Dark Cell (Soul)? (IJSER, September 2013)
[21] Darwin Sir is Wrong?! (IJSER, October issue, 2013)
[22] Prehistoric Pyramids are RF Antenna?!... (IJSER, October issue, 2013)
[23] HUMAN IS A ROAM FREE CELL PHONE?!... (IJIRD, September issue, 2013)
[24] NEUTRINOS EXIST IN EARTH ATMOSPHERE?!... (IJERD, October issue, 2013)
[25] EARLY UNIVERSE WAS HIGHLY FROZEN?!... (IJOART, October issue, 2013)

[26] UNIVERSE IS LIKE SPACE SHIP?!... (AJER, October issue, 2013)

[27] ANCIENT EGYPT IS DRAVIDA NAD?!... (IJSER, November issue, 2013)

[28] ROSETTA STONE IS PREHISTORIC "THAMEE STONE" ?!... (IJSER, November issue, 2013)

[29] The Supernatural "CNO" HUMAN?... (IJOART, December issue, 2013)

[30] 3G HUMAN ANCESTOR?... (AJER, December issue, 2013)

[31] 3G Evolution?... (IJIRD, December issue, 2013)

[32] God Created Human?... (IJERD, December issue, 2013)

[33] Prehistoric "J" – Element?... (IJSER, January issue, 2014)

[34] 3G Mobile phone Induces Cancer?... (IJERD, December issue, 2013)

[35] "J" Shall Mean "JOULE"?... (IRJES, December issue, 2013)

[36] "J"- HOUSE IS A HEAVEN?... (IJIRD, January issue, 2014)

[37] The Supersonic JET FLIGHT-2014?... (IJSER, January issue, 2014)

[38] "J"-RADIATION IS MOTHER OF HYDROGEN?... (AJER, January issue, 2014)

[39] PEACE BEGINS WITH "J"?... (IJERD, January issue, 2014)

[40] THE VIRGIN LIGHT?... (IJCRAR, January issue 2014)

[41] THE VEILED MOTHER?... (IJERD, January issue 2014)

[42] GOD HAS NO LUNGS?... (IJERD, February issue 2014)

[43] Matters are made of Light or Atom?!... (IJERD, February issue 2014)

[44] THE NUCLEAR "MUKKULAM"?... (IJSER, February issue 2014)

[45] WHITE REVOLUTION 2014-15?... (IJERD, February issue 2014)

[46] STAR TWINKLES!?... (IJERD, March issue 2014)

[47] "E-LANKA" THE TAMIL CONTINENT?... (IJERD, March issue 2014)

[48] HELLO NAMESTE?... (IJSER, March issue 2014)

[49] MOTHERHOOD MEANS DELIVERING CHILD?... (AJER, March issue 2014)

[50] E–ACHI, IAS?... (AJER, March issue 2014)

[51] THE ALTERNATIVE MEDICINE?... (AJER, April issue 2014)

[52] GANJA IS ILLEGAL PLANT?... (IJERD, April issue 2014)

[53] THE ENDOS?... (IJERD, April issue 2014)

[54] THE "TRI-TRONIC" UNIVERSE?... (AJER, May issue 2014)

[55] Varied Plasma Level have impact on "GENETIC VALUE"?... (AJER, May issue 2014)

[56] JALLIKATTU IS DRAVIDIAN VETERAN SPORT?... (AJER, May issue 2014)

[57] Human Equivalent of Cosmo?... (IJSER, May issue 2014)

[58] THAI-e ETHIA!... (AJER, May issue 2014)

[59] THE PHILOSOPHY OF "DALIT"?... (AJER, June issue 2014)

[60] THE IMPACT OF HIGHER QUALIFICATION?... (AJER, June issue 2014)

[61] THE CRYSTAL UNIVERSE?... (AJER July 2014 issue)

[62] THE GLOBAL POLITICS?... (AJER July 2014 issue)

[63] THE KACHCHA THEEVU?... (AJER July 2014 issue)

[64] THE RADIANT MANAGER?... (AJER July 2014 issue)
[65] THE UNIVERSAL LAMP?... (IJOART July 2014 issue)
[66] THE MUSIC RAIN?... (IJERD July 2014 issue)
[67] THIRI KURAL?... (AJER August 2014 issue)
[68] THE SIXTH SENSE OF HUMAN?... (AJER August 2014 issue)
[69] THEE… DARK BOMB?... (IJSER August 2014 issue)
[70] RAKSHA BANDHAN CULTURE?... (IJERD August 2014 issue)
[71] THE WHITE BLOOD ANCESTOR?... (AJER August 2014 issue)
[72] THE PHILOSOPHY OF “ZERO HOUR”?... (IJERD August 2014 issue)
[73] RAMAR PALAM?... (AJER September 2014 issue)
[74] THE UNIVERSAL TERRORIST?... (AJER September 2014 issue)
[75] THE “J-CLOCK”!... (AJER September 2014 issue)
[76] “STUDENTS” AND “POLITICS”?... (EJAE September 2014 issue)
[77] THE PREGNANT MAN?... (AJER September 2014 issue)
[78] PERIAR IS ATHEIST?... (IJSER September 2014 issue)
[79] A JOURNEY TO "WHITE PLANET”?... (AJER September 2014 issue)

REFERENCE

[1] Intensive Internet “e-book” study through, Google search and wikipedia
[2] M.Arulmani, “3G Akkanna Man”, Annai Publications, Cholapuram, 2011
[3] M. Arulmani; V.R. Hemalatha, “Tamil the Law of Universe”, Annai Publications, Cholapuram, 2012
[4] Harold Koontz, Heinz Weihriah, “Essentials of management”, Tata McGraw-Hill publications, 2005
[5] M. Arulmani; V.R. Hemalatha, “First Music and First Music Alphabet”, Annai Publications, Cholapuram, 2012
[6] King James Version, “Holy Bible”
[7] S.A. Perumal, “Human Evolution History”
[8] “English Dictionary”, Oxford Publications
[9] Sho. Devaneyapavanar, “Tamil first mother language”, Chennai, 2009
[10] Tamilannal, “Tholkoppiar”, Chennai, 2007
[11] “Tamil to English Dictionary”, Suravin Publication, 2009
[12] “Text Material for E5 to E6 upgradaton”, BSNL Publication, 2012
[13] A. Nakkiran, “Dravidian mother”, Chennai, 2007
[14] Dr. M. Karunanidhi, “Thirukkural Translation”, 2010
[15] “Manorama Tell me why periodicals”, M.M. Publication Ltd., Kottayam, 2009
[16] V.R. Hemalatha, “A Global level peace tourism to Veilankanni”, Annai Publications, Cholapuram, 2007
[17] Prof. Ganapathi Pillai, “Sri Lankan Tamil History”, 2004
[18] Dr. K.K. Pillai, “South Indian History”, 2006
[19] M. Varadharajan, “Language History”, Chennai, 2009
[20] Fr. Y.S. Yagoo, “Western Sun”, 2008
[21] Gopal Chettiar, “Adi Dravidian Origin History”, 2004
[22] M. Arulmani; V.R. Hemalatha, “Ezhem Nadu My Dream” - (2 Parts), Annai Publications, Cholapuram, 2010
[23] M. Arulmani; V.R. Hemalatha, “The Super Scientist of Climate Control”, Annai Publications, Cholapuram, 2013, pp 1-3

American Journal of Engineering Research (AJER)
e-ISSN : 2320-0847 p-ISSN : 2320-0936
Volume-3, Issue-10, pp-14-24
www.ajer.org

Research Paper Open Access

A JOURNEY TO "WHITE PLANET"?...

(A New theory on "White Mars")

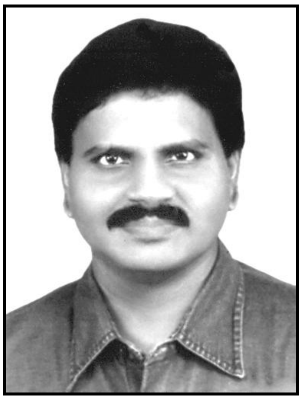

M.Arulmani, B.E.
(Engineer)

V.R.Hema Latha, M.A., M.Sc., M.Phil.
(Biologist)

ABSTRACT: CONGRADULATIONS TO MOTHER INDIA!... for having reached the **MARS PLANET** (also called as "**RED PLANET**") and become "**PIONEER**" in search of existence of life and possibility of Transforming future human populations into MARS PLANET for **inhabitation** for overcoming the earth climate issues and **subsistence of Life**.

This scientific research article focus that "**WHITE MARS**" shall be considered as the only planet in the entire cosmo Universe suitable for supporting and subsistence of human life besides "**EARTH PLANET**". Hence journey has to be continued till further to reach **WHITE MARS** near white hole **J-RADIATION** region of universe for further exploration.

This research further focus that there are different types of Mars planet such as **White Mars, Dark Mars, Blue Mars, Green Mars, Red Mars** consider exist in "**different galaxies**" under different Environmental conditions. **White mars** shall be considered as the **1st stage** and **red mars** shall be considered as the **5th stage** of location in the material universe under "**strong downward gravity**" of different level.

It is further focused that the '**HUMAN ANCESTOR**' shall be considered lived in **WHITE MARS** in the early universe with **extraordinary intelligence and wisdom**. During the course of expanding universe the human ancestor considered **TRANSFORMED TO EARTH PLANET** from white mars due to varied climatic condition. The transformation shall be considered like '**INFANT**' transformed from '**MOTHER'S WOMB**' which is considered as '**ONE WAY JOURNEY**' and '**RETURN JOURNEY**' is not possible until and '**REBIRTH**'.

> *"**WHITE MARS** belong to white galaxy (also called **milky galaxy**) shall be considered as "**Mother of all planets**". Other mars planets belong to **Dark galaxy, Blue galaxy, Green galaxy, Red galaxy** shall be considered as supporting galaxies responsible for various environmental conditions of universe and not meant for supporting **inhabitation of human life**".*
>
> ***- Author***

It is focused that the living Earth Planet in the Universe considered located at the stage say '**TAMBARAM**' and '**Red Mars**' considers located at the stage "**ST. THOMAS MOUNT**". The **white mars** considers located at stage of '**PARK STATION**'. Hence, further journey has to be performed through various stages of **GUINDY, SAIDAPET, EGMORE** to reach white Mars ultimately.

"WISH YOU HAPPY JOURNEY 2014
- M. Arulmani,
Tamil based Indian

KEY WORDS:
a) Philosophy of "**White Mars**"?...
b) Philosophy of "**Dark Mars**"?...
c) Philosophy of "**Blue Mars**"?...
d) Philosophy of "**Green Mars**"?...
e) Philosophy of "**Red Mars**"?...
f) Philosophy of "**Planet Ring**"?...

I. INTRODUCTION:

Thanks to "**NASA**" of United States of America for pioneering the mars exploration through '**MARTIAN**' since 1883 for **benefit of global population** for possibility of future inhabitation of human population to overcome the present globe warming environment, and better harvesting of solar energy from **other galaxies**.

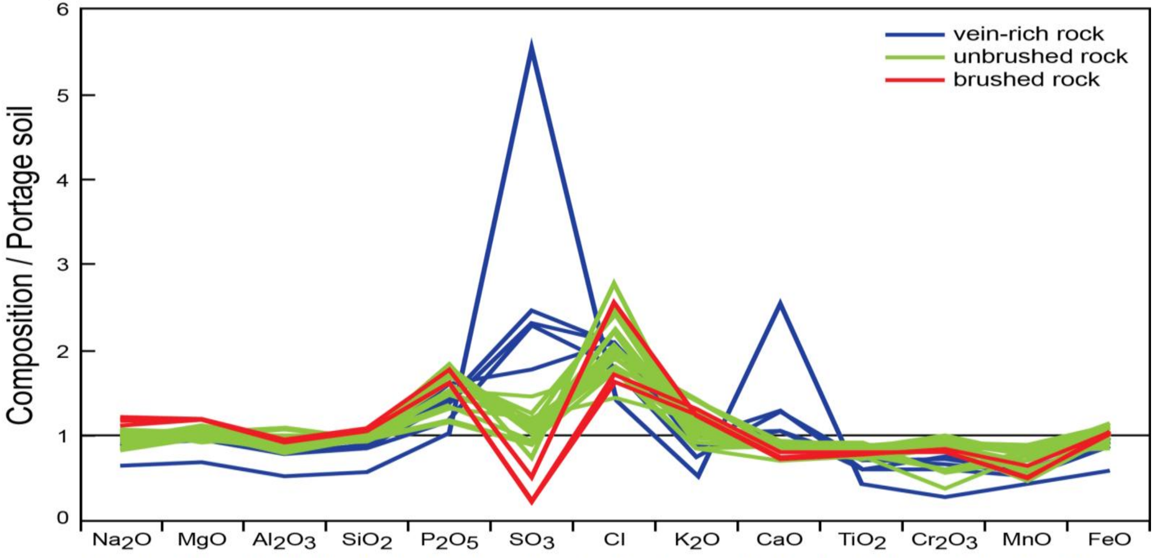

Composition of "Yellowknife Bay" rocks – rock veins are higher in calcium and sulfur than "Portage" soil – APXS results – Curiosity rover (March, 2013).

This scientific research article speculates that **HUMAN ANCESTORS** already lived in **White Mars of white galaxy** with outstanding Intelligence and wisdom capable of controlling effectively the fundamental parameters of **SUN, EARTH, MOON** considered as **FOUNDATION OF UNIVERSE** rather than '**planets of solar**

system'. It is further focused that the human ancestors lived in white mars shall be considered as having genetically varied characteristics say "**MALE PREGNANCY**" and the "**FEMALE PREGNANCY**" shall be considered as transformed from **white Mars ancestors** when population started living on **EARTH PLANET** during subsequent "**Nuclear Age**".

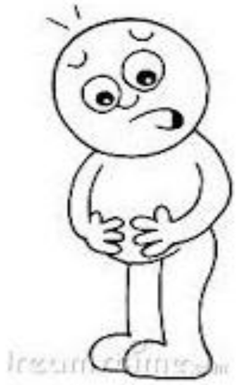

WHITE MARS ANCESTOR
(Model Male Pregnancy)

It is further focused that "**human ancestors**" of white Mars shall be considered as worshiped as '**GOD**' in the early universe. The philosophy of roman god of mars, greek god of Ares and other thousands of gods Earth planet might be derived from the philosophy of "**God of white mars**".

II. HYPOTHESIS AND NARRATION

a) Philosophy of white galaxy?...

Case study on Astronomical science focus that there are thousands of galaxies exist accommodating various planets, comets, asteroids, meteors orbiting within the respective galaxy. **Do galaxies serve any purpose for sustainability of human life?... Can human populations survive without existence of so many galaxies?...**

It is hypothesized that "**Human Ancestors**" considered lived in white mars under environment of only single galaxy say "**White galaxy**". The white galaxy considered contains only three planets say **white sun, white earth, white moon** having centered by **white mars**.

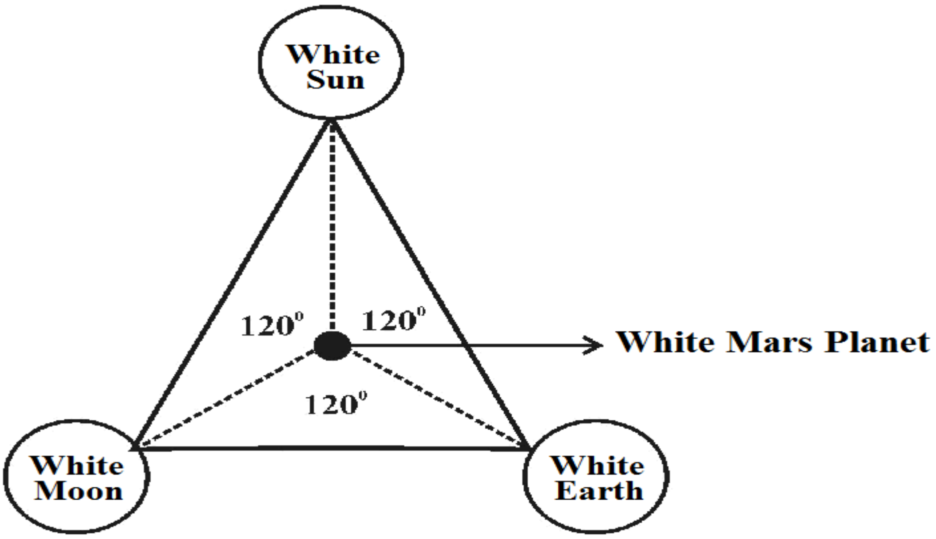

(MODEL WHITE GALAXY)

During the course of expanding universe the **white galaxy** gave birth to many other galaxies say **Dark galaxy** (also called as plasma galaxy) **Blue galaxy, Green galaxy, Red galaxy** in different nuclear ages. The human ancestors lived in white mars consider transformed to earth planet at one stage and started living under existence of four distinguished galaxies exist above Earth planet and undergone varied genetic characteristics in different nuclear age. The philosophy of growth of various galaxy shall be described as below:

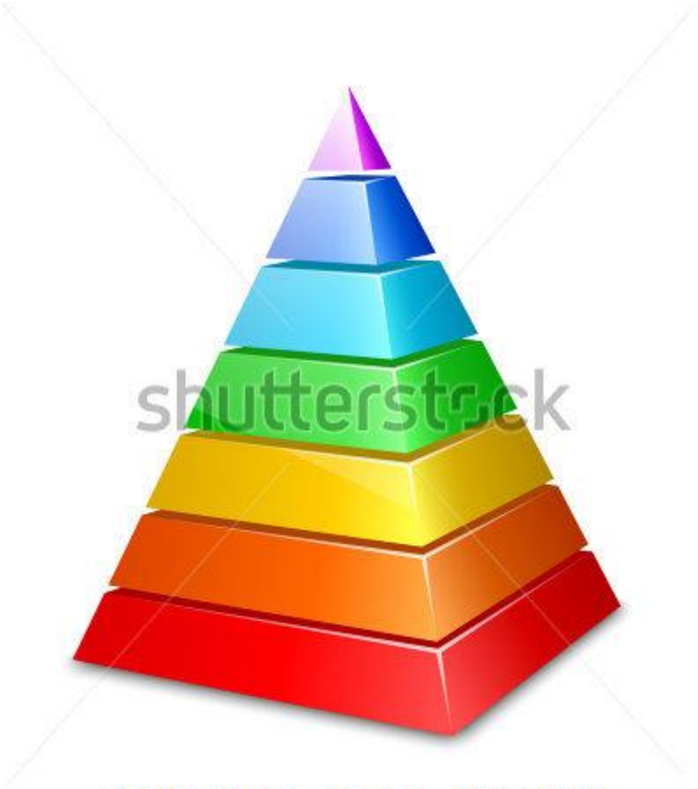

(MODEL GALAXIES)

Sl.No.	Name of galaxy	Mother planet	Three-in-one planets
1.	White galaxy	**White mars**	White sun, white earth, white moon
2.	Dark galaxy	**Dark mars**	Dark sun, Dark earth, Dark moon
3.	Blue galaxy	**Blue mars**	Blue sun, Blue Earth, Blue moon
4.	Green galaxy	**Green mars**	Green sun, green earth, green moon
5.	Red galaxy	**Red mars**	Red sun, red earth, red moon

It is further hypothesized that the **stage** of various galaxy and varied characteristics shall be hypothetically described as below for easy understanding.

i) **Foundation of Universe**
(Sun, Earth, Moon) - **Tambaram** (0 KM)

ii) **Red galaxy**
(UV, RF, IR) - **St.Thomas Mount** (5 KM)

iii) **Green galaxy**
(Only UV, RF) - **Guindy** (10 KM)

iv) **Blue galaxy**

(Only UV) - **Saidapet** (15 KM)
v) **Dark Galaxy**
(Plasma stage) - **Egmore** (20 KM)
vi) **White galaxy**
(e radiation) - **Park Station** (25 KM)
vii) **J. Radiation**
(White hole region - **Mint** (30 KM)
virgin light)

b) Case study on Red Planet MARS?...

Case study shows that **MARS PLANET** (also called as Red Planet) is the fourth planet from the sun and third smallest in the solar system having similar characteristics of Earth planet having possibility of Human Inhabitation. Greek also called Red planet as '**Pyrolis**" the Fiery (Fire star). Red planet further consider significantly less dense than Earth and no existence of **magnetic field** currently but the once the magnetic field might exist and subsequently lost during the course of expanding universe. The reddish colour is due to abundance of Hematite in its surface rocks.

It is hypothesized that the white galaxy and white mars shall be considered composed of only **WIND, RAIN, MUSIC** essential for supporting human life and subsistence of human life. Further the white mars planet shall be considered exist under "**SUPER SOLID STATE**" (White Element) beyond **TRIPLE POINT** of law of thermodynamics and all matters of universe shall be considered derived from 'white mars'. Further it is focused that the wind, music, rain shall be totally free from atomic elements like **Hydrogen, carbon, Nitrogen, Ozone** and consider composed of only ions of photon, electron, proton due to impact of "**J-RADIATION**" having definite charge and electric, magnetic, optic properties. The '**Wind**' (Free from oxygen) shall be considered like 1000 times pure than conventional **OZONE** having low PH value.

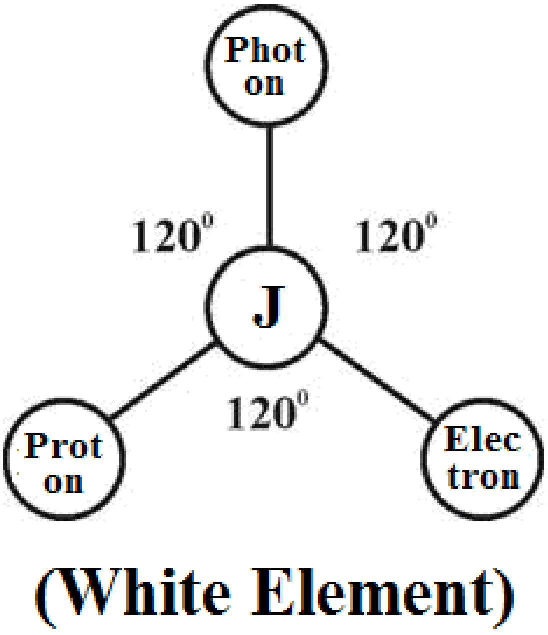

"The origin of various atomic elements like Hydrogen, Carbon, Nitrogen, Ozone (HCNO) and complex molecules shall be considered evolved in other Blue, Green, Red Galaxies in different Nuclear Ages".

Author

c) Case study on Etymology of Word MARS?...

It is hypothesized that the etymology of word MARS and other prehistoric astronomical words shall be considered derived from proto Indo Europe root as described below:

S.No.	Word	PIE	English Meaning
1.	J.Radiation	Thee	Virgin light
2.	Mars	Mari-e	Rain, Ray
3.	Radiation	Thri-e	Lightning
4.	Galaxy	Kal-e	Atmosphere

d) Philosophy of Male Pregnancy in white mars?...

It is hypothesized that the male parent (also called as **Male Angel**) responsible for male pregnancy by '**asexual means**' by impact of **J-Radiation** and the white population (**virgin population**) shall be considered as produced and multiplexed. The female angel shall be considered as responsible only for assisting Male Angel for safe delivery. The Female Angel (**Queen**) shall also be called as "**Mother of Mars**" (Virgin).

(i)

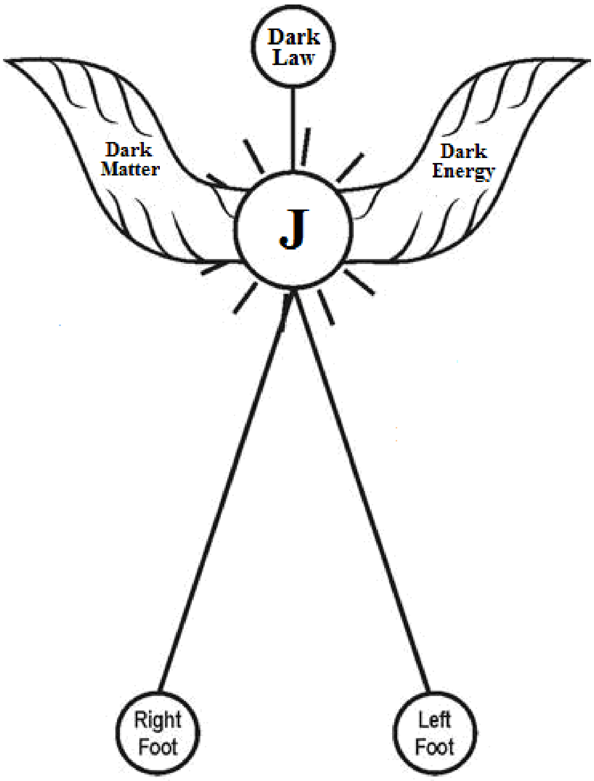

MODEL MALE ANGEL
(Male Pregnancy)

(ii)

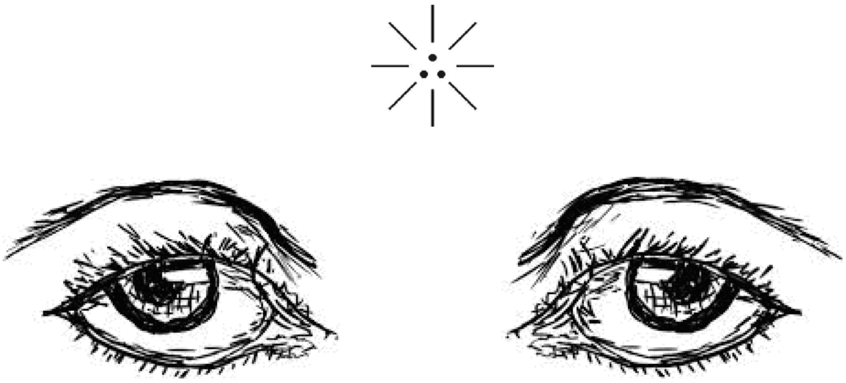

MODEL FEMALE ANGEL
(Mother of Mars)

It is further focused that the philosophy of mars symbol considered derived from philosophy of "**Mars Trisomy**". Mars Trisomy shall mean fundamental trisomy chromosome of **White mars organisms** having genetic characteristics of Angel populations (**Angel family**) responsible for **male pregnancy and Egg laying**. It is hypothesized that trisomy chromosome might be genetically undergone changes during '**Plasma Age**' (in Dark galaxy) and organisms with **diploid chromosome and female pregnancy** might be formed during inhabitation of human population on the Earth planet.

e) Case study on Tesla Study?...

An 1893 soap ad playing on the popular idea that Mars was populated.

Case study shows that in 1989 Nikola Tesla observed repeated signals that he later speculated that the signals might have come from another planet possibly Mars. It is hypothesized that in the expanding Universe the various Mars planets such as **White Mars, Dark Mars, Blue Mars, Green Mars, Red Mars** exists in various galaxies shall be considered as the source of energy derived from J-Radiation.

f) Case study on Planet Ring?...

Planetary ring refers to ring of cosmic dust and other small particles orbiting around a planet in a flat disc shaped region. It is hypothesized that the formation of planetary ring of each planet existing in the Universe shall be considered as two segments i.e. upper segment is influenced with upward gravity and lower segment considered influenced with downward gravity. The ring like region shall be considered as zero gravity of the planet. It is further focused that the different orientation of planets in the Universe shall be considered as orientation towards the respective Mars planet of the respective galaxies and considered exists under equilibrium condition otherwise called as **ORBIT RESONANCE**.

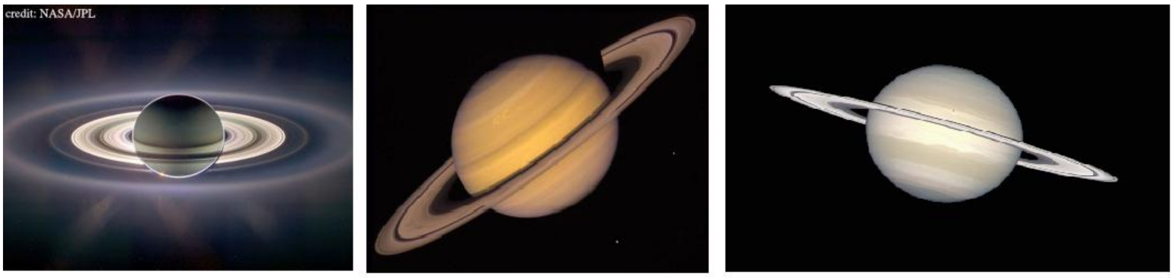

(MODEL DISTINGUISHED GRAVITY ORIENTATION)

III. CONCLUSION:

In the current solar system Sun is considered as center of the planetary system without consideration of comets, asteroids, meteors also orbiting in the respective solar system. It is hypothesized that the whole Universe shall be considered as different galaxies in which **MARS** shall be considered as the center of the solar system and **WHITE MARS** shall be considered as the mother of whole Universe.

It is further focused that the concept of **HEAVEN** shall be considered as the supernatural system in which galaxies shall be considered as integral part of heaven. Further the integrated galaxy system shall be considered equivalent to **STOMACH OF GOD** of white Mars.

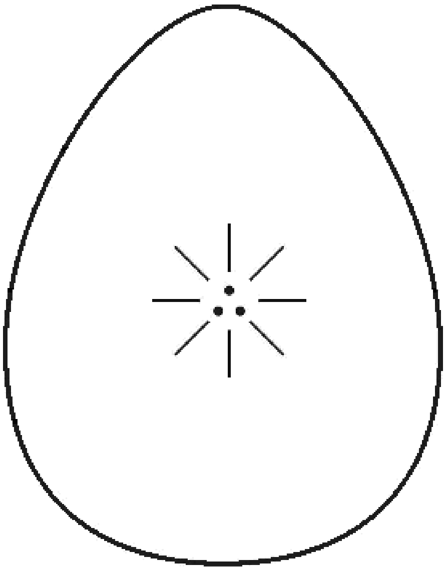

STOMACH OF GOD
(Galaxy System)

*"The **White Mars** expedition is a bold move that will add significantly to our understanding of how to deal with the challenge of human exploration of the **Red Planet**."*

- Robert Zubrin, President, US Mars Society

IV. Previous Publication:

The philosophy of origin of first life and human, the philosophy of model Cosmo Universe, the philosophy of fundamental neutrino particles have already been published in various international journals mentioned below. Hence this article shall be considered as **extended version** of the previous articles already published by the same author.

[1] Cosmo Super Star – IJSRP, April issue, 2013

[2] Super Scientist of Climate control – IJSER, May issue, 2013

[3] AKKIE MARS CODE – IJSER, June issue, 2013

[4] KARITHIRI (Dark flame) The Centromere of Cosmo Universe – IJIRD, May issue, 2013

[5] MA-AYYAN of MARS – IJIRD, June issue, 2013

[6] MARS TRIBE – IJSER, June issue, 2013

[7] MARS MATHEMATICS – IJERD, June issue, 2013

[8] MARS (EZHEM) The mother of All Planets – IJSER, June issue, 2013

[9] The Mystery of Crop Circle – IJOART, May issue, 2013

[10] Origin of First Language – IJIRD, June issue, 2013

[11] MARS TRISOMY HUMAN – IJOART, June issue, 2013

[12] MARS ANGEL – IJSTR, June issue, 2013

[13] Three principles of Akkie Management (AJIBM, August issue, 2013)

[14] Prehistoric Triphthong Alphabet (IJIRD, July issue, 2013)

[15] Prehistoric Akkie Music (IJST, July issue, 2013)

[16] Barack Obama is Tamil Based Indian? (IJSER, August issue, 2013)

[17] Philosophy of MARS Radiation (IJSER, August 2013)

[18] Etymology of word **"J"** (IJSER, September 2013)

[19] NOAH is Dravidian? (IJOART, August 2013)

[20] Philosophy of Dark Cell (Soul)? (IJSER, September 2013)

[21] Darwin Sir is Wrong?! (IJSER, October issue, 2013)

[22] Prehistoric Pyramids are RF Antenna?!... (IJSER, October issue, 2013)

[23] HUMAN IS A ROAM FREE CELL PHONE?!... (IJIRD, September issue, 2013)

[24] NEUTRINOS EXIST IN EARTH ATMOSPHERE?!... (IJERD, October issue, 2013)

[25] EARLY UNIVERSE WAS HIGHLY FROZEN?!... (IJOART, October issue, 2013)

[26] UNIVERSE IS LIKE SPACE SHIP?!... (AJER, October issue, 2013)

[27] ANCIENT EGYPT IS DRAVIDA NAD?!... (IJSER, November issue, 2013)

[28] ROSETTA STONE IS PREHISTORIC "THAMEE STONE" ?!... (IJSER, November issue, 2013)

[29] The Supernatural "CNO" HUMAN?... (IJOART, December issue, 2013)

[30] 3G HUMAN ANCESTOR?... (AJER, December issue, 2013)

[31] 3G Evolution?... (IJIRD, December issue, 2013)

[32] God Created Human?... (IJERD, December issue, 2013)

[33] Prehistoric “J” – Element?... (IJSER, January issue, 2014)

[34] 3G Mobile phone Induces Cancer?... (IJERD, December issue, 2013)

[35] “J” Shall Mean “JOULE”?... (IRJES, December issue, 2013)

[36] “J”- HOUSE IS A HEAVEN?... (IJIRD, January issue, 2014)

[37] The Supersonic JET FLIGHT-2014?... (IJSER, January issue, 2014)

[38] “J”-RADIATION IS MOTHER OF HYDROGEN?... (AJER, January issue, 2014)

[39] PEACE BEGINS WITH “J”?... (IJERD, January issue, 2014)

[40] THE VIRGIN LIGHT?... (IJCRAR, January issue 2014)

[41] THE VEILED MOTHER?... (IJERD, January issue 2014)

[42] GOD HAS NO LUNGS?... (IJERD, February issue 2014)

[43] Matters are made of Light or Atom?!... (IJERD, February issue 2014)

[44] THE NUCLEAR “MUKKULAM”?... (IJSER, February issue 2014)

[45] WHITE REVOLUTION 2014-15?... (IJERD, February issue 2014)

[46] STAR TWINKLES!?... (IJERD, March issue 2014)

[47] “E-LANKA” THE TAMIL CONTINENT?... (IJERD, March issue 2014)

[48] HELLO NAMESTE?... (IJSER, March issue 2014)

[49] MOTHERHOOD MEANS DELIVERING CHILD?... (AJER, March issue 2014)

[50] E–ACHI, IAS?... (AJER, March issue 2014)

[51] THE ALTERNATIVE MEDICINE?... (AJER, April issue 2014)

[52] GANJA IS ILLEGAL PLANT?... (IJERD, April issue 2014)

[53] THE ENDOS?... (IJERD, April issue 2014)

[54] THE “TRI-TRONIC” UNIVERSE?... (AJER, May issue 2014)

[55] Varied Plasma Level have impact on “GENETIC VALUE”?... (AJER, May issue 2014)

[56] JALLIKATTU IS DRAVIDIAN VETERAN SPORT?... (AJER, May issue 2014)

[57] Human Equivalent of Cosmo?... (IJSER, May issue 2014)

[58] THAI-e ETHIA!... (AJER, May issue 2014)

[59] THE PHILOSOPHY OF “DALIT”?... (AJER, June issue 2014)

[60] THE IMPACT OF HIGHER QUALIFICATION?... (AJER, June issue 2014)

[61] THE CRYSTAL UNIVERSE?... (AJER July 2014 issue)

[62] THE GLOBAL POLITICS?... (AJER July 2014 issue)

[63] THE KACHCHA THEEVU?... (AJER July 2014 issue)

[64] THE RADIANT MANAGER?... (AJER July 2014 issue)

[65] THE UNIVERSAL LAMP?... (IJOART July 2014 issue)

[66] THE MUSIC RAIN?... (IJERD July 2014 issue)

[67] THIRI KURAL?... (AJER August 2014 issue)

[68] THE SIXTH SENSE OF HUMAN?... (AJER August 2014 issue)

[69] THEE… DARK BOMB?... (IJSER August 2014 issue)

[70] RAKSHA BANDHAN CULTURE?... (IJERD August 2014 issue)

[71] THE WHITE BLOOD ANCESTOR?... (AJER August 2014 issue)

[72] THE PHILOSOPHY OF “ZERO HOUR”?... (IJERD August 2014 issue)

[73] RAMAR PALAM?... (AJER September 2014 issue)

[74] THE UNIVERSAL TERRORIST?... (AJER September 2014 issue)

[75] THE “J-CLOCK”!... (AJER September 2014 issue)

[76] “STUDENTS” AND “POLITICS”?... (EJAE September 2014 issue)

[77] THE PREGNANT MAN?... (AJER September 2014 issue)

[78] PERIAR IS ATHEIST?... (IJSER September 2014 issue)

REFERENCE

[1] Intensive Internet “e-book” study through, Google search and wikipedia
[2] M.Arulmani, “3G Akkanna Man”, Annai Publications, Cholapuram, 2011
[3] M. Arulmani; V.R. Hemalatha, “Tamil the Law of Universe”, Annai Publications, Cholapuram, 2012
[4] Harold Koontz, Heinz Weihriah, “Essentials of management”, Tata McGraw-Hill publications, 2005
[5] M. Arulmani; V.R. Hemalatha, “First Music and First Music Alphabet”, Annai Publications, Cholapuram, 2012
[6] King James Version, “Holy Bible”
[7] S.A. Perumal, “Human Evolution History”
[8] “English Dictionary”, Oxford Publications
[9] Sho. Devaneyapavanar, “Tamil first mother language”, Chennai, 2009
[10] Tamilannal, “Tholkoppiar”, Chennai, 2007
[11] “Tamil to English Dictionary”, Suravin Publication, 2009
[12] “Text Material for E5 to E6 upgradaton”, BSNL Publication, 2012
[13] A. Nakkiran, “Dravidian mother”, Chennai, 2007
[14] Dr. M. Karunanidhi, “Thirukkural Translation”, 2010
[15] “Manorama Tell me why periodicals”, M.M. Publication Ltd., Kottayam, 2009
[16] V.R. Hemalatha, “A Global level peace tourism to Veilankanni”, Annai Publications, Cholapuram, 2007
[17] Prof. Ganapathi Pillai, “Sri Lankan Tamil History”, 2004
[18] Dr. K.K. Pillai, “South Indian History”, 2006
[19] M. Varadharajan, “Language History”, Chennai, 2009
[20] Fr. Y.S. Yagoo, “Western Sun”, 2008
[21] Gopal Chettiar, “Adi Dravidian Origin History”, 2004
[22] M. Arulmani; V.R. Hemalatha, “Ezhem Nadu My Dream” - (2 Parts), Annai Publications, Cholapuram, 2010
[23] M. Arulmani; V.R. Hemalatha, “The Super Scientist of Climate Control”, Annai Publications, Cholapuram, 2013, pp 1-3

American Journal of Engineering Research (AJER)
e-ISSN: 2320-0847 p-ISSN : 2320-0936
Volume-3, Issue-10, pp-25-33
www.ajer.org

Research Paper Open Access

Energy Equations for Computation of Parabolic-Trough Collector Efficiency Using Solar Position Coordinates

I. S. Sintali, G. Egbo and H. Dandakouta
Department of Mechanical Engineering
Faculty of Engineering and Engineering Technology
Abubakar Tafawa Balewa University, Bauchi

ABSTRACT: *This paper presents the development of energy equations for computation of the efficiency of Parabolic-Trough Collector (PTC) using solar coordinates. The energy equations included the universal time*(UT)*, day (n), month (M), year (Y), delta T* (ΔT)*,llongitude*(γ)*and latitude* (ϕ) *in radian. The heliocentric longitude (H), geocentric global coordinates and local topocentric sun coordinates were considered in the modeling equations. The thermal efficiency* η_{th} *of the PTC considered both the direct*$\left(E_{gd}\right)$ *and reflected* $\left(E_{gr}\right)$ *solar energy incident on the glass-cover as well as the thermal properties of the collector and the total energy losses* (Q_{losses})*in the system. The developed energy equations can be used to predict the performance (efficiency) of any PTC using the meteorological and radiative data of any particular location.*

Key words:*Parabolic-trough Collector, Energy, solar coordinates, thermal efficiency, meteorological and radiative.*

I. INTRODUCTION

1.1 Background of the study

In the design of solar energy systems, it is most important to predict the angular relationship between the sun's rays (solar coordinates) and a vector normal to the aperture or surface of the collector at a particular location on the earth (Topocentric Location). "Topocentric" means that the sun position is calculated with respect to the observer local position at the earth surface. When the sun is observed from a position on the earth, the point of interest is to know the position of the sun relative to a coordinate system that is located at the point of observation not at the center of the earth. The position of the sun relative to these coordinates can be fixed by two angles; solar altitude angle **(**α**)** and the solar azimuth angle(A). These are as shown in figure 1[1]

Williams and Raymond, [1] stated that solar altitude angle **(**α**)** at a point on the earth is the angle between the line passing through the point and the sun and the line passing through the point tangent to the earth and passing below the sun. The solar azimuth angle **(**A**)** is the angle between the line under the sun and the local meridian pointing to the equator, or due south in the northern hemisphere. It is positive when measured to the east and negative when measured to the west. The solar zenith angle **(** θ_z**)** is the angle between a solar ray and local vertical direction and it is the complement of **(**α**)**.

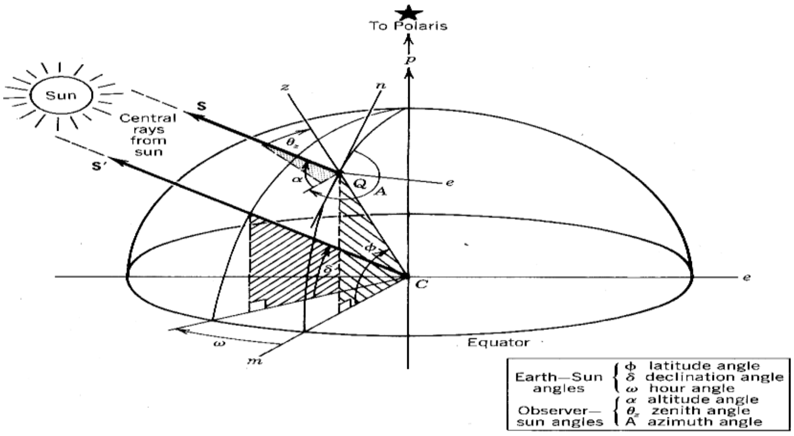

Fig. 1: Composite View of Parallel Sun Rays Relative to the Earth Surface and the Earth CenterCoordinates

The time of the year is specified by the topocentric solar declination (δ_t). The time of the day is specified by the hour angle (h_t). The hour angle is defined as zero at local solar noon and increases by 15° for each hour. Solar time is location dependent and is generally different from local time, which is defined by time zones and other approximation. Some situations such as performance correlations, determination of true south, and tracking algorithms require an accurate knowledge of the difference between solar time and the local time [2].

The definition of a parabola provides that all paraxial rays striking the parabolic reflector are reflected toward the line-focus as shown in figure 2. Parabolic-trough Collector (PTC) consists of a reflecting surface made by bending highly polished stainless steel reflector and fixed on a parabolic contour. The reflecting surface may also be made of polished mirror. The parabolic contour is supported by steel framework and mounted on a reflector support structure.A hand-wheel operated tilting mechanism permits adjustment of declination, in order to track the sun, thus, maintains the focusing of the solar radiation on the receiver. The receiver assembly comprises of the absorber-tube covered with a glass-cover tube to reduce heat losses, is placed along the focal line of the receiver as shown in figure 3.

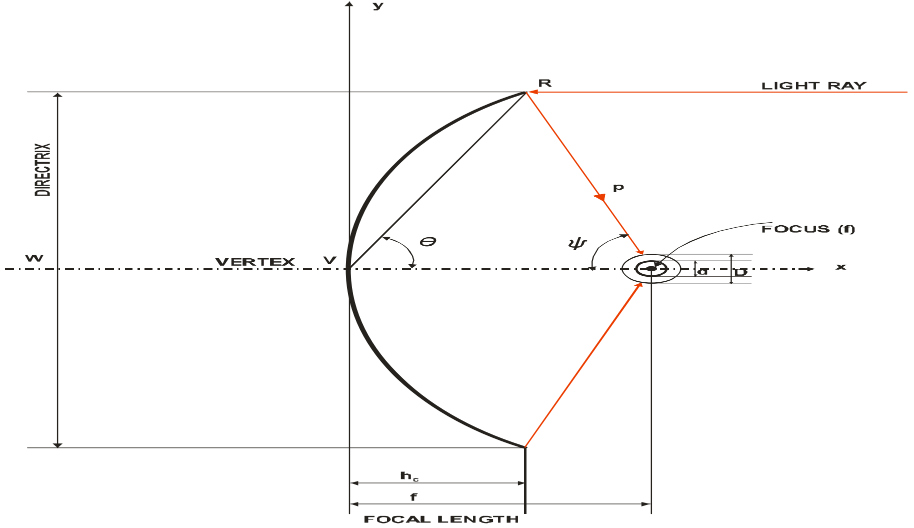

Fig 2: Geometry of Solar Parabolic-trough Collector

Concentration is achieved by using the reflector to channel natural concentration of energy on the reflector's aperture area into a significantly smaller area, the receiver assembly that is mounted on the focal line of the parabola. Typically, concentrator systems will not work efficiently without tracking, so at least single-axis tracking is required. This is as a result of the continuous changing sun's position in the sky with respect to time of the day as the sun moves across the sky.

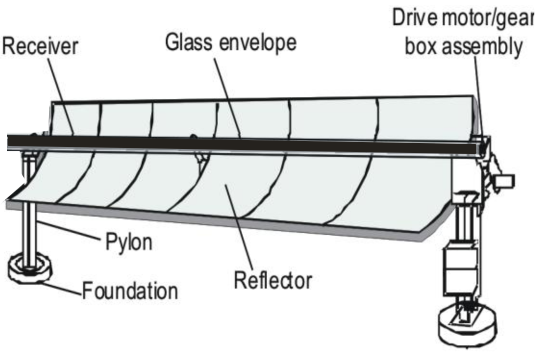

Fig 3: Parabolic-trough Concentrator

The accuracy of the solar tracking depends to a great extent on the solar coordinates at a particular location and at a given instant.This would greatly influence the solar radiation collection and thus the efficiency of the system. This necessitates the need to develop energy equations for computation of PTC efficiency using solar coordinates.

Other critical factors to be considered in the analysis of the solar concentrating collector are its material properties. When radiation strikes a body, part of it is reflected, a part isabsorbed and if the material is transparent, a partis transmitted. The fraction of the incidentradiation reflected is the reflectance (ρ), thefraction of the incident radiation transmitted isthe transmittance (τ) and the fraction absorbed isthe absorptance (α) as shown schematically in figure 4.

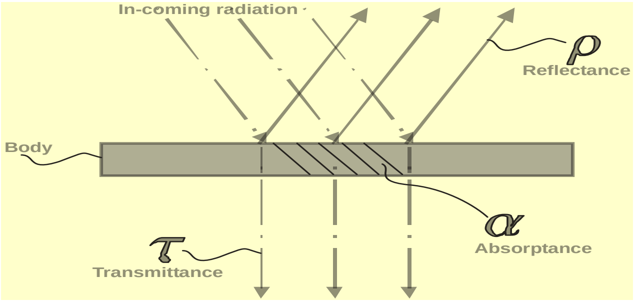

Fig. 4: Reflection, Absorption and Transmission of incident solar radiation by a solidbody.

Absorption of solar radiation is what solar heat collector is all about; therefore, a blackbody surface is ideal surface for making any solar collector's absorbing surface. For this reason, the latter is usually made as black as possible so that it will have a high absorption capacity.

II. DEVELOPMENT OF SOLAR PARABOLIC-TROUGH ENERGY EQUATIONS USING SOLAR COORDINATES

In developing the model equations for computing the efficiency of PTC using solar coordinates, the input parameters are determined by the time scales because of the importance of using the correct time in the calculation of solar position for solar radiation application.

2.1 Determination of Delta T(ΔT)

Delta T(ΔT) is a measure of the difference between a time scale based on the rotation of the Earth (Universal time UT) and an idealized uniform time scale at the surface of the Earth (Terrestrial time TT). The values of ΔT can be obtained from the (TT – UT) smoothed data provided in Bulletin B of the International Earth Rotation and Reference Systems, (IERRS) [3]. The value of ΔT was obtained for the year 2014 to be approximately 67.7 seconds.

2.2 Determination of Universal Time (UT)

The Universal Time (UT), or Greenwich civil time, is used to calculate the solar position based on the earth's rotation and is measured in hours from 0-hour at midnight. The minutes and seconds must be converted into fraction of an hour.

2.3 Determination of Time Scale (t_G and t)

The time scale, (t_G and t)are the Julian day and the Ephemeris Julian day respectively. These are used to overcome the drawbacks of irregularly fluctuating mean solar time due to elliptical shape of the earth's orbit i.e. the interval between two successive passages of the sun through the meridian, is not constant.They are defined as follows [4]:

$$t_G = INT\big(365.25(Y - 2000)\big) + INT\big(30.6001(M + 1)\big) + n + \frac{UT}{24} - 1158.5 \qquad \text{Eqn. 1}$$

$$t = t_G + \frac{\Delta T}{86400} \qquad \text{Eqn. 2}$$

Where*INT* is the integer of the calculated terms, *Y* is the year;*M* is the month of the year, n is the day of the month with decimal time and UT is the Universal Time.

2.4 Longitude γ and Latitude ϕ

Sun position is also very location-dependent, so it is critical that the longitude and latitudeof the site are known before calculations are carried out.

2.5 Determination of Heliocentric Longitude of the Earth

According toReda and Andreas, [4]"Heliocentric"means that the earth position is calculated with respect to the center of the sun. The heliocentric longitude (H) is the sum of four termsdefined as follows;

$$H = L_y + L_m + L_h + L_p \qquad \text{Eqn. 3}$$

Where:

$$L_y = 1.74094 + 1.7202768683e^{-2t} + 3.34118e^{-2}\sin\sigma + 3.488e^{-4} \times \sin 2A_o \qquad \text{Eqn. 4}$$

$$A_o = 1.72019e^{-2t} - 0.0563 \qquad \text{Eqn. 5}$$

$$L_m = 3.13e^{-5} \times \sin(0.2127730t - 0.585) \qquad \text{Eqn. 6}$$

$$L_h = 1.26e^{-5} \times \sin(4.243e^{-3t} + 1.46) + 2.35e^{-5} \times \sin(1.0727e^{-2t} + 0.72) + 2.76e^{-5} \times \sin(1.5799e^{-2t} + 2.35) + 2.75e^{-5} \times \sin(2.1551e^{-2t} - 1.98) + 1.26e^{-5} \times \sin(3.1490e^{-2t} - 0.80) \qquad \text{Eqn. 7}$$

$$L_p = (((-2.30796e^{-7}t_2 + 3.7976e^{-6})t_2 - 2.0458e^{-5})t_2 + 3.976e^{-5})t_2^2 \qquad \text{Eqn. 8}$$

With$t_2 = 0.001t$ Eqn. 9

WhereL_y, L_m, L_h, and L_p are linear increase with annual oscillation, moon perturbation, harmonic correction and polynomial correction respectively. The time scale t_2 is introduced in order to have more homogenous quantities in the products within the polynomial, avoiding too rough rounding approximation[5].

2.4 Correction to Geocentric Longitude Due to Nutation ($\Delta\gamma$)

"Geocentric" means that the sun position is calculated with respect to the earth center[4]. One problem is that the sun's apparent diurnal and annual motions are not completely regular, due to the ellipticity of the Earth's orbit and its continuous disturbance by the moon and planets. Consequently, the complex interactions between the bodies produce a wobbly motion of the earth rather than completely smooth motion, thus the need to compute the correction to geocentric longitude defined by the following relation [5]:

$$\Delta\gamma = 8.33e^{-5} \times \sin(9.252e^{-4t} - 1.173) \qquad \text{Eqn. 10}$$

2.5 Determination of the Earth Axis Inclination (ϵ)

This is the inclination of the center of the earth axis to the sun and is correlated as follows [5]:

$$\varepsilon = -6.21e^{-9t} + 0.409086 + 4.46e^{-5} \times \sin(9.262e^{-4t} + 0.397) \qquad \text{Eqn. 11}$$

2.6 Determination of Geocentric Global Solar Coordinates

This is the coordinates of the sun with respect to the earth's center.

2.6.1 Computation of geocentric solar longitude (γ_g)

The geocentric solar longitude may be estimated using the following relation[5]:

$$\gamma_g = H + \pi + \Delta\gamma - 9.932e^{-5} \qquad \text{Eqn. 12}$$

2.6.2 Computation of geocentric right ascension (α_a)

The ascension angle (α_a) is defined by [5]:

$$\alpha_a = arctan\,(sin\gamma_g\, cos\varepsilon cos\gamma_g) \qquad \text{Eqn. 13}$$

Where*arctan* is an arctangent function that is applied to maintain the correct quadrant of the α where α is in the range from $-\pi$ toπ.

2.6.3 Computation of geocentric declination (δ)

The geocentric solar declination is the declination of the sun with respect to the earth's center. The angle between the earth's equatorial plane and the earth-sun line varies between $\pm 23.45^o$ throughout the year. This angle is called the declination(δ).At the time of the year when the northern part of the earth's rotational axis is inclined toward the sun; the earth's equatorial plane is inclined 23.45° to the earth-sun line. At this time, the solar noon is at its highest point in the sky and the declination angle$(\delta) = \pm 23.45^o$ as illustrated in figure 5. This condition is called the summer solstice [6]. Thus, the declination can be computed at any given instant by equation 14.

$$\delta = arcsin\ (sin\varepsilon sin\gamma_g) \qquad \text{Eqn. 14}$$

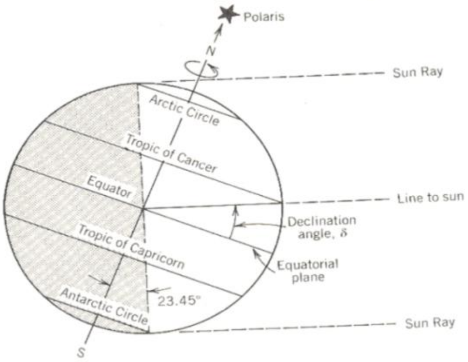

Fig. 5: Solar Declination Angle

2.7 Computation of Local Hour Angle of the Sun (*h*)

The hour angle is the angle through which the earth must turn to bring the meridian of a point directly in line with the sun's rays. It is measured positively west ward from the observer and it may be expressed in hours, minutes and seconds or degrees, minutes radians. One hour is equivalent to $\frac{2\pi}{24} = 0.262 rad or \frac{360^o}{24} = 15^o$ [4]:

$$h = 6.3003880990 t_G + 4.8824623 + 0.9174\Delta\gamma + \gamma - \alpha_a \qquad \text{Eqn. 15}$$

2.7 Computation of Parallax Correction to Right Ascension ($\Delta\alpha$)

The parallax correction may be computed using the following correlation [5]:

$$\Delta\alpha = -4.26e^{-5} \times cos\phi sinh \qquad \text{Eqn. 16}$$

2.9 Computation of Topocentric Sun Coordinates

According to Reda and Andreas, [5] topocentric sun coordinatesmeans that the sun position is calculated with respect to the observer local position at the earth surface.Grena[5] mentioned that topocentric sun coordinates affects the sun positions by many seconds of arc.

2.9.1 Topocentric right ascension (α_t)

The topocentric ascension angle is correlated as [5]:

$$\alpha_t = \alpha_a + \Delta\alpha \qquad \text{Eqn. 17}$$

2.9.2 Topocentric solar declination (δ_t)

This is the declination as expressed in section 2.6.3 with respect to the local observer position. This angle is given as [5]:

$$\delta_t = \delta - 4.26e^{-5} \times (sin\phi - \delta cos\phi) \qquad \text{Eqn. 18}$$

Whereδgeocentric declination and ϕ observer local latitude

2.9.3 Topocentric hour angle

This is as explained in section 2.7 and is determined with respect to the local observer position [5]:

$$h_t = h - \Delta\alpha \qquad \text{Eqn. 19}$$

$$ch_t = \cosh + \Delta\alpha sinh \quad \text{(Approximate cosine of } h_t\text{)} \qquad \text{Eqn. 20}$$

$$sh_t = sinh + \Delta\alpha cosh \quad \text{(Approximate sine of } h_t\text{)} \qquad \text{Eqn. 21}$$

2.10 Determination of Solar Elevation Angle, Without Refraction Correction (e_o)

Atmospheric refraction is the deviation of light or other electromagnetic wave from a straight line as it passes through the atmosphere due to the variation in air density as a function of altitude and is given by [7]:

$$e_o = asin\ (sin\phi sin\delta_t + cos\phi cos\delta_t ch_t) \qquad \text{Eqn. 22}$$

2.11 Atmospheric Refraction Correction to the Solar Elevation (Δe)

This correction factor is correlated as [8]:

$$\Delta e = \frac{0.08421P}{\left[(273+T)\tan\left(\frac{e_0 + 0.0031376}{e_0 + 0.089186}\right)\right]} \qquad \text{Eqn. 23}$$

Where T is Temperature at a particular time of the day and P is the pressure at that same time.

2.12 Local topocentric sun coordinates

2.12.1 Topocentric Zenith angle (θ_z)

The solar zenith angle θ_z is the angle between a solar ray and local vertical direction and it is the complement of the altitude$A$ as illustrated in figure 1.

$$\theta_z = \frac{\pi}{2} - e_0 - \Delta e \qquad \text{Eqn. 24}$$

2.12.2 Topocentric Azimuth angle (A)

The solar azimuth is the angle between the line under the sun and the local meridian pointing to the equator, or due south in the northern hemisphere. It is positive when measured to the east and negative when measured to the west as illustrated in figure 1.

$$A = atan2(sh_t ch_t \sin\phi - \tan\delta_t \cos\phi) \qquad \text{Eqn. 25}$$

2.12.3 Topocentric Altitude angle (α)

The solar altitude at a point on the earth is the angle between the line passing through the point and the sun and the line passing through the point tangent to the earth and passing below the sun as shown in figure 1.

$$\alpha = \sin\phi\sin\delta_t + \cos\phi\cos\delta_t\cos h_t \qquad \text{Eqn. 26}$$

Where; ϕ is the local latitude.

2.12.4 Solar incidence angle

In the design of solar energy systems, it is most important to be able to predict the angle between the sun’s rays and a vector normal to the aperture or surface of the collector. This angle is called the angle of incidence θ_i ; the maximum amount of solar radiation reaching the surface (or geometric aperture) is reduced by cosine of this angle. The other angle of importance is the tracking angleρ_t.

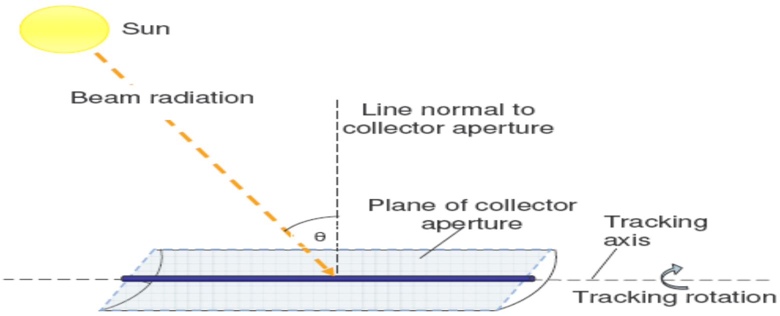

Fig.6: Solar Parabolic-trough Tracking Aperture where tracking rotation is about the axis.

Most type of medium and high-temperature collectors require a tracking drive system to align at least one and often both axes of the collector aperture perpendicular to the sun’s central ray. This is illustrated in figure 6.

For practical application when the tracking axis is oriented in the north-south direction the incidence angle,θ_i, and the tracking angle, ρ_t, and are given by equation 27 and 28 respectively [9]:

$$\cos\theta_i = \sqrt{1 - \cos^2\alpha_a \cos^2 A} \qquad \text{Eqn. 27}$$

$$\tan\rho_t = \frac{\sin A}{\tan\alpha_t} \qquad \text{Eqn. 28}$$

2.13 Heat Gain, Heat Transfer and Heat Absorbed by the PTC

The solar radiation incident on the concentrator is reflected on to the receiver (absorber tube) located at the focal line through which working fluid flows and which is covered by concentric-transparent glass cover. As the temperature of the receiver increases, heat transfer processes take place. Energy in transition under the motive force of a temperature difference between components of the collector forms the basis for the determination of heat gained and heat losses to and from one component to another.

The basic components of the PTC are as follows:

- The concentrator (reflecting surface)
- A receiver assembly comprising of a circular absorber tube with suitable coating, enclosed inside a concentric-transparent glass-cover; and
- The working fluid.

These are illustrated in figure 7 below:

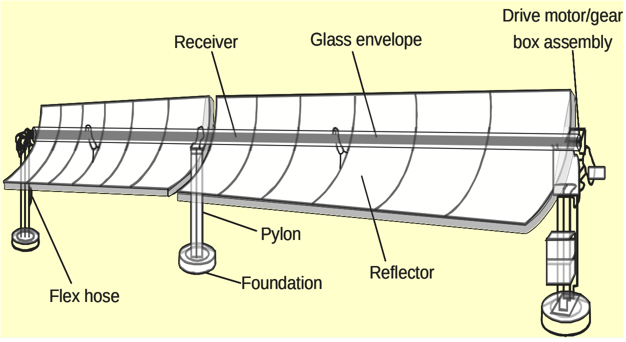

Fig.**7:** Basic Components of the Parabolic-Trough Collector

Energy balance equations for a PTC by *Egbo et al*,[10] considered the heat-energy-gain, the heat-energy-loss and the heat-energy-transfer between the components, i.e. the reflecting surface, the glass-cover and the absorber-tube, the thermal properties of the materials of the components and geometric dimensions of the SPTC. The equation for the enveloping glass-cover temperature developed by *Egbo et al,* [10] is given as follows;

2.13.1 Energy Equations for the Enveloping Glass-Cover

The energy balance equation for the enveloping glass-cover can be written as follows;

$$2\alpha_g RL\left[\left(I_{beam} * R_b\right) + I_{diff}\right] + \rho_c \alpha_g \left[\frac{(W-D)L}{\pi}\right]\left(I_{beam} * R_b\right) + \frac{A_t \sigma\left(T_t^4 - T_g^4\right)}{\frac{1}{\varepsilon_t} + \frac{A_t}{A_g}\left[\frac{1}{\varepsilon_g} - 1\right]} -$$

$$\sigma \varepsilon_g A_g\left(T_g^4 - T_{sky}^4\right) - A_g h_c\left(T_g - T_{sur}\right) = m_g c_{p_g} dT_g/dt \qquad \text{Eqn. 29}$$

Where: absorptance of the glass-cover material (α_g), outer radius of the enveloping glass-cover (R),outer diameter of the enveloping glass-cover (D),length of the concentrator (L), tilt factor (R_b), beam radiation on a horizontal surface (I_{beam}), diffuse radiation (I_{diff}), reflectance of the concentrator (ρ_c), aperture width of the concentrator (W), surface area of the enveloping glass-cover (A_g), mass of the enveloping-glass-cover material (m_g), specific heat capacity of the enveloping-glass-cover material (Cp_g), surface area of the absorber-tube (A_t), Stefan-Boltzmann's constant of radiation (σ), temperature of the absorber-tube (T_t), temperature of the enveloping glass-cover (T_g),emittance of the enveloping glass-cover material (ε_g),emittance of the coating material on the absorber-tube (ε_t), sky temperature (T_{sky}), ambient temperature (T_{surr}) and convective heat transfer coefficient (*h*), temperature gradient of the enveloping-glass-cover (dT_g/dt) as shown in figure 9

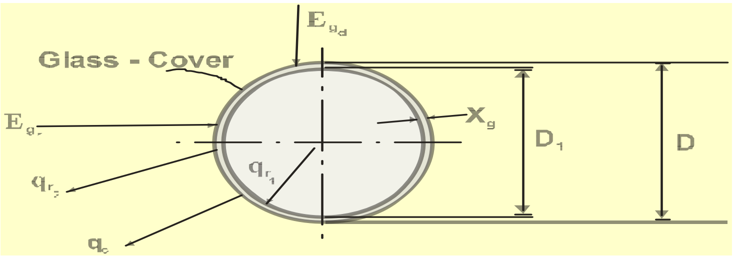

Fig. 9: The enveloping glass-cover showing heat Gain and heat Loss

For purpose of solar concentrator design, it is often necessary to convert the beam radiation data on a horizontal surface to radiation on a tilt surface by using a conversion ratio R_b [10]. The value of R_b depends solely on the solar topocentric angles. Consequently, the beam radiation incident on the aperture of the concentrating collector becomes $I_{beam} * R_b$.

$$R_b = \frac{\cos(\phi-\rho)\cos\delta_t \cos h_t + \sin(\phi-\rho)\sin\delta_t}{\cos\phi\cos\delta_t\cos h_t + \sin\phi\sin\delta_t} \qquad \text{Eqn. 30}$$

2.13.2 Heat Gained and Heat Lost by the Absorber-Tube

The energy balance for the absorber-tube is as shown in figure 10 and can be written as in equation 31 follows;

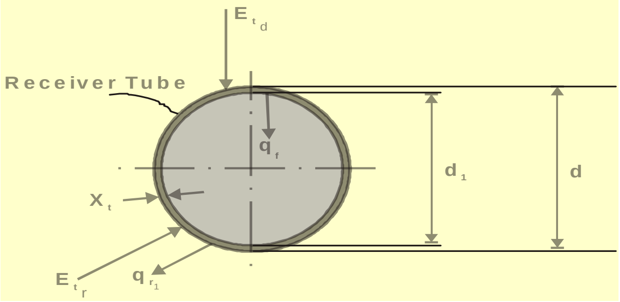

Fig. 10: Representation of heat gain and heat loss by absorber-tube.

$$\alpha_t\tau_g\left(\frac{2RL}{\pi}\right)\left[\left(I_{beam} * R_b\right) + I_{diff}\right] + \alpha_t\tau_g\rho_c\left[\frac{(W-D)L}{\pi^2}\right]\left[I_{beam} * R_b\right] - \frac{A_t\sigma\left(T_t^4 - T_g^4\right)}{\frac{1}{\varepsilon_t} + \frac{A_t}{A_g}\left[\frac{1}{\varepsilon_g} - 1\right]} - \frac{A_{in}\left(T_t - T_f\right)}{\left[\frac{1}{h_f} + \frac{A_{in}\ln\left(\frac{r}{r_i}\right)}{2\pi KL}\right]} = m_t c_{p_t} dT_t/dt$$

Eqn. 31

Where: absorptance of the absorber-tube material (α_t), transmittance of the enveloping glass-cover material (τ_g), surface area of the tube based on internal diameter of absorber-tube (A_{tin}) and temperature of the fluid (T_f), convective heat transfer coefficient of the fluid (h_f), inner radius of the absorber-tube (r_1) and outer radius of the absorber-tube (r), mass of the absorber-tube material (m_t), specific heat capacity of the enveloping-glass-cover material (Cp_t) and temperature gradient of the absorber-tube (dT_t/dt)

2.13.3. Energy Equation for the Working Fluid

The equation for the fluid temperature developed by *Egbo et al*,[10] is given as follows;

$$\frac{A_{in}\left(T_t - T_f\right)}{\left[\frac{1}{h_f} + \frac{A_{in}\ln\left(\frac{r}{r_i}\right)}{2\pi KL}\right]} - \frac{2A_c\left(T_f - T_{surr}\right)}{\frac{1}{h_c} + \frac{1}{h_f}} = m_f c_{p_f} dT_f/dt \qquad \text{Eqn. 32}$$

Where: mass of the working fluid (m_f), specific heat capacity of the working fluid (Cp_f) and temperature gradient of the working fluid, ($\frac{dT_f}{dt}$)

2.13.4. The Thermal Efficiency of the Parabolic-Trough Collector(η_{th})

The thermal efficiency of the Parabolic-trough Collector is given by;

$$\eta_{th} = 1 - \frac{Q_{losses}}{Q_{input}} \qquad \text{Eqn. 33}$$

WhereQ_{losses} is the total heat losses and Q_{input} is the total heat supplied to the receiver.

The hourly heat supplied to the receiver (Q_{input}) can be computed as follows:

$$Q_{input} = \left[\left(I_{beam} * R_b\right) + I_{diff}\right][WL] \qquad \text{Eqn. 34}$$

The total heat losses in the system (Q_{losses}) is considered as the sum of the radiative heat-loss from the surface of the enveloping glass-cover to the surroundings (q_{r_2}), the convective heat loss from the surface of the enveloping glass-cover to the surroundings (q_c) and the conductive/convective heat loss from the fluid to the surroundings (q_1). This can be expressed as follows;

$$Q_{losses} = q_{r_2} + q_c + q_1 \qquad \text{Eqn. 35}$$

III. CONCLUSION

The energy equations for computation of Solar Parabolic-trough Collector Efficiency using solar coordinates in Bauchiwere developed. The input data considered for the model equations are the Universal Time(UT), Delta T(ΔT), Date (day n, months M, and years Y), longitude γ and latitude ϕ (in radians) of Bauchi. The data also include the geometric global coordinates and local topocentric sun coordinates. The thermal efficiency $(\eta_{th})$of the Parabolic-trough collector, considered both the total energy supplied to the receiver Q_{input} and the total energy losses Q_{losses} in the system. The developed energy equations can be used to predict the efficiency of the solar PTC at any location.

REFERENCE

[1]. William, B. S. and Raymond, W. H. “Solar Energy Fundamentals and Design with Computer Applications”. John Wiley and Sons Inc. New York, pp. 38-62, 1985

[2]. John, R. H., Richard, B. B. and Gary, C. V. “Solar Thermal Energy Systems; Analysis and Design”. McGraw-Hill Book Company, New York pp. 54-78, 1982.

[3]. International Earth Rotation and Reference Centre. *Current values and longer term predictions of Delta T (2000 to 2050)*. Retrieved February 21, 2012; from: *http//asa.usno.navy.mil/seck/DeltaT.html*

[4]. Reda, I. and Andreas, A. “Solar Position Algorithm for Solar Radiation Applications”. *Elsevier, Solar Energy* 76(5), 577-589, 2004.

[5]. Grena, R. “An Algorithm for the Computation of the Solar Position”. *Elsevier, Solar Energy* Vol. 82, pp. 462-470, 2008.

[6]. Blanco-Muriel, M., Alarcon-Padilla, D. C., Loea-Moratalla, T. and Lara-Coira, M. ”Computing the Solar Vector”. *Elsevier, Solar Energy*, 70(5), pp. 431-441, 2001.

[7]. Wilkinson, B. J. “The effect of atmospheric refraction on the solar Azimuth”. *Elsevier Solar Energy*.Vol. 30, pp. 295, 1983.

[8]. Muir, L. R. “Comments on The effect of atmospheric refraction on the solar azimuth”. *Elsevier, Solar Energy,* Vol. 30, pp. 295, 1983.

[9]. Williams, B. and Geyer, M. “Power form the Sun. Retrieved March 03, 2004; from: http:/www.powerfrom the sun.net/book, 2003.

[10]. Egbo, G. I., Sambo A. S. and Asere, A. A. “Development of Energy Equations for Parabolic-trough Solar Collector” *Nigerian Journal of Engineering Research and Development.*4(1), pp. 28-36, 2005.

American Journal of Engineering Research (AJER)
e-ISSN : 2320-0847 p-ISSN : 2320-0936
Volume-3, Issue-10, pp-34-40
www.ajer.org

Research Paper Open Access

Performance Evaluation of Flat Plate Solar Collector (Model Te39) In Bauchi

Gambo Buhari Abubakar, Gerry Egbo
Department of Mechanical Engineering Abubakar Tafawa Balewa University, Bauchi

ABSTRACT: *This paper presents the thermal performance of solar flat plate water heater (Model TE 39) in Bauchi weather conditions (lat. 10.50° N, long. 10.00° E). Fluid was circulated through the imbedded copper tubes in the flat plate collector and inlet and outlet temperatures of the fluid were noted at intervals of five minutes. The experimental-time was between 11:00-13:00 hours daily for a period of 28 days. The result shows that the outlet water temperatures were dependant on the weather condition (solar radiation intensity, cloud cover) with outlet water temperature of 55℃ and 70.5% optimum efficiency of the collector obtained at 12:05pm. This shows that the use of this flat plate solar collector will be viable for domestic heating application under Bauchi prevailing weather condition.*

Key words: *flat plate collector, solar intensity radiation, thermal performance.*

I. INTRODUCTION

Energy is the rate at which work is done and is an essential ingredient of socio-economic development and economic growth [1]. Energy is an essential input to all aspects of modern age and is indeed, the livewire of industrial and agricultural production, the fuel for transportation as well as for the generation of electricity in conventional thermal power plant. The nature and extent of energy demand and utilization in a national economy are, to a large extent, indicative of its level of economic development. For rapid and secured economic advancement in a productive economy, the country must pay maximum attention to the development and utilization of its energy resources and to the security of supply of its energy needs [2].

Presently, the world heavily relies on fossil fuels of oil, gas and coal to meet its energy requirements providing about 80% of the total global energy demand while renewable energies of solar, hydro, biomass and geothermal; and nuclear powers are contributing only 13.5% and 6.5% respectively [3].

The uses of renewable energy sources present an alternative use to fossil fuels. They are inexhaustible, freely available and environmentally friendly. A considerable proportion of the energy need of man could be met by the utilization of solar energy as an alternative energy source of heating water using the flat plate solar collector for domestic application.

Solar collectors capture incident solar radiation energy and convert it to heat. Solar collectors are basically classified into two general categories: Non-concentrating solar collectors and Concentrating solar collectors. In the non-concentrating solar type, the collector aperture area (i.e. the area that intercepts the solar radiation) is the same as the absorber area (i.e. the area absorbing the radiation). For temperatures below 100^{o}C, flat-plate collectors of the non-concentrating type are generally used [7]. In the concentrating collectors, the area intercepting the solar radiation is greater than the absorber area. They are basically used for temperatures greater than100℃ [7].

The flat-plate collectors are the most common used collectors for residential water and space-heating applications. A typical flat plate collector is an insulated metal box with a glass or plastic cover called the glazing and a dark-colored absorber plate. The glazing can be transparent or translucent. Translucent (transmitting light only) low-iron glass is common glazing material for flat-plate collectors because of high transmission of total available solar energy. The glazing allows the light to strike the absorber plate but reduces the amount of heat that can escape. The sides and bottom of the collector are usually insulated to minimize heat losses [9].

The flat plate water heater under investigation (i.e. Model TE 39) comprises a collecting plate which is constructed from two sheets of preformed stainless steel welded together to form integral parallel water channels. The surface of the plate in enclosed in an air tight box having a clear acrylic cover. Heat losses from the rear surface of the plate are minimized by the use of a layer insulting material. A small centrifugal pump circulates water through the absorber plate rate. The collector is supported on a base frame and is hinged so that its inclination may be adjusted [10]

The study is to evaluate the performance of the flat plate solar collector in Bauchi prevailing weather condition and assess its viability for domestic application.

II. EXPERIMENTATION

Figure 1: Experimental Set-up

The solar collector was set to angle of inclination equal to that of Bauchi and maintain throughout the experiment (i.e.10.23°). The collector was supply with water from a storage vessel connected unto it. Temperatures were measured at the water storage vessel T_1; at inlet to collector T_2; at outlet from the collector T_3 and shade temperature of the atmosphere T_4 with the aid of a mercury thermometer (0-100°C). A solarimeter was used to obtain the global solar radiation. A calibrated vessel (0-5 liters) measure the volume of water discharged (liters or centimeters) while a stop watch was used to measure the time (seconds) for volume of water discharged. The experimental time was between 11:00-13:00 p.m for period of twenty-eight days.

2.1 Determination of heat absorbed by the circulating water

Since the effective area of the collector is $14m^2$, E_1 incident energy, is equal to the radiation intensity I.

$$H = \frac{v}{t}(T_3 - T_1) \times 4186.8 \qquad \dots.(1) \qquad [10]$$

Where,

$H =$ Heat absorbed by the circulating water(W), $V =$ Volume of water discharge in liters

$t =$ Measured time for volume (s), $T_1 =$ Temperature of cold water at inlet (°C)

$T_3 =$ Temperature at outlet from the collector (°C), $4186.8 =$ constant

2.2 Determination of the losses and the efficiency of the flat plate solar collector

Under conditions of steady radiation, the steady flow energy flow equation for the apparatus is given by:

$$E_1 + E_p = H + L \qquad \dots..(2) \qquad [10]$$

The losses can therefore be calculated as:

$$L = E_1 + E_p - H \qquad \dots..(3) \qquad [10]$$

Where:

$E1 =$ Incident energy(W/m2), $Ep =$ Energy input from the circulating pump(W), $L =$ Losses (W)

And also the losses can be calculated in relationship to the shade temperature by the formula below:

$$L = const. \times [(T_2 + T_3)/2 - T_4]^{1.3} \qquad \dots..(4) \qquad [10]$$

Where: $T_2 =$ Temperature at inlet to the collector (°C), $T_4 =$ Shade temperature of the atmosphere (°C).

The losses (L) from the collector are due mainly to the process of natural convection in the surrounding air.

2.3 The overall efficiency is calculated by:

$$\eta = (H - E_p)/E_1 \qquad \ldots.(5)$$ [10]

2.4 Summary of the result obtained

The purpose of the experiment is to obtain the relationship between the rate of heat absorbed by the collector and the mean temperature of the water passing through it. The parameters considered are: mean temperature difference of water ($T_3 - T_1$), the mean shade temperature of the atmosphere, the solar radiation and corresponding heat absorbed by the collector, losses and the collector efficiency.

Table 1: Experimental Result

Time: 11:30am-12:30pm						
Time	**$T_3 - T_1$ °C**	**T_4 °C**	**E_1**	**H**	**L**	**EFFICIENCY(η)**
11:05 am	21.3	22.2	466.7	496.4	210.8	68.0
11:10 am	20.4	22.2	466.7	490.5	216.7	66.9
11:15 am	19.8	22.1	466.7	466.8	240.4	63.3
11:20 am	18.9	22.1	466.7	445.2	261.1	60.0
11:25 am	18.3	22.2	466.7	424.1	283.0	57.0
11:30 am	19.3	22.2	466.7	441.8	265.3	55.8
12:05 pm	26.5	27.9	653.2	698.0	271.4	70.5
12:10 pm	25.7	28.2	653.2	660.5	308.9	66.4
12:15 pm	24.9	28.3	653.2	613.0	355.5	61.4
12:20 pm	23.5	28.6	653.2	579.4	390.0	57.8
12:25 pm	23.4	28.6	653.2	575.9	393.5	57.1
12:30 pm	23.2	28.6	653.2	566.4	403.0	55.9

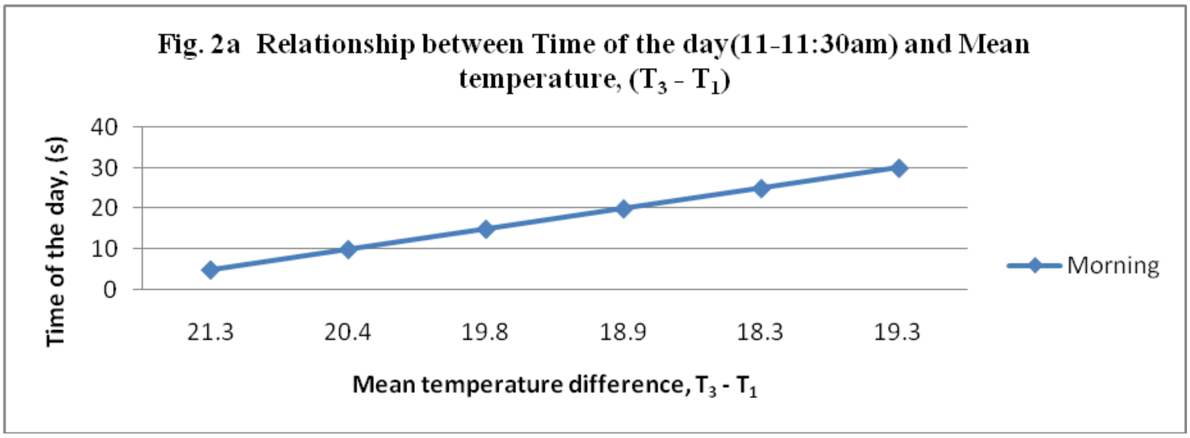

Fig. 2a Relationship between Time of the day(11-11:30am) and Mean temperature, (T_3 - T_1)

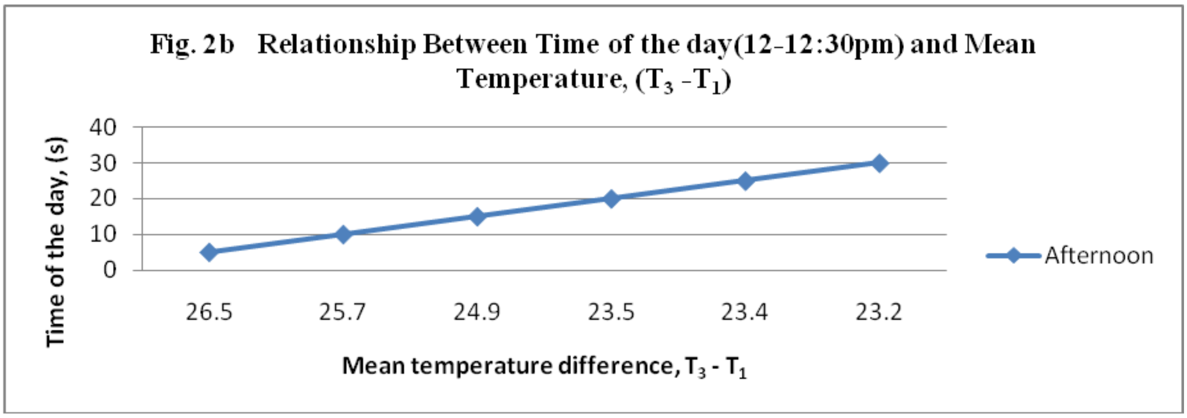

Fig. 2b Relationship Between Time of the day(12-12:30pm) and Mean Temperature, (T_3 -T_1)

Fig. 2 Relationship of Time of the day and mean temperature difference

Fig. 2a and 2b show the relationship of time of the day with mean temperature difference by the circulating fluid, the graph follows a trend of direct proportionality. The graphs show that as the time of the day increases the mean temperature difference increases vice versa.

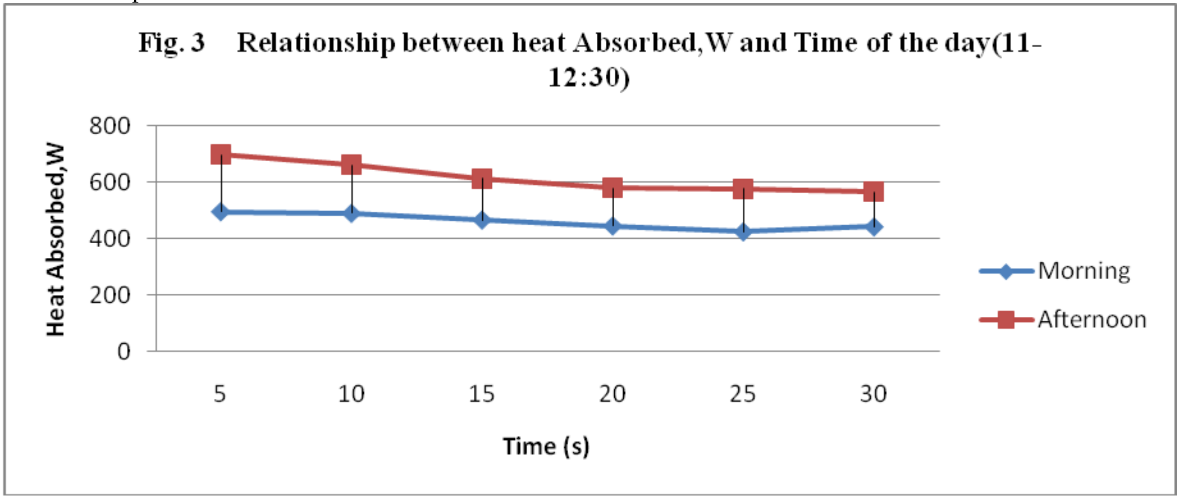

Fig. 3 Relationship of Heat absorbed and Time of the day

Fig.3 shows the relationship the relationship of Heat absorbed and time of the day. The heat absorbed by the collector was observed to be higher at the beginning of the experiment and decreases steadily as the experiment progresses with time. This is because the temperature difference between the fluids collected at the outlet of the collector and the inlet of the collector decreases. Thereby, decreasing the heat absorbed by the collector.

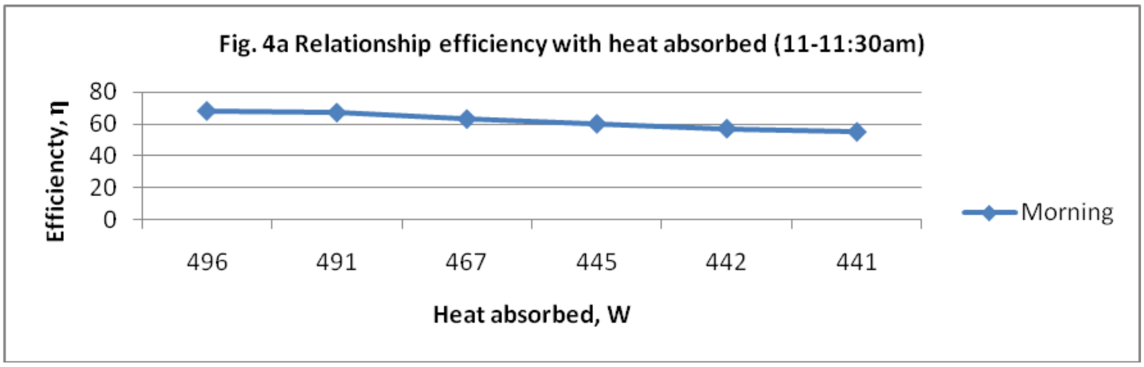

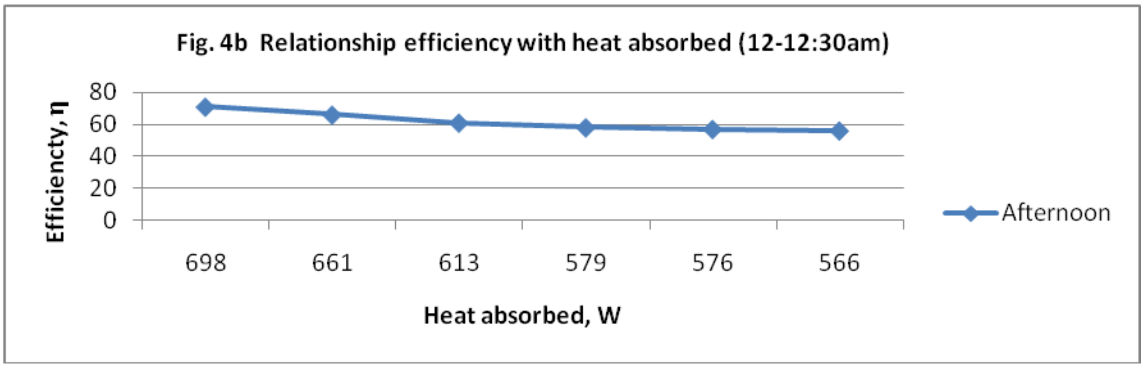

Fig.4 Relationship of efficiency with heat absorbed by circulating fluid

Fig. 4a and Fig. 4b show the relationship of efficiency with heat absorbed by the circulating fluid, the graph follows a trend of direct proportionality. For constant incident energy, the efficiency of the flat plate collector depends on the heat absorbed by the circulating water. This gives a linear graphs for both experiment (conducted in the morning and afternoon). Since the efficiency is the ratio of power output and power input. The incident energy being the power input to the collector, the heat absorbed by the circulating water is the power output from the collector. The heat absorbed by the collector depends on so many factors such as air mass factor.

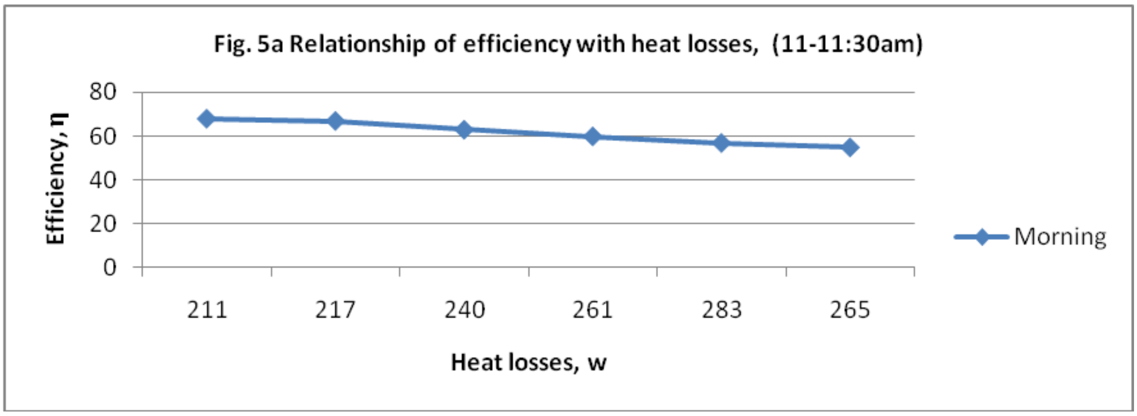

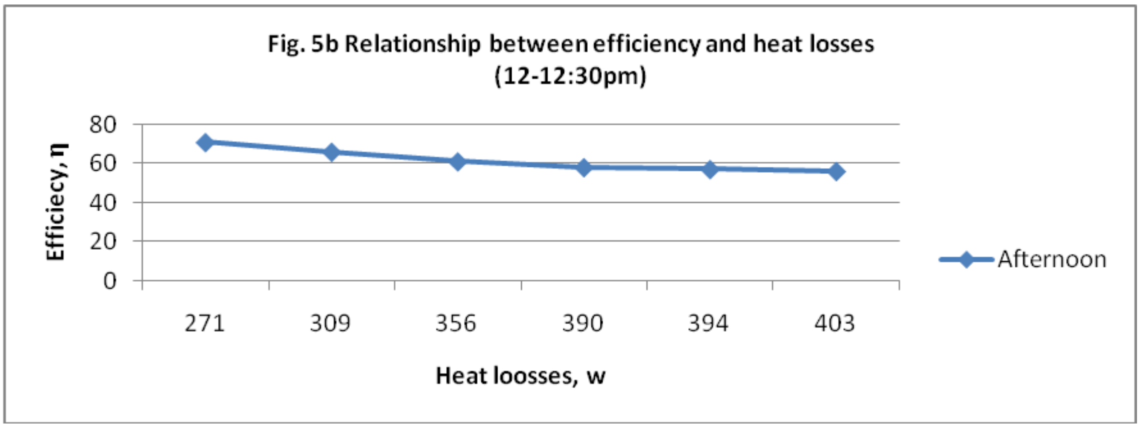

Fig.5 Relationship of efficiency with losses from the collector

Fig. 5a and Fig. 5b shows the relationship of efficiency with losses, the losses are the unused energy input from the collector, which is the long wave reflected radiation from the collector surface. The graphs show that, at higher heat loss from the collector, the efficiency is low and at lower heat loss from the collector, the efficiency of the flat plate collector is higher.

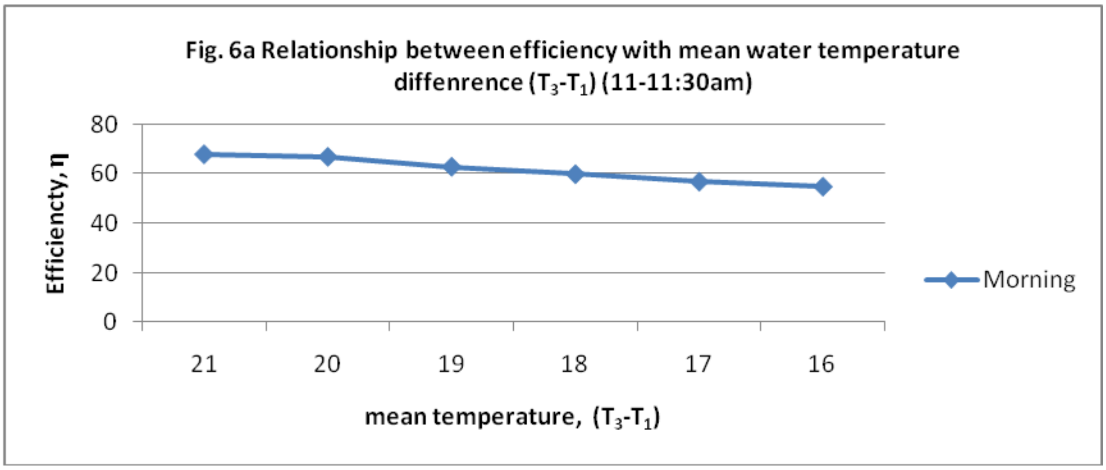

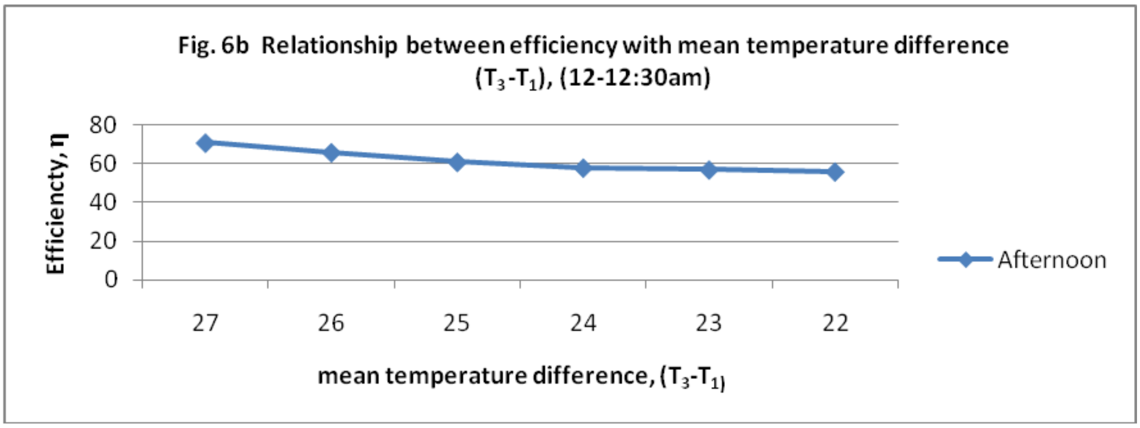

Fig. 6 Relationship of efficiency with mean water temperature difference

Fig. 6a and Fig. 6b show the relationship of efficiency with mean water temperature difference, this will take an order of direct proportionality as thus; the efficiency of the flat plate collector is directly proportional to the heat absorbed by the circulating fluid and the heat absorbed by the circulating fluid is dependent on the temperature difference of the fluid passing through the collector mean. The practical conclusion to be drawn from this is that, the higher the difference between the fluid at the outlet and the inlet the higher the efficiency of the collector.

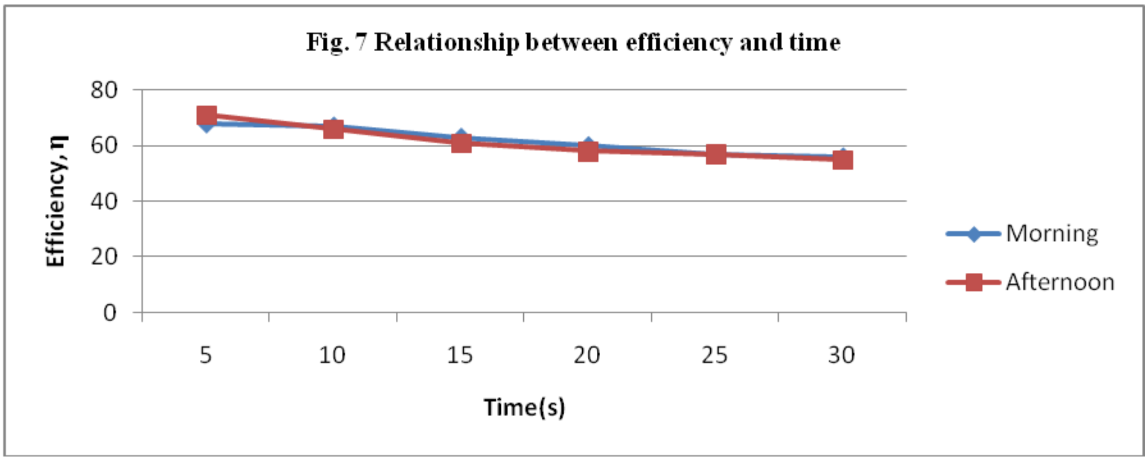

Fig. 7 Relationships between efficiency with time of the day

Fig. 7 shows the efficiency of the flat plate collector for the values obtained for the experiment conducted in the morning (11-11:30am) and afternoon (12-12:30pm). The maximum efficiency of the flat plate collector was gotten as 12:05 as 70.5% while the lowest is obtained at 55.9%. The efficiency of thecollector was observed to be higher at the beginning of the experiment and decreases steadily as the experiment progresses with time. This is because the temperature difference between the fluids collected at the outlet of the collector and the inlet of the collector decreases, thereby decreasing the heat absorbed by the collector and invariably causing a decrease in the efficiency of the flat plate collector. A comparative efficiency of the flat plate collector obtained in the morning and that of the afternoon shows that efficiency of the flat plate collector is comparatively higher in the morning compare to that obtainable in the afternoon.

III. CONCLUSION

The efficiency of the collector was observed to be higher at the beginning of the experiment and decreases steadily as the experiment progresses with time, though some variations that can be ascribed to the effect of wind speed were observed. The comparison between the efficiencies shows that efficiency of the flat plate collector is comparatively higher in the morning period as experimentally determined against that obtained in the afternoon due to the moderately higher incident energy observed in the afternoon. In conclusion, at a steady radiation, the higher the heat absorbed, the higher the efficiency of the collector. The use of the flat plate solar collector (Model TE 39) for domestic and commercial heating purposes in Bauchi is viable since reasonable temperatures (outlet from the collector, T_3) were realized.

REFERENCES

[1]. Sambo, A. S. (2005). Renewable Energy Technologies for National Development Status, Prospects and Policy Direction. Nigeria Engineers Vol.39, No 1, pp23-31.

[2]. Egbo G. I. (2005), "Performance Evaluation of Parabolic Trough Solar Collector", Nigerian Journal of Engineering Research and Development, NJERD Vol 4, No pp.45-51.

[3]. Munear T, Asift M. (2005). Energy Supply, its demand and security issues for developed and emerging economies. Renewable and Sustainable Energy Review.

[4]. Ganechari, S.M and Sandeep, K. (2005). Alternative Energy Sources. Paper presented at the National Seminar on Alternative energy sources. Thakar Polytechnic, Thakar complex, Kindavali, Mumbai, India.

[5]. Donald O., Ibrahim M, Ade A. (2007). "Annular-Gap Effect of A Parabolic Trough Collector (Model TE 38)" A Project Submitted To Mechanical/Production Engineering Programmed, ATBU Bauchi, Unpublished.

[6]. Energy Commission of Nigeria and United Nations Development Programme (2005).

[7]. National Workshop on Review of Renewable Energy Master Plan.

[8]. S. P Sukhatme, Solar Energy, Principle of thermal collection and Storage. Indian Institute of Technology, Mumbai.

[9]. Thomas, A. and Thomas, S.A. (1994) "Energy Conversion Management; Tracking Concentrating Solar Collectors and Their Components And Subsystems".

[10]. Gladstone, Samuel (2007) "Nuclear Weapons". Microsoft Student Encarta, Redmond, W.A: Microsoft Corporation.

[11]. Plinth and partners, (1984) "Manual of Flat Plate Solar Energy Collector, Model TE39" Berkshire, RG11 2QG, England.

American Journal of Engineering Research (AJER)
e-ISSN : 2320-0847 p-ISSN : 2320-0936
Volume-3, Issue-10, pp-41-47
www.ajer.org

Research Paper Open Access

Black Hole and Greyhole Attack in Wireless Mesh Network

[1]Rupinder Kaur, [2]Parminder Singh
Student, IT Deptt. CEC, Landran, Mohali,
Assit.Professor,IT Deptt, CEC, Landran, Mohali,

Abstract: *Security is an important need in wireless mesh networks to give safe and shared information between wireless non-static nodes. In wireless network nodes has ability to act correctly and route the packets. Wireless mesh networks unusual method of producing,keeping and sharing information ability of mobile objects to show spontaneous and cheap adjusting arrangement itself.There are different types of communication devices in technology by which performance is measured.There is a major issue which take part in network and provide security from various kinds of malicious attacks.There are various attacks such as black hole attack,wormhole attack,Greyhole attack, and evesdropping attack.Black hole and Greyhole attacks are network layer attacks that spoils the performance by falling the packets.The black hole and Grey hole are the problem of security that consider in wireless networks.Black hole and Greyhole attack is one type of way of interrupting attack and can cause large amount of damage to network.Black hole attack is act like ad-hoc network; which create network and attack on packets.In black hole attack where a false node not make correct paths in public to receiver node during the direction finding process. Theattacker achieves this attack when all the similar kinds of nodes communicate and make network to each other. It is very important to protectthe network layer from these attack which is also a great issues in wireless mesh network.*

Greyhole attack is very difficult to detect in wireless mesh network.In this paper,its an overview about black hole attack and grey hole in wireless mesh network and define problem statement about them. Secondly, its take study about related work in which many authors perform on these attacks and then its discuss about proposed method.Thirdly,the results are simulated carried out in OPNET simulator where black hole attack and grey hole attack shows the performance and Its analysis the throughput in network.

Keywords---Black hole attack, Grey hole attack,MRP, OLSR, RREQ, RREP,RERR,OPNET.

I. INTRODUCTION

Wireless mesh network is combination of independent nodes that shared information with each other by making a multi-hop radio network and keeping joined in a non-static manner.Network changes its topology suddenly and without reason.There is lack of system support where each node play role like router and different node connect anywhere and go away from the network at any time.Wireless mesh network is type of dynamic network structures.In different form,an object in classical wireless LAN,all nodes are dynamic and changes in topology is done suddenly in wireless mesh network,which cause difficult job to the security of wireless network.As a result,attacker joins the network and grabbed packets and leaves the network. Black hole and Greyhole attacks are the two traditional attack under wireless mesh network,which spoil the network topology and degrade the network performance. In this paper,Its analysis the behaviour of wireless network and IEEE 802.11b protocol and then Its focus on black hole attack and Grey hole attack which coming in network and then apply OLSR proactive routing protocol and analysis the effect of these attacks on network. To build the awareness of this paper which is not forgotten is well managed as follows:Part II,provide the study about related research work,which contain existing methods to solve the same problem or related problem.In Part III Its discuss about our proposed work and its advantages of OLSR protocol. In Part IV Its analysis and describe the environment which help to show our results. Alsoits discuss about the simulation parameters. A number of simulation results are provided to notice the performance of our proposed method. Lastly,Its make conclusion and future scope.

1.1 .BLACK AND GREY HOLE ATTACK

Black hole means incoming and outgoing of information is dropped ,without telling the source node that the information did not communicate with planned receiver node. Black hole attack as its name specifies that, the attacker attacks and discards the whole packets from receiver node. A black hole node done its job in the following strategies: one time RREQ(route request) and RREP(route reply) message is received by source node ,then attacker send RREP message directly and shows that it is real receiver node. The sender node having fake RREP from attacker, after that real RREP message is discarded. Under these condition, the sender node post packets to black hole in the place of receiver node. When the sender node transfers the packets through black hole, then attacker dropped them without replies as RERR (route error) message. The Grey hole present the same attitude and behaviour like black hole. The difference is that the Grey hole does not drop whole packets, it dropped some part of packets. The packets are dropped by false node which is known as attacker node. The black hole and Grey hole attack will carry a large amount of effect to the performance of wireless mesh network. In previous study, the authors bring out experiments on black hole and Grey hole by measuring its Grey magnitude. Grey magnitude means if It’s have value of seed is 50 then its probability of dropping the packets is 50%.In part IV of this paper ,Its analyse the different behaviour of nodes.

II. RELATED WORK

JiItsn et al[13] presented the adaptive approach to detect black hole and grey hole attack in ad-hoc networks.They generated a Path based detection algorithm where each node not necessary watch all nodes,but it only observe the next node in current path.In this ,they analysis the false positive probability taking constant threshold and dynamic threshold.Also ,they analysis the great impact of performance under different grey magnitude values. Patcha et al[1] proposed a proper way of prevention of black hole attack.To handle collision among nodes they introduced the watchdog method.In this algorithm,nodes are divided into three parts in network i.e.trusted,watchdog and ordinary nodes.Every watchdog node that is chosen should watch carefully its normal node neighbours and notice whether they can be behaved as trusted or malicious node. Deng et al[11] have proposed a technique for detecting a malicious nodes which is present as a chain in ad-hoc network,that malicious node is known as black hole and Grey hole node.In this,total load traffic is categorised into small set of blocks and at initial step make a backbone of strong nodes on ad-hoc network.Strong nodes mean nodes having well in terms of radio range and power computing.Remaining nodes which are not considered as strong nodes is aregular node.The disadvantage of this technique is that the strong node consider as trusted node ,and if attacker attack on that nodes;then algorithm is failed and black hole and Grey hole is generated. Geo et al[22] presented aggregate signature algorithm to trace packet dropping nodes. Theybind up into three algorithms.(1) creating proof algorithm.(2) The checkup algorithm.(3)The diagnosis algorithm. The advantage of this presented work are(1)The bandwidth overhead is low.(2) Thesecurity issues are fulfilled.(3) No need of bidirectional communication link.(4)There is broad scope for applications.

III. PROPOSED WORK

Black hole and Greyhole attack is a major problem in wireless mesh network.Our proposal is based on the analysing these attacks in 802.11b network environment and calculate is through put in both attack,that how black hole and Grey hole node effect the throughput.Its implement it by taking nodes as vector; i.e. one node is link with two nodes in x-axis and y-axis, and further make links as vector quantity. In this each node is connected to next nodes and packets broadcast it.Thereis all mobile nodes,which is not fixed in position and all nodes are connected with one IP called backbone.Firstly, it’s make scenario of wireless nodes and deploys random way point on each node and then change wireless LAN parameters. It’s give each node as unique basic service station number and also set channel for these service station and then transfer the packets and generate graph of network without attacks. Secondly,after that Its change one node as false node and generate black hole then transfer the packets and generate graph.by this false node our packets shows source value but receiver node value is zero,that means whole packets are dropped and at receiver node information is not retrived.Ater this, Its make that false node as Grey hole node,configure it by taking variable seeds and generate graph of that scenario.Finally Its configure this scenario by taking OLSR(optimized link state routing protocol) protocol in each statics then compare the performance.OLSR is also stored all the information in tables.It updates the topology of network which is changed in wireless mesh network.In network layer OLSR protocol accumulated throughput is calculated.

These all works has some advantages which are as follows:

1. In this, each node is connected to two nodes and all the information is stored in tables.
2. Its require no encryption on topology control, so information sharing is easy.
3. There is not necessary to watch all nodes, one node record link of just two nodes by which it link.

IV. SIMULATION ENVIRONMENT

The prevention is implementing in OPNET simulator and performance is analyzed in term of network throughput and load. Simulation of black hole and Greyhole attack on the OPNET is achieved by having a false node. This node is detected through secure path scheme having OLSR protocol in order to stop the behavior of false node. In following scenario which is set of 30 mobile nodes. These mobile nodes are moving with constant speed of 10 m/s and simulation time taken as 1000 seconds. Area of simulation is taken as 1500*1500 metersand mobility model is random way point with speed 10 m/s and transmitting power is by default 0.005 watts. The random environment is chosen in wireless mesh network and other specification of simulation isas follows:

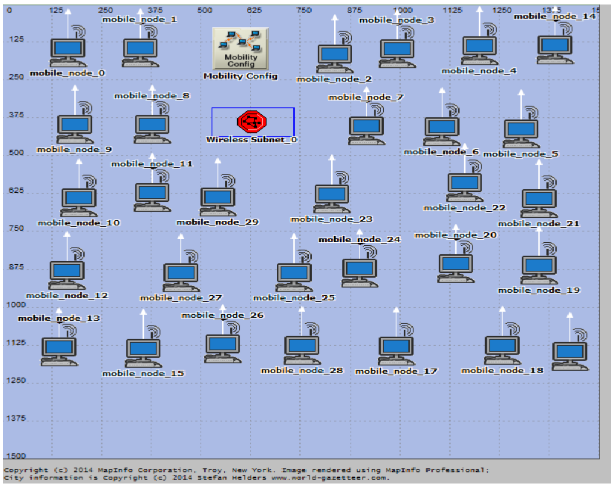

Fig 1. Scenario of 30 nodes

Fig 1, shows the scenario in which wireless subnet having address 255.255.192.2 by which 30 nodes are connected and communicate.The host address of node is starting from 192.168.5.0/26,192.168.5.130,192.168.5.64 and end at 192.168.5.65 .These nodes communicate with the help of broadcast ip address ,i.e192.168.5.63 .Our main goal is to check which attack is more dangerous effect on network performance .The last but not least stage and very vital of the time is given to this stage.

V. SIMULATION RESULTS

In random simulation environment, the first step is to determine the throughput and network load on network performance.Results are analysed carefully by obtaining from OPNET simulation.Its simulate anetwork of 30 mobile nodes.In OPNET there is set of two types of statics i.e. global and node.Initial take a uniform scenario with no black hole and grey hole attacks. There is no prevention is applied, then attacks will occurs. The false node is choose randomly in simulation test, and decreases the throughput and increases the network load on network. The simulation results are presented in fig 2. And fig 3; which shows the network performance without attacks and with both attacks,i.e. black hole and Grey hole attack as follows:

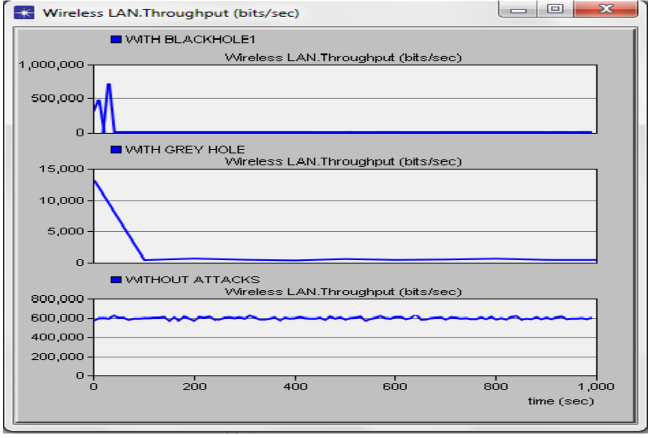

Fig 2: Network Throughput in wireless LAN

Firstly, in without attack graph itstransmits the packets in the form of bits from source to receiver node. After this Its generated one false node in network ,that false node is black hole or Grey hole node then performance of network is vary which shows as follows:

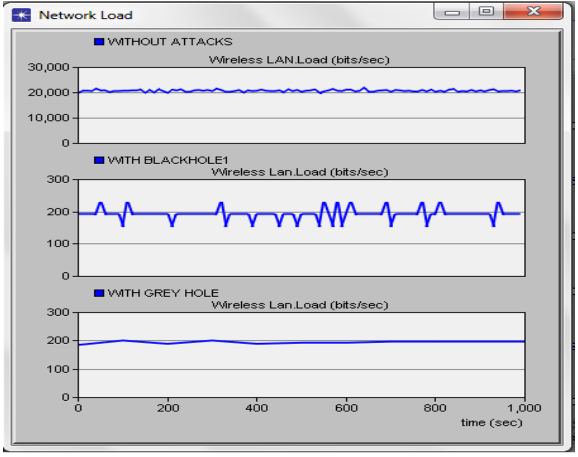

Fig 3: Network Load in wireless LAN

Based on these above results, Secure path prevention technique is generated and analysis the network performance.After implementingthe secure path scheme and prevent the network from attack and shows the drastic changes in the performance of throughput and network load. First its detect the node from route table that stored inOLSR table as shortest path. Its take that value from the table which does not show the route between source to receiver node which means attack will occur. Ifit'sfinding that kind of value, thenits drop that route and prevent network from attacks. The effect on throughput with attacks and after prevention is calculated as follows:

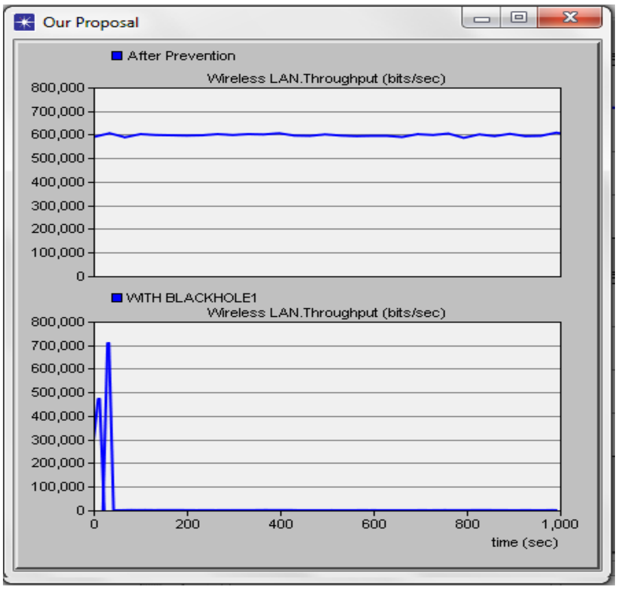

Fig 4: Network Throughput in black hole attack

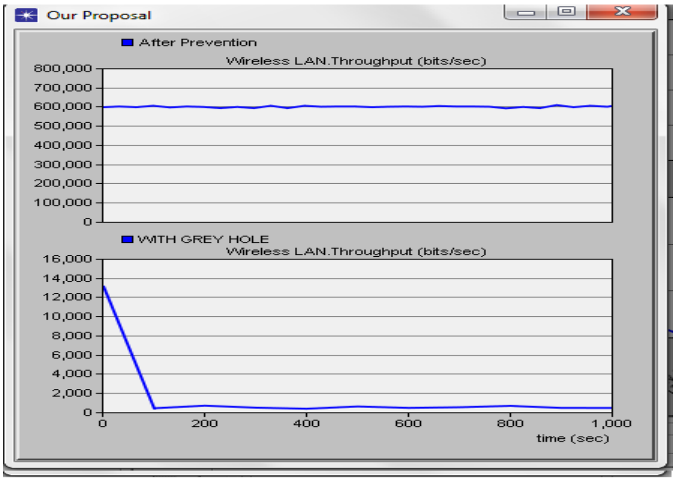

Fig 5: Network Throughput inGreyhole attack

This technique is provides good performance for detecting attacks and work without any modification of protocol and without special environment assumptions. When the nodes found no route to receiver node in table, that means attacks occurs and with the help of prevention technique it drop that route and improves the network performance. Black hole and grey hole attack is a routing layer attacks in which data is revolves from other node. The transmission of packets on multiple nodes and dropping of packets is mostly occurring on routing layer. Routing protocol is targeted by the attack. Greyhole attack having great influencing attack on Wireless mesh network.By this it also find variation in network load which show as following graphs.

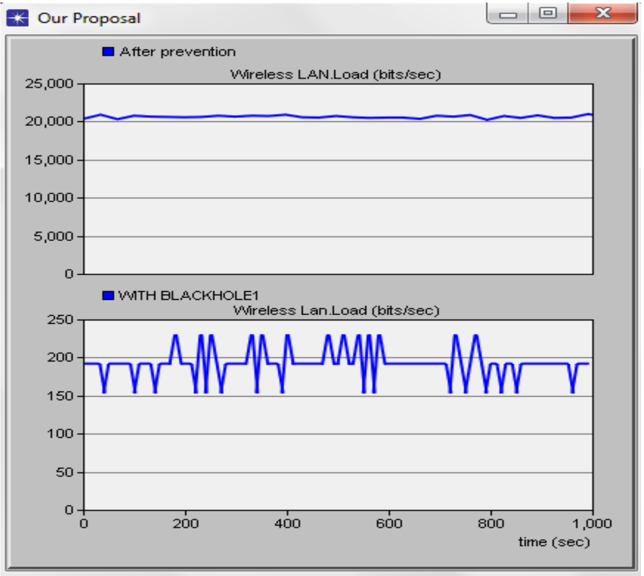

Fig 6:Network Load in black hole attack

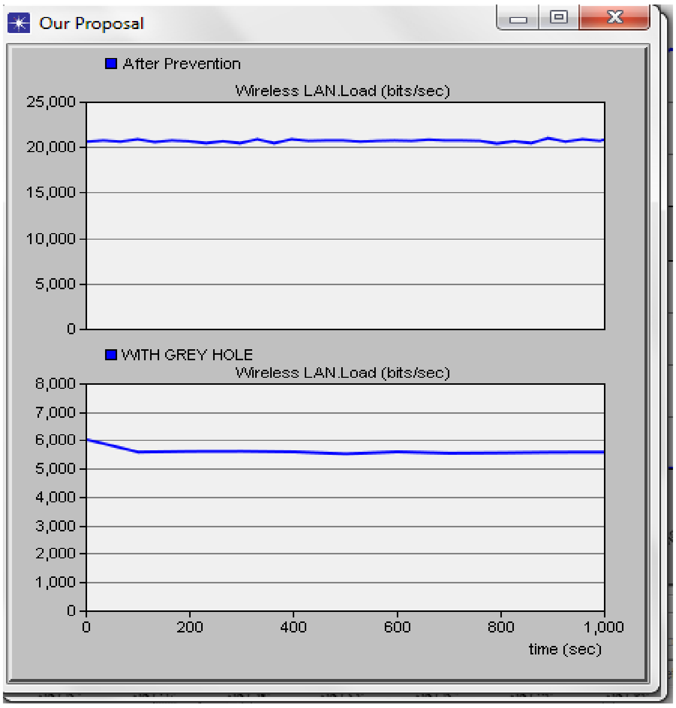

Fig 7: Network Load inGreyhole attack

VI. CONCLUSION

Security is the important feature in wireless mesh network.In this paper,the black hole and grey hole attack is come on network layer.due to movable nature,wireless mesh network have many Itsakness.Our aim is to prevent the network layer from these attack in which false node act as regular node.That node is difficult to detect, because the nodes here in this type of attack are very much unpredictable and volatile as they varies from normal to adversary and adversary to normal nodes.In this paper,Its apply OLSR protocol and find out that it stops some effect of these attacks,but Its cannot safe network from these attacks purely.Its also find that black hole attack is easy to detect than Grey hole attack.At performance level,there is not much difference in both attacks.

VII. FUTURE SCOPE

Network layer is full of attacks.If secure network layer then its safe many information from attackers.To study the related researches,its find how attack occur in network layer.Our main goal is to detect and present black hole attack and Greyhole attack and cause security better so that performance of network is not degrade.

REFERENCES

[1] A.Patcha, A.Mishra, ”Collaborative Security architecture of black hole attack prevention in mobile ad hoc networks[C]”,Radio and Wireless Conference,2003,pp.75-78

[2] B. Sun, Y. Guan, ,J. Chen ,U.W Pooch, ”Detecting Black hole attack In Mobile Ad-hoc Netwoks[C]”.5th EuropeenPersonel Mobile Communications Conference,2003,pp. 490-495.

[3] C. Karlof, D.Wagner, “Secure routing in wireless sensor networks: Attacks and countermeasures, Special Issue on Sensor Network Applications and Protocols”, vol 1 (2-3), 2003,pp.1293 –1303

[4] Dr. A. A. Gurjar, Professor, Department Of Electronics & Telecommunication, Sipna’s C.O.E.T, Amravat and A. A. Dande, Second Year (M.E.), Computer Engineering, Sipna’s C.O.E.T, Amravat “ Black Hole Attack in Manet’s: A Review Study” International Journal of IT, Engineering and Applied Sciences Research (IJIEASR) ISSN: 2319-4413 Volume 2, No. 3, March 2013,pp. 12-14.

[5] D.Djen, L. Khelladi, and A.N. Badache, “A survey of of Security issues in Mobile Ad Hoc Network,” Communication Surveys & Tutorials , IEEE,vol. 7 no. 4, ,pp. 2-28,2005.

[6] D.Boneh,C.Gentry,B.Lynn,H.Shachem,”Aggregate and Verifiably Encrypted Signature from Bilineer Maps ”,Advances in Cryptology-EUROCRYPT’03,LNCS 2656,Berlin,Spinger-Veralg,2003,pp.416-432.

[7] Elizabeth M. Royer, and Chai-KeongToh, “A Review of Current Routing Protocols for Ad Hoc Mobile Wireless Networks,” IEEE Personal Communications, April 1999, pp. 46-55.

[8] F.Stanjano, R.Anderson, “The Resurrecting Duckling: Security Issues for Ubiquitous Computing,” Vol. 35, Apr, 2002, pp. 22-26.

[9] HesiriItserasinghe and HuirongFu,”Preventing Cooperative Black Hole Attacks in Mobile Ad Hoc Networks”, International Journal of Software Engineering and Its Applications,Vol. 2, No. 3, July, 2008,pp.39-54.

[10] H. Deng, W. Li, and D. P. Agrawal.“Routing Security in Adhoc Networks.” In: *IEEE* Communications Magazine, Vol. 40, No. 10, Oct. 2002,pp. 70-75.

[11] Hongmei Deng, Itsi Li, and Dharma P. Agrawal, “Routing Security in Wireless Ad Hoc Network,” IEEE Communications Magzine, vol. 40, no. 10, October 2002,pp70-75.

[12] J. Cai, P. Yi, J. Chen, Z. Wang, N. Liu, An adaptive approach to detecting black and Grey hole attacks in ad hoc network, in: 4th IEEE International Conference on Advanced Information networking and Applications, IEEE Computer Society, 2010, pp.775–780.

[13] JiItsn CAI,Ping YI,JialinCHEN,Zhiyang WANG,Ning LIU,”An adaptive approach to detecting black and Grey hole attacks in Adhoc networks”,24th IEEE International Conference on Advanced Information networking and application,2010,pp.775-891.

[14] LathaTamilselvan,VSankaranarayanan,”Prevention Of Blackhole Attack in MANET”,In proceeding of 3nd International Conference on Wireless Broadband and Ultra Wideband Communication, Aug 2007,pp.21-21

[15] 15] M. A. Shurman, S. M. Yoo, and S. Park, “Black hole attackin wireless ad hoc networks,” in ACM 42nd Southeast Conference (ACMSE’04), Apr. 2004, pp. 96-97.

[16] N. H. Mistry, D. C. Jinwala and M. A. Zaveri,“MOSAODV: Solution to Secure AODV against Black hole Attack“, (IJCNS) International Journal of Computer and Network Security, Vol. 1, No. 3, December 2009.pp.42-45.

[17] O. Kachirski and R. Guha, “Effective intrusion detection using multiple sensors in wireless ad hoc networks”, In Proceedings of the 36th Hawaii International Conference on System Sciences,2003, pp. 57-61.

[18] R.Agrawal, R. Tripathi, S. Tiwari, “Performance evaluation and comparison of aodv and dsr under adversarial environment”, International Conference on Computational Intelligence and Communication Networks, IEEE Computer Society, 2011, pp.596–600.

[19] R.H.Jhaveri, S.J.Patel, D. Jinwala, “A novel approach for Greyhole and blackhole attacks in mobile ad hoc networks”, Second International Conference on Advanced Computing and Communication Technologies, IEEE Computer Society, 2012, pp. 556–560.

[20] Satoshi Kurosawa, Hidehisa Nakayama, Nei Kato, Abbas Jamalipour, and Yoshiaki Nemoto. “Detecting Blackhole Attack on AODV based Mobile Ad hoc networks by Dynamic Learning Method”. International Journal of Network Security, Vol.5, No.3,Nov 2007, pp.338–346.

[21] W. Heinzelman, A. Chandrakasan, H. Balakrishnan, “Energy efficient communication protocol for wireless microsensornetworks”,IEEE Transactions on Wireless Communications ,vol 1 (4) ,2002,pp. 660–670.

[22] X.P.Geo,W.Chen,”A Novel Grey hole Attack Detection Scheme for Mobile Adhoc Networks[C]”,IFIP International Conference On Network and Parallel Computin Workshop,2007,pp. 209-214.

[23] Xiaoyan Hong, KaixinXu, and Mario Gerla, “Scalable Routing Protocols for Mobile Ad hoc Networks,” IEEE Network,Vol.16(4),July/August2002,pp.11-21.

[24] Y. A. Huang and W. Lee, “Attack analysis and detection for ad hoc routing protocols,” in The 7th International Symposium on Recent Advances in Intrusion Detection (RAID’04), pp. 125-145, French Riviera, Sept. 2004.

[25] Y. Zou, K. Chakrabarty, “Sensor deployment and target localization based on virtual forces”, TItsnty- Second Annual Joint Conference of the IEEE Computer and Communications Societies, Vol. 2, IEEE Computer Society, 2003, pp. 1293–1303.

[26] Y. Law, P. J. Havinga, “how to secure sensor network”, International Conference on Sensor Networks and Information Processing, IEEE Computer Society, 2010, pp. 89–95.

[27] Y.-C. Hu, D.B. Johnson, and A. Perrig, “SEAD: Secure Efficient Distance Vector Routing for Mobile Wireless Adhoc Networks,” Proc.4th IEEE Workshop on Mobile Computing Systems and Applications, Callicoon, NY, June 2002, pp. 3-13.

American Journal of Engineering Research (AJER)
e-ISSN : 2320-0847 p-ISSN : 2320-0936
Volume-3, Issue-10, pp-48-54
www.ajer.org

Research Paper Open Access

Model Development and Simulation of Nitrification in SHARON Reactor in Moderate Temperature by Simulink

Dr. Adnan Abbas Al-Samawi[1] and Mohammed Siwan Shamkhi[2]
[1]*(Prof. Emeritus of Environmental Engineering, University of Technology, Iraq)*
[2]*(Civil Engineeringdept., Wasit University, Iraq)*

ABSTRACT : *In order to reduce the nitrogen compounds in WWTP effluent according to legislations, nitrogen of reject water is removed in separate unit by applying innovative cost effective process named SHARON (Single reactor High activity Ammonium Removal Over Nitrite) process which is feasible to apply in moderate weather and more cost effective process due to elimination the heat exchanger required to keep the reject water of high temperature. In addition to the save in oxygen requirement to oxide ammonium by preventing nitrite oxidation and the saving in external COD addition for denitrification. Also, there is no need for large reactor volume because HRT equal to SRT. Significant mathematical model of nitrification process in SHARON reactor was developed based on substances and organisms mass balance as well as organisms kinetics. A relatively favorable consistency was obtained between the experimental and the predicted results of model. A high correlation of (R^2=0.946) between model predictions and experimental data sets.*

KEYWORDS : *SHARON, nitrification, model, moderate temperature.*

I. INTRODUCTION

The presence of nitrogen compounds is a significant problem in wastewater treatment process. It is difficult to obtain and maintain sufficient nitrifiers in wastewater treatment plants with short sludge retention time (SRT) [12]. Because the nitrifiers growth is slow due to effects of environment change in biological reactor such as toxic shock and pH [3]. For nitrification design in conventional activated sludge processes safety factor is used to get long SRT to increases the concentration of mixed liquor suspended solids (MLSS) which requires large and clarifiers tanks and other sludge conditioning units to accommodate the accumulation of solids [11]. High nitrogen wastewater is typically generated in reject water (side stream wastewater) such as anaerobic sludge digestion and drying bed filtrates. During sludge treating before final disposal to reduce the volume of sludge by removal of water, which constitutes 97-98% of sludge and to reduce the volatile content to eliminate the harm and threat to human health, the nitrogen is fraction in the organic matter is converted to soluble ammonia. The reject water from dewatering of hydrolyzed sludge has high ammonium content, typically 500-1500 *mg/l* and it is 20-30 times stronger than that of influent [14]. Reject water recycling to the main stream of wastewater treatment plant increase the total nitrogen load with 15-20% [6,13], but because the flows are relatively low, they are about 1% of the main line, cost effective nitrogen removal in small reactors can be achieved [9]. Among the possible treatment options are SHARON process(Single reactor system for High activity Ammonium Removal Over Nitrite). The aim of a mathematical model during simulation is to describe the performance of SHARON process. Thus, a model can contribute for better understanding of process operation and kinetics. There were two types of models were combined to described the process; 1) mass balance model that described mass transport in SHARON reactor; 2) and kinetic model which described the growth rate of ammonium oxidizing organism and nitrite oxidizing organism depend on the reactor conditions. The equations described mass balance in well mixed bioreactor for unsteady state was ordinary differential equations. The growth of ammonium oxidizer organism and nitrite oxidizer organism was associated with dissolved oxygen consumption , pH variation and temperature variation.

II. NITRIFICATION MODEL

The proposed mathematical model focuses on the prediction of the substrates removal and microorganism growth in the system. The model had to be able to predict the change of DO and pH. The main process parameters include oxygen concentration, temperature and HRT The model considers two substrates, ammonium and nitrite, and two groups of microorganisms, ammonium oxidizers and nitrite oxidizers were taking into account. The SHARON reactor is continuous stirred tank reactor (CSTR) and consists liquid and gas phases were made to facilitate the numerical solution of the model. In addition, quantitative and qualitative uniform istribution of organisms and substrates in the reactor was considered and interphase transport of oxygen is considered. The model assumed that the feed stream does not contain any ammonium oxidizer or nitrite oxidizer organisms.The ammonium consider available with high concentration which sufficient for growth process.

III. MATERIAL BALANCES

Based on equations (1-6), the equilibrium reactions considered as follows:
The stoichiometric reaction for oxidation of ammounium to nitrite:

$$NH_4^+ + 1.5O_2 \rightarrow 2H^+ + H_2O + NO_2^- \qquad \text{..... (1)}$$

The stoichiometric reaction for oxidation of nitrite to nitrate:

$$NO_2^- + 0.5O_2 \rightarrow NO_3^- \qquad \text{..... (2)}$$

All the reactions take place in aquatic system in which the carbonic acid bicarbonate equilibrium take place according the following :

$$H_2O + CO_2 \longleftrightarrow H_2CO_3 \longleftrightarrow H^+ + HCO_3^{-+} \qquad \text{..... (3)}$$

Representing the bacterial composition as ($C_5H_7NO_2$) and by combining equation (1) and (2) with equation (3)yield the following equations:

$$NH_4^+ + 1.5O_2 + \ 2HCO_3^- \rightarrow NO_2^- + 2H_2CO_3 + H_2O + 58{\sim}84\ Kcal \qquad \text{..... (4)}$$

$$13NH_4^+ + \ 23\ HCO_3^- \rightarrow 8\ H_2CO_3 + 10\ NO_2^- + 3\ C_5H_7NO_2 + 19\ H_2O \qquad \text{.....(5)}$$

$$NH_4^+ + \ 10\ NO_2^- + 4\ H_2CO_3 + \ HCO_3^- \rightarrow 10\ NO_3^- + 3\ H_2O + 3\ C_5H_7NO_2 \qquad \text{.....(6)}$$

The dynamic model, which consists of four differential equations, is based on substrate and organism mass balances around the reactor. For continuous flow, continuous stirred tank reactor (CSTR) the general equation for the substrate material balance may be expressed as below:

$$Accumulation\ = In - Out\ + Generation \qquad \text{.....(7)}$$

The same expression can be applied for organism material balance. In the differential equations, all the terms associated with ammonium, nitrite and nitrate concentrations are expressed as *mg/l* of N.
The mass balance of ammonium nitrogen is:

$$\frac{ds_1^{NH3}}{dt} = \frac{Q}{\forall}(S_0^{NH3} - S_1^{NH3}) - \mu^{am}\frac{x_1^{am}}{y^{am}} \qquad \text{.....(8)}$$

The mass balance of nitrate nitrogen can be written as:

$$\frac{ds_1^{NO2}}{dt} = \frac{Q}{\forall}(S_0^{NO2} - S_1^{NO2}) - \mu^{nit}\frac{\mu_1^{nit}}{y^{nit}} \qquad \text{.....(9)}$$

The oxygen transfer from gas phase to liquid follow the two films theory for gas transfer, which assume the gas – liquid interface include gas film and liquid film through which the gas is transfer by molecular diffusion. The diffusion in the liquid phase is usually the control for overall rate of mass transfer because of much lower diffusivity in this phase. Also, the gas film thickness is much smaller than liquid film thickness because mobility of molecular in gas phase is much greater than liquid phase. The net transfer from the gas phase to the liquid phase is given by:

$$\frac{ds_{O2}^{liquid}}{dt} = ka\left(S_{O2}^{sat} - S_{O2}^{liquid}\right) \qquad . \qquad \text{....(10)}$$

Henry’s law which states “the weight of gas that can be dissolved in given volume of liquid is directly proportional to the pressure that the gas exerts above the liquid” assumed to apply at the interface to calculate the saturation concentration of oxygen in wastewater as below [5]:

$$S_{O2}^{sat} = K_H P_{O2} \qquad \text{.....(11)}$$

The saturation concentration of oxygen in wastewater will be different from that of fresh water as:

$$S_{wO2}^{sat} = \beta S_{O2}^{sat} \quad .....(12)$$

Whereβ =0.8. The mass transfer coefficient of oxygen expressed in (d^{-1}), is related to superficial gas velocity which expressed in (*m/s*). for air water bubble columns with coarse bubble, the linear relationship can be used [16]:

$$ka = 0.6\, U_g \quad .....(13)$$

According [1], the superficial gas velocity can be taken as (*0.02m/s*). the mass transfer coefficient varies with temperature according Arrhenius equation as below:

$$ka_T = ka\ \theta^{(T-20)} \quad .....(14)$$

The common value of reported is 1.024 for mechanical and diffused aeration device [10].

Based on equations (11) to (14), equation (10) can be written as:

$$\frac{dS_{O2}^{liquid}}{dt} = 0.6\, U_g\, \theta^{(T-20)}\left(\beta S_{O2}^{sat} - S_{O2}^{liquid}\right) \quad .....(15)$$

Based on equation (1), the stoichiometric requirement of oxygen for ammonium oxidation is 3.43 mg of O_2 per mg of *NH4-N* [11]. The oxygen utilization term for the oxidation of ammonium per unit volume of reactor per unit time is:

$$O_{2_{consumed}} = 3.43\ \times oxidation\ rate\ of\ NH_4^+ asN \quad .....(16)$$

Where, $oxidation\ rate\ of\ NH_4^+ asN = \mu^{am} \frac{X_1^{am}}{Y^{am}}\ asN$ .....(17)

The oxygen balance in liquid for nitrification phase of SHARON reactor can be written as:

$$\frac{dS_{O2}^{liquid}}{dt} = 0.6\, U_g\, \theta^{(T-20)}\left(\beta S_{O2}^{sat} - S_{O2}^{liquid}\right) - 3.43\mu^{am}\frac{X_1^{am}}{Y^{am}}\ (mg/l.sec) \quad .....(18)$$

Organisms balances

The mass balances of the ammonium oxidizer and nitrite oxidizer organisms around the reactor can be expressed as:

$$\frac{dX_1^{am}}{dt} = \frac{Q}{\forall}\left(X_0^{am} - X_1^{am}\right) + \mu^{am}.X_1^{am} \quad .....(19)$$

$$\frac{dX_1^{nit}}{dt} = \frac{Q}{\forall}\left(X_0^{nit} - X_1^{nit}\right) + \mu^{nit}.X_1^{nit} \quad .....(20)$$

Since the feed stream does not contain any ammonium oxidizer or nitrite oxidizer organisms.
So, the equations (19) and (20) can be written as:

$$\frac{dX_1^{am}}{dt} = -\frac{Q}{\forall}X_1^{am} + \mu^{am}.X_1^{am} \quad .....(21)$$

$$\frac{dX_1^{nit}}{dt} = -\frac{Q}{\forall}X_1^{nit} + \mu^{nit}.X_1^{nit} \quad .....(22)$$

IV. ESTIMATION OF GROWTH RATES OF NITRIFICATION ORGANISM

All biochemical experiments carry out previously on different organism culture indicate that the kinetics are influenced by many factors such as substrate concentration, product concentration, pH, temperature, dissolved oxygen and various inhibitors. The specific growth rate is commonly expressed by multiplication of Monod type expressions of each individual term. According [15,16], the specific growth rate coefficient for mmonium oxidizer and nitrite oxidizer can be expressed as:

$$\mu^{am} = \mu^{am}_{max} \cdot \frac{S_1^{NH_3}}{K^{am}_{NH_3}+S_1^{NH_3}} \cdot \frac{S_1^{O_2}}{K^{am}_{O_2}+S_1^{O2}} \qquad \text{.....(23)}$$

$$\mu^{nit} = \mu^{nit}_{max} \cdot \frac{S_1^{NO2}}{K^{nit}_{NO2}+S_1^{NO2}} \cdot \frac{S_1^{O_2}}{K^{nit}_{O_2}+S_1^{O2}} \qquad \text{.....(24)}$$

The temperature dependency of maximum specific growth rates of ammonium oxidizer organism and nitrite oxidizer organism was taking into account using the Arrhenius equation:

$$\mu_T = \mu_{20} e^{\theta(T-T_r)} \qquad \text{.....(25)}$$

The dependence of maximum specific growth rates of ammonium oxidizer organism and nitrite oxidizer organism was modeled using the relationship of Van Hulle et al.; 2007 [16]:

$$OUR = OUR_{max} \frac{K_{pH}}{K_{pH}-1+10^{\left(pH_{opt}-pH\right)}} \qquad \text{.....(26)}$$

Where, $K_{pH} = 8.21$ and $pH_{opt} = 7.23$. Equation (26), is applied here for maximum specific growth rates of ammonium oxidizer organism and nitrite oxidizer organism instead of oxygen uptake rate (*OUR*).

$$\mu = \mu_{max} \frac{K_{pH}}{K_{pH}-1+10^{\left(pH_{opt}-pH\right)}} \qquad \text{.....(27)}$$

Based on the above considerations, the following expressions for the specific growth rate of ammonium and nitrite oxidizes organisms are proposed:

$$\mu^{am} = \mu^{am}_{max} \cdot \frac{S_1^{NH_3}}{K^{am}_{NH_3}+S_1^{NH_3}} \cdot \frac{S_1^{O_2}}{K^{am}_{O_2}+S_1^{O2}} \cdot \frac{K_{pH}}{K_{pH}-1+10^{\left(pH_{opt}-pH\right)}} \cdot e^{\theta(T-20)} \qquad \text{.....(28)}$$

$$\mu^{nit} = \mu^{nit}_{max} \cdot \frac{S_1^{NO2}}{K^{nit}_{HNO2}+S_1^{NO2}} \cdot \frac{S_1^{O_2}}{K^{nit}_{O_2}+S_1^{O2}} \cdot \frac{K_{pH}}{K_{pH}-1+10^{\left(pH_{opt}-pH\right)}} \cdot e^{\theta(T-20)} \qquad \text{.....(29)}$$

The values of parameters was used in the model were selected by literature survey and presented in Table (1) . The specific yield value used were 0.15 $mg\ NH_4^+\text{-}N/L$ for ammonia oxidizer [2].

V. RESULTS

A simulink which is graphical extension to MATLAB program version 7.11.0.584(R2010b) was applied to solve the set of equations suggested for the developed model.The implementation of SHARON process in Simulink model has been shown in Figure (1).

Model predictions : The kinetics parameters and constants related to the performance of SHARON process Table (1) were characterized and adopted to develop a theoretical relationship of variation for the substrate concentration (ammonium and nitrite). The yield coefficient as well as the dilution rate and the experimental influent concentration of ammonium were experimentally determined.

The variation of ammonium, nitrite, and nitrate are given in Figure (2). The variation of DO concentration during aerobic phase of SHARON process taking in account the saturation DO concentration for water of temperature 27.48 ℃ which represent the average temperature during operation of lab scale SHARON reactor experiment to simulate the weather condition is given in Figure (3).

Comparison of model predictions and experimental results : Comparisons between the predicated result and experimental results shown in Figure (4). In general, the model predictions significantly and successfully agree with the experimental data sets. A reasonable agreement between the predicated results and experimental results can be recognized. Overall, the model predictions successfully show a very good correlation (R^2=0.946) with the experimental data sets. The slight variations between the model predictions and experimental results may be attributed to the simplifications and assumptions made in the developed model such as (1) a uniform distribution of microbial populations in the reactor was assumed; (2) the influent ammonium is well distributed in the reactor; (3) constant reactor temperature and pH was assumed; (4) and no DO consumption by aerobic heterotrophic organism was assumed.

FIGURES AND TABLES

Table (1): the parameters as well as the constants used for the model development and imulation for nitritation of SHARON process model.

Parameter	Symbol	unit	Value	Reference
maximum specific growth rate of ammonia oxidizer	μ_{max}^{am}	d^{-1}	1.22	[7]
maximum specific growth rate of nitrite oxidizer	μ_{max}^{nit}	d^{-1}	0.02 to .17	[8]
ammonia substrate saturation for ammonia oxidizers	$K_{NH_2}^{am}$	mg/L	5.14	[4]
nitrite acid substrate saturation for nitrite oxidizers	K_{NO2}^{nit}	mg/L	0.27	[4]
oxygen substrate saturation for ammonia oxidizers	$K_{O_2}^{am}$	mg/L	0.23	[17]
oxygen substrate saturation for nitrite oxidizers	$K_{O_2}^{nit}$	mg/L	1.5	[17]
Arrhenius constant for ammonia oxidizers	θ	-	0.094	[17]
Arrhenius constant for nitrite oxidizers	θ	-	0.061	[17]

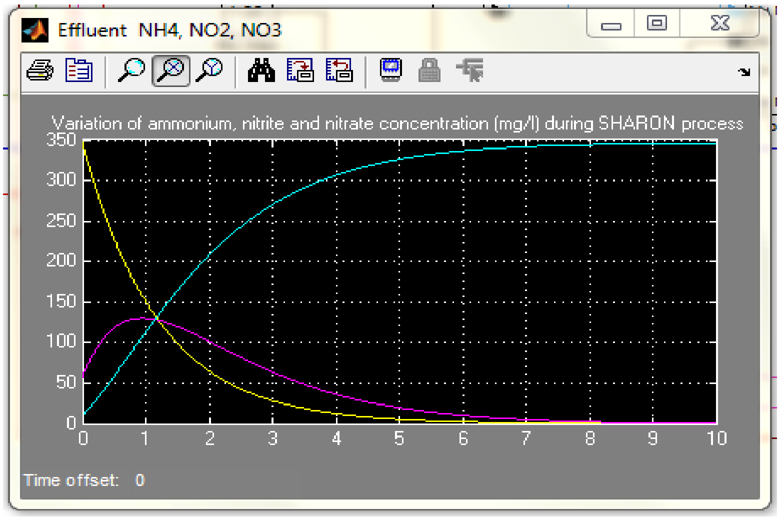

Figure (2): Simulink simulation of effluent ammonium (Yellow), nitrite (Cyan) and nitrate (Magenta) concentration during SHARON process operation

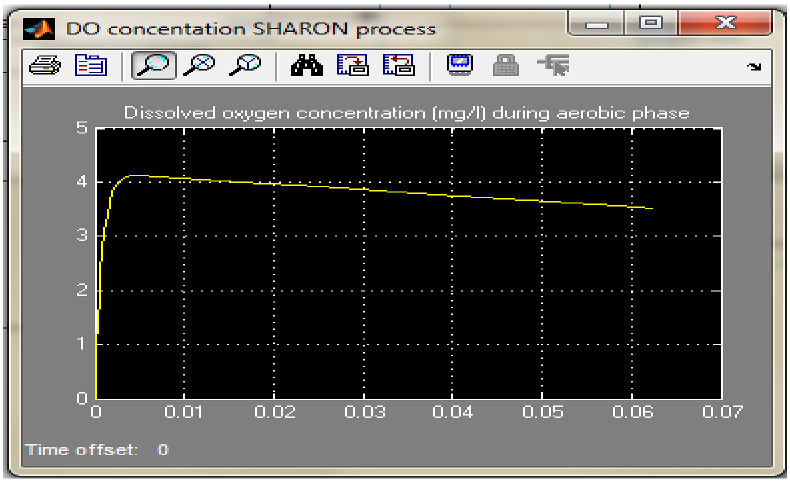

Figure (3): Simulink simulation of DO concentration for aerobic phase of SHARON process.

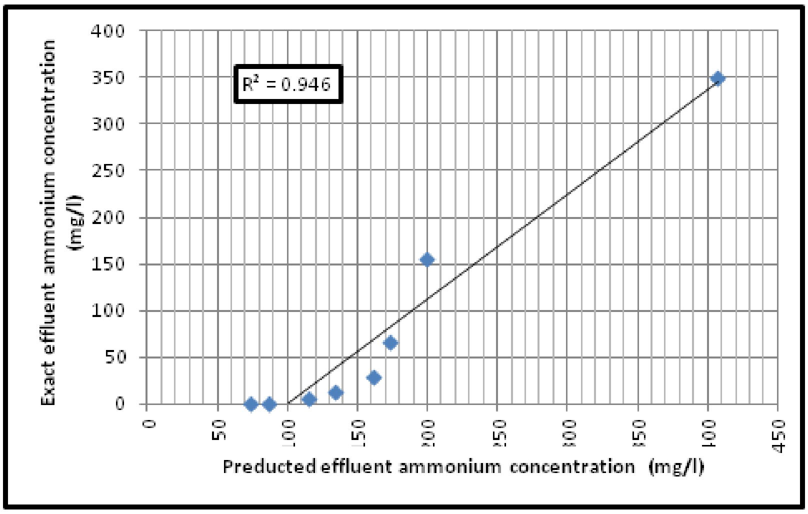

Figure (4): Correlation between exact and predicted by model of effluent ammonium concentration during SHARON process.

VI. CONCLUSION

Significant mathematical model of nitrification process in SHARON reactor was developed based on substances and organisms mass balance as well as organisms kinetics. A relatively favorable consistency was obtained between the experimental and the predicted results of model. A high correlation of (R^2=0.946) between model predictions and experimental data sets.

VII. NOMENCLATURE

S	substrate concentration (mg/L as N)	P_{O2}	partial pressure of O_2 (atm), determined by Dalton’s law.
Q	flow rate (l/sec)	U_g	superficial gas velocity (*m/s*)
$\frac{Q}{\forall}$	dilution rate (d^{-1})	T	temperature °C
$\forall$	reactor volume (*l*)	θ	Arrhenius constant
X	organism concentration (mg/l)	K	substrate saturation coefficient (mg/l)
μ^{am}	ammonium oxidizer organism specific growth rate coefficient(d^{-1})	μ_T	maximum specific rate at real temperature

Y^{am}	yield coefficient of ammonium oxidizer coefficient	μ^{am}_{max}	maximum specific growth rate of ammonium oxidizer(d^{-1})
S^{liquid}_{O2}	concentration of oxygen gas in water (*mg/l*)	μ^{nit}_{max}	maximum specific growth rate of nitrite oxidizer(d^{-1})
ka	mass transfer coefficient	μ_{20}	maximum specific rate at reference temperature =20℃
S^{sat}_{O2}	saturation concentration of oxygen gas in water (*mg/l*)	θ	Arrhenius constant
K_H	Henry's law constant (*mg/l/atm*)	T_r	reference temperature (℃)

REFERENCES

[1] Al Ezzi, A. A. R., Najmuldeen, G. F., 2013. The Effects of Superficial Gas Velocity and Liquid Phase Properties on Gas Holdup and Mass Transfer In An Airlift Reactor. *American Journal of Engineering Research (AJER)*. Volume-02, Issue 11, pp-25-32.

[2] Chen, J., Zheng, P., Yu, Y., Mahmood, Q., Tang, C.,2010. Enrichment of high activity nitrifers to enhance partial nitrification process. *Bioresource Technology*. 101, 7293–7298.

[3] Coskuner, G., Curtis, T.P., 2002. In situ characterization of nitrifiers in an activated sludge plant: detection of Nitrobacter Spp. Journal of Applied Microbiology. Vol. 93, 3, 431-437.

[4] Dinçer, A., Kargi, F., 2000. Kinetics of sequential nitrification and denitrification processes. *Enzyme and Microbial Technology*. 27, 37–42.

[5] Droste, R., 1997, Theory and practice of water and wastewater treatment, John Wiley & Sons, Inc., USA.

[6] Fux , C, Boehler, M., Huber, P., Brunner, I., Siegrist, H., 2002, Biological treatment of ammonium-rich wastewater by partial nitritation and subsequent anaerobic ammonium oxidation (anammox) in a pilot plant. *Journal of Biotechnology* .99 , 295- 306.

[7] Guven, D., Kutlu, O., Insel, G., Sozen, S., 2009, Model-based process analysis of partial nitrification efficiency under dynamic nitrogen loading. *Bioprocess Biosyst. Eng.*, 32:655–661.

[8] Hellinga, C., Schellen, A. A. J. C., Mulder, J. W., van Loosdrecht, M. C. M., Heijnen, J. J., 1998, The Sharon process: an innovative method for nitrogen removal from ammonium rich wastewater. Water Science and Technology. 37, 135-142.

[9] Kampschreur, M. J., van der Star, W. R. L., Wielders, H. A., 2008. Dynamics of nitric oxide and nitrous oxide emission during full-scale reject water treatment. *Water Research*. 42, ,812 – 826.

[10] Karia, G. L. and Christian, R. A., 2009. Wastewater Treatment Concepts and Design approach. PHI Learning Private Limited, India, pp: 365.

[11] Metcalf & Eddy, Inc., Revised by G. Tchobananoglous, F.L. Burton, 2005, Wastewater engineering: treatment, disposal and reuse. McGraw-Hill, McGraw-Hill series.

[12] Shi, X. Y., Sheng, G. P., Li, X. Y., Yu, H. Q., 2010. Operation of a sequencing batch reactor for cultivating autotrophic. *Bioresource Technology*. 101 , 2960–2964.

[13] Thorndhahl, H., 1993. Nitrogen Removal from Returned Liquors. *J.IWEM* 492 496.

[14] van Kempen, R., Mulder, J. W., Uijterlinde, C. A., Loosdrecht, M.C.M., 2001. Overview: full scale experience of the SHARON process for treatment of rejection water of digested sludge dewatering. .: 44, 1, 145–152.

[15] Van Hulle,S. W. H., Volcke, E. I. P., Teruel, J. L., Donckels,B., van Loosdrecht, M. C. M., Vanrolleghem, P. A., 2007. Influence of temperature and pH on the kinetics of the Sharon nitritation process. *Journal of Chemical Technology and Biotechnology*. 82:471–480.

[16] Volcke E.I.P. (2006). Modelling, analysis and control of partial nitritation in a SHARON reactor. *PhD thesis, Ghent University*, Belgium.

[17] Wyffels, S., Van Hulle, S. W.H., Boeckx, P., Volcke, E. I. P., Van Cleemput, O., Vanrolleghem, P. A., Verstraete, W., 2004. Modeling and Simulation of Oxygen Limited Partial Nitritation in a Membrane-AssistedBioreactor (MBR). *BIOTECHNOLOGY AND BIOENGINEERING*, 86, 5, 531-542.

American Journal of Engineering Research (AJER)
e-ISSN : 2320-0847 p-ISSN : 2320-0936
Volume-3, Issue-10, pp-55-60
www.ajer.org
Research Paper Open Access

Developing a Mathematical Model to Dampen the Effect of Chromatic Dispersion in Optic Fibre Carrying-Capacity Due To External Pressure

*[1]C.O. Ezeagwu; [2]J.Eke; [3]I.C. Oshuoha; [4]I. Ofili
[1]Department of Electrical & Computer Engineering, Nnamdi Azikiwe University, Awka, Anambra State,
[2] Department of Electrical &Electronics Engineering, Enugu State University of Science & Technology, Enugu, Enugu State,
[3]Department of Mechanical Engineering, University of Agriculture Makurdi, Benue State,
[4]Projects Development Institute (PRODA), Enugu, Enugu State

Abstract: Telecommunications requires a medium to propagate the signals from source to destination without signal impairment .The optical fibre has been rated the best medium ,but for long haulage ,wavelength multiplex (WDM) has to be installed which introduces dispersion The information carving capacity of a fibre is then limited by the phenomenon called dispersion .This introduces small change in the transmit time for signals travelling through the fibre The arrival of different wavelength at different time and the interspersing of the signal bits causes signal broadening at the destination ,resulting degradation of blurred images for data and noisy audio output, A mathematical model is developed to counter the effect of external pressure in aiding the fast spreading of these signals, known as -p compensation method.

Keywords: Telecommunication, impairment, signal broadening, long-haulage , carrying capacity

I. INTRODUCTION

Telecommunication is simply the coding and decoding of information from source to destination by electronic means. A medium is required for the transportation of this information from source to destination. The available media that can be used to carry the signals include but not limited to wired cables of copper, coaxial, optic fibre, and wireless medium waves infrared, Bluetooth, radio signals, and very small aperture terminal (V-sat) satellite. This work concentrates solely on optic fibre medium that relies on the principles of light rays for signal transmission. It consists of isolated medium which contains strands of glass fibre that carries more information over long distance than electrical signals being routed over orthodox copper cable, coaxial cable, or radio waves. Consequently, the increase in the demand for broadband backbone has led to concerted efforts on studies, analysis, planning, installation and maintenance of optic fibre network. When the optic fibre network is well articulated, planned and designed its transmission capabilities by principles of light ray propagation, is over hundreds of kilometres with large bandwidth potentials, unattended. Telecommunications service providers have to face continuously growing bandwidth demands in all networks areas, from local area (subscriber/end user terminal to long-haul to access network. Sequel to the fact that installing new communication links would require huge Investments, telecommunications carriers prefer to increase the capacity of their existing fibre links by using possible expandable method (multiplexing) which means introducing wavelength division multiplex (WDM) thereby bringing in dispersion into the system. The major problem of the wave length division multiplex (WDM) is how to avoid the interference/ distortion that normally arises from transmitting the signals belonging to different operators into one fibre as this will lead to over lapping bearing in mind that this will cause signal broadening (chromatic dispersion) in the channel.

II. MATERIALS AND METHODS

In view of developing protection against pressure for future installations and to satisfy the academic benefits of this research, a mathematical modelling was developed which will apply negative compensation to the effect of external pressure on the fibre optics cable. The model takes cognisance of the fact that wave length (λ),aligns with wave parameters, pressure aligns with force the modelling is as follows: Since the propagation

constant and phase velocity are involved in fibre transmission context, Fourier and Taylor series (Power series) will be adopted in the modelling formulations of this research. This will further help in characterizing the system. In Fibre optics, the velocity of propagation of light or the speed of signal propagation depends on the wavelength of the fibre. Optic fibre is affected by two kinds of dispersion, intermodal and intramodal dispersion, each of them leads to pulse broadening inside the fibre. This is the reason why multimode fibres are not very popular in optic fibre communication systems. Intramodal dispersion or group velocity dispersion (GVD), chromatic dispersion (CD) or fibre dispersion will usually exists in both single mode fibre and multimode fibre.
But in our model, let the two intramodal dispersion be material M_d and waveguide dispersion W_d.
M_d essentially depends on the source spectral width S_w and is less at longer wavelengths λ_1. The reason for W_d. is that propagation constant β is a function of fibre core size S_c and wave length λ. So, W_d results because the propagation constant (β) is a function of S_c and λ. Moreover the refractive indexes R_i of the core and the cladding could be different, so light propagates differently in them because, the core and cladding R_i are different so light propagates differently in each. At higher bit rates (>10Gb/s), chromatic dispersion (CD) becomes so serious that it degrades information capacity and fibre transmission distance due to pulse broadening, i.e. travel at different group velocities (v_g). Now, given that pulse broadening stems from frequency dependence of β, Using Taylor's series expansion of propagation constant, $\beta(\omega)$ around the carrier frequency, ω_c, we now obtain:

$$\beta(\omega)=\beta_0+\beta_1(\omega-\omega_c)+{}^{1}/_{2!}\,\beta_2(\omega-\omega_c)^2+{}^{1}/_{3!}\,\beta_3(\omega_c)(\omega-\omega_c)^3+ \quad \text{……….(1)}$$

From equation (1),β(ω) can be used to estimate CD for arbitrary modulation formats impaired by arbitrary amounts of CD and noise based on an analytical formula for the CD in terms of the phase of the optical signal at four frequencies. The model could be used to monitor performance in reconfigurable heterogeneous optical networks and in the design of general purpose coherent receiver systems.
If the signal is impaired only by CD, then the Fourier transform, $\hat{u}$, of the coherently-received signal, u, is given by

$$\hat{u}(\omega) = \hat{v}(\omega)\left(\textstyle\sum_{n=0}^{N-1} b_n \exp(i\omega_n T)\exp\left({}^{i\beta\omega^2}/_{2}\right)\exp(i\theta_0 + i\omega\theta_0)\right) \quad \text{.........(2)}$$

Where ω is angular frequency, $v = v(t)$ is the pulse shape at the transmitter, b_n is the *n-th* data symbol, T is the symbol period, b is the total dispersion, and t_0 and θ_0 are unknown time and phase offsets.
Just like in equation (2).applying z-transform: let *f(z)* be analytic in the domain D (dispersion) and applying z-transform, let $z = a$; be any point in D ,Then there exist precisely one power series with centre a, which represents *f(z)*, this series then is of the form

$$f(z) = \textstyle\sum_{n=0}^{\infty} b_n \ (q-a))^n \quad (3)$$

Applying binomial expansion in $f(z)$ and taken necessary factors into consideration i,e, have a non zero radius convergence R then it represents some analytical function in the disk as in [1]:
For $|z-a| < R$, let

$$f(z) = b_0 + b_1(z-a) + b_2(z-a)^2 + b_3(z-a)^3 + \cdots + b_{n+1}(z-a)^{n+1} \quad (4)$$

$$\beta(w) = \beta(w_o) + \beta_1(w_0)(w-w_0) + \frac{1}{2}\beta_2(w_0)(w-w_0)^2 + \frac{1}{6}\beta_3(w_0)(w-w_0)^3 \quad (5)$$

where $\beta_m(w_0)$ denotes the nth derivative β with respect to w evaluated at $w-w_0$, that is,

$$\beta_m = \left(\frac{\delta^m\beta}{\delta w^m}\right)_{w-w_0} \quad (6)$$

The first term causes a shift, and the product $[\beta_0(w_0) - \beta_{0y}(w_o)].z.$ (i.e., z times the difference in the x and y components of (β_0) describes the polarization evolution of the optical wave.
In the second term of equation (1), the factor $\beta_1(w_0)z$ produces a group delay $\tau_g = {}^{z}/_{V_g}$, where z is the distance travelled by the pulse and $V_g = {}^{1}/_{\beta_1}$ is the group velocity.
Using the delay equation as stated in equations (4) and (5) according to[1],

$$\frac{\tau_g}{L} = \frac{1}{V_g} = \frac{1}{c}\frac{d\beta}{dk} = -\frac{\lambda^2}{2\pi c}\frac{d\beta}{d\lambda} \quad (7)$$

where L is the distance travelled by the pulse, β is the propagation constant along the fibre axis, $k = 2\pi/\lambda$, and the *group velocity*

$$V_g = c\left(\frac{d\beta}{dk}\right)^{-1} = \left(\frac{\partial\beta}{\partial w}\right)^{-1} \quad (8)$$

Is the velocity at which the energy in a pulse travels along a fibre.
The phase velocity, V_p, of a wave in a given uniform medium is given by:

$$V_p = \frac{c}{n} = \frac{\omega}{k} \qquad (9)$$

Where c is the speed of light in a vacuum and n is the refractive index of the medium, wavelength λ, ω is the optical frequency and k is the propagation constant.

For visible light:

$$1 < n(\lambda_{red}) < n(\lambda_{yellow}) < n(\lambda_{blue}) \qquad (10)$$

or

$$\frac{dn}{d\lambda} = 0 \qquad (11)$$

The group velocity Vg is related to the phase velocity by

$$V_g = c\left(n - \lambda\frac{dn}{d\lambda}\right)^{-1} \qquad (12)$$

Phase velocity can also be represented as

$$V_p = \left(\frac{dk}{d\omega}\right)^{-1} = \frac{1}{k} \qquad (13)$$

Where k = propagation constant and ω for optical frequency. The term $\frac{dk}{d\omega}$ represents the first order coefficient. Due to the different in velocity experienced by various optical frequencies the output pulse is scattered and dispersed in the time domain. The delay experienced by the optical frequency ω over a fibre length *L* is as given by equation (13) which is equivalent to phase velocity.
Let $\Delta\omega$ be the optical bandwidth, the extent of pulse broadening $\Delta\tau$ is given in the following equation.

$$\tau = \frac{L}{V_g} \qquad (14)$$

Chromatic dispersion defined with reference to wavelength, hence the dispersion coefficient D expressed in unit ps/(nm-km) is defined as

$$D = \frac{\Delta\tau}{\Delta\omega\lambda}\frac{d\omega}{d\lambda} = k\frac{d\omega}{d\lambda} = -\frac{2\pi c}{\lambda^2}k'' \qquad (15)$$

Second order dispersion parameter

$$S = \frac{dD}{d\lambda} = \left(\frac{2\pi c}{\lambda^2}\right)^2 k'' + \left(\frac{4\pi c}{\lambda^3}\right)k'' \qquad (16)$$

Where λ is the operating wavelength, n is the refractive index, c is the free speed of light. The dispersion parameter D is known for a fibre and is 17ps/(km-nm) for a single mode fibre. The GVD parameter k is expressed in ps^2/km [3].

III. DESIGN MODEL FOR FIBRE DEPLOYMENT

Sequel to the above wave derivative the value of v_g is the group phase velocity, then the need to find the relationship between velocity and pressure (force) plays a great role to solving this problem. Ordinarily, the pressure equation *(p);* is given by Pressure (P) = force (f)/area (a) And force *(f)*= mass*(m)*×acceleration*(a)* Where *m* = mass of the earth above the fibre and a= v_g = group velocity, equation (8) becomes *F* = weight of the earth(ω)×V_g Following the above derivative where V_g is the group phase velocity, we seek to establish the relationship with velocity and force-pressure.
Basically, pressure *P= force/Area*
Where force *F* = *ma* where *m* = mass of the soil domain for the fibre.
F =*ma* =Weight of the soil $[c(\frac{d\beta}{dk})^{-1})]$ Figure 1 shows a fibre pipeline deployment layout carrying signal *x* with a density *dx* that modulates an optical source. The design of the pipeline involves the determination of the inside diameter of the pipe *D* and its wall thickness *t* for the signal flow. We shall assume that the modulated optical signal excites all modes equally at the input end of the fibre hence carrying equal amount of energy.

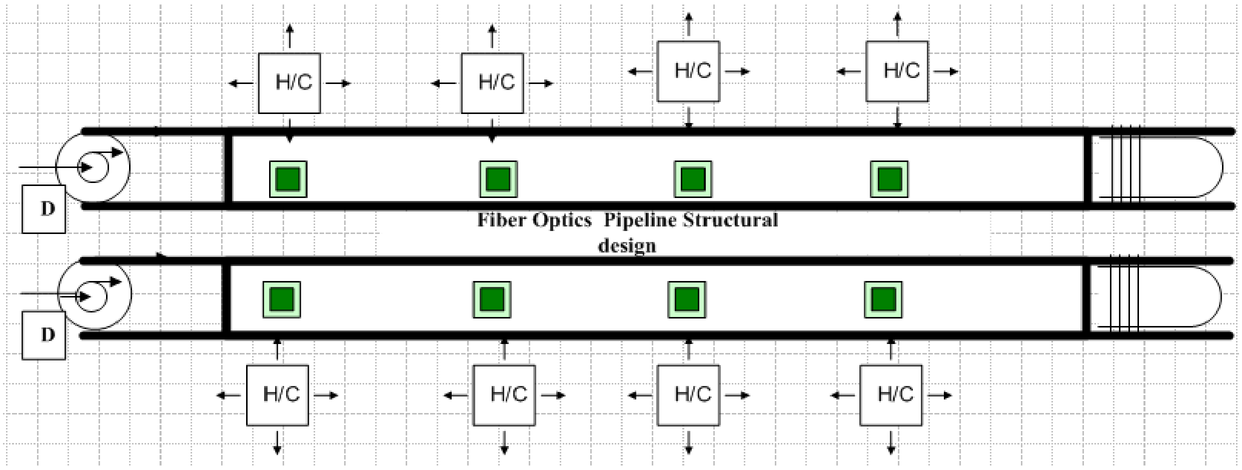

Fig. 1a Structural Pipeline Deployment and Design

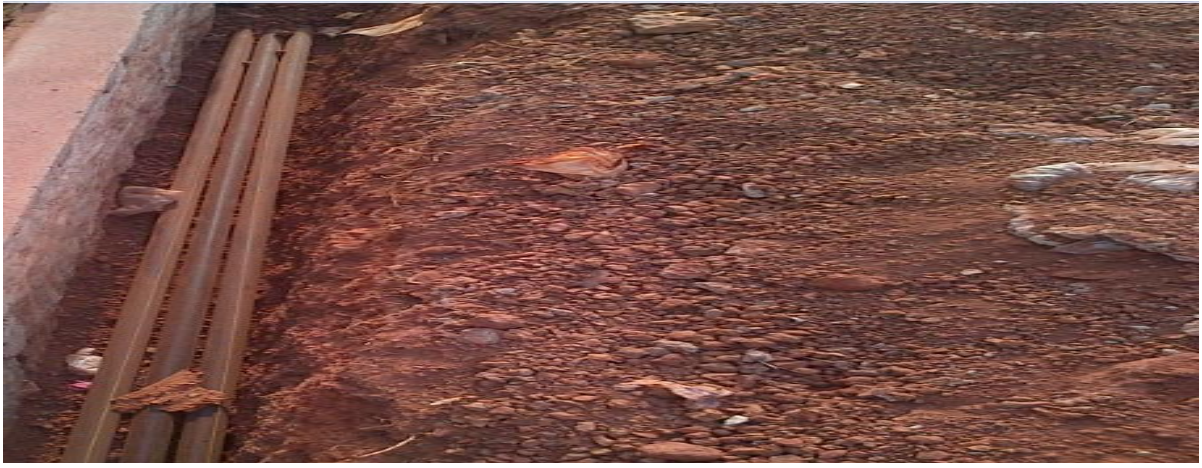

Fig. 1b Structural Pipeline Deployment and Design

On the fibre trench, the forces that are prevalent on the fibre is developed below. In the fibre, the stress on the wall cannot be equally distributed as the load varies, hence the tangential and radial forces are developed from engineering point of view.
Let the tangential stress maximum be at the inner surface and minimum at the outer surface, while the radial stress will be maximum at the inner surface and zero at the outer surface. The lames equation [2], remains significant in this context.

i. **Equation for Inside Diameter of the Fibre Pipe**: This depends on the quantity of the signal to be delivered, as such, Let,

A represent the cross sectional Area of the fibre pipe
D represents the diameter of the fibre pipe
V represents the velocity of fibre pipeline signal per minute
Q represents Quantity of fluid carried per minute
But the Quantity Q of signal flowing per minute is given by:

$$\mathbf{Q = A*V = \frac{\pi}{4}*D^2*V} \qquad (17)$$

Solving for D yields

$$\mathbf{D = \sqrt{\frac{4}{\pi}*\frac{Q}{V}} = 1.13\sqrt{\frac{Q}{V}}} \qquad (18)$$

ii. Wall Thickness of the fibre Pipeline *t*

From figure 1a , *t* is considered next in order to withstand the internal signal fluid pressure *p* in the thin or thick cylindrical fibre pipeline.
Essentially, the thin cylindrical equation will be applied when:

i. Stress across the fibre pipeline section is uniform
ii. The internal diameter of the fibre pipeline section *D* is >20t; i.e D/t>20

iii. The allowable stress σ_t is more than six times the pressure inside the fibre pipe *P* ie. $\sigma_t > 6$

According to the thin cylindrical equation 19, wall thickness *t* of the fibre pipeline is given by

$$\mathbf{t} = \frac{P.D}{2Q_t} = \frac{P.D}{2Q_t\eta_t} + \mathbf{C} \qquad (19)$$

Where, η_t is the Efficiency of fibre pipeline longitudinal joint and ***C*** is the Weishack constant

IV. Design Model For fibre Pipeline Stress

Consider a cylindrical shell of a pressure vessel carrying signal which was subjected to a high internal pressure *p*, the wall of the cylinder must be made extremely thick ***t***. The factors under consideration are the pressure (forces) and the cylindrical fibre with core and cladding surfaces.

Assuming that the tensile stresses are uniformly distributed over the section of the walls, let,

r_0 represent outer radius of the cylindrical shell
r_i represent inner radius of the cylindrical shell
t represent thickness of the cylindrical shell = $r_0 - r_i$
p represents intensity of internal pressure
μ represent Poisson's ratio
σ_t represents tangential stress
σ_r represents radial stress

Using lame's law which states that assuming that the longitudinal fibres of the cylindrical shell are strained, the tangential stress at any radius *x* is give by

$$\sigma_t = \frac{p_i(r_i)^2 - p_0(r_0)^2}{(r_0)^2 - (r_0)^2} + \frac{(r_i)^2(r_0)^2}{x^2}\left[\frac{p_i - p_0}{(r_0)^2 - (r_i)^2}\right] \qquad (20)$$

Now, radial stress at any radius *x* is given by

$$\sigma_r = \frac{p_i(r_i)^2 - p_0(r_0)^2}{(r_0)^2 - (r_0)^2} - \frac{(r_i)^2(r_0)^2}{x^2}\left[\frac{p_i - p_0}{(r_0)^2 - (r_i)^2}\right] \qquad (21)$$

Considering the internal pressure only ($P_i = P$) which assists the spreading of the pulse very fast. In this case, let external pressure, $P_0 = 0$,

From Equation 20, the tangential stress at any radius *x* is give by.

$$\sigma_t = \frac{p_i(r_i)^2}{(r_0)^2 - (r_0)^2}\left[1 + \frac{(r_0)^2}{x^2}\right] \qquad (22)$$

$$\sigma_r = \frac{p_i(r_i)^2}{(r_0)^2 - (r_0)^2}\left[1 + \frac{(r_0)^2}{x^2}\right] \qquad (23)$$

From equation (22) and (23), the tangential stress is a tensile stress whereas the radial stress is a compressive stress.

Again, the tangential stress is Maximum at the inner surface of the pipeline ie. $x = r_i$ and it is minimum at the outer surface of the shell ie. $x = r_0$

By taking the value of $\boldsymbol{x = r_i}$ and $\boldsymbol{x = r_0}$ in Equation (21) and (22), the Maximum tangential stress at the inner surface of the pipeline is given by,

$$\sigma_{(t_{Max})} = \frac{P[(r_0)^2 + (r_i)^2]}{(r_0)^2 - (r_i)^2} \qquad (24)$$

While the minimum tangential stress at the outer surface of the shell is given by,

$$\sigma_{(t_{Min})} = \frac{2P[(r_i)^2]}{(r_0)^2 - (r_i)^2} \qquad (25)$$

$$\sigma_{(t_{Max})} = -p \text{ (Compressive) and at } \sigma_{(t_{Min})} = 0 \qquad \mathbf{(26)}$$

Therefore, Equations (25) and (26) becomes the major maximum and minimum stress equation for the fibre pipeline design. Now, the tangential stress is always maximum at the inner surface of the core ie when $x = r_1$ and is minimum at the outer surface where $x = r_o$

V. CONCLUSION AND RECOMMENDATION

Conclusively, this model, gives adequate impedance matching to any external force which would have led to signal degradation leading to various dispersion failures (group velocity dispersion- GVD, polarisation mode dispersion- PMD, material dispersion and chromatic dispersion- CD). When implemented, it will ensure that the intelligent signals being propagated are decoded accurately.

Hence, it is recommended that this neutrality of external pressure can be carried using sensor simulation by subsequent researchers.

REFERENCE

[1] Gerl Keiser, (2000), Optical Fibre Communications 3rd edition; Mcgraw-Hill International Editions Khurmi R.S and Gupta, J.K (2005), Machine Design, 1st edition, S Chand publishers; Pp 196- 227.

[2] Shaham ,S, "Chromatic Dispersion Compensation by Signal Predistortion, Linear and Non Linear filtering," Communication System Group, Department of Signal & Systems, Chalmers University of Technology, Gotebory, Sweden 2010.

American Journal of Engineering Research (AJER)
e-ISSN : 2320-0847 p-ISSN : 2320-0936
Volume-3, Issue-10, pp-61-67
www.ajer.org
Research Paper Open Access

Measurement of Electrocardiographic Signals for Analysis of HeartConditions and Problems

Mbachu, C. B[1], Nwosu, A. W[2]
[1, 2]*Department of Electrical and Electronic Engineering, Anambra State University,Uli, Nigeria.*

ABSTRACT:*People who suffer from heart or heart-related diseases mostly experience heart attacks if these diseases are not detected early enough and treated. This underscores the need for a very reliable means of detecting these diseases to save the patients from these attacks which are increasing in proportion all over the world. Electrocardiography (ECG) is the electrical activity of the heart and it generates a biomedical signal referred to as ECG signal or simply ECG, and the appearance of this signal conveys much clinical information regarding the conditions and problems of a patient. Therefore proper interpretation of this signal is very vital in the diagnosis of heart problems. ECG signal amplitude is very small, about 1.0 mV and the signal is naturally contaminated by other biomedical and non-biomedical signals. The biomedical signals are electroencephalogram, electromyogram and baseline wander, while the non-biomedical signal is power line interference. These contaminating signals must be removed from the ECG signal during measurement otherwise it will convey incorrect clinical information concerning the patient's heart conditions and problems. Digital filters are employed in removing these contaminating signals and a good quality digital filter is able to remove these contaminants and still preserve the integrity of the signal. In this paper ECG signal acquisition technique, processing and interpretation are presented. Three different filters are considered: low pass andhigh pass filters and adaptive noise canceller. Matlab software tool is used to observe and record results.*

KEYWORDS:*ECG, leads, frequency spectrum, filter*

I. INTRODUCTION

Electrocardiography (ECG) is the electrical activity of the heart, and this activity generates a biomedical signal known as electrocardiographic (ECG) signal or simply ECG. The morphology of this ECG signal conveys much clinical information regarding the heart conditions and problems of a patient. Measurement of ECG signal starts with signal acquisition and this can berealised by placing electrodes directly on the arms, legs and chest [1]. ECG signal is naturally contaminated by other biomedicalsignals which include electroencephalogram(EEG) which is due to the electrical activity of the brain,electromyogram (EMG) which is due to the electrical activity of the muscles, and baseline wander which is due to respiration. It is also contaminated by a non-biomedical signal, 50/60Hz powerline interference, which is due to power supply source to the ECG measuring system. The frequency range of ECG signal is from 0.5Hz to 100Hz, baseline wanders around 1Hz frequency while EEG is above 100Hz. The EMG signal frequency can be below or overlaps with ECG signal frequency depending on body muscle movement. These signals which constitutenoise to the ECG signal must be removed during ECG measurement otherwiseit will convey incorrect clinical information regarding the patient's cardiac conditions and problems. Digital filters are used to remove these noise signals. A typical noise- free ECGis shown in fig. 1 and comprises three waves and one complex. The waves are P, T and U waves and the complex is QRS complex [2,3]. Interpretation of the signal is done by considering the shapes of the signal, the waves and complex and also the period or frequency of the signal and time intervals of the waves and complex. Different researchers have worked on ECG signal acquisition, processing and interpretation. Abdul *et al* [1] worked on the 12-lead and 3-lead ECG data acquisition systems. The authors processed the ECG signal with analogue high pass, low pass and 50Hz notch filters with analogue instrumentation amplifier amplifying the analogue ECG signal before application to the analogue filters. In [4] Ajayanalysed the 12 lead ECG signal acquisition system and processed the acquired signal exactly as done by Abdul*et al* in [1]. In [5]Anatolie*et al* carried out ECG signal acquisition and processing in their dynamic analysis of heart rate variability parameters. They used a dual channel amplifier module and a portable data acquisition module that communicates with a computer throughUSB port. Philip*et al* in [6] developed an algorithm forassessment of quality of ECGs acquired via mobile telephones and used the algorithm to assess and evaluate 1,500 12-lead ECG signals acquired on mobile telephones. In reducing powerlineinterference in ECG signal, notch, Wiener and adaptive filters can be used [7]. Comparison of the performance of the three different filters by the authors showsthat the adaptive filter removes 50Hz power interference better than the other two. Geeta and Bhaskar [8] carried out a performance evaluation of finite impulse response(FIR) filters designed with different windows in the reduction of 50Hz powerline interference in ECG signal. In [9]Mikheld and Khaled developed wavelet transform thresholding algorithm for ECG signaldenoising. The authors used four different ECG signals to study the effect of threshold value of descrete wavelet transform coefficients. These signals are considered as original and noise-free ECG signals with different morphologies.

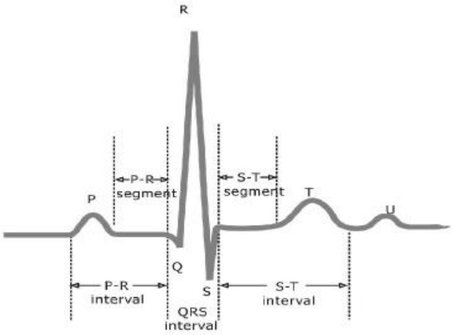

Fig. 1: Typical ECG signal

Source [2]

II. ECG SIGNAL ACQUISITION

Depolarisation of the cardiac cells is the central electrical event of the heart. This occurs when the cardiac cells, which are electrically polarized, lose their internal negativity [9].Depolarisation is distributed from cell to cell, producing a wave of depolarization that can be transmitted across the entire heart and takes place during every heartbeat.This wave represents a flow of electricity and it can be captured ordetected by electrodes placed on the skin of the body at designated sites or locations. Once depolarization is complete, the cardiac cells are able to restore their resting polarity through a process called repolarisation. This flow of electricity can also be captured by the same recording electrodes.The leadin the context of an ECG refers to the voltage difference between two of the electrodes placed on the skin and it is this difference that is recorded by ECG recording equipment known as electrocardiograph (ECG). There are 3-lead, 5-lead, 6-lead and 12-lead ECGmeasurement systems. Fig. 2 shows a 3-lead ECG system, consisting of the acquisition stage, processing stage and the display unit. The acquisition stage consists of 3 electrodes representing lead I, lead II and lead III, and an analogue instrumentation amplifier(IA).Lead I is the voltage between left arm (LA) and right arm (RA), that is LA – RA. Lead II is the voltage between left leg (LL) and right arm (RA),that is LL – RA. Lead III is the voltagebetween left leg (LL) and left arm (LA), that is LL – LA or Lead II – Lead I. This Lead III voltage is derived from Lead II and Lead I. A raw ECG signal has very low amplitude of about 1mV and therefore for effective filtration the low amplitude raw ECG signal is amplified first by the analogue instrumentation amplifier (IA). At the output of the instrumentation amplifier, acquisition is complete and the acquired signal is ready for processing and display.

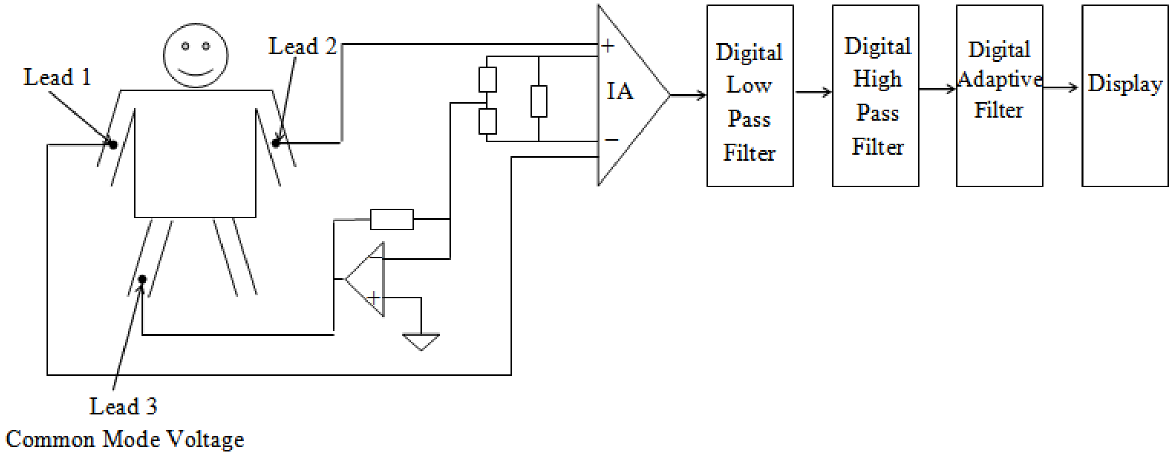

Fig.2: 3-Lead ECG Measurement System

ECG Right Leg Driver : The essence of the ECG right leg driver is to remove common mode noise generated from the body [11]. The two signals entering the instrumentation amplifier are summed, inverted and amplified in the right leg driver being fed back to an electrode attached to the right leg. The other electrodes pick up this signal to cancel the noise.

III. ECG SIGNAL PROCESSING

After acquisition of an ECG signal the signal is still contaminated by artifacts like baseline wander, encephalographic (EEG) signal and powerline interference. The patient should be still and quiet during acquisition so that the electromyographic artifact is reduced to the barest minimum. Filters are used to remove other artifacts. Matlab is used for the design.

Design of Low Pass Filter :A Finite Impulse Response (FIR) digital low filter is designed using Kaiser Window [12]. This filter removes the EEG noise and any other frequency above the upper cut off frequency of 100Hz used here. The sampling frequency is 1000Hz while the order of the filter is 100. The resulting magnitude response is shown in figures 3.

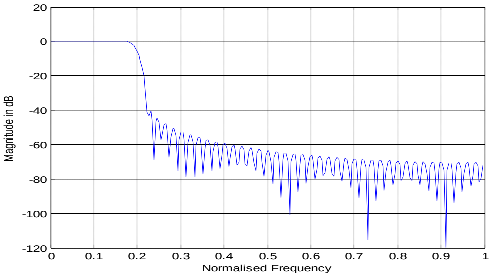

Fig 3 Magnitude response of the low pass filter

Design of High Pass Filter : An FIR digital high pass filter is designed with Kaiser Window.This filter removes the baseline wander noise and any other noise below the lower cut- off frequency of 0.5Hz used here. The sampling frequency is 1000Hz while the order of the filter is 100. The magnitude response of the filter is depicted in figures 4.

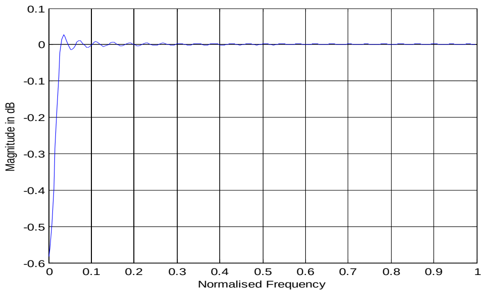

Fig 4: Magnitude response of the high pass filter

Design of Adaptive Filter : An FIR digital adaptive noise canceller is designed with a step size of 0.0010 and order of 100 to remove the 50Hz powerline noise in the ECG. The sampling frequency is 1000Hz. This filter is particularly useful in a situation where the power supply frequency to the ECG measurement system is not stable, because the adaptive noise canceller tracks the powerline interference frequency as it changes. The magnitude response is in fig 5.

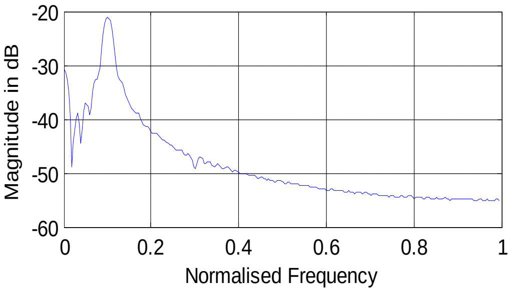

Fig. 5 Magnitude response of the adaptive filter

IV. RESULTS

In this section the various designed digital filters in section 3 are used to filter a noisy ECG signal and the effect of each filter is recorded. There are four groups in the presentation of the results; the results of the low pass, high pass, and adaptive filters, and a cascade of the three filters. An ECG signal of 3.5mV amplitude corrupt with baseline wander, EEG and 50Hz powerline noise of 0.1mV each is shown in fig 6 while the frequency spectrum or periodogram is depicted in fig 7.

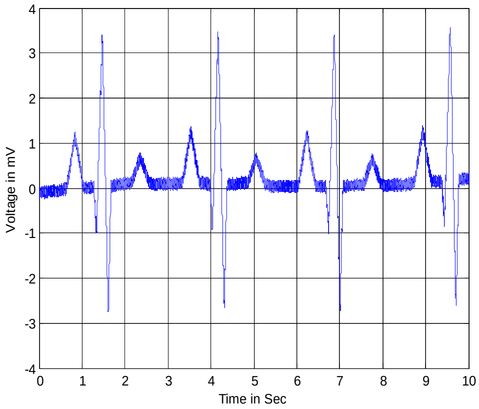

Fig 6: Corrupt ECG signal

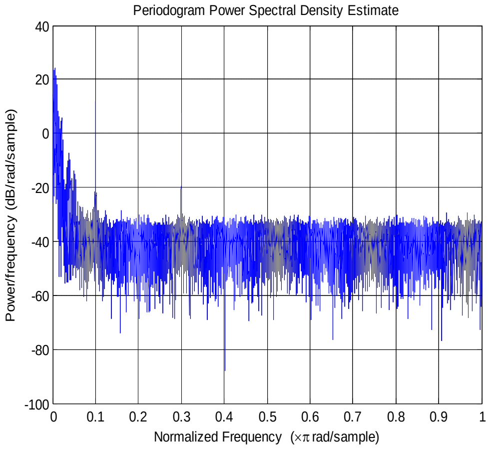

Fig 7: Frequency spectrum of the corrupt ECG signal

Filtration with Low Pass Filter : The noisy ECG signal of fig 6 is passed through the low pass filter and the output is depicted in fig 8 while the frequency spectrum of the output appears as in fig 9. From fig 7 the average power of the raw ECG signal above 100Hz is about -26.25dB whereas from fig 9 the average power of the filtered ECG signal above 100Hz (0.2 in the figure) is about-50.25 dB, implying that the filter has filtered off high frequency noise from the ECG signal.

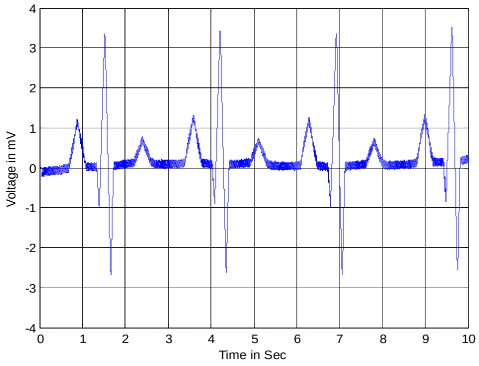

Fig 8: ECG signal after low pas filter filtering

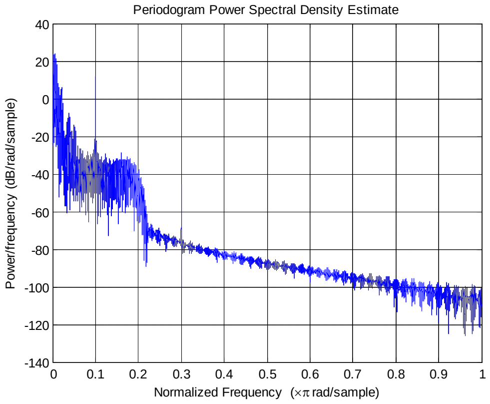

Fig 9: Frequency spectrum of ECG after low pass filtering

Filtration with High Pass Filter : The noisy ECG signal of fig. 6 is filtered with the high pass filter and the output is recorded as fig. 10 while the frequency spectrum of the output is as in fig. 11. From fig. 7, the average power of the raw ECG signal below the frequency of 0.5Hz is approximately 23.75dB, whereas from fig 11 the average power of the filtered ECG signal at a frequency below 0.5Hz (0.001 in the figure) drops to 21.5dB and the implication is that the high pass filter has reduced the baseline wander and other low frequency noise from the ECG signal.

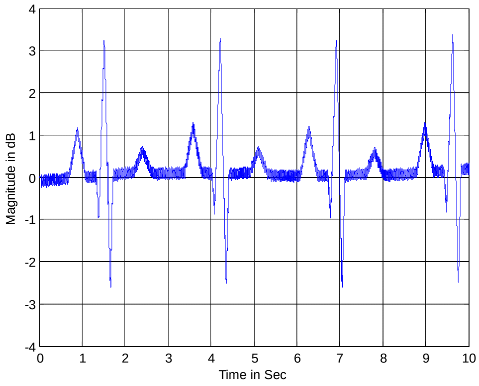

Fig 10: ECG Signal after high pass filtering

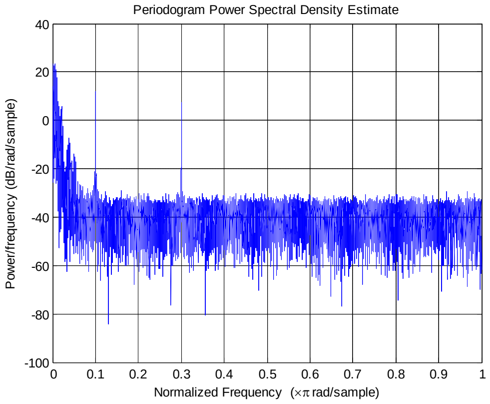

Fig. 11: Frequency spectrum of ECG after high pass filtering

Filtration with the Adaptive Filter : The noisy or raw ECG signal is applied to the input of the adaptive noise canceller. The filtered output is shown in fig. 12 while the frequency spectrum is shown in fig 13. From fig. 7 the power of the raw ECG signal at 50Hz is 10dB but from fig. 13 the power of the filtered ECG signal at 50Hz is lowered to -37.5dB which is a confirmation that the adaptive noise canceller has removed the 50Hz powerline interference from the ECG signal.

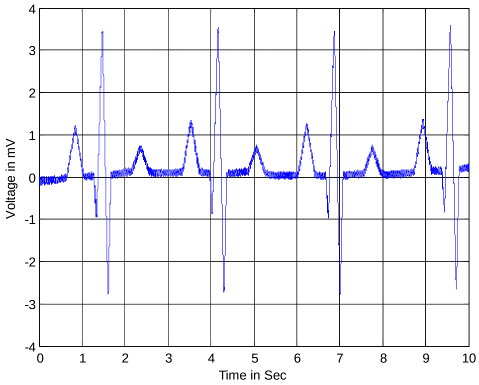

Fig. 12: ECG signal after adaptive filtering

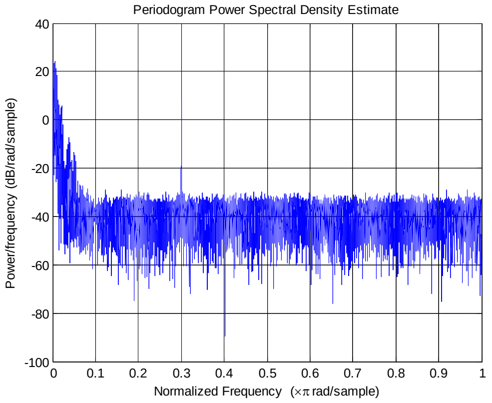

Fig. 13: Frequency spectrum of ECG after adaptive filtering

Filtration with a Cascade of Low Pass, High Pass and Adaptive Filters : The raw ECG signal of fig. 7 is applied to the input of the cascade and the output is depicted in fig. 14. Comparing fig 6 and fig. 14 it can be clearly seen that the cascade has drastically reduced the avalanche of noises in the raw ECG signal.

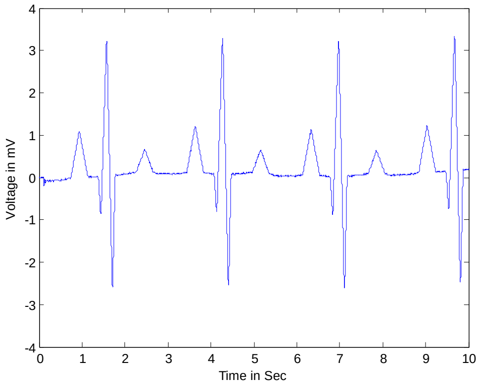

Fig. 14: ECG after cascade filtering

V. INTERPRETATION OF ECG

ECG signal conveys clinical information concerning the heart conditions of a patient. Any abnormality in the heart may change the normal morphology or frequency of the signal or both. The type and degree of change is a measure of the nature and degree of the health condition. Activation of atrial myocardium of the heart produces the P wave [3] as shown in fig. 1. During Sinus rhythm the initial part of the P wave represents the right atrial activation and the terminal part of the P wave represents activation of the left atrium by the sinus impulse with some overlap in the middle. The QRS complex as shown in fig 1 arises from the depolarization of the ventricular muscle of the heart. After depolarization of heart cells, repolarisation begins. The T wave arises from the repolarisation of the ventricular muscle of the heart. The U wave that sometimes follows the T wave is a second order effect of an uncertain origin and is of little diagnostic significance.Each heart beat produces one cycle of ECG signal. Therefore the frequency of ECG signal, that is the number of cycles produced by a patient's heart per second , which can be translated to the number cycles or beats per minute (bpm) by multiplying number of cycles per second by 60 can be used to determine whether the heart beat rate of a patient is normal or not. Normally, human heart beat rate is between about 60bpm to 150bpm depending on age [13]. Heart arrhythmias include Tachycardia which is when the heart rate is above 150bpm, andBracardia which iswhen the heart rate is below 60bpm. Other heart abnormalities include but not limited to left ventricular hypertrophy which manifests in the ECG signal as inverted T wave and old myocardial infarction which manifests in the ECG signal in form of prolonged Q.

VI. DISCUSSION

The magnitude responses of the three digital filters designed show that the filters are stable because there is no sustained oscillation in each one. The results of the filtrations show that each filter drastically reduced the noise specifically meant for it to filter. For example the noise levels of the raw ECG signal at frequency of 0.5Hz, 100Hz and 50Hz lowered at those respective frequencies when the signal was applied to the filters. The output of the cascade of the three filters produced a clean ECG signal without distortion which confirms the compatibility of the filters to one another and the optima of the orders of the filters.

VII. CONCLUSION

Accurate measurements of ECG signals are very vital in the diagnoses of heart and heart-related diseases because the rate and morphology of ECG signals convey much clinical information regarding the heart. It has been established that digital filters are indispensable in ECG measurement because they remove the inherent noises that impair reliable interpretation of the signals. Reasonable acquisition of ECG signals starts with electrodes as transducers and therefore good quality electrodes are recommended.

REFERENCES

[1] Abdul QayoomBhat, Vineet Kumar and Sunil Kumar (2013).Design of ECG Data Acquisition System. International Journal of Advanced Research in Computer Science and Software Engineering (IJARCCSE), Vol. 3, issue 4, 2013.

[2] Manish Kansal, Vija Kumar, Dinesh Arora and Hardeep Singh Saini (2011). Designing and Implementation of Digital Filter for Removal of Power Supply Noise. International Journal of Soft Computing and Engineering (IJSCE), Vol. 1, Issue 4, Pp. 242 – 246.

[3] [3]Stefan Jurko and GregorRosinaj (2006).High Resolution of ECG Signals by Polynomial Approximation. Radio Engineering, Vol. 5, no 1, Pp. 32 – 37.

[4] Ajay Bharadwaj (Feb. 2011). Accurate ECG Signal Processing. EE Times Design, Pp. 1 – 7 (www.eetimes.com/design).

[5] Anatolie BOEV, Marcel STANCIU and Brandusa PANTELIMON (2011).ECG Measurement and Acquisition System for Dynamic Analysis of Heart Rate Variability Parameters. U. P. B. Science Bulletin Series C., Vol. 73, Issue 1, Pp. 191 – 198.

[6] Philip Langley, Luigi Yuri Di Marco, Susan King, David Duncan, Costanzo Di Maria, WenfengDuan, MarjanBojarnejad, DingchangZheng, John Allen and Alan Murray (2011). An Algorithm for Assessment of Quality of ECGs Acquired via Mobile Telephones. Computing in Cardiology, Vol 38, Pp. 281 – 284.

[7] [7] Yatindra Kumar and Gorav Kumar Malik (2010).Performance Analysis of Different Filters for Powerline Interference in ECG Signal.International Journal of Computer Application, Vol. 3, No 7, Pp. 1- 6.

[8] GeetaKadam and Bhaskar P. C. (2012). Reduction of PLI in ECG Signal Using FIR Filter. International Journal of Computational Engineering (IJCER), Vol.2,Issue2 pp314-319.

[9] MikheldAlfaouri and KhaledDaqrouq (2008). ECG Signal Denoising by Wavelet Transform Thresholding. American Journal of Applied Sciences Vol. 5, Issue 3, Pp. 276 – 281.

[10] Biopac Systems Inc. (2013). Application note 109.www.biopac.com

[11] Patrick O. Bobbie, ChaudaryZeeshanArif, HemaChaudhari and SagarPujari. Electrocardiogram (EKG) Data Acquisition and Wireless Transmission.

[12] Shenoi B. A. (2006) Introduction to Digital Signal Processing and Filtering Design. John Wiley and Sons, USA, Canada.

[13] Yuheng Chen, Leslie Goldberg, and Christine Moran.ECG Acquisition and Diagnostic System.Rice.www.owlnet.rice

American Journal of Engineering Research (AJER)
e-ISSN : 2320-0847 p-ISSN : 2320-0936
Volume-3, Issue-10, pp-68-74
www.ajer.org
Research Paper Open Access

A Finite Impulse Response (Fir) Adaptive Filtering Technique for the Monitoring Of Foetal Health and Condition

Mbachu, C. B[1], Arinze, A. W.[2]
[1, 2]*Department of Electrical and Electronic Engineering, Anambra State University, Uli,*
Anambra State, Nigeria

ABSTRACT :*Foetal heart rate and its in-between beat variability are two vital biomedical recordings for ascertaining the foetal health and condition inside its maternal womb. Naturally, the foetal electrocardiographic signal which is generated by the foetal heart beat is mixed with the maternal electrocardiographic signal and other background noise arising from maternal muscle activity and foetal motion. The morphology of the foetal ECG describes the medical state of the foetus. This ECG must have to be extracted from the contaminating signals before it can be interpreted correctly and clinically. In this paper a design and implementation of an adaptive FIR filter that separates the foetal and maternal ECG signals, and a static FIR low pass filter that removes the high frequency noise from the foetal ECG is proposed. Matlab software is used to design and simulate the results.*

KEYWORDS:*FECG, MECG, ANC, Noise*

I. INTRODUCTION

Foetal electrocardiographic (FECG) signal is a waveform that is generated by foetal heart rate and its beat-to-beat variability. Similarly the maternal electrocardiographic (MECG) signal is a waveform that is generated by maternal heart rate and its beat-to-beat variability. The morphology of the FECG contains much clinical information regarding the health and condition of the foetus. Incidentally, biomedical research has shown that this FECG signal is mixed up with other signals which include MECG signal and background noise resulting from maternal electromyogram (EMG) and foetal motion and these signals degrade the quality of the FECG. For correct clinical FECG measurement and interpretation, the MECG and the background noise associated with the FECG must be reduced to the barest minimum. Different researchers have used different approaches to effect this reduction. In [1] Amin et al used adaptive linear neural network (ADALINE) to separate the FECG from composite ECG, comprising FECG and MECG. This approach is very convenient to the patient during long-term monitoring of the foetus. In [2] Suzanna et al used a method that consists of a sequential analysis approach, in which the “a priori” information about the interferencesignals associated with FECG is used for the detection of the FECG and this method can be used for FECG detection both during pregnancy and labour. The authors evaluated the method on a set of 20 abdominal recordings from pregnant women with different gestational ages and obtained a superior performance when compared with independent component analysis (ICA) method. In [3] Mansoureh et al proposed a multivariate singular spectrum analysis (MSSA) approach for extracting and separating the mother heart signal, foetal heart signal and the noise component from the combined ECG signals. The method is targeted on noisy recordings and the algorithm was validated by using some noisy simulated signals and real life signals. Arias – Ortega and Gaitan – Gonzalez [4] proposed a sequential processing method, in which the detection and cancellation of maternal QRS complexes followed by foetal QRS complex involving hardware suitable processing techniques, for single channel abdominal ECG algorithm for real – time maternal and fetal heart rate monitoring. The authors tested the algorithm on a group of 25 different gestational age pregnant women signals, and performance was very satisfactory. MahaShadaydeh et al [5] extracted foetal ECG from maternal ECG by using adaptive voterra filter. The adaptive voterra filter (AVF) is capable of synthesisingthe non-linear relation between the mother thoracic ECG signal and the abdominal signal which contains a transformed mother ECG, the foetal ECG and other noise elements. An adaptive multi-sensory noise canceller structure was adopted for the extraction purpose and the AVF update algorithm of RLS was proposed. The result showed superior effectiveness over some methods.

Dr.Walid A.Zgallai [6] combined an adaptive cubic LmFvoterra filter and artificial neutral network classifier to improve the detection of foetal heart beat, in his bi – spectral contour matching method of non – invasive foetal heart beat. Swarnalatha and Prasad [7] investigated the use of wavelet transform denoising along with two stage adaptive filtering technique for foetal ECG extraction from the abdominal ECG. The authors used wavelet transform to decompose the abdominal signal into its two components of MECG and FECG and the FECG is extracted by adaptive filtering technique. Results showed that the technique is capable of extracting FECG even when it is embedded with complex maternal signal. Mariano Ruffo et al [8] used foetal phonocardiography (FPCG) and foetal electrocardiography (FECG) with passive, fully non-invasive low cost digital recording systems in effectively monitoring of the foetus. The authors presented the use of FECG, FPCG and their combination in order to detect the foetal heart rate (FHR) and potential functional anomalies. They also presented signal processing methodologies, suitable for long-term assessment, to detect heart beat events such as first and second heart sounds and QRS waves, which provide reliable measurement of heart rate, and offer the potential of new information about measurement of the systolic time intervals and foetus circulatory impedance. Jimenez-Gonzalez A. and James C. J. in [9] developed a method of separating foetal heart sounds and maternal activity from single-channel phonograms for effective monitoring offoetal health condition and this method involves:

(1) Using temporal decomposition source Separation (TDSEP), (2) Increasing the number of components to be extracted to higher number of ten and (3)Using K-means to find and group components corresponding to the same sources such as FHS, maternal or line-noise. Results showed a better quality and more objective extraction of foetal heart sounds (s_{1-S2}), maternal activity and line-noise. In [10] Ebrahim et al proposed the use of genetic algorithm (GA)-based adaptive filter method in extracting foetal heart signal via two-channel arrangement. In this two channel approach, an electrode is placed on the mother's thoracic and the other placed on the mother's abdomen. The authors argued that the signal recorded from the mother's thoracic represents the maternal heart signal while the composite signal recorded from the mother's abdomen represents the foetal heart signal, the maternal heart signal, the maternal electromyogram, the 50Hz powerline interference and random electronic noise. According to the authors the GA is employed to avoid convergence into local extremum, that is the GA is recruited whenever the adaptive filter is suspected of reaching a local extremum. The maternal thoracic ECG serves as a reference signal to the LMS based adaptive filter. In [11] Hasan M. A. et al reviewed the various existing methodologies and developed algorithms on FECG signal detection and analysis to provide efficient and effective ways of understanding the FECG signal and its nature for foetal monitoring. The methodologies and algorithms reviewed by the authors include wavelet transform, artificial intelligence, ICA and blind source separation, linear adaptive filter framework, genetic algorithm approach, matching pursuits (MP) approach, SVD method, successive cancellation algorithm and adaptiveneuro-fuzzy logic technique. In [12] KokBengGan et al designed and *developed a low-poweroptical system* for monitoring the foetal heart rate. The signal of interest in this monitoring is the photoplethysmogram (PPG) which is generated when a beam of light is modulated by blood pulsations. In this non-invasive technique light intensity, formed by light emitting diode, is modulated by the maternal as well as foetal blood circulation, producing a combined signal which is detected by a photo detector and separated via digital signal processing. The technique was proved to give a satisfactory performance. Camps G et al [13] used neutral network based on finite impulse response filter to extract foetal ECG from maternal ECG, while Kam A. and Cohen A. in [14] combined IIR adaptive filtering and genetic algorithms in the detection of foetal ECG.

In this paper we consider a non-invasive technique of combination of an adaptive and a static FIR filters for the extraction of FECG from the composite EEG(MECG+FECG) and thehigh frequency random noises. The adaptive LMS-based FIR filter separates the MECG from the composite ECG and high frequency random noise resulting from foetal motion and maternal EMG, while the static FIR filter removes the random noise from the FECG, leaving a clean FECG only. The introduction of the static filter makes this work different from other related works for foetal ECG separation.

II. FOETAL SEPARATION PROCESS

The diagram for the separation process is shown in fig1. Abdominal electrodes placed at the maternal abdomen pick up the abdominal ECG (AECG). This abdominal ECG comprises the MECG, FECG and the higher frequency random noise. The AECG is applied to main input of the adaptive filter via the abdominal leads as shown in fig1. The thoracic electrodes placed at the maternal chest pick up the MECG and this is coupled to the reference input of the adaptive filter via the chest leads to serve as the reference input signal to the adaptive filter. The filter output is an estimated value of the reference input signal, here the MECG. The estimation is done by convolution of the filter coefficients and the reference input signal until an estimated signal that is as close as possible to the reference input is obtained. The estimated signal is subtracted from the AECG, producing an error signal “e”. This error signal corresponds to FECG and the high frequency random noise. The error signal is further applied to the low pass static FIR filter to remove the high frequency randomnoise, hence leaving only the FECG to appear at the system output as the output signal.

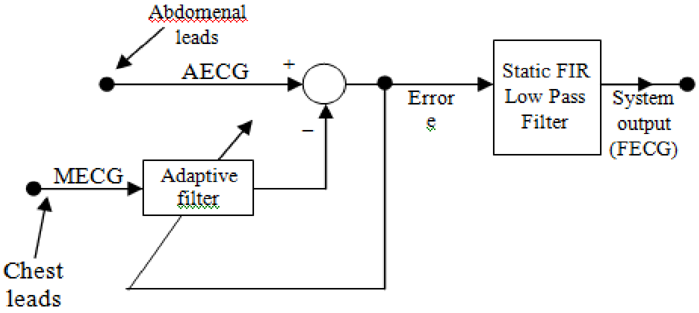

Fig 1: Foetal Monitoring System

III. DESIGN OF THE ADAPTIVE FILTER

With a sampling frequency of 1000HZ, adaptive step-size of 0.00087and filter order of 100, the impulse, magnitude, phase and Z – plane responses of the adaptive filter are shown in figures 2, 3, 4 and 5 respectively.

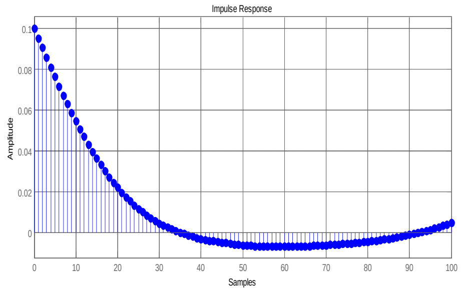

Fig 2: Impulse Response of the Adaptive Filter

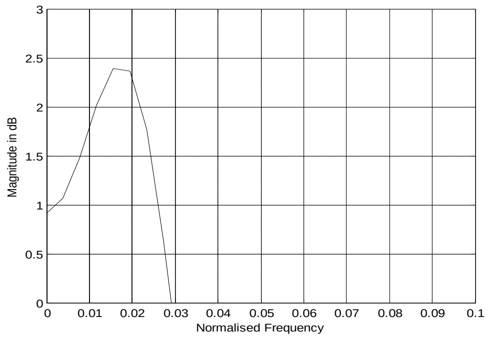

Fig 3: Magnitude Response of the Adaptive Filter

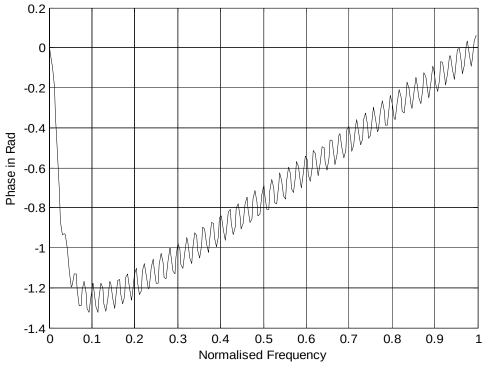

Fig 4: Phase Response of the AdaptiveFilter.

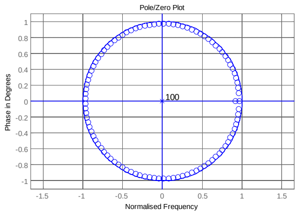

Fig 5: Z-plane Response of the AdaptiveFilter

IV. DESIGN OF FIR LOW PASS FILTER

With a sampling frequency of 1000HZ, cutoff frequency of 100Hz and static filter order of 100, the impulse, magnitude and phase responses of the static low pass filter are depicted as figures 6, 7 and 8 respectively.

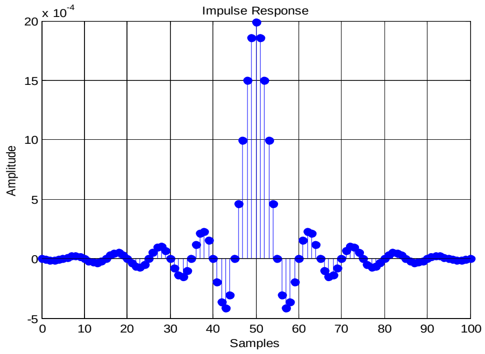

Fig 6: Impulse Response of Low PassFilter

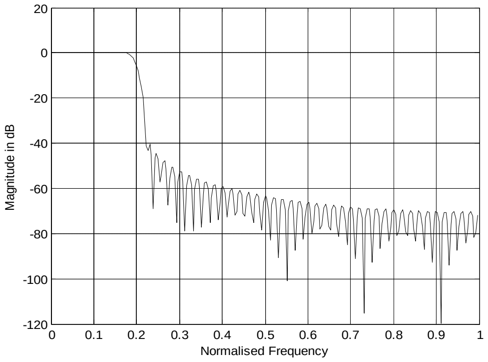

Fig 7: Magnitude Response of Low Pass Filter

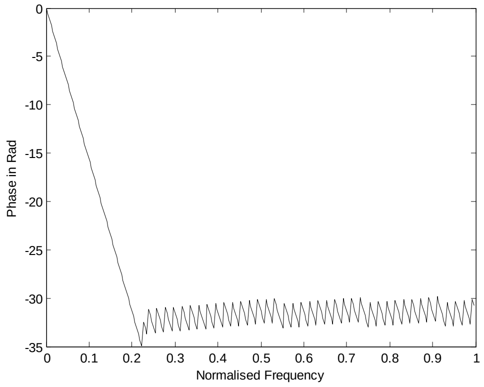

Fig 8: Phase Response of the Low PassFilter

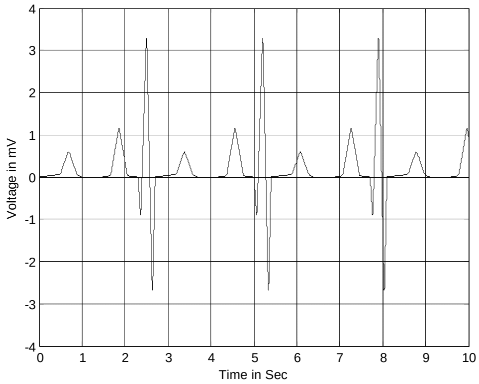

Fig. 9: Maternal ECG FromMatlab

V. RESULTS

A maternal ECG of 3.5 millivolt amplitude resulting from a heart beat of about 89 beats per minute is presented in fig 9 above. Naturally foetal ECG amplitude is less than that of maternal ECG but foetal heart beats faster than the maternal heart. Typically foetal heart beat rate ranges from 120 to 160 beats per minute [3]. Fig 10 represents a typical foetal ECG signal with a heart beat rate of 139 beats per minute and amplitude voltage of 0.25mV. Fig 11 shows the abdominal ECG (AECG) consisting of the 3.5 millivolts MECG, 0.25 millivolt FECG and 0.02 millivolt high frequency random noise. The AECG is applied to the foetal monitoring system of fig 1. The error signal which represents the output of the adaptive section of the system is depicted in fig 12. This error signal is FECG corrupt with high frequency noise. The system output which emulates a clean FECG is provided in fig. 13.

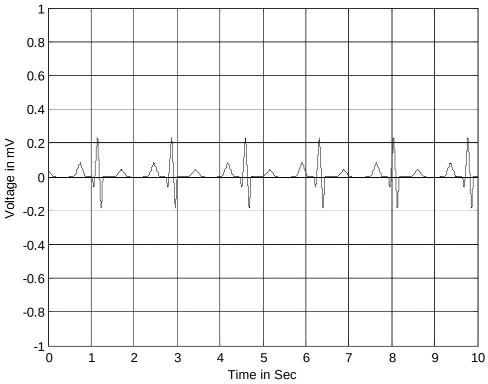

Fig 10: Foetal ECG from Matlab

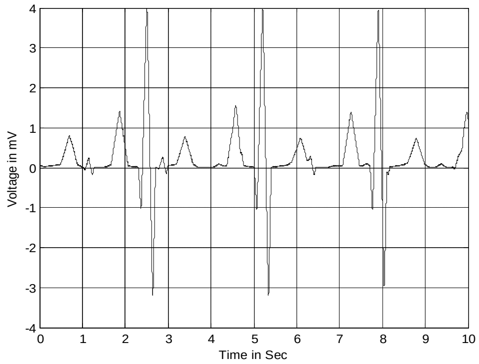

Fig 11: Abdominal ECG from Matlab

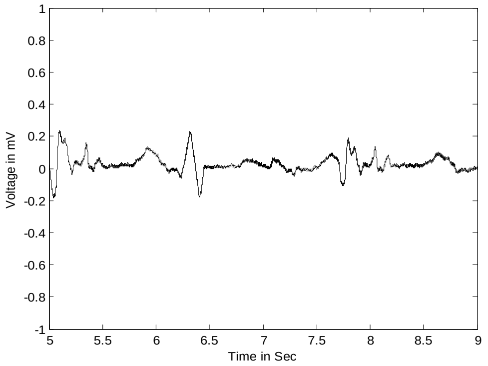

Fig 12:FoetalECGAfter Adaptive filtering Only

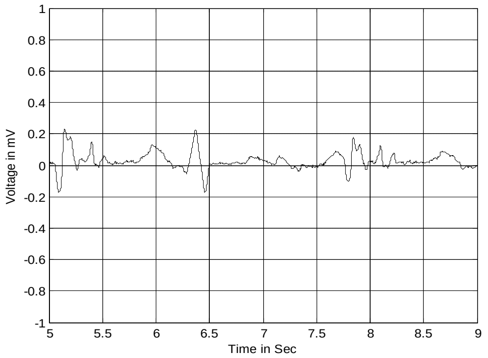

Fig 13:FoetalECG After Adaptive and Low Pass Filtering

VI. DISCUSSION

The impulse and magnitude responses of the adaptive filter as depicted in figures 2 and 3 respectively show that the adaptive filteris stable since the responses do not have sustained oscillations. The z-plane response of fig. 5 shows stability because all the poles and zeros are confined within a unit circle.The phase response of fig. 4 shows a good degree of linearity which implies that the adaptive filter will not distort any applied complex signal. Similarly figures 6 and 7 indicate that the designed low pass filter is stable, while the phase response of fig. 8 is linear within the required frequency range.Fig. 11 shows that the foetal ECG is swallowed up by maternal ECG in the womb. This maternal ECG and the other associated noise signals must be removed before the appearance of the foetal ECG can be determined. Fig. 12 shows the foetal ECG after the maternal ECG is removed. The appearance still indicates presence of noise, and this noise is the random noise arising from foetal motion. Fig. 13 shows a better foetalECG because the low pass filter has reduced the random noise. It can be observed that this ECG of fig. 13 is closer to the uncorrupt foetal ECG of fig. 3, though with small distortion due to presence of overlapping random noise. However, it is good enough for correct clinical interpretations.

VII. CONCLUSION

It has been established in this research that digital filters are very useful in the accurate measurement of foetal ECG. Adaptive filters extract the maternal ECG which swallows up the foetal ECG in the abdomen. Without the adaptive filter the output will appear like a corrupt maternal ECG signal during measurement. The low pass filter plays a vital role in the reduction of the high frequency noise that corrupts the foetal ECG.

REFERENCES

[1]. Amin M. S, MamunMd, Hashin F. H. and Husain H. Separation of Foetal Electrocardiography (ECG) from Composite ECG Using Adaptive Linear Neural Network for Fetal Monitoring. International Journal of the Physical Sciences, Vol. 6 (24), pp 5871 – 5876, 16th Oct, 2011.

[2]. Suzanna M. M Martens, Chiara Rabotti, Massimo Mischi and Rob J. Sluijter. A Robust Fetal ECG Detection Method for Abdominal Recordings. Physiological Measurements, Vol. 28, pp 373 – 388, 10 P Publishing Ltd, 2007.

[3]. MansourehChodsi, HosseinHassani and SaedSanei. Extracting Fetal Heart Signal From Noisy Maternal ECG by Multivariate Singular Spectrum Analysis. Statistics and its Interface, Vol. 3, pp 399 – 411, 2010

[4]. Arias-Ortega R. and Gaitan-Gonzalez M. J. Single Channel Abdominal ECG Algorithm for Real-Time Maternal and Fetal Heart Rate Monitoring. Revista Mexicana De IngenieraBiomedica, Vol. xxxi, Num. 2, pp 111 – 118, December, 2010.

[5]. MahaShadaydeh, Yegui Xiao and RababKriedieh Ward. Extraction of Fetal ECG Using Adaptive Voterra Filters. The 16th European Signal Processing Conference, Lausanne, Switzerland, August 25 – 29, 2008.

[6]. Walid A Zgallai. Non-Invasive Foetal Heartbeat Detection Using Bispectral Contour Matching. International Conference on Electronics, Biomedical Engineering and its Applications, Dubai, pp 239 – 243, January 7 – 8, 2012.

[7]. Swarnatha R. and Prasad D. V. Interference Cancellation in FECG Using Wavelet-Adaptive Filtering Technique. Journal of Engineering and Applied Sciences, Vol. 4, nos 5 – 6, pp 353 – 357, 2009.

[8]. Mariano Ruffo, Mario Cesarelli, Craig Jin, Gaetano Gargiulo, Alistair McEwan, Collin Sullivan, Paolo Bifulco, Maria Romano, Richard W. Shephard and Andre Van Schaik. Non – Invasive Foetal Monitoring with Combined ECG-PCG System. Biomedical Engineering Trends in Electronics, Communications and Software, pp 348 – 366, January, 2011. www.intechopen.com

[9]. Jimenez-Gonzalez A. and James C. J. Source Separation of Foetal Heart Sounds and Maternal Activity from Single-Channel Phonograms: A Temporal Independent Component Analysis Approach. Computers in Cardiology, Vol. 35, pp 949 – 952, 2008.

[10]. EbrahimKholdi, NooshinBigdeli and KarimAfshar. A New GA-Based Adaptive Filter for Fetal ECG Extraction. World Academy of Science, Engineering Technology, Vol. 54, pp 240 – 244, 2011.

[11]. Hasan M. A., Reaz M. B. I., Ibrahimy M. I., Hussain M. S., and Uddin J. Detection and Processing Techniques of FECG Signal for Fetal Monitoring. Biological Procedures Online, Vol. 11, No 1, pp 263 – 295, 2009. www.springerlink.com

[12]. KokBengGan, Edmond Zahedi and Mohd. Ali. Application of Adaptive Noise Cancellation in Transabdominal Fetal Heart Rate Detection Using Photoplethysmography. Pp 142 – 156. www.interopen.com

[13]. Camps G., Martinez M. and Sofia E. Fetal ECG Extraction Using an FIR Neural Network IEEE, Computers in Cardiology, Vol. 28, pp 249 – 252, 2001.

[14]. Kam A. and Cohen A. Detection of Foetal ECG with IIR Adaptive Filtering and Genetic Algorithms. IEEE International Conference on Acoustics, Speech and Signal Processing, Vol. 4, pp 15 – 19, 1999.

American Journal of Engineering Research (AJER)
e-ISSN : 2320-0847 p-ISSN : 2320-0936
Volume-3, Issue-10, pp-75-83
www.ajer.org
Research Paper Open Access

An Interpolation Process on the Roots of Hermite Polynomials on Infinite Interval

Rekha Srivastava
Deptt. Of Mathematics And Astronomy Lucknow University, Lucknow, INDIA

ABSTRACT: For given arbitrary numbers $d_k, k = 1(1)n-1, d_k^*, k = l(1)n-1$ and $d_k^{**}, k = 1(1)n$, we seek to determine explicity polynomials $R_n(x)$ of degree atmost 3n-3 (n even), given by:

(1)
$$R_n(x) = \sum_{k=1}^{n-1} d_k U_k(x) + \sum_{k=1}^{n-1} d_k^* V_k(x) + \sum_{k=1}^{n} d_k^{**} W_k(x),$$

Such that

$$R_n(y_k) = d_k, \quad k = 1(1)n-1,$$
$$R_n^{'}(y_k) = d_k^*, \quad k - 1(1)n-1$$
$$\text{and}$$
$$R_n(x_k) = d_k^{**}, k = 1(1)n,$$

where $\{x_k\}_{k=1}^{n}$ are the zeros of n^{th} Hermite polynomial $H_n(x)$ and $\{y_k\}_{k=1}^{n-1}$ are the zeros of $H_n^{'}(x)$.
Let the interpolated function f be continuously differentiable satisfying the conditions:

$$\overset{Lim}{|x|} \to +\infty x^{2v} f(x) \rho(x) = 0, \quad \gamma = 0, 1, 2., \ldots..$$
and
$$\overset{Lim}{|x|} \to +\infty x^{2v} \rho(x) f'(x) = 0, \quad \text{where } \rho(x) = e^{-x^2/2},$$

further in (1) $d_x = f(y_k), \ k = (1)n-1,$

$$d_k^* = f'(y_k), \delta\kappa = \circ\left(e^{\delta y^2 k} \omega(f', \frac{1}{\sqrt{n}} \right), k = 1(1)n-1, \circ < \delta < 1$$

$d_k^{**} = f'(x_k), k = 1(1)n$, then for the sequence of inter polynomials $R_n(n = 2, 4, \ldots)$, we have the estimate

$$e^{-vx^2} \left| f(x) - R_n(f, x) \right| = 0(\omega(f'; \frac{1}{\sqrt{n}}) \log n), \quad v > \frac{3}{2}$$

Which holds the whole real line, O does not depend on n and x and ω is the modulus of continuity of f' introduce by G. Freud.

Keywords: Hermite, Interpolation

I. INTRODUCTION

Earlier Pal [8] proved that when function values are prescribed on one set of n points and derivative values on another set of $n-1$ points, then there exists no unique polynomial of degree $\leq 2n-1$, but prescribed function value at one more point not belonging to the former set of n points there exists a unique polynomial of degree $\leq 2n-1$. Eneduanya [2] proved its convergence on the roots of $\pi_n(x)$.

Let $$-\infty < x_{n,n} < x^*_{n-1} < \ldots < x^*_{2,n} < x_{1,n} < \infty$$

be a given system of $(2n-1)$ distinct points. $L \cdot$ Szili [11] determined a unique polynomial R_n lowest possible degree 2n-1 (for n even) given by:

$$R_n(x) = \sum_{i=1}^{n} Y_{i,n} A_{i,n}(x) + \sum_{i=1}^{n-1} Y^*_{1,n} B_{i,n}(x),$$

satisfies the conditions:

$$R_n(x_{i,n}) = Y_{i,n}, \quad \text{i} = 1, 2, \ldots n$$

$$R'_n(X^*_{v,n}) = Y'_{v,n}, \quad v = 1, 2, \ldots n-1$$

and

$$R_n(0) = 0$$

If the interpolated function f is continuously differential

$$f(0) = 0 \text{ and } \overset{Lim}{|x| \to \infty} e^{-x^2/2} x^{2v} f(x) = 0, \quad v = 0, 1, 2, \ldots$$

$\overset{Lim}{|x| \to \infty} f'(x) e^{-x^2/2} = 0$, then the sequence $\{R_n(x)\}$ satisfies the relation

$$e^{-vx^2} \left| f(x) - R_n(x) \right| = 0(\omega(f', \frac{1}{\sqrt{2}}) \log n), \quad v > 1$$

which holds on the whole real line and 0 does not depend or n and x.

Further K.K. Mathur and R.B. Saxena [6] extended the results of L. Szili to the case of weighted (0,1,3,)-interpolation on Infinite interval.

In this paper, we consider a special problem of mixed type, (0,1;0)-interpolation on the zeros of Hermite polynomial

(1.1) Let $\{X_k\}_{k=1}^{n}$ and $\{y_k\}_{k=1}^{n-1}$ be the zeros of $H_n(x)$ and $H_n'(x)$, where

The fundamental polynomials of Lagrange interpolation are given by

(1.2) $$1_k(x) = \frac{H_n(x)}{H'_n(x_k)(x - x_k)}, \quad k = 1(1)n.$$

and

(1.3) $$L_k(x) = \frac{H'_n(x)}{H'_n{}'(y_k)(x - y_k)}, \quad k = 1(1)n-1$$

In this paper, study the following:

$(0,1:0)-$ Interpolation on Infinite Interval.

Let n be even, then for given arbitrary sequence of numbers $\{d_k\}_{k=1}^{n-1}, \{d_k^*\}_{k=1}^{n-1}$ and $\{d_k^{**}\}_{k=1}^{n}$, there exists a unique polynomial $R_n(x)$ of degree $\leq 3n-3$, such that

$$\begin{cases} R_n(y_k) = d_k, & k = 1(1)n-1 \\ R_n^{'}(y_k) = d_k^*, & k = 1(1)n-1 \\ and & \\ ,R_n(y_k) = d_k^{**}, & k = 1(1)n \end{cases} \tag{1.4}$$

For n odd, $R_n(x)$ does not exist uniquely. Precisely we shall prove the following:

Theorem 1:

For n even,

$$R_n(x) = \sum_{k=1}^{n-1} d_k U_k(x) + \sum_{k=1}^{n-1} d_k^* V_k(x) + \sum_{k=1}^{n} d_k^{**} W_k(x), \tag{1.5}$$

where $U_k(x)$, $k = 1(1)n-1$ and $W_k(x)$, $k = 1(1)n$ are the fundamental polynomial of the first kind and $V_k(x)$, $k = 1(1)n-1$ are the fundamental polynomials of the second king of mixed type $(0,1:0)$ interpolation. Each such fundamental polynomial is of degree at most $3n-3$, given by:

$$U_k(x) = \frac{H_n(x) L_k^2(x)\left[1 - 2y_k(x - y_k)\right]}{H_n(y_k)}, \quad k = 1(1)n-1 \tag{1.6}$$

$$V_k(x) = \frac{H_n(x) H_n^{'}(x) L_k(x)}{H_n(y_k) H_n^{''}(y_k)}, \quad k = 1(1)n-1 \tag{1.7}$$

and

$$W_k(x) = \frac{H_n^{',2}(x) 1_k(x)}{H_n^{',2}(H_k)}, \quad k = 1(1)n. \tag{1.8}$$

where $1_k(x)$ and $L_k(x)$ are given by (1.2) and (1.3) respectively

Theorem 2:

Let the interpolated function $f : R \to R$ be continuous differentiable, such that

$$\begin{cases} \lim_{|x| \to +\infty} x^{2k} f(x) \rho(x) = 0 \quad (k = 0,1,\ldots) \\ and \\ \lim_{|x| \to +\infty} \rho(x) f'(x) = 0, \text{ where } \rho(x) = e^{-\beta x^2}, \circ \leq \beta < 1. \end{cases} \tag{1.9}$$

Further, taking the numbers δ_k as:

(1.10) $$\delta_k = 0\left(e^{\delta y_k^2}\right) w\left(f';\frac{1}{\sqrt{n}}\right),\ k = 1(1)n-1,\ \circ < \delta < 1,$$

where w is the modulus of continuity of f', then

(1.11) $$R_n(f,x) = \sum_{k=1}^{n-1} f(y_k)U_k(x) + \sum_{k=1}^{n-1} \delta_k V_k(x) + \sum_{k=1}^{n} f(x_k)W_k(x)$$

satisfies the relation:

$$e^{-vx^2}\left|f(x) - R_n(x)\right| = 0\left(\log n\ w\left(f';\frac{1}{\sqrt{n}}\right)\right),\quad v > \frac{3}{2}.$$

which holds on the whole real line and 0 does not depend on n and x.

Remark.

$w(f,\delta)$ denotes the special form of modulus of continuity introduced by G. Freud [3] given by:

(1.12) $$w(f,\delta) = \underset{\circ \le t \le \delta}{Sup}\left\|W(x+t)f(X+t) - W(x)f(x)\right\| + \left\|T(\delta x)W(x)\right\|$$

where

$$T(x) = \begin{cases} |x|, & \text{for } |x| \le 1 \\ 1, & \text{for } |x| > 1 \end{cases}.$$

and $\|\bullet\|$ denotes the sup-norm in $C(R)$. If $f \in C(R)$ and $\underset{|x|\to\infty}{\text{Lim}} W(x)f(x) = 0$, then $\underset{\delta\to\circ}{\text{Lim}} w(f,\delta) = 0$.

II. PRELIMINARIES.

In this section, we shall give some well known result which we shall use in the sequel.

The differential equation satisfied by $H_n(x)$ is given by:

(2.1) $$H_n''(x) - 2xH_n'(x) + 2nH_n(x) = 0$$

(2.2) $$H_n'(x) = 2nH_{n-1}(x).$$

From (1.2), we have

(2.3) $$1_K(x_j) = \begin{cases} 0 & j \ne k \\ & \text{for} \\ 1 & j = k \end{cases},\quad k = 1(1)n$$

(2.4) $$1_k^{'}\left(x_j\right)=\begin{cases}\dfrac{H_n^{'}\left(x_j\right)}{H_n^{'}\left(x_k\right)\left(x_j-x_k\right)}, & j\neq k\\ x_k\ , & j=k.\end{cases}$$

Form (1.3), one has

(2.5) $$L_k\left(y_j\right)=\begin{cases}0 & j\neq k\\ & \text{for} \quad , \quad k=1(1)n-1\\ 1 & j=k\end{cases}$$

(2.6) $$x_k^2 \square \frac{k^2}{n}$$

(2.7) $$H_n(x)=0\left\{n^{-1/4}\sqrt{2^n n!}\left(1+3\sqrt{|x|}e^{x^{2/2}}\right)\right\}, x\in R$$

(2.8) $$H_n^{'}(x)\geq c2^{2+1}\left[\frac{n}{2}\right]!e^{\delta x_k^2}, 0<\delta<1.$$

(2.9) $$\sum_{i=0}^{n-1}\frac{H_i(y)H_i(x)}{2^i i!}=\frac{H_n(y)H_{n-1}(x)-H_{n-1}(y)H_n(x)}{2^n(n-1)!(y-x)}$$

From (1.2) and (2.9) at $y=x_k$, we have

(2.10) $$\left|1_k(x)\right|=\frac{0(1)2^{n+}n!\sqrt{n}e^{\frac{^{v}1}{2}\left(x^2+x_k^2\right)}}{H_n^{'2}\left(x_k\right)},\quad v_1>1$$

(2.11) $$\sum_{k=1}^{n}e^{-\in x_k^2}0\left(\sqrt{n}\right),\quad \text{where} \quad \in>0$$

(2.12) $$\sum_{k=1}^{n}e^{\delta x_k^2}\left(H_n^{'}\left(x_k\right)\right)^{-2}=0\left(2^{n+1}n!\right)^{-1},\quad 0<\delta<1$$

and

(2.13) $$\frac{2^n\left[\left(\frac{n}{2}\right):\right]^2}{(n+1):}\square\, n^{-1/2},\quad \text{n}=1,2,\ldots$$

III. PROOF OF THEOREM 1.

Using the results given in preliminaries and a little computation, one can easily see that the polynomials given (1.6), (1.7) and (1.8) satisfy the conditions:

For $k=1(1)n-1$

(3.1)
$$\begin{cases} U_k(y_i) = \begin{cases} 0 & j \neq k \\ & \text{for} \\ 1 & j = k \end{cases}, \quad j = 1(1)n-1, U_k^{'}(y_j) = 0, \ j = 1(1)n-1 \\ \text{and} \\ U_k(x_j) = 0, \quad j = 1(1)n \end{cases}$$

For $k = 1(1)n-1$

(3.2)
$$\begin{cases} V_k(y_j) = 0, \ j = 1(1)n-1, \quad V_k^{'}(y_j) = \begin{cases} 0 & j \neq k \\ & \text{for} \\ 1 & j = k \end{cases}, \quad j = 1(1)n-1 \\ \text{and} \\ V_k(x_j) = 0, \quad j = 1(1)n \end{cases}$$

For $k = 1(1)n$

(3.3)
$$\begin{cases} W_k(y_j) = 0, \ j = 1(1)n-1, \ W_k^{'}(y_j) = 0, \ j = 1(1)n-1 \\ W_k(x_j) = \begin{cases} 0 & j \neq k \\ & \text{for} \\ 1 & j = k \end{cases}, \quad j = 1(1)n \end{cases}$$

IV. TO PROVE THEOREM 2, WE NEED

Lemma 4.1

For $k = 1(1)n-1$ and $x \in (-\infty, \infty)$, we have,

$$\left|L_k(x)\right| = 0\left(\frac{2^n n! e^{\frac{v_1}{2}\left(x^2 + y_k^2\right)}}{\sqrt{n} H_n^2(y_k)}\right), \quad v_1 > 1 \ \text{and} \ k = 1(1)$$

where $L_k(x)$ is given by (1.3).

Proof.

From (2.9) at $y = y_k$ and using (1.3) and (2.2), we get

$$\left|L_k(x)\right| \leq \frac{2^n (n-1)!}{H_n^2(y_k)} \sum_{i=0}^{n-1} \frac{1}{2^i i!} \left|H_i(x)\right| \left|H_i(y_k)\right|,$$

which on using (2.7) leads the lemma.

V. Estimation of the fundamental polynomials

Lemma 5.1:

For $k = 1(1)n-1$ and $x \in (-\infty, \infty)$

$$\sum_{k=1}^{n-1} e^{\beta y_k^2} \left|U_k(x)\right| = 0\left(\sqrt{n}\right) e^{vn^2}, v > \frac{3}{2} \text{ and } 0 \le \beta < 1,$$

where $U_k(x)$ is given by (1.6).

Proof.

From (1.6), we have

when $\left|x - y_k\right| < n^{1/2}\Big|$

$$\sum_{k=1}^{n-1} e^{\beta y_k^2} \left|U_k(x)\right| \le \sum_{k=1}^{n-1} \frac{e^{\beta y_k^2} L_k^2(x) \left|H_n(x)\right|}{\left|H_n(y_k)\right|}.$$

$$+ \sum_{k=1}^{n-1} \frac{2e^{\beta y_k^2} \left|x_k\right| \left|x - y_k\right| L_k^2(x) H_n(x)}{\left|H_n(y_k)\right|}$$

(5.1) $$= I_1 + I_2$$

Using (2.7), (2.13) and lemma 4.1, we get

(5.2) $$I_1 = 0\left(\sqrt{n}\right) e^{\beta x^2}, v > \frac{3}{2}$$

Similarly, owing to (2.6), (2.7), (2.13) and lemma 4.1, we have

(5.3) $$I_2 = 0\left(\sqrt{n}\right) e^{\beta x^2}, v > \frac{3}{2}$$

On combining (5.2) and (5.3), we get the lemma.

When $\left|x - y_k\right| > n^{1/2}$, using (1.3), we have

$$\sum_{k=1}^{n-1} e^{\beta y_k^2} \left|U_k(x)\right| \le \sum_{k=1}^{n-1} \frac{e^{\beta y_k^2} \left|H_n(x)\right| L_k^2(x)}{\left|H_n(y_k)\right|}$$

$$+ \sum_{k=1}^{n-1} \frac{2e^{\beta y_k^2} \left|y_k\right| \left|H_n(x)\right| \left|H_n'(x)\right| \left|L_k(x)\right|}{\left|H_n(y_k)\right| \left|H'_n(y_k)\right| \,\Big|}$$

$$= I_3 + I_4$$

From lemma 4.1,(2.7) and (2.13) we get

(5.4) $$I_3 = 0\left(\sqrt{n}\right)e^{vx^2}, \quad v > \frac{3}{2}$$

Similarly, using (2.6), (2.7), (2.13), lemma 4.1, (2.1) at $x = y_k$ and (2.2) we get

(5.5) $$I_4 = 0\left(\sqrt{n}\right)e^{vx^2}, \quad v > \frac{3}{2}$$

Owing to (5.4) and (5.5), we get the lemma.

Lemma 5.2

For $k = 1(1)n-1$ and $x \in (-\infty, \infty)$, we have

$$\sum_{k=1}^{n-1} e^{\beta y_k^2}\left|V_k(k)\right| \leq \sum_{k=1}^{n-1} \frac{e^{\beta y_k^2}\left|H_n(x)\right|\left|H_n'(x)\right|\left|L_k(x)\right|}{\left|H_n(y_k)\right|\left|H_n''(y_k)\right|}$$

Using (2.1) at $x = y_k$, (2.2), (2.7), (2.13) and lemma 4.1, we get the required lemma.

Lemma 5.3

For $k = 1(1)n$ and $x \in (-\infty, \infty)$

$$\sum_{k=1}^{n} e^{\beta x_k^2}\left|W_k(x)\right| = 0\left(e^{vx^2}\right), v > \frac{3}{2} \text{ and } 0 \leq \beta < 1.$$

Where $W_k(x)$ is given by (1.8).

Proof.

From (1.8), we have

$$\sum_{k=1}^{n} e^{\beta x_k^2}\left|W_k(x)\right| \leq \sum_{k=1}^{n} \frac{e^{\beta x_k^2} H_n'^2(x)\left|l_k(x)\right|}{H_n'^2(x_k)}$$

Using (2.8), (2.10), (2.12) and (2.13), we get the lemma.

VI. IN THIS SECTION, WE MENTION CERTAIN THEOREMS OF G. FREUD AND L. SZILI REQUIRED IN THE PROOF OF THEOREM 2.

Theorem (G. Freud, Theorem 4[4] and theorem 1[3])

Let $f : R \to R$ be continuously differentiable. Further, let

$$\lim_{|x| \to +\infty} x^{2k}\rho(x) f(x) 0, \; k = 0,1,2,.... \;.$$

and

$$\lim_{|x| \to +\infty} x^{2k}\rho(x) f'(x) = 0,$$

then there exist polynomials $Q_n(x)$ of degree $\leq n$, such that

(6.1) $$\rho(x)\left|f(x)-Q_n(x)\right| = 0\left(\frac{1}{\sqrt{n}}\right)\omega\left(f';\frac{1}{\sqrt{n}}\right), \quad x \in R,$$

where ω stands for modulus of continuity defined by (1.12) and $\rho(x)$ the weight function.

Szili ([11] lemma 4, theorem 4) established the follow

(6.2) $$\rho(x)\left|Q_n^{(r)}(x)\right| = 0(1), r - 0,1 : \; x \in R$$

VII. PROOF OF THE MAIN THEOREM 2.

(7.1) $$Q_n(x) = \sum_{k=1}^{n-1} Q_n(y_k)U_k(x) + \sum_{k=1}^{n-1} Q_n^{'}(y_k)V_k(x) + \sum_{k=1}^{n} Q_n(x_k)^{'} W_k(x)$$

From (7.1) and (1.11), we have

$$\left|R_n(x) - f(x)\right| \leq \left|R_n(f - Q_n)(x)\right| + \left|Q_n(x) - f(Y)\right|$$

$$e^{-vx^2}\left|R_n(x) - f(x)\right| \leq e^{-vx^2}\left|Q_n(x) - f(x)\right|$$
$$+ e^{-vx^2}\sum_{k=1}^{n-1} e^{-\beta y_k^2}\left|f(y_k) - Q_n(y_k)\right|\left|U_k(x)\right|e^{-\beta y_k^2}$$
$$+ e^{-vx^2}\sum_{k=1}^{n-1} \delta_k\left|V_k(x)\right|$$
$$+ e^{-vx^2}\sum_{k=1}^{n-1} e^{-\beta y_k^2}\left|Q_n^{'}(y_k)\right|\left|V_k(x)\right|e^{-\beta y_k^2}$$
$$+ e^{-vx^2}\sum_{k=1}^{n} e^{-\beta y_k^2}\left|f(x_k)\right| - Q_n\left|W_k(x)\right|e^{-\beta y_k^2}$$

Owing to (6.1), (6.2), (1.10) and lemmas 5.1-5.3, theorem follows

Acknowledgement

In this Paper I have got good cooperation from Prof. K.K. Mathur.

REFERENCES

[1] Blazs, J.: Sulyosott (0,2)-interrolacio ultraszferibus polinomk gyokein, MTA III; Oszt. Kozl, 11(1961), pp. 305-338.

[2] Enduanya, S.A. : On the convergence of interpolation polynomials, Analysis, Maths., 11(1985), pp. 12-22.

[3] Freud, G.: On polynomials approximation with the weight exp $\left(-\frac{1}{2}x^{2k}\right)$, ibid, 24 (1973), pp. 367-371.

[4] Freud, G.: On two polynomial inequalities I, Acta Math, Acad. Sci. Hung., 22 (1971), pp. 109-116.

[5] Freud, G.: On two polynomial inequalities II, ibid., 23 (1972) pp. 137-145.

[6] Mathur, K.K. and Sexena, R.B.: On weighted (0,1,3)-interpolation on the abscissas as zeros of Hermite polynomials. Acta. Math Hung., 62 (1-2) (1993), pp. 31-47.

[7] Mathur, K.K. and Srivastava Rekha.: Pal-type Hermite Interpolation on Infinite- interval, Journal of Mathematical Analysis and Applications 192, 346-359 (1995).

[8] Pal L.G.: A new modification of the Hermite Fejer interpolation, Analysis Math. 1 (1975), pp. 197-205.

[9] Szego, G.: Orthogonal polynomials Amer. Math. Soc. Coll. Publ. New York, 1959.

[10] Szili, L.: A convergence theorem for the Pal method of interpolation on the roots of Hermite polynomials, Anal. Math. 11(1985) pp. 75-84.

[11] Szili, L.: Wieghted (0,2)-interpolation on the roots of Hermite polynomials. Annales Univ. Sci. Budapest. Eotvos Sect. Math. 27 (1984), pp. 153-166.

American Journal of Engineering Research (AJER)
e-ISSN : 2320-0847 p-ISSN : 2320-0936
Volume-03, Issue-10, pp-84-89
www.ajer.org

Research Paper Open Access

Smart White Cane – An Elegant and Economic Walking Aid

Rohit Sheth[1], Surabhi Rajandekar[2], Shalaka Laddha[3], Rahul Chaudhari[4]
[1234]*Department of Electronics and Telecommunication Engineering,PVG's College of Engineering and Technology,Pune*

ABSTRACT:*the main aim of this research paper is to provide a simple, affordable yet an efficient solution for the visually impaired. The idea behind the design of the stick was to keep it structurally similar i.e. thin, lightweight and easy to handle, yet give an active feedback to the user regarding hazards in his walking path. The smart white cane uses the ultrasonic sensors arranged in such a way that it detects pits, potholes, downfalls, a staircase (up and down), low lying and knee level obstacles and even those above the waist. The user is notified about the same by the pre-recorded sound messages and a haptic feedback in form of vibrations. This can considerably alleviate the risk of the user injuring himself.*

INDEXTERMS: *ATMega328,Ultrasonicsensor, Sound IC,White cane, walking aid.*

I. INTRODUCTION

There are approximately 37million people across the globe who are blind, over 15 million are from India.Even for the non-visually impaired the congestion of obstacles is sometimes problematic, it's even worse for the visually impaired. People with visual disabilities are often dependent on external assistance which can be provided by humans, trained dogs, or special electronic devices as support systems for decision making. Existing devices are able to detect and recognize objects that emerge on the floor, but a considerable risk is also includes the objects that are at a sudden depth, or obstacles above waist level or stairs. Thus wewere motivated to develop a smart white cane to overcome these limitations.The most common tool that the blind currently use to navigate is the standard white cane. We decided to modify and enhance the walking cane, since blind are only able to detect objects by touch or by cane. The user sweeps the caneback and forth in front of them. When the cane hits an object or falls off of the edge of a stair, the user then becomes aware of the obstacle –sometimes too late. We wanted to provide additional feedback to the user to warn him of objects *before* he runs into them. We accomplished this goal by adding ultrasonic sensors at specific positions to the cane that provided information about the environment to the user through audio feedback.

Smart white cane is specially designed to detect obstacles which may help the blind to navigate care-free. The vibration feedback and the audio messages will keep the user alert and considerably reduce accidents. The cane will warn whenever there are steps ahead and communicate whether they are going up or down accordingly. The intensity of vibrations is an indication of the closeness of an obstacle in the walking path of the user.

II. LITERATURE SURVEY

Numerous attempts have been made in the society to help the blind. "Project Prakash" [1] is a humanitarian mission to help the blind children especially by training them to utilize their brains to learn a set o objects around them. In [2], the stick has a ping sonar sensor to sense the distant objects. It also has a wet detector to detect the water. The micro-controller used is PIC microcontroller. The microcontroller circuit is on the outside of the stick but is protected with a code so its security cannot be breached. The only feedback given to the user is through the vibration motor.In [3], three sensors are used viz. ultrasonic, pit sensor and the water sensor. Even this is a PIC based system. The feedback given is through the vibration as well as the speaker/headphones. There is a GPS system where-in the user has to feed his location. No information on how a blind man would do that. Also they haven't mentioned anything about the size and shape of their cane and neither about the placement of their circuitry.

In [4], the author has made a detachable unit consisting of an ultrasonic sensor and a vibration motor. It can be fit on any stick. It detects obstacles up to 3m. The vibration feedback varies in the intensity as the obstacles comes nearer. Many different approaches have been taken with the primary purpose of creating a technology to aid the visually impaired. The priorities set by different authors are different leaving a scope of improvement in every application.

SYSTEM DESIGN AND IMPLEMENTATION

Figure 1:Block Diagram of the system

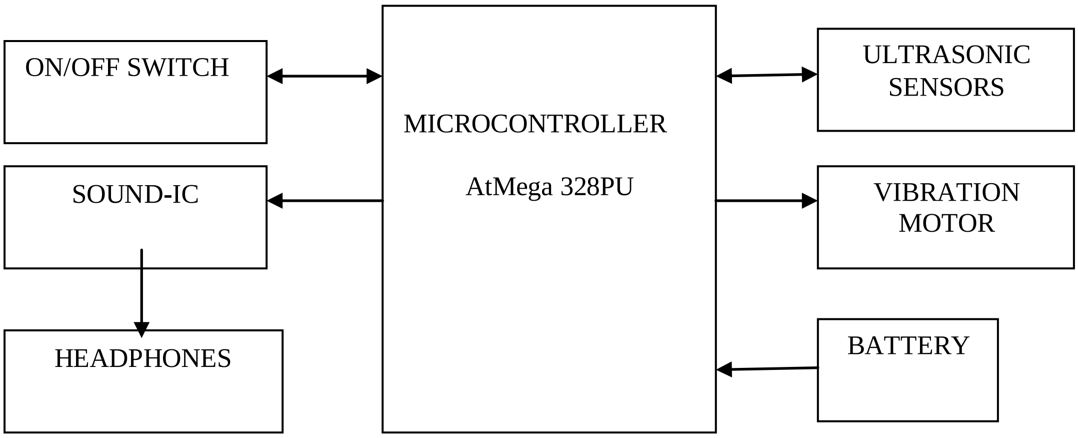

CIRCUIT DIAGRAM

SHEET 1-

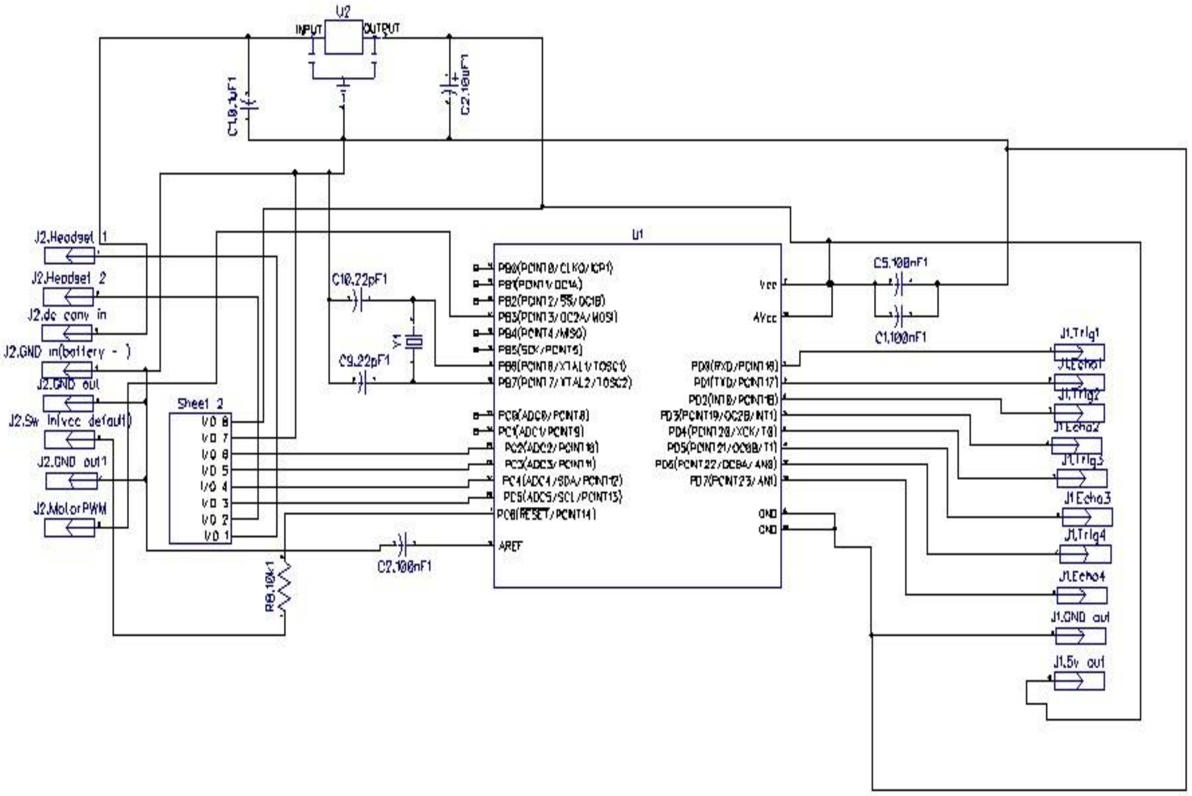

Sheet 2: Sound IC (Hierarchical Block)

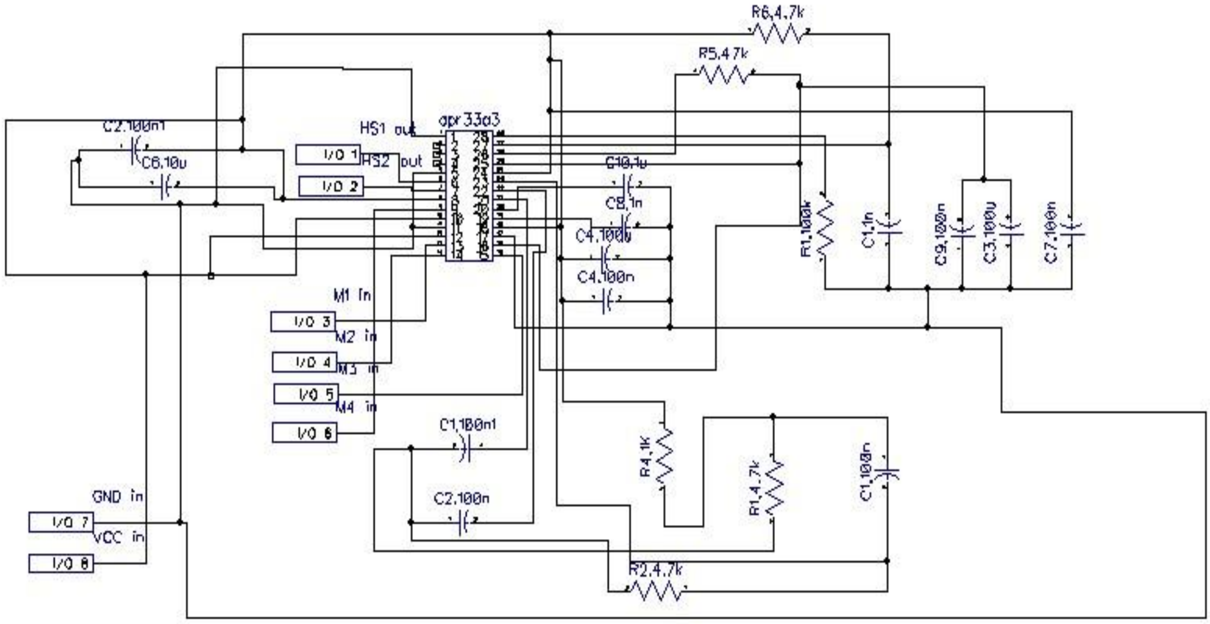

The major components of the Smart White Cane are as follows:

- ATMega328PU microcontroller
- HC-SR04 Ultrasonic Sensor Module
- Sound IC – APR33a3
- Vibration Motor

1. **ATmega328-PU µC:**
   Features:
   28 Pin I/O
   RESET Pin NO. 1 (ACTIVE LOW)
   Crystal Pins at 9-10 PIN
   Software Declarable Serial Ports

2. **HC-SR04 Ultrasonic Sensor module**
   Features:
   Working Voltage - DC 5 V
   Working Current - 15mA
   Working Freq. - 40Hz
   Max Range - 4m
   Min Range - 2cm
   Measuring Angle - 15 degree
   Trigger Input Signal - 10uS TTL pulse
   Echo Output Signal - Input TTL lever signal and the range in proportion
   Dimension - 45*20*15mm

3. **APR33a3**
   Features:
   Operating Voltage Range: 3V ~ 6.5V
   Single Chip, High Quality Audio/Voice Recording & Playback Solution
   Voice Recording Length APR33A3- 680 sec
   Audio Processor- Powerful 16-Bits Digital
   Memory - Non-volatile Flash
   Built-in Audio-Recording Microphone Amplifier
   Resolution - 16-bits
   Averagely 1, 2, 4 or 8 voice messages record & playback

III. HARDWARE DESCRIPTION

We decided to place our entire circuitry inside the cane.
The following considerations were made:

- The Stick shouldn't be bulky.
- Enough space to accommodate PCB and sensors.
- PCB should be as small as possible.
- Should be sturdy so as to protect the PCB.

Thus we choose a PVC pipe with a 3.5cm diameter and Height of 2.8feet.

To reduce the size of our PCB we choose all components as SMD with 0805 dimensions for capacitors and resistors wherever possible and also an SMD package of voltage regulator 7805(T0-252-Dpack) along with SOIC DIP packages for both Atmega328 and Apr33a3.

For vibration feedback, we provided the vibration motor at the handle (like the ones in mobile phones) and also for voice messages we have given headset port also at the handle.

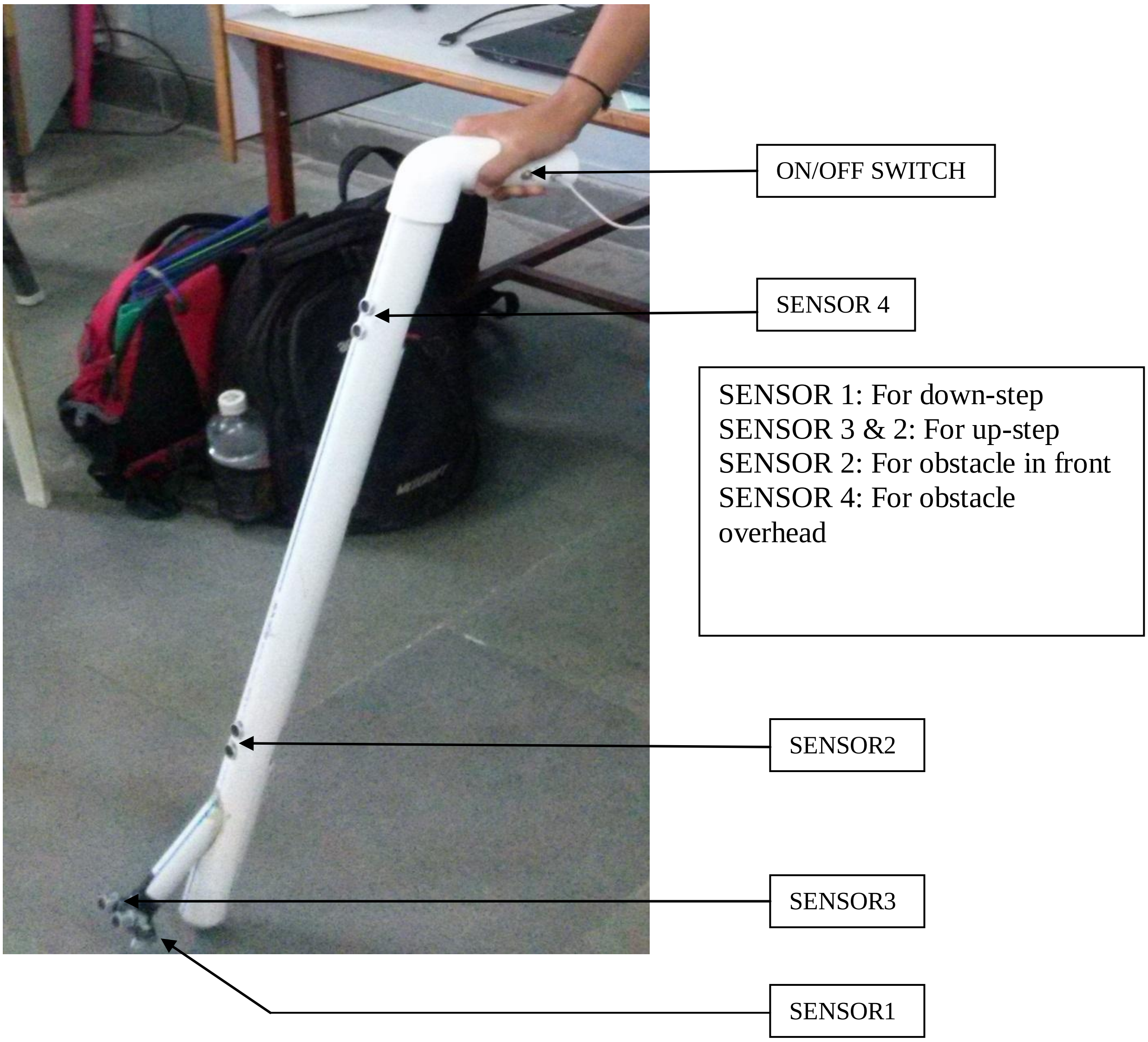

SENSOR 1: For down-step
SENSOR 3 & 2: For up-step
SENSOR 2: For obstacle in front
SENSOR 4: For obstacle overhead

IV. SALIENT FEATURES

- Affordability **-** The estimated price for mass production should not exceed Rs.500. As majority of blind population in the developing countries are poor, this provides an economical solution.
- Versatility – Apart from the low level obstacles even the ones above waist and types of staircases can be determined.
- Design –
  The bottom wheel – The blind generally tap while sweeping which is avoided by using a wheel.
- The entire circuitry along with the battery compartment is concealed inside the stick reducing the risk of damage to the circuit and reducing bulkiness.
  Handle – ON/OFF switch, vibration feedback and the audio jack is provided on the handle itself.
- Audio feedback – Short pre-recorded messages informing the user about the obstacles are played. The priority of the obstacles is set on the basis of the risk

V. CONCLUSION

The smart white cane is a practically feasible product and convenient to carry around like any other walking stick. This could also be considered a crude way of giving the blind a sense of vision. This also reduces the dependency on other family members, friends and guidance dogs while walking around. It can serve as a benchmark in aid for the blind like crutches are for the paraplegic.

Future Scope: A global positioning method will used to find the position of' the user using the global positioning system (GPS) and guidance to their destination will be given to the user by voice navigation.A wall-following function can also be added so that the user can walk straight along a corridor in an indoor environment. Some more applications like vehicle detection, slippery floor, on-coming vehicle detection and fire or smoke alarm can also be included.

REFERENCES

[1] Project Prakash" http://web.mit.edu/bcs/sinha/prakash.html
[2] Mohammad Hazzaz Mahmud, "Smart walking stick - an electronic approach to assist visually disabled persons" http://www.ijser.org/researchpaper%5CSmart-walking-stick-an-electronic-approach-to-assist- visually-disabled-persons.pdf
[3] G.Gayathri, "Smart Walking Stick for visually impaired"http://ijecs.in/issue/v3-i3/8%20ijecs.pdf
[4] Singh Vaibhav, "'SMART' CANE FOR THE VISUALLY IMPAIRED: DESIGN AND CONTROLLED FIELD TESTING OF AN AFFORDABLE OBSTACLE DETECTION SYSTEM"http://assistech.iitd.ernet.in/doc/Transed2010_Smar t_Cane.pdf
[5] Mohd Helmy Abd Wahab, "Smart Cane: Assistive Cane for visually impaired people http://arxiv.org/ftp/arxiv/papers/1110/1110.5156.pdf

American Journal of Engineering Research (AJER)
e-ISSN : 2320-0847 p-ISSN : 2320-0936
Volume-03, Issue-10, pp-90-98
www.ajer.org

Research Paper Open Access

Modified Wilkinson Compact Wide Band (2-12GHz) Equal Power Divider

Sandeep kumar[1], Mithilesh kumar[2]
[1]*(Electronics Engineering Department, University College of Engineering RTU, Kota, Rajasthan, India)*
[2]*((Electronics Engineering Department, University College of Engineering RTU, Kota, Rajasthan, India)*

ABSTRACT : *A novel compact wideband (2-12 GHz) Wilkinson equal power divider on microstrip line is proposed in this paper. In this paper, a novel approach to the design of a Wideband (2-12) power divider is presented. In order to achieve the wideband performance, the divider is established by introducing variable width of microstrip line between input lines to output lines of different impedance. Finally, a compact power divider is designed, and it is demonstrated that 3 dB powers splitting from one input port to two output ports is achieved. In addition, good impedance matching at all the three ports and excellent isolation between two output ports are obtained over the specified 2-12 GHz WB range. The simulated and measured input return loss is approximately 21 dB at center frequency 7.92 GHz. The average insertion loss, and group delay are around 3 dB (including the 3-dB power-dividing insertion loss) and around 0.09 ns over across the WB. In addition, the measured and simulated isolation between the output ports is approximately 25 dB at center frequency 7.92 GHz.*

KEYWORDS - *impedance matching, microstrip components, Power divider, power-dividing ports, wideband (WB), Wilkinson power divider, Ultra-wide band (UWB).*

I. INTRODUCTION

A power divider for RF power division and combination is basic passive component and applied to many millimeter-wave systems and needed in many microwave applications such as phased antenna arrays and power amplifiers, antenna feeders, etc. Because WB technology has the characteristics of low cost, high data transmission rate, and very low power consumption, it is promising and attractive in many industrial electronic systems [9]. However, its narrow bandwidth is a serious barrier for the WB application. Among them, the wideband (WB) devices have attracted great interest in industrial communities on exploring various WB industrial electronic systems since the U.S. Federal Communications Commission released the unlicensed use of UWB (3.1–10.6 GHz) for commercial communication applications in 2002 [10]. The disadvantage of Waveguide based power divider is with an increasing number of power-dividing ports, the radius of the radial waveguide in [4] or the conical line in [6] will increase, which will cause higher order modes to be presented in the radial -waveguide or conical-line power dividing cavity due to discontinuities, and cannot be suppressed effectively, but in microstrip based power divider has not this type problem.

A UWB power divider with good isolation performance is proposed in [5], this divider is formed by installing a pair of branching in Stepped-impedance lines to two symmetrical output ports. Another different method to achieve UWB is inter- connection of two ways Wilkinson power divider is given in [2]. And other method is dividing ratio equalization of power divided combiner used in a power amplifier [3]. In this paper the structure is a planar structure, here planar structure means taken ground then substrate and at the last patch. Many structures are fabricated for power divider is based on waveguide structure [4].

In this paper, a novel approach to the design of an Ultra-Wideband power divider is presented. In order to achieve the ultra-wideband performance, the divider is established by introducing variable width of microstrip line between input lines to output line of different impedance. Good insertion/return losses are achieved as demonstrated in simulation and measurement. In the following, the design results indicate that the proposed WB power divider has several advantages, such as wide bandwidth, large one input and two output ports (compact and simple design), excellent input impedance matching, low insertion loss, good balance of amplitude and phase at output ports, and flat group delay within the WB. It can be noted that such a structure can be utilized to a WB active power-combining system and can include large numbers of active power devices to provide high power. Obviously, this type of microstrip planar UWB power divider is different from the waveguide based power dividers [7]–[8].

II. STRUCTURE AND DESIGN OF TWO-WAY POWER DIVIDER

2.1 STRUCTURE OF PROPOSED POWER DIVIDER

Fig.1 shows the schematic diagram of the traditional two-section Wilkinson power divider with matched port. For better coupling and impedance matching, as can be seen in Fig. 2. The proposed WB power divider is simulated with commercial software CSTv11 and measured by Agilent N5230C network analyzer. The dimensions of a power divider with relative good performance were determined. The isolating resistor *R*=100Ω. Basically here the structure is based on the method of microstrip variable width. And for improving the large bandwidth using variable width technology which is shown in Fig.2 shown the width and length of substrate. The WB power divider has simulated and measured on the FR-4 substrate with a dielectric constant of 4.01 and a thickness of 1.0 mm. and the isolator resistor R=100Ω has used. And all dimensions are shown in TABLE 1.

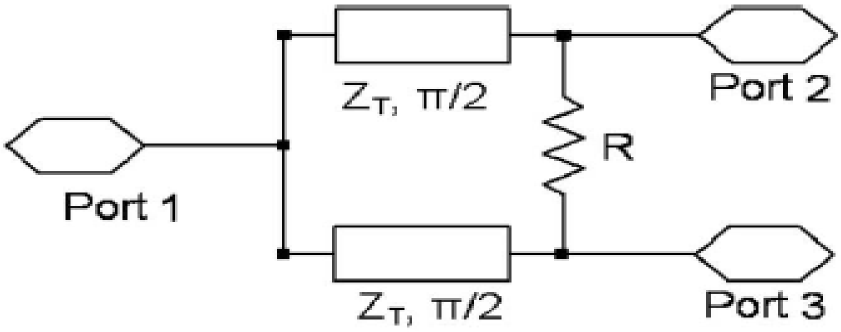

Fig.1 Traditional two-way Wilkinson power divider

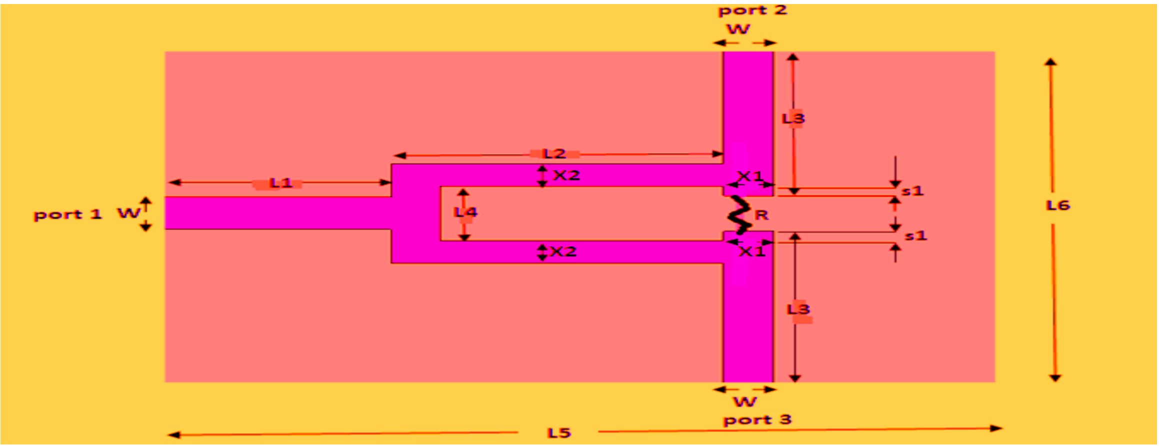

Fig.2 Layout of Proposed WB Power Divider (Simulated Structure on CST) (Dimension 15mm × 10.3mm)

Fig.3 fabricated Structure of Proposed WB Power Divider (Dimension is 15 mm×10.3 mm)

TABLE 1: DIMENSIONS OF THE POWER DIVIDER (UNIT: MILLIMETERS)

Dimension	L1	L2	L3	L4	L5
Calculated value	4.1	6.0	4.2	1.7	15
Dimension	L6	X1	X2	W	S1
Calculated value	10.3	0.9	0.7	1.0	0.3

2.2 CIRCUIT DESIGN OF PURPOSED POWER DIVIDER

Fig.3 (a) shows a standard circuit model of two-way power divider. Here loads are represented by R_1, R_2 and Z_{21}, Z_{22} and θ_1 for characteristic impedances and electrical lengths of the upper and lower transmission lines. The characteristic impedances and electrical lengths of additional transmission lines are denoted by Z_{22} and θ_2 .

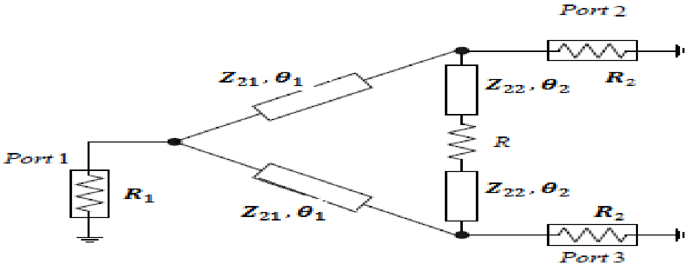

Fig. 3(a) circuit model

2.3 EVEN-MODE ANALYSIS

We define the fed power ratio of port 3 to port 2 to be k^2 to 1. The following equation holds under the condition that the voltages at port 2 and port 3 are equal.

$$k^2 = \frac{|S_{31}|^2}{|S_{21}|^2} \tag{1}$$

When the circuit shown in Fig. 3(a) is excited by the even-mode, the circuit can be divided into two equal circuits as shown in Fig. 3(b). When the ratio of the upper circuit elements to the lower circuit elements is k^2 to 1.the two equal circuits have symmetric voltage distribution, and no currents flow to the isolation resistor [1], [11].

Therefore,

$$R_{12} = (1+k^2)\,R_1 \tag{2}$$

Let Y_{INb}^{eve} denote input admittance from port 2 to port 1. From the matching condition, the relationship between Y_{INb}^{eve} and terminal admittance $1/R_2$ is given by the following equation

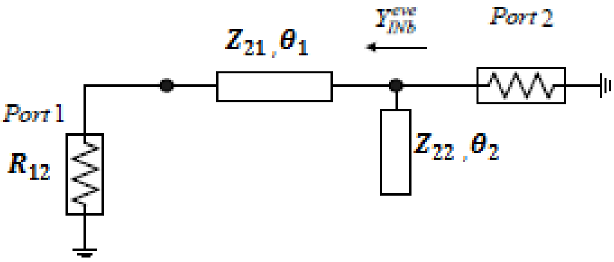

Fig.3 (b) even mode symmetrical circuit of equivalent circuit

$$Y_{INb}^{eve} = \frac{Z_{21}+jR_{12}\tan\theta_1}{Z_{21}(R_{12}+jZ_{21}\tan\theta_1)} + j\frac{\tan\theta_2}{Z_{22}} = \frac{1}{R_2} \tag{3}$$

From the real part of (3)

$$\frac{Z_{22}}{Z_{21}} = -\frac{Q}{P} \tag{4}$$

and from the imaginary part,

$$1-\frac{Z_{21}^2}{R_{12}R_2} = 1-\frac{Z_{21}^2}{(1+k^2)R_1} = \frac{P}{(\tan\theta_1)^2} \tag{5}$$

where

$$P = \frac{R_{12}}{R_2} - 1 = \frac{(1+k^2)R_1}{R_2} - 1 \tag{6}$$

$$Q = (\tan\theta_1)\,(\tan\theta_2) \tag{7}$$

2.4 ODD-MODE ANALYSIS

When ports 2 and 3 are excited by an equal amplitude and out-of-phase current, the circuit is divided as shown in Fig. 3(c).

Therefore, we get the following equation:

$$k^2 = \frac{|S_{31}|^2}{|S_{21}|^2} \tag{8}$$

Calculating the below circuit likewise by even-mode analysis,

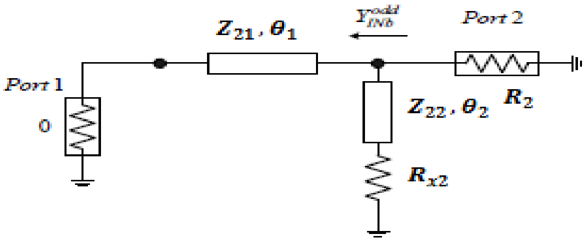

Fig.3 (c) odd mode symmetrical circuit of equivalent circuit

$$Y_{INb}^{odd} = \frac{Z_{22}+jR_{x2}\tan\theta_2}{Z_{22}(R_{x2}+jZ_{22}\tan\theta_2)} + \frac{1}{jZ_{21}\tan\theta_1} = \frac{1}{R_2} \tag{9}$$

From the real part,

$$1-\frac{R_{x2}}{R_1} = 1-\frac{(\tan\theta_2)^2}{P} \tag{10}$$

and from the imaginary part

$$\left\{\frac{Z_{22}}{Z_{21}} + Q\right\}R_{x2} = \frac{Z_{22}^2}{R_2}Q \tag{11}$$

Solving (4), (5), (10), and (11),

$$Z_{21} = \sqrt{\frac{(1+k^2)Z_{22}{}^2 R_1 R_2}{(1+k^2)R_1 R_2 + Z_{22}{}^2(1-P)}} \tag{12}$$

$$R_{x2} = \frac{Z_{22}{}^2\,P}{(1+k^2)R_1} \tag{13}$$

$$R = (1+\frac{1}{k^2})\,R_{x2} = \frac{Z_{22}{}^2\,P}{k^2 R_1} \tag{14}$$

$$\theta_1 = \tan^{-1}[\pm\sqrt{\{\frac{(1+k^2)R_1 R_2 P}{(1+k^2)R_1 R_2 - Z_{21}{}^2}\}}] \tag{15}$$

$$\theta_2 = \tan^{-1}[\pm\sqrt{P\{1-\frac{Z_{22}{}^2 P}{(1+k^2)R_1 R_2}\}}]$$

$$= \tan^{-1}[\pm\sqrt{P\{1-\frac{Z_{22}{}^2 P}{(1+k^2)R_1 R_2}\}}] \tag{16}$$

Equation (6) must be positive from (14) and (16). Therefore

$$\frac{R_2}{R_1} < 1 + k^2 \tag{17}$$

Since the above equations are incomplete, one parameter needs to be determined to determine all of the circuit parameters. If the sign of (15) is negative, the sign of (16) must be positive by (4) and (7). Regarding the ranges of all values, firstly, (15) gives the ranges of Z_{21} and θ_1, and, secondly, (15) gives the range of Z_{22}. Finally the ranges of θ_2 and R are determined. Consequently,

$$\sqrt{(1+k^2)R_1 R_2} \geq Z_{21} > 0 \tag{18}$$

$$\sqrt{\frac{(1+k^2)R_1 R_2}{P}} \geq Z_{22} > 0 \tag{19}$$

$$(1+k^{-2})R_1 \geq R > 0 \tag{20}$$

$$\pi\,(n+1) - \tan^{-1}\sqrt{P} > \theta_1 \geq n\pi + \frac{\pi}{2} \tag{21}$$

$$m\pi + \tan^{-1}\sqrt{P} > \theta_2 \geq m\pi \tag{22}$$

Where n and m are any integer

Once one of these parameters is given within these ranges, all other values are determined. If k^2 and R_1=R_2=1, the above expressions are the same as the expressions presented by Horst [12].

III. SIMULATION AND RESULTS

Fig.6 shows the simulated and measured results of the designed WB power divider. Fig.6 as can be seen in this graph, the input power has been split equally to the two output ports. The isolation is less than -10 dB, and the two insertion loss and the return loss show the excellent performance over the WB band Very good input port matching is achieved with $S11$, simulated -21.2 dB and measured -21 at the design frequency (7.92 GHz) as shown in Fig. 6, and the agreement between both full-wave simulators can be clearly seen. Fig.7 (a) shows that the transmission parameters ($S21$and $S31$) are very close to their theoretical values of simulated 3 dB and measured -2.91 dB at the design WB, which shows the equal-split behavior of this divider. The small discrepancies could be due to losses and discontinuities. Fig. 8 shows the isolation between the 2-way power divider output ports. As mentioned before, the isolation between the output ports at the design frequency (7.92 GHz) is as good as that in the Wilkinson power divider. From Fig.8, it can be seen that $S23$ equal to simulated -25.2 dB and measured -24.28 at design frequency 7.92 GHz, while it is noted that the best isolation seems to be between ports 2 and 3 less than -10 dB at the WB. Fig.5 shows the output ports matching, Parameters $S22$ and $S33$, WB power divider. As mentioned in the introduction, the output ports are matched at the design frequency, and according to Fig. 5, the output ports return losses are all less than -10 dB at the design frequency (7.92 GHz). In addition, the simulated group delays show good linearity within WB, as shown in Fig. 9. The mean of flat group delay is the signal from input port to output ports reach at same time so there is no delay. Here at WB the total group delay is 0.09 ns which is very negligible group delay between output signals. All simulated and measured results are shows in TABLE 2.

TABLE 2: SIMULATED AND MEASURED RESULTS OF WIDE-BAND POWER DIVIDER

S. No.	Freq. Band (GHz)	Reso-nant Freq. (GHz)	Isolation (dB)		Return Loss (dB)		Group delay (ns)	Insertion loss (dB)	
			Simulated	Measured	Simulated	Measured	Simulated	Simulated	Measured
1	2-12	7.92	25.2	24.28	S11=21.2 S22=17.85 S33=17.82	S11=21 S22=18.2 S33=18.4	0.090	3	2.91

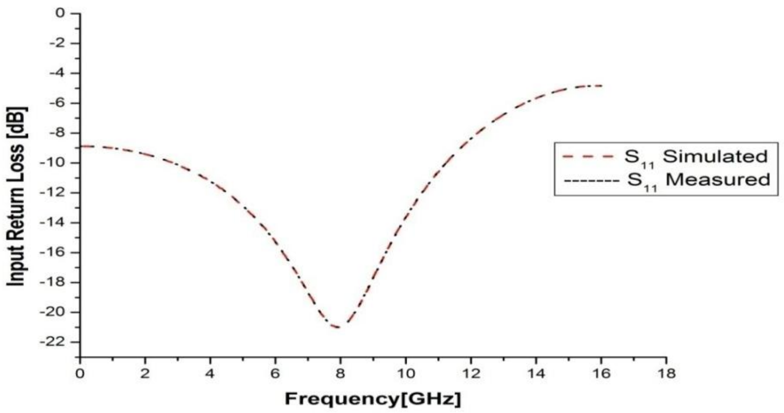

Fig.4 Return loss of Proposed Power Divider

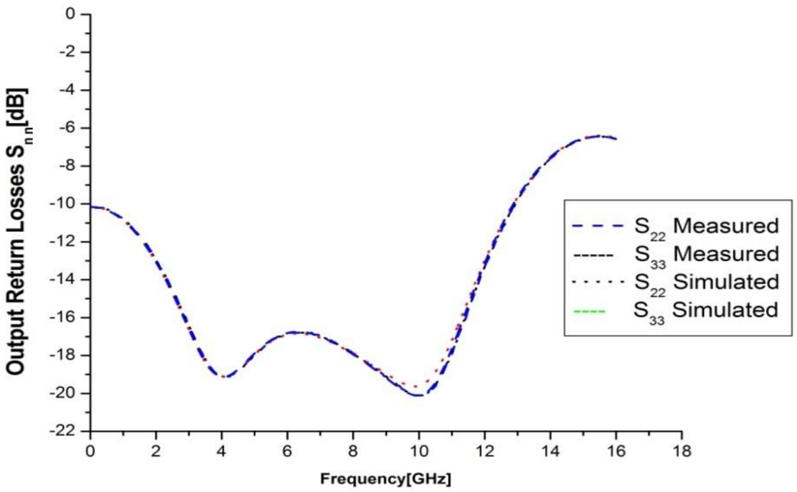

Fig.5 Return loss at output ports (n=2, 3)

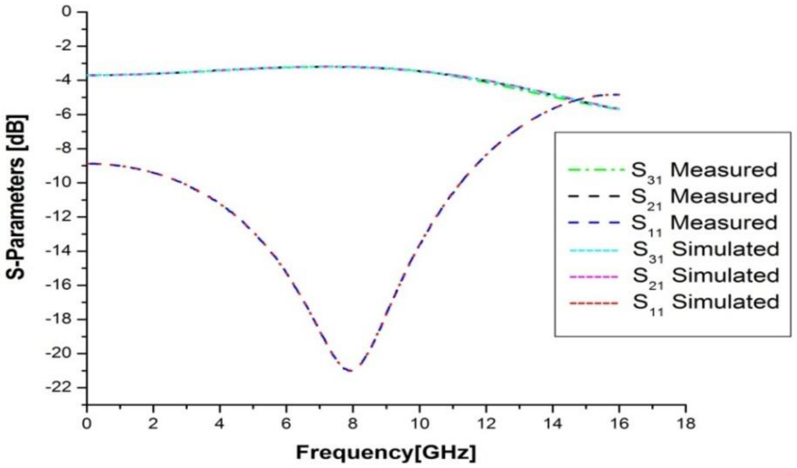

Fig.6 Simulated and measured result of the proposed power divider

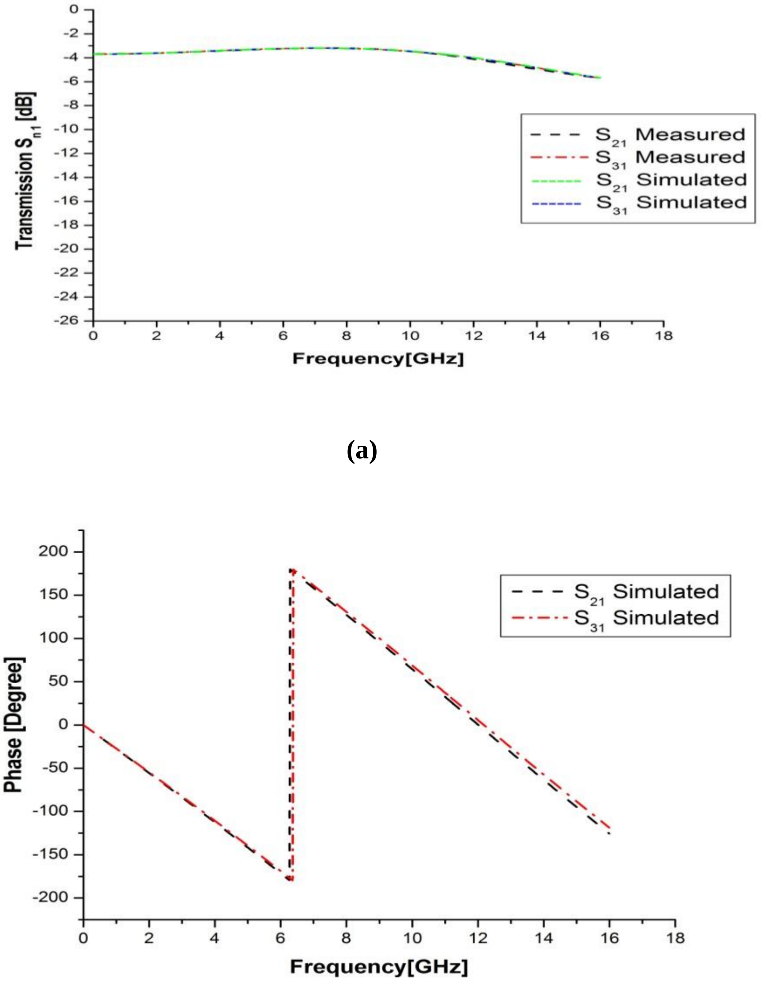

(a)

(b)

Fig.7 Simulated Transmission coefficients of WB power divider (*n* = 2, 3). (a) Amplitude. (b) Insertion Phase

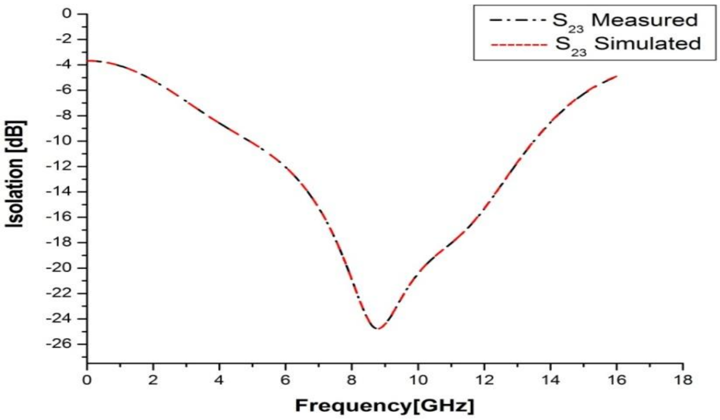

Fig.8 Isolation between output ports

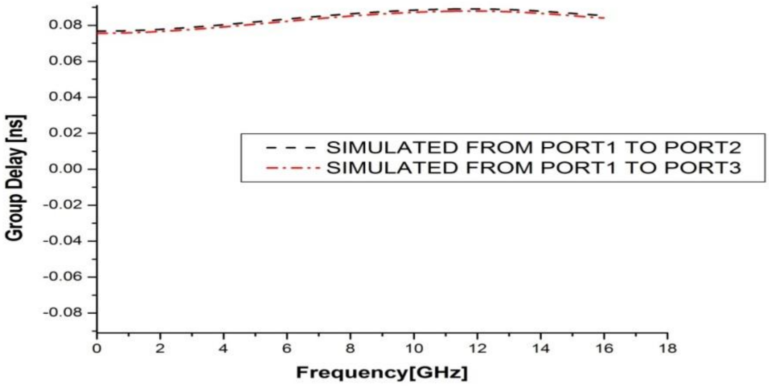

Fig. 9 Simulated and measured group delays of the proposed power divider

IV. CONCLUSION

In this paper, a unique method of designing an ultra-wideband (WB) equal power divider using the divider is established by introducing variable width of microstrip line between input lines to output line of different impedance on microstrip line is proposed. Through the simulation, good power splitting, impedance matching and isolation can be obtained. The structure occupies an area of 15mm × 10.3 mm. The circuit integration is enhanced because of the special placement of the isolation elements. Simulated and measured results show that it makes the 3 dB power divider work preferably in a wide bandwidth. All simulated and measured result matched by measured result. It is proven by calculation that the response of the dividers is symmetrical about the center frequency.

REFERENCES

[1]. L. I. Parad and R. L. Moynihan, “Split-Tee power divider,” IEEE Trans Microw. Theory Tech., vol. MTT-13, pp. 91-95, Jan. 1965.
[2]. Jiafeng Zhou, Kevin A. Morris, and Michael J. Lancaster, “General Design of Multiway Multisection Power Dividers by Interconnecting Two-Way Dividers”. IEEE Transaction on Microwave Theory and Techniques, Vol. 55, no. 10, October 2007.
[3]. J. Y. Tarui, K. Nakahm, Y. Itoh, and M. Maisunaga, “A method for dividing ratio equalization of power divided combiner used in apower amplifier,” IEICE Trans. (GI), vol. J81-C-I, no.9, pp.553-558, Sept. 1998.
[4]. Y.-P. Hong, D. F. Kimball, P. M. Asbeck, J.-G. Yook, and L. E. Larson, “Single-ended and differential radial power combiners Theory implemented with a compact broadband probe,” IEEE Trans. Microw. Tech., vol. 58, no. 6, pp. 1565–1572, Jun. 2010.
[5]. Sai Wai Wong, Lei Zhu, “Ultra-wideband Power Divider With Good and Wireless Components Letters, vol. 18, Issue 8, pp. 518-520, Aug. 2008.
[6]. D. I. L. de Villiers, P.W. van derWalt, and P.Meyer, “Design of a ten-way conical transmission line power combiner,” IEEE Trans. Lett Microw. Theory Tech., vol. 55, no. 2, pp. 302–308, Feb. 2007. Compon vol. 16, no. 8, pp. 452–454, Aug. 2006.
[7]. K. Song, Y. Fan, and Z. He, “Broadband radial waveguide spatial combiner,” IEEE Microw. Wireless Compon. Lett., vol. 18, no. 2, pp 73–75, Feb. 2008.
[8]. K. Song and Q. Xue, “Planar probe coaxial-waveguide power combiner/ divider,” IEEE Trans. Microw. Theory Tech., vol. 57, no. 11,pp. 2761–2767, Nov. 2009.

[9]. Y. Koike, S. Ishii, and R. Kohno, “DS/chirp hybrid industrial WB for ranging and high reliability communications,” in Proc.14th APCC, 2008, pp. 1–5.

[10]. “Revision of part 15 of the commission’s rules regarding ultra-wideband transmission system, first note and order,”Federal Communication Commission, Washington, DC, ET-Docket 98-153, 2002.

[11]. R. B. Ekinge, “A new method of synthesizing matched broadband TEM- mode three-ports,” *IEEE Trans. Microw. Theory Tech*., Vol. MTT-19, pp. 81-88, Jan. 1971.

[12]. C. I. G., Hsu, L. Ching-Her, et al, “Tri-Band Bandpass Filter With Sharp Passband Skirts Designed Using Tri-Section SIRs,” *IEEE* Microw. Wireless Compon. Lett., Vol. 18, No.1, 19-21, 2008.

American Journal of Engineering Research (AJER)
e-ISSN : 2320-0847 p-ISSN : 2320-0936
Volume-03, Issue-10, pp-99-109
www.ajer.org

Research Paper Open Access

Design and Development of Shell and Tube Heat Exchanger for Harar Brewery Company Pasteurizer Application (Mechanical and Thermal Design)

Dawit Bogale
Lecturer in School of Mechanical and Industrial Engineering
Bahir Dar Institute of Technology,Bahir Dar, Ethiopia

ABSTRACT: *A heat exchanger is a device that is used to transfer thermal energy (enthalpy) between two or more fluids, between a solid surface and a fluid, or between solid particulates and a fluid, at different temperatures and in thermal contact****[1]****.From different types of heat exchangers the shell and tube heat exchangers with straight tubes and single pass is to be under study. Here the redesign takes place because of temperature fluctuation at the 9th zone of the pasteurizer in the Harar Brewery Company. Thermal and mechanical design is run in order to optimize the output temperature of the cold fluid at the last heat exchanger in which it is sprayed on the beer ready for customer use. In thermal design part geometry optimization is done through trial and error. And for Mechanical design part the natural frequency& vortex shedding of different components of heat exchangers are investigated through governing equations of vibrations under dynamic fluid with in tubes. Using computational fluid dynamics (CFD) the heat transfer of the two fluid is investigated using FEM* ***simulation software's Gambit1.3 and Fluent 6.1****and the performance of the STHEx determined in terms of variables such as pressure, temperature, flow rate, energy input/output, mass flow rate and mass transfer rate that are of particular interest in STHEx analysis.*

KEYWORDS: *Enthalpy, Gambit 2.4.6 and Fluent 6.1, Simulation, CFD, STHEx, Pasteurizer*

I. INTRODUCTION

In heat exchangers, there are usually no external heat and work interactions. Typical applications involve heating or cooling of a fluid stream of concern and evaporation or condensation of single- or multicomponent fluid streams. In other applications, the objective may be to recover or reject heat, or sterilize, pasteurize, fractionate, distill, concentrate, crystallize, or control a process fluid. In a few heat exchangers, the fluids exchanging heat are in direct contact. In most heat exchangers, heat transfer between fluids takes place through a separating wall or into and out of a wall in a transient manner. In many heat exchangers, the fluids are separated by a heat transfer surface, and ideally they do not mix or leak**[1]**.But because of vibration induced due to the dynamics of the fluid in the tube there may be linkage in the baffle and the shell wall. The use of the baffles in heat exchangers is to enhance heat transfer through turbulence of the shell side flow and to reduce the vibration (Natural frequency) of the tube.

The STHEx under study for this paper is found in Harar Brewery Company at the 9th zone of the pasteurizer. Here the pasteurizer works in engineering principle's in order to make the bottles adopt for water with maximum temperature and that of minimum temperature. The detail of the working principle of machine is shown in Figure 1 below.

Here for the STHEx in Harar brewery company the two system fluids in which heat is going to be exchanged is water and steam(H_2O in gas state). Steam with mass flow rate of 6000kg/hr enters at 160^0C shell side in which a cool water at 25^0C enters the tube side and out at a designed temperature of 35.5^0C and steam with outlet temperature of shell side at 80^0C but the problem is the out let temperature of the cold fluid will fluctuates frequently and this result in undesirable test in the beer. Having the above information at hand geometry optimization is run using general thermal equations for STHEx heat transfer Q (heat load), pressure drop across the system and optimum insulation insulation cost is calculated. And geometry optimization is done considering tube length, thickness and tube patterns (Triangular or Rectangular Pattern) by doing so the overall heat transfer, Pressure drop and cost are studied and the allowable design is chosen from thermal design point of view. This paper is different from the other papers on STHEx is that here both mechanical design and thermal design is considered including Simulation to investigate the heat transfer of the two fluids.Simulation refers to process of comparing information on the behavior &characteristics of the real system by analyzing, studying or observing the model of the system such a model may be subjected to a variety of operating and environmental conditions and theperformance of the of STHEx determined in terms of variables such as pressure, temperatureflow rate, energy input/output, mass flow rate and mass transfer rate that are of particular interest in STHEx analysis.

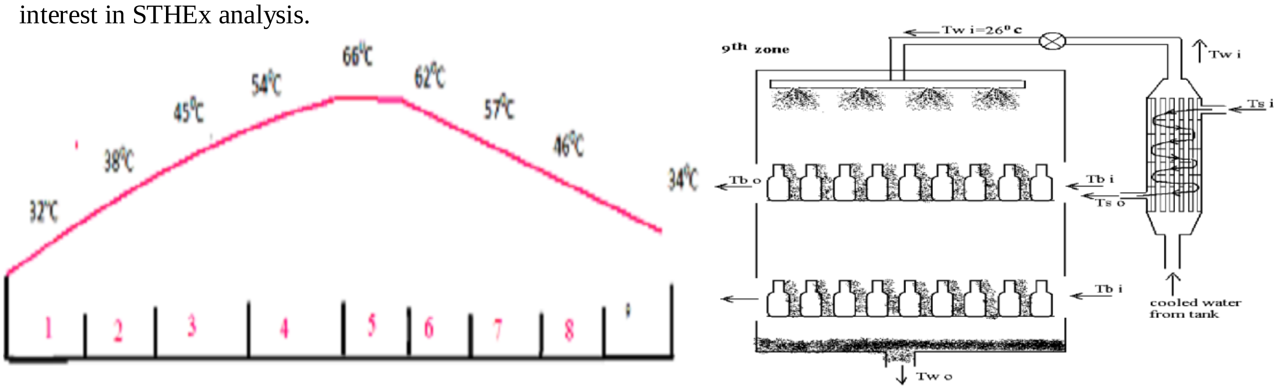

Figure1. Shows a) 9 Zone Temperature (^{0}C) Vs. Time (min) b) 9th zone bottle pasteurized using STHEx9

II. LITERATURE

Shell-and-tube heat exchangers are commonly used in petro-chemical and energy industries for their relatively simple manufacture and adaptability to different operating conditions. Many thermal engineers try to increase the efficiency STHEx by considering different parameters which affects heat transfer between the shell and the tubes.An experimental investigation of heat transfer enhancement for STHEx has been done by the Xi'an Jiootong University, Xi'an, China, Department of Refrigeration and Cryogenics Engineering, School of Energy and Power Engineering**[2].**For the purpose of heat transfer enhancement, the configuration of a STHEx was improved through the installation of sealer in the shell side .the gaps between the baffle plates and shell is blocked by the sealers, which effectively decrease the short-circuit flow in the shell side.The result of heat transfer experiment show that the shell-side heat transfer coefficient of the improved heat exchanger increased by 18.2-25.5%, the overall coefficient of heat transfer increased by 15.6-19.7%, and the exergy efficiency increased by 12.9-14.1%.pressure losses increased by 44.6-48.8% with the sealer installation, but the increments of required pump power can be neglected compared with the increment of heat flux. The heat transfer performance of the improved heat exchanger is intensified, which is an obvious benefit to the optimizing of heat exchanger design for energy conservation**[2]**.

Other experimental investigation on heat transfer enhancement for STHEx has been done by Amirkabir university of technology, faculty of technology, Teheran iran they tried to obtain experimentally the heat transfer coefficient and pressure drop on STHEx for three different types of copper tubes (smooth, corrugated and with micro-fin) also experimental data has been compared with theoretical data available. and correlation have been suggested for both Nusseltnumber for the three tube types the experimental setup has three STHEx in conjunction with electric boilers and chiller as well as air cooled condenserFor comparison of experimental and theoretical results bell's method is used variation of Nu and Eu with respect to Re.Pr is shown and they tried to conclude the following points, first the experimental values of Nu are higher than the predicted values, especially for smooth and corrugated tubes, but are closer for micro fin tubes, two the experimental values for pressure drop are higher than those of predicted empirically this is due to complicated flow pattern at low Reynolds number is given it is seen that micro-fin having the lowest Nu this is may be due to trap of the fluid inside tiny space between fins which prevent mixing of main streams when the flow is not turbulent**[3].**The 3Rdproject in STHEx is enhancing the heat transfer performance of triangular pitch and tube evaporators using an spray technique by southern Taiwan university , department of

mechanical engineering this study show that in compact STHEx the dry out problem can be delayed by use of an interior spray method in which each heater tube within the bundle is sprayed simultaneously by to nozzles. The experimental results show that the shell side heat transfer coefficient obtained using the proposed spray technique are significantly higher than conventional flooded type evaporator the experimental setup was a refrigerant flow loop to circulate it through the test section the refrigerant is HCFC and the test section was fabricated from stainless steel the copper heater tube and nozzle tube fastened at opposite sides plates**[4].**

III. METHODOLOGY

Design is an activity aimed at providing complete descriptions of an engineering system, part of a system, or just of a single system component design methodology for a heat exchanger as a component must be consistent with the life-cycle design of a system.

There are two main design for this paper even for general design of STHEx

3.1. Thermal Design

Heat exchanger thermal/hydraulic design procedures top in involve exchanger rating (quantitative heat transfer and pressure drop evaluation)and/or exchanger sizing. Only two important relationships constitute the entire thermal design.Two of the simplest (and most important) problems are referred to as the rating and sizing problems.

3.1.1. Rating Problem

Determination of heat transfer and pressure drop performance of either an existing exchanger or an already sized exchanger (to check vendor's design) is referred to as a rating problem. Inputs to the rating problem are the heat exchanger construction, flow arrangement and overall dimensions, complete details on the materials and surface geometries on both sides, including their non-dimensional heat transfer and pressure drop characteristics (j or Nu and f vs. Re),{ fluid flow rates, inlet temperatures, and fouling factors. The fluid outlet temperatures, total heat transfer rate, and pressure drops on each side of the exchanger are then determined in the rating problem. The rating problem is also sometimes referred to as the performance orsimulation problem.

3.1.2. Sizing Problem

In a broad sense, the design of a new heat exchanger means thedetermination/selection of an exchanger construction type, flow arrangement, tube/plate and fin material, and the physical size of an exchanger to meet the specifiedheat transfer and pressure drops within all specifiedconstraints. However, in a sizingproblem for an extended surface exchanger, we will determine the physical size (length,width, height, and surface areas on each side) of an exchanger.For a STHEx a sizing problem in general refers to the determination of shell type, diameter and length, tube diameter and number, tube layout, pass arrangement, and so on. Inputs to the sizing problem are surface geometries (including their dimensionless heat transfer and pressure drop characteristics), fluid flow rates, inlet and outlet fluid temperatures, fouling factors, and pressure drops on each fluid side.

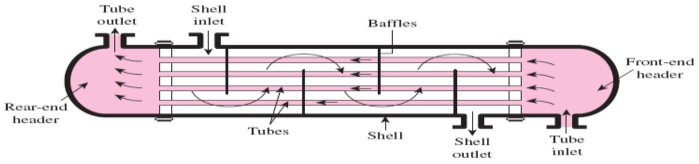

FIGURE 11–4

The schematic of a shell-and-tube heat exchanger (one-shell pass and one-tube pass).

Figure2. Shows shell and tube heat exchanger**[5]**

IV. RESULTS AND DISCUSSION ANALYSIS AND DESIGN EQUATIONS OF STHEX

The beer from the 8th zone enters the 9th zone at 46^0C which is the desired temperature let us calculate the out let temperatures of the hot water in which it is going to be used to cool(decrease the final temperature) the beer for the final processing. Let us compute the mass flow rate of the beer in our zone. HBSC produce 90 million bottles of beer per year it works 6 days per week and 16 hours per day. so it works for(365-(13+4*12))/16=4864 hr\year the volume flow rate of the beer in this zone isV_b=90e6*0.33/48640=6160.0855 lit/hr or V_b=6.1258kg/sec.

1.1. Determination Of hi

The mass flow of water (hot water comes out of HEx) is determined from

(Mcp)beer=(Mcp)water

Equation1

but the specific heat of 2.16 and that of water is 4.186 the percentage presence of alcohol is 4.25% and the rest is water. so that the specific heat of Harar beer is determined from

Cpb=0.0425*2.16+0.9575*4.186=4100 J/kg`c

Hence the mass flow rate of the water to this zone per second is

Mw=6kg/sec
The heat lost from the beer during heat transfer process with the hot water in which the hot water absorbs heat. In the9th zone the total heat loss

$Q_{loss} = M_b * C_{cp} * \Delta T_b$ =301392W Equation2

To know the lost from one bottle beer the diameter at the base of the bottle is 6 cm so that the number of beer along the length and width of the 9th zone pasteurizer respectively is

NobL=3/0.06=50 bottles Nobw=4/0.06=66.03 bottles

The heat lost from one bottle = total heat lost/ total no of bottles=30139w/ 6600 =45.64 w

The convective heat transfer coefficient for the beer if we take the 9th zone as one system and the heat film condensation take place on the vertical bottles of beer as in tubes the beer is at a saturation temperature of 46^0C and

Assumptions-

- steady operation condition exists
- the bottles of beer is isothermal
- the bottles considered as a cylinder
- the convective heat transfer coefficient for the beer and the water is the same and also be the same properties each bottle are maintained at a surface temperature of 36^0C

Properties:-The properties of water at the saturation temperature of 46^0C are

hfg=2393e3 J/kg ρv=0.069 kg/m

The properties of liquid at the film temperature of

$T_f = \frac{T_{sat}-T_s}{2}$=$41^0$CEquation3

The modified latent heat of vaporization Equation4

Hfg*= $Hf_g + 0.68C_{pl}\,(T_{Sat} - T_S\,)$

Nothing that ρv<<<ρl(since 0.06<<<991) the heat transfer coefficient for a condensation on a single vertical (bottles) is determined and laminar film condensation takes place and the height of the bottle h=10.8cm

Now let us compute the temp at which the hot water leaves the heat exchanger and sprayed on the beer. We know that the heat lost by the hot beer is equal to the conduction heat transfer along the thickness of the bottle and the convective heat transfer to the hot water. This is given by

Qlost/bottle=$h_i*A_{internal}*\Delta Ti=k*A_{average}*\Delta T_0=h_o*A_{exter}*\Delta T_0$

$=h_i*A_{int}*(T_b-T_{si})=k*A_{avg}*(T_{s,i}-T_{s,o})/\Delta x=h_o*A_{exter}*(T_{s,o}-T_{w,o})$

The temperature of the internal surface Ts,i is

Q loss/bottle=$h_i*A_{int}\,(T_b-T_{s,i})$ Equation5

The conduction heat transfer

Q_{loss}/bottle= $h_o*A_{ext}*\Delta T_c/\Delta x$ Equation6

And the convection heat transfer

Q_{loss}/bottle=$h_o*A_{ext}*\Delta T_{conv}$hence$T_{w0}=32^0$C

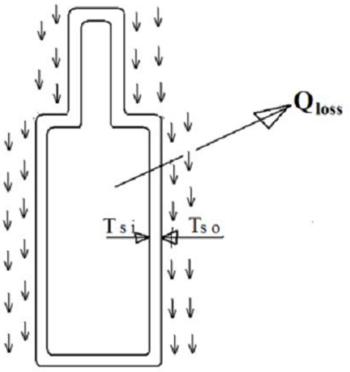

Figure3. Shows bottle beer under showering by hot H_2O

And from the first law of thermodynamics the heat lost by beer is equal to the heat absorbed by the hot water so that

$Mb=C_{pb}*\Delta T_w$ Equation7

So the inlet temperature of water is $T_{wi}=26.24^0$C which is inlet temperature for the 9^{th} zone tank and outlet temperature for this STHEx. So the out let temperature of the water from the tube becomes $T_{wi}=26.24^0$C which is the heat exchanger designed(desired) temperature

Steam with mass flow rate of 6000kg/hr enters at 160^0C shell side and in which a cool water at 15^0C enters the tube side and out at a designed temperature of 26.24^0C and the shell side at 80oc the shell and tube heat exchanger used now is Lm in length and parameters(Datas) from the company STHEx at the 9^{th} zone tank is as follows

tube outer dia Do=19.05mm pt=25.4mm shell inner dia Ds-i=155.18mm
length L=1.01m Clearance C=Pt-Do=6.35mm

pressure drop due friction during heat transfer

$\Delta Pf = \frac{fLNp}{di} * \frac{PV^2}{2gc}$ Equation8

1 pass tube &shell $Ntube = \frac{Mw}{\rho*Ain*V}Ren = \frac{Vm*Dh}{v}$

$Nu_{d}=hDh/k=0.023*Red^{0.8}*Pr^{0.4}$

hi=Nud*k/Dh &f=(0.79lnRed-1.64)

from the above equations we have the following result in the table1 below

From the table by optimization it is selected a row with tube internal diameter of 18mm and tube number of 28 and pressure drop of 199.54 (less).

0.015	Vm	N	Red	f	Nud	hi	ΔPf(kpas)
	1.773	40	29047.79	0.02382	179.79	7253.93	253.72
	2.2166	32	36305.65	0.02258	213.71	8622.48	375.71
	2.533	28	41499.19	0.02188	237.84	9596.06	475.67
	2.627	27	43039.23	0.02169	244.84	9879.69	507.19
	1.555	37	28125.74	0.02401	174.23	6367.39	178.19
0.01656	1.818	32	32882.69	0.02312	197.43	7215.25	234.53
	2.078	28	37585.39	0.02239	219.72	8029.89	295.31
	2.155	27	38978.39	0.02220	226.21	8267.05	316.42
	2.530	23	45760.84	0.02139	257.18	9398.87	420.22
	1.539	32	30256.89	0.02359	184.72	6210.69	157.77
0.018	1.759	28	34582.11	0.02284	205.56	6911.38	199.54
	1.824	27	35860.02	0.02265	211.61	7114.79	212.78
	2.239	22	44018.96	0.02158	249.32	8382.69	305.47
	2.59	19	50978.64	0.02086	280.38	9426.99	396.03

1.1.1. Shell side design (Estimation of ho)

First the tube side layout is to be selected considering different important points which enhance heat transferand from maintenance point of view in our case the HBScSTHEx has triangular pitch arrangements, so from table for 1 pass shell and tube and tube outer diameter of 19.05mm has Pt=25.4mm

Calculating the hydraulic diameter of the triangular pitch

$$De = 4 * \left[\frac{\frac{Pt(0.86*Pt)}{2} - \frac{\pi Do^{2}}{8}}{Do/_{2}}\right]$$ **Equation9**

Now let us estimate the shell side Pressure drop & the heat transfer coefficient but the cross sectional area

$$As = \frac{DsCB}{Pt}$$ **Equation10**

but the optimum baffle spacing from TEMA standardization the baffle spacing is somewhere between 0.4 and 0.6 of shell inner dia (Ds). With optimum design baffle spacing of 0.5Ds so that B=0.5*0.2205=0.11026m

We know that the shell side velocity is limited to 0.6 - 1.5 m/s &assuming Vs=1.5 m/s maximum shell characteristics area using equation

1.1.2. The mass velocity

The velocity in the shell in the range of 0.6 - 1.5, taking 1.5 m/s let us calculate **ho** by counter checkin2e3<Res<1e6

$$Red = \frac{VsDe}{kf} Nus = \frac{hoDe}{kf}$$ **Equation11**

From the above equation ho can be calculated

$$ho = \frac{Nus*kf}{De}$$ **Equation12**

Since the heat exchanger operates in counter flow manner so that the mean temperature difference ΔTlm relation is different unlike the parallel flow and others types of flow and derivate by the factor F_t which is called temperature correction factor

$T_{lm} = F_t * \Delta T_{lm} * C_f$In our case Ft=<1 **Equation13**

F can be found by calculating first the S&R ratios which are called temperatures effectiveness and heat capacity ratio respectively where

$$S = \frac{t_o - t_i}{T_i - T_o} = \frac{\Delta Tactu}{\Delta Tmax} \text{and} R = \frac{T_i - T_o}{t_o - t_i}$$ **Equation14**

Since our HEx is a single shell, single tube pass so that the temperature correction factor is calculated from

$$f_t = \frac{\sqrt{R^2+1}\ln\frac{1-S}{1-RS}}{(R-1)\ln\frac{2-S(R+1-\sqrt{R^2+1}}{2-S(R+1+\sqrt{R^2+1}}}$$ **Equation15**

ΔT1=Ti-to and ΔT2= To-ti from the figure4 below **Equation16**

And the log mean temperature difference is evaluated from the relation

$$\Delta T_{ln} = \frac{\Delta T_1 - \Delta T_2}{\ln\frac{\Delta T_1}{\Delta T_2}}$$ **Equation17**

But the flow includes both counter flow and cross flow so that

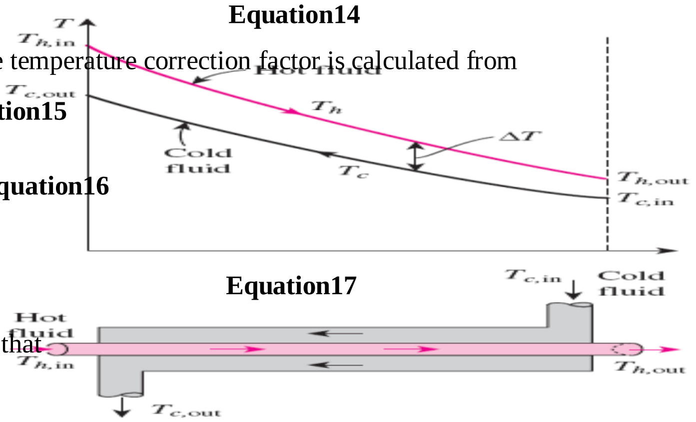

ΔT1m=Ft *ΔT1m*cf
Therefore let us calculate the desired length at the out let
temperatures of tube by counter check methodFigure4. Shows temperature of cold and hot fluid**[5]**
Q=UAΔT1m.cf = UNπPoLΔT1n **Equation18**
The overall heat transfer Co-efficient

$$U = \frac{1}{h_i}\frac{D_o}{D_i} + \frac{1}{h_o} + \frac{\frac{D_o}{2} * \ln\frac{D_o}{D_i}}{k} + R_{fi}\frac{D_o}{D_i} + R_{fi}$$ **Equation19**

Table2. Shows design of the STHEx total length

V(m/s)	Res	Nus	ho	U	L(m)
0.6	43920.29	145.39	5517.01	1846.81	1.69
0.9	85880.44	181.72	6895.37	1891.39	1.58
1.0	73200.49	192.56	7306.69	1921.39	1.56
1.2	87840.58	212.78	8077.38	2065.64	1.52
1.3	95160.63	222.45	8440.92	2088.65	1.50
1.4	102480.68	231.709	8792.07	2109.49	1.48
1.5	109800.73	240.67	9132.11	2128.51	1.47

The final design length at the assumed V=1.5 m/s is
L=1.87m Res=109800.73 Nus= 240.67 ho=9132.11 U=2027

1.1.3. Tube side pressure drop

Tube side pressure drop is a quantity of interest in shell & tube heat exchanger, in the analysis of tube flow is important parameter. Since this quantity is directly related to the power requirement of the pump to maintain flow then the required pumping power for this HEx to over come
A specified pressure drop ΔP is determined from
Wpump=V*ΔP= m*ΔP/ρ **Equation20**

The Reynolds number from the calculation result at the corresponding velocity is greater than 4000. So that the flow is turbulent in this shell& tube HEx design. which is much shorter than the total length of the tube therefore, we can assume fully developed turbulent flow in the entire length tube. The surface temperature Ts of the tube at any location can be determined from the tube cross sectional and heat transfer area
$A_c= \pi*D_i^2/4A_{hta}=PLq_s= Q/AT_s= T_m+q_s/h_i$ **Equation21**

1.1.4. The shell side pressure drop

Pressure drop for the shell side is given by
$\Delta P_s= f*(N_b+1)D_s/D_e*\rho V^2/2gc$ **Equation22**
The number of baffles is determined from
(Nb+1)B=L**Equation23**

1.2. MECHANICAL DESIGN

1.2.1. STRESS ANALYSIS ON SHELL

Considering our cylindrical shell as a pressure vessel of thin shell in which the wall thickness of the shell (t) is less than 1/10 of the internal diameter of the shell (d) or the internal fluid pressure is less than 1/6 of th e allowable stress then it is called a thin shell. In our case the shell are and there are pipes in which water flowing outside the pipe so that our shell is an example of open and pressure vessel, so that the circumferential or hoop stresses are induced by the fluid pressure when a thin cylinder shell is subjected to an internal pressure , it is likely to fail in the following two ways

1. It may fail along the longitudinal section (i.e. circumferentially) splitting the cylinder into two troughs as shown in figure below

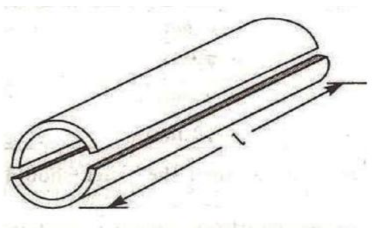

Figure5. Circumferential failure**[6]**

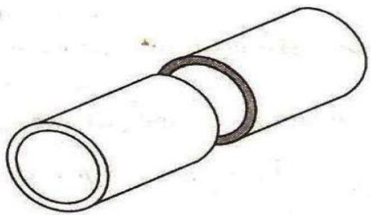

Figure6. Transverse section (longitudinally)**[6]**

2. It may fail across the transverse section (longitudinally) splitting the cylindrical in two cylinder shell Circumferential or hoop stress a tensile stress acting in a direction tangential to the circumferential or hoop stress

$$t = \frac{pd}{2\sigma_{ti}}$$ **Equation24**

In case of ductile materials circumferential stress$\sigma_{ti} = 0.8\sigma_y$

For brittle material$\sigma_{ti} = 0.125\sigma_u$

1.2.1.1. Longitudinal stress

Consider a thin cylindrical shell subjected to an internal pressure. Tensile stress acting in the direction of the axis is called longitudinal stress in this case the total force acting on the transverse section (along Y-Y) Intensity of pressure cross sectional area is

$$\sigma_{t2} = \frac{pd}{4t}$$ **Equation25**

From the above we see that the longitudinal stress is half of the circumferential stress therefore the design of a shell pipe must be based on the maximum stress i.e. hoop stress

1.2.1.2. Maximum shear stress

We know that according to maximum shear stress theory the maximum shear stress is one half the the algebraic difference between the maximum and minimum principal stress i.e the hoop stress and longitudinal stress. Therefore maximum shear stress

$$S = \frac{\sigma_{ti} - \sigma_{t2}}{2}$$ **Equation26**

1.2.2. INTEGRAL FLANGE DESIGN FOR TUBE SHEET

Dimensions of A flange joint for a stainless steel shell pipe 220mm dia to carry a pressure of 0.4 N/mm^{2}and from table for stainless steel allowable tensile stress t=14 N/mm^{2}c=9mm

Therefore thickness of the pipe

$$t = \frac{pd}{2\sigma_t} + c$$ **Equation27**

Other dimensions of a flanged joint for a cast iron shell pipes may be fixed as follows. Nominal dimensions of the boltd=0.75t+10 **Equation28**

Number of bolts n= 0.0275D+1.6, Thickness of the flange, t_f=1.5t+3, Width of the flange, B=2.3d, Outside diameter of the flange Do=d+2t+2B, Circumferential pitch of the bolts Pc=πDp/n = π*300/8Pc =117.8 mm. In order to make the joint lack proof the value of Pc should be between$20\sqrt{d_i}$ and $30\sqrt{d_i}$where di is the bolt holedia

Since the circumferential pitch as obtained (117.8mm) above is within 100 to 150 therefore the design is safe.

$$N = \frac{d_o - d_i}{2}$$ **Equation29**

$$\frac{D_o}{D_I} = \sqrt{\frac{y - Pm}{y + (Pm + 1)}}$$ **Equation30**

While there is an enormous variety of specific design features that can be used in shell and tube exchangers, the number of basic components is relatively small. These are shown and identified.

1.2.3. VIBRATION ANALYSIS

1.2.3.1. Flow Induced Vibrations (FEI) In STHEx

Of the different excitation mechanism of flow induced vibration, only fluid elastic instability is the primary concern in all flow mediums. Others mechanisms have less importance in certain flow media. For example turbulent buffering is not primary concern in gas flow since the low of the gas does not result in a very high hydrodynamic force.Hence, design restrictions are imposed to limit acoustic resonance and FEI.

1.2.3.1.1. Approaches to fiv analysis

Two approaches are normally followed to predict FIV effect of shell and tube heat exchanger:

- **Finite element method modeling technique**This model simulates the time- dependent motion of a multi-span heat exchanger tube in the presence of tube and baffle plate clearance, and the resulting wear is determined. This approach is normally followed for heat exchanger especially STHEx.

- **Limiting amplitude of vibration**This approach linearizes the structural by assuming as classical beams with support plates offering simple support at the intermediate points and clamped at the tube sheet ends.

1.2.3.1.2. Empirical Nature of FIV Analysis

It is important to note that flow-induced vibration of shell and tube heat exchanger is physical phenomenon that cannot be explained by simple empirical correlations. It is most difficult to analyze due to reasons like:

- Tube bank dynamic is a multi-body problem. The tubes are supported by multiple baffles with holes slightly larger than the tube diameter.
- The interaction between the tube and the support plates is characterized by impacting as well as sliding motion. This makes the system nonlinear in nature.
- The tube and surrounding fluid form a fluid form a fluid-structure coupling that results in motion-dependent fluid forces that rise to added mass, couple models, and damping.
- Generally the flow field is quite complex, non- uniform, and quite unsteady, and the incidence of flow on the tubes is at variable angles to the longitudinal axis.
- Structural complexity arises due to time-variant flow-dependent boundary conditions. Mechanical tolerances, initial straightness, fit-up, and tube buckling due to manufacturing process add complexities in defining boundary conditions.
- Effect of tube bundle parameters such as transverse and longitudinal pitches, tube layout pattern, pass partition lanes, shell to tube bundle clearance, number of tube rows, etc. on the Occurrence of FIV cannot be correctly evaluated. For this reasons, most of the method in the analysis of the tube bank dynamics are semi-empirical in nature. To render the problem amenable for most analytical studies and experimental investigation. The flow conditions are idealized as:
- The flow is uniform and steady
- The incident of the flow is either axial or normal to the tubes
- The tube motion is linearized and it is assumed that the frequencies are well defined.
- The baffles support provides a simply supported condition.

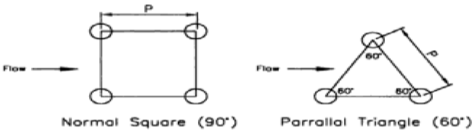

1.2.3.1.3. Fiv (Flow Induced Vibration) mechanisms

Some of the mechanisms in shell and tube heat exchanger are as follows:

1.2.3.1.3.1. Vortex shedding

Consider a bluff body such as cylinder in cross flow with the tube axis perpendicular to the flow. As the fluid flows past the tube the wake behind the tube is no longer regular as a result of vortex shedding the following conditions happened.

- The vortex shedding frequency shifts to the structural frequency, developing the condition called "lock-in" or "synchronization." The lock in phenomena leads to high-amplitude vibration with substantial energy input to the tube.
- The lift force becomes a function of structural amplitude.
- The drag force on the structure increases. However, the magnitude of the oscillating drag force is smaller than the oscillating lift force.
- The strength of the shed vortices increases.

The criteria for avoiding lock-in due to vortex shedding in the first two to three rows in a tube bank are :

a. If the reduced velocity for the fundamental vibration mode (n=1) is satisfied by the relation

$\frac{U}{f_n D} < 1$For n=1 **Equation31**

Both lift and drag direction lock-in are avoided.

b. For a given vibration mode if the reduced damping C_n is large enough,

$C_n > 64$

Then lock-in will be suppressed in that vibration mode.

c. If for a given vibration mode

$\frac{U}{f_n D} < 3.3 C_n > 1.2$then lift direction lock-in is avoided and drag direction lock-in is suppressed.

d. The reduced damping C_n is calculated by the equation

$M_n = \int_{L_i}^{L_o} m(x) \varphi^2{}_n (u) du$ **Equation32**

1.2.3.1.3.2. TURBULENCE-INDUCED EXITATION MECHANISM

1.2.3.1.3.2.1. Turbulence

In general, higher flow rates promote and maintain high turbulence in the fluid, which is desirable for enhanced heat transfer, but the high turbulence is a source of structural excitation. STHEx tubes responds in a random manner to turbulence in the flow field. In addition to structural excitation, turbulence in the flow can affect the existence and strength of other excitation mechanism, namely, vortex shedding.

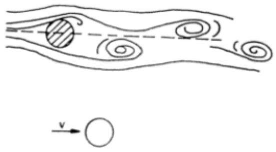

Figure7. shows vortex shedding past single tube**[6]**

1.2.3.1.3.3. FLUID ELASTIC INSTABILITY

Fluid flow across an array of elastic tubes can induce a dynamic instability, resulting in very large amplitude tube vibrations once the critical cross-flow velocity is exceeded. This is a relatively common occurrence in shell and tube heat exchangers. Once the critical cross flow velocity is exceeded, vibration amplitude increases very rapidly with cross flow velocity V, usually as $V^n$where n=4 or more compared with an exponent in the range $1.5 < n < 2.5$ below the instability threshold.

A sudden change in vibration patterns within the tube array indicates instability and is attained when the energy input to the tube mass-damping system exceeds the energy dissipated by the system.

1.2.3.1.3.3.1. ACCEPTANCE CRITERIA TO AVOID FEI

To avoid FEI, acceptance criteria are:

Normal criterion$U_{cr} < U$**Equation33**

Conservative criterion$\frac{U}{U_{cr}} <= 0.5$ **Equation34**

1.3. Simulations (Computational Fluid Dynamics CFD)of STHEX

Simulation refers to process of comparing information on the behavior &characteristics of the real system by analyzing, studying or observing the model of the system such a model may be subjected to a variety of operating and environmental conditions and the performance of the of STHEx determined in terms of variables such as pressure, temperature flow rate, energy input/output, mass flow rate and mass transfer rate that are of particular interest in STHEx analysis.

There are several reasons for simulating a system behavior through its mathematical &numerical model in this respect simulation can be used to

- Evaluate different designs for selection of an acceptable design
- Study system behavior under design conditions
- Determine the effects of different design behavior variables for optimization
- Improving or modifying existing systems
- Investigate the sensitivity of the design to different variables with regards to the extent of their influenced or significance

In this case simulated 2D of the shell and tube heat exchanger and we have observed the different parameters that affect the operation of exchanger. The following are some of them; first to simulate we have start with creating geometry.

Let us start by drawing the two dimensional geometry of the problem (STHEx) which is done by simple sketch by hand and then drawn and defined on the gambit software to be meshed

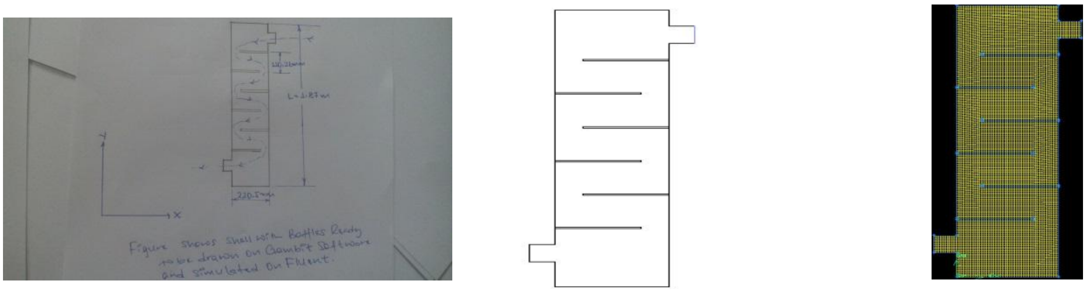

Figure8. a).STHEx drawn by hand b).STHEx drawn on Gambit c). STHEX Meshed on Gambit

As u can see the mesh is fine as a result of giving large interval count along each sides to have good results of simulation. Then after defining the boundary condition and entity we just exported in to the fluent. There the beauty of the thermal is shown. Contours are colorful graphics which indicates the properties and the results of the system.

1.3.1. VELOCITY CONTOURS

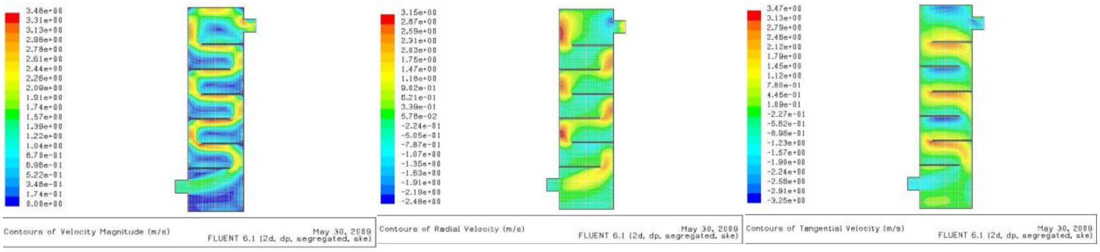

Figure9.a).Velocity magnitudeb).Radial Velocity c). Tangential Velocity

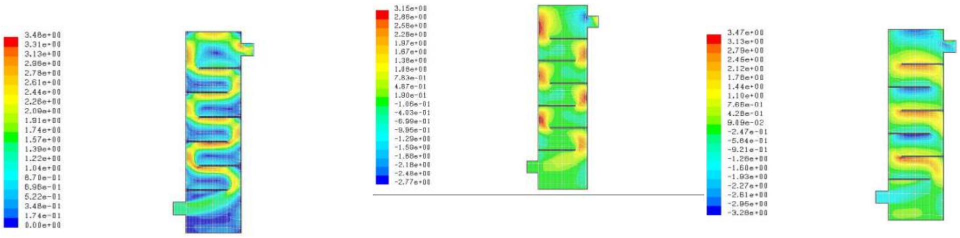

Figure10.a).Relative Velocity b).Relative Y Velocityc).Relative Tangential Velocity

1.3.2. PRESSURE CONTOURS

Which shows the pressure difference down the length of the heat exchanger from the color we observed that the pressure drop increases

- Because of the presence single segemental baffles and
- Gradient

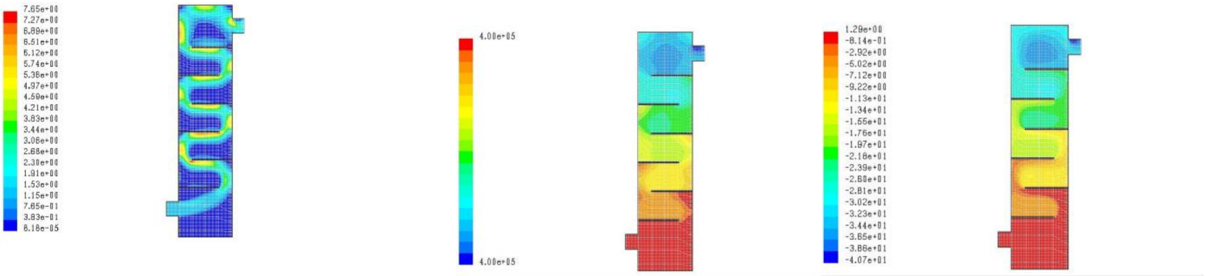

Figure11.a).Contours of dynamic pressure b).Absolute pressure c).Total pressure

1.3.3. TEMPERATURE CONTOUR

The temperature contour is as you can observe from the diagram it is uniform becuose

- Only single fluid is analyzed since there is no heat transfer

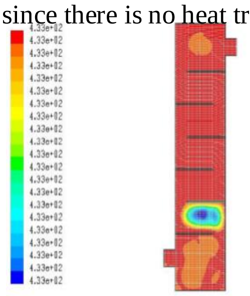

Figure12. Temperature contour

V. CONCLUSION

As all knows shell and tube heat exchanger are the most important devices in that installed to assist some plants and several industries like Harar Brewery Share Company but here the STHEx at the 9th zone was malfunctioned that is the temperature of the cold fluid would fluctuate between 35^0C-40^0C.Then some optimization and redesign of the machine is done for both mechanical and thermal designs and the simulation fo the heat transfer between the two fluid is analyzed using the concept of CFD (Computational Fluid Dynamics) using Gambit and Fluent software's. The final result of the STHEx in HBSC which is the redesigned STHEX can achieve or efficiently work to achieve the required outlet temperature 34^0C the temp at which the beer is ready for customer for use.

REFERNCES

[1]. Ramesh K. Shah, D. P. (2003). Fundamentals of Heat Exchanger Design. New Jercy and Canada: John Wiley & sons Inc

[2]. ZHANG Xiao-jun1, W. X.-L.-R. (2010). Numerical Simulation of Flow Field in Shellside of Heat Exchanger in Nuclear Power Plant. CNKI, 50-62.

[3]. R. Hosseinia, A. H.-G. (April 2007). Experimental determination of shell side heat transfer coefficient and pressure drop for an oil cooler shell-and-tube heat exchanger with three different tube bundles. Science Direct-ELSEVIER, 1001–1008.

[4]. Chang, T.-B. (2009). Enhancing the heat transfer performance of triangular-pitch shell-and-tube evaporators using an interior spray technique. Research Gate, 14-19.

[5]. Boles, Y. A. (2006). Thermodynamics: An Engineering Approach. McGraw-Hill.

[6]. Kurmi, 2006. Design of Machine Elements

Bibliography

Dawit Bogale is currently working as a Lecturer in School of Mechanical and Industrial Engineering, Bahirdar University, Bahirdar, Ethiopia. He did his ***BSc in Mechanical Engineering at Jimma Universisty,Ethiopia*** and ***Specialized his MSc in Applied Mechanics at Addis Ababa Institute of Technology (AAiT)*** in the year 2012 and 2013 respectively.

"There's no place like home except Grandma's. This paper is dedicated to My Grandmother who spent 15 years of her life with me. I love you my grandmother Yeshiye Wedneh."

American Journal of Engineering Research (AJER)
e-ISSN : 2320-0847 p-ISSN : 2320-0936
Volume-03, Issue-10, pp-110-120
www.ajer.org

Research Paper Open Access

Bernoulli-Euler Beam Response to Constant Bi-parametric Elastic Foundation Carrying Moving Distributed Loads

Ogunyebi S.N
Department of Mathematical Sciences, Ekiti State University, Ado-Ekiti, Ekiti State, Nigeria.

ABSTRACT: *A study of the dynamic response of Bernoulli-Euler beam to constant bi-parametric elastic foundation to moving distributed forces is presented. The transformed equation governing the system is obtained by means of the Galerkin's technique. The cases of the dynamic response of the beam to distributed loads of equal magnitude are studied. Numerical examples are given in order to determine the effects of various parameters on the response of the simply-supported Bernoulli-Euler beam.*

Keywords- Deflection, foundation modulus, Resonance, Shear force, Simply supported beam.

I. INTRODUCTION

Beams are of great importance in construction engineering. This may be due to their light weight and this has contributed to their widely usage.

The dynamic response of Bernoulli-Euler beam have been extensively studied especially for simply supported beams [1], [2], [3], [4], [5]. In most of the previous works, the problem of assessing the dynamic response of Bernoulli-Euler beam carry moving loads, has been restricted to the case when the loads are simplified as moving concentrated forces [6], [7], [8] and mostly placed on Winkler elastic foundation [9], [10].

The classical Winkler model has various applications in construction engineering and this model suffers several criticisms as it has some shortcomings due to the discontinuity of the adjacent displacement [11]. To tackle this deficiency, a better model that introduced shear interaction between adjacent Winkler spring elements was introduced [12].

Several authors in the area of structural dynamics have thoroughly investigated the dynamics and stability of the Winkler-type foundation model by both approximate methods [13] and exact approaches [14]. In 1991, [15] presented some finite element models for the static analysis of Euler-Bernoulli beam resting on a Winkler-type foundation. In 2010, Omolofe [16] investigated the dynamic response to moving load of an elastically supported non-prismatic Bernoulli-Euler beam on variable elastic foundation and obtained analytical solutions for which the numerical solutions are displayed in plotted curves.

In this paper, the problem of dynamical analysis of Bernoulli-Euler when it is simply supported and resting on constants bi-parametric elastic foundation under moving distributed forces are presented. All the components of inertia terms are considered in the analysis. While section II describes the theory and brief description of the problem under investigation, section III focuses on the technique involved in the transformation of the fourth order partial differential equation of the dynamical system. Some remarks on the analytical solution so obtained are reported in section IV and finally, numerical results are displayed in plotted curves in section V.

II. THEORY AND FORMULATION

The problem of the displacement response of simply-supported Bernoulli-Euler beam resting on constant bi-parametric elastic foundation carry moving distributed loads is governed by the fourth order partial differential equation

$$EI\frac{\partial^4}{\partial x^4}Y(x,t)+\mu\frac{\partial^2}{\partial t^2}Y(x,t)-N\frac{\partial^2 Y(x,t)}{\partial x^2}+Q_m(x)Y(x,t)+MH(x-ct)P_fY(x,t)=P(x,t)$$
(2.1)

where E is the young modulus, $Y(x,t)$ is the transverse displacement, $Q_m(x)$ is the bi-parametric elastic foundation, $P(x,t)$ is the moving load. Also, $H(x,ct)$ is the Heaviside function defined as

$$H(x,ct)=\begin{cases}0, & \text{for } x<0\\ 1, & \text{for } x>0\end{cases} \tag{2.2}$$

In this paper, when the effect of the mass of the moving load on the beam is considered, $P(x,t)$ takes the form

$$P_f(x,t)=MH(x,ct)\left[g-\left(\frac{\partial^2}{\partial t^2}+2c\frac{\partial^2}{\partial x\partial t}+c^2\frac{\partial^2}{\partial x^2}\right)Y(x,t)\right] \tag{2.3}$$

The boundary conditions for our dynamical system are arbitrary and the initial conditions without any loss of generality are taken to be

$$Y(x,0)=0=\frac{\partial}{\partial t}Y(x,0) \tag{2.4}$$

The relationship that exists between the foundation reaction and the lateral deflection $Y(x,t)$ is given by

$$Q_m(x)=GmY(x,t)-\frac{\partial}{\partial x}\left(Km\frac{\partial}{\partial x}Y(x,t)\right) \tag{2.5}$$

where Gm and Km are two constant parameter of elastic foundation. Thus, Gm is the constant foundation stiffness and Km is the variable shear modulus. To this end, equation (2.5) can be written as

$$Q_m(x,t)=GmY(x,t)-K'm\frac{\partial Y(x,t)}{\partial x}-Km\frac{\partial^2 Y(x,t)}{\partial x^2} \tag{2.6}$$

Substituting equations (2.2) to (2.6) into equation (2.1), one obtains

$$EI\frac{\partial^4}{\partial x^4}Y(x,t)+\mu\frac{\partial^2}{\partial t^2}Y(x,t)-N\frac{\partial^2}{\partial x^2}Y(x,t)+GmY(x,t)-\frac{d}{dx}\left[Km\frac{d}{dx}Y(x,t)\right]MH(x-ct)$$

$$\left[\frac{\partial^2}{\partial t^2}Y(x,t)+2C\frac{\partial^2}{\partial x\partial t}Y(x,t)+C^2\frac{\partial}{\partial x^2}Y(x,t)\right]=MgH(x-ct) \tag{2.7}$$

III. MATHERIALS AND METHOD

A close form solution to equation (2.7) does not exist, so the elegant Galerkin's method described in [10] is employed to tackle the fourth order partial differential equation. The method is presented in the form

$$Y_j(x,t)=\sum_{i=1}^{j}W_i(t)U_i(x) \tag{3.1}$$

where $U_i(x)$ is chosen such that the desired boundary conditions are satisfied. And since we are considering simply supported boundary condition, $U_i(x)$ is defined thus,

$$U_i(x)=\frac{\sin i\pi x}{L} \tag{3.2}$$

Substituting equation (3.1) into equation (2.7), taking note of equation (3.2) one obtains

$$\sum_{i=1}^{j}\Big[EIU_i^{IV}(x)W_i(t)+\mu U_i(x)\ddot{W}_i(t)+GmU_i(x)W_i(t)-KmU_i'(x)W_i(t)-KmU_i''(x)W_i(t)$$

$$+M\left(\frac{x}{L}+\frac{2}{i\pi L}\sum_{i=1}^{\infty}\sin\frac{i\pi x}{L}\cos\frac{i\pi t}{L}+C_0\right)\left[\ddot{W}_i(t)U_i(x)2C\dot{W}_i(t)U_i'(x)+C^2W_i(t)U_i''(x)\right]\Bigg]$$

$$=\frac{MgL}{\pi i}\left[\cos\frac{\pi ict}{L}-\cos\pi i\right] \qquad (3.3)$$

where $H(x-ct)$ have been defined as

$$H(x-ct)=\frac{x}{L}+\frac{2}{i\pi L}\sum_{i=1}^{\infty}\sin\frac{i\pi x}{L}\cos\frac{i\pi t}{L}+C_0 \qquad (3.4)$$

imposing orthogonaliy condition, equation (3.3) after simplification becomes

$$\int_0^L\left\{\sum_{i=1}^{j}\Big[EIW_j(t)U_i^{iv}(x)+\mu\ddot{W}_j(t)U_i^{iv}(x)+GmW_i(t)U_i(x)-KmW_i(t)U_i'(x)-KmW_i(t)U_i''(x)\right.$$

$$\left.+\frac{M}{\mu}\left(\frac{x}{L}+\frac{2}{i\pi L}\sum_{i=1}^{\infty}\sin\frac{i\pi x}{L}\cos\frac{i\pi ct}{L}+C_0\right)\left[\ddot{W}_i(t)U_i(x)+2C\dot{W}_i(t)U_i'(x)+C^2W_i(t)U_i''(x)\right]\Bigg]\right\}$$

$$=U_k(x)\frac{MgL}{\pi i}\left[\cos\frac{\pi ict}{L}-\cos\pi i\right] \qquad (3.5)$$

which can be re-written as

$$\sum_{i=1}^{j}\Bigg[\ddot{W}_i(t)H_{i1}(i,k)+H_{i2}\left(\frac{EI}{\mu}H_{i2}(i,k)+\frac{S(x)}{\mu}H_{i3}(i,k)-\frac{K(x)}{\mu}H_{i4}(i,k)-\frac{K(x)}{\mu}H_{i5}(i,k)\right)W_i(t)$$

$$+\frac{M}{\mu L}H_{i6}(i,k)\ddot{W}_i(t)+\frac{2M}{\mu i\pi L}\sum_{i=1}^{\infty}\cos\frac{i\pi ct}{L}H_{i7}(i,k)\ddot{W}_i(t)+\frac{MC_0}{\mu}\ddot{W}_i(t)H_{i8}(i,k)$$

$$+\frac{2cM}{\mu}\dot{W}_i(t)H_{i9}(i,k)+\frac{2M}{\mu i\pi L}\sum_{i=1}^{\infty}\cos\frac{i\pi ct}{L}H_{i10}(i,k)\ddot{W}_i(t)+\frac{C_0 2c}{\mu}\dot{W}_i(t)H_{i11}(i,k)+\frac{Mc^2}{\mu}\dot{W}_i(t)H_{i12}(i,k)$$

$$\frac{2Mc^2}{\mu i\pi L}\sum_{i=1}^{\infty}\cos\frac{i\pi ct}{L}H_{i13}(i,k)+\frac{C_0c^2}{\mu}H_{i14}(i,k)=\frac{MgL}{\pi i}\left[\cos\frac{\pi ict}{L}-\cos\pi i\right] \qquad (3.6)$$

where

$$H_{i1}(i,k)=\int_0^L U_k(x)U_i(x)dx \quad ; \quad H_{i2}(i,k)=\int_0^L U_k(x)U_i^{iv}(x)dx$$

$$H_{i3}(i,k)=\int_0^L U_k(x)U_i(x)dx \quad ; \quad H_{i4}(i,k)=\int_0^L U_k(x)U_i'(x)dx$$

$$H_{i5}(i,k)=\int_0^L U_k(x)U_i''(x)dx \quad ; \quad H_{i6}(i,k)=\int_0^L U_k(x)U_i(x)dx$$

$$H_{i7}(i,k)=\int_0^L U_k(x)U_i(x)\sin\frac{i\pi x}{L}dx \quad ; \qquad H_{i8}(i,k)=\int_0^L U_k(x)U_i(x)dx$$

$$H_{i10}(i,k)=\int_0^L U_k(x)U_i'(x)\sin\frac{i\pi x}{L}dx \quad ; \qquad H_{i11}(i,k)=\int_0^L U_k(x)U_i'(x)dx=H_{i4}(i,k)$$

$$H_{i12}(i,k)=\int_0^L U_k(x)U_i''(x)dx \quad ; \qquad H_{i13}(i,k)=\int_0^L U_k(x)U_i''(x)\sin\frac{i\pi x}{L}dx$$

$$H_{i14}(i,k)=\int_0^L U_k(x)U_i''(x)dx \tag{3.7}$$

equation (3.5) when re-arranged gives

$$\ddot{W}_i(t)+\varepsilon_0^2W_i(t)+\Gamma_0\left[\left(H_{i6}(i,k)+\frac{2}{i\pi}\sum_{i=1}^{\infty}\cos\frac{i\pi ct}{L}H_{i7}(i,k)+LC_0H_{i8}(i,k)\right)\ddot{W}_i(t)\right.$$

$$+\left(2CLH_{i9}(i,k)+\frac{2}{i\pi}\sum_{i=1}^{\infty}\cos\frac{i\pi ct}{L}H_{i10}(i,k)+2C_0LH_{i11}(i,k)\right)\ddot{W}_i(t)$$

$$\left.+\left(C^2LH_{i12}(i,k)+\frac{2C^2}{i\pi}\sum_{i=1}^{\infty}\cos\frac{i\pi ct}{L}H_{i13}(i,k)+C_0C^2LH_{i14}(i,k)\right)\right]$$

$$=\frac{MgL}{\mu\pi i}\left[\cos\frac{\pi ict}{L}-\cos\pi i\right] \tag{3.8}$$

so that

$$\ddot{W}_i(t)+\varepsilon_0^2W_i(t)+\Gamma_0\left[\frac{L^2}{\pi^2}\left(\frac{1}{(i+k)^2}-\frac{1}{\pi^2(i-k)^2}\right)+\left(\frac{8ikL}{\pi^2\left[(n-k)^2-m^2\right]\left[(n+k)^2-m^2\right]}\sum_{n=1}^{\infty}\frac{\cos n\pi ct}{L}\right)\right.$$

$$+\left.\frac{L^2c_o}{2}\right]\ddot{W}_i(t)+\left[2cL+\frac{4i^2\pi(n^2+k^2-i^2)}{\pi^2\left[(n+k)^2-m^2\right]\left[(n-k)^2-m^2\right]}-\frac{4n^2c_oL}{k^2-n^2}\right]\dot{W}_i(t)$$

$$+\left[c^2n^2L\left(\frac{1}{(n+k)^2}-\frac{1}{(n+k)^2}\right)+\left(\frac{8ikL}{\pi^2\left[(n-k)^2-m^2\right]\left[(n+k)^2-m^2\right]}\right)+\left(\frac{c^2\pi^2n^2c_o}{2}\right)\right]W_i(t)$$

$$=\frac{MgL}{\mu\pi i}\left[\cos\frac{\pi ict}{L}-\cos\pi i\right] \tag{3.9}$$

Further arrangements of equation (3.9) give

$$\ddot{W}_i(t)+\varepsilon_0^2W_i(t)=\frac{MgL}{H_{i1}(i,k)\mu i\pi}\left[1-(-1)^i+\cos\frac{i\pi ct}{L}\right] \tag{3.10}$$

where

$$\varepsilon_0^2 = \frac{1}{H_{i1}(i,k)}\left[\frac{EI}{\mu}H_{i2}(i,k) + \frac{Gm}{\mu}H_{i3}(i,k) - \frac{Km}{\mu}H_{i4}(i,k) - \frac{Km}{\mu}H_{i5}(i,k)\right] \quad (3.11)$$

and by Laplace methods, one obtains

$$W_i(t)S^2 + \varepsilon_0^2 W_i(t) = \frac{MgL}{H_{i1}(i,k)\mu i\pi}\left[\frac{S}{S^2+\Omega_i^2} - \frac{(-1)^i}{S}\right] \quad (3.12)$$

where

$$\Omega_i = \frac{ic\pi}{L} \quad (3.13)$$

then from equation (3.12)

$$W_i(t)\left[S^2 + \varepsilon_0^2\right] = \frac{MgL}{H_{i1}(i,k)\mu i\pi}\left[T_a - T_b\right] \quad (3.14)$$

where

$$T_a = \frac{S}{S^2+\Omega_i^2} \times \frac{1}{S^2+\varepsilon_0^2} \quad ; \quad T_b = \frac{R_0}{S} \times \frac{1}{S^2+\varepsilon_0^2} \text{ and } R_i = \frac{(-1)i}{S} \quad (3.15)$$

when solutions of T_a and T_b are substituted into equation (3.14), one obtains

$$W_i(t) = \frac{MgL}{H_{i1}(i,k)\mu i\pi}\left[\frac{\cos\Omega_i t - \cos\varepsilon_0 t}{\varepsilon_0^2 - \Omega_i^2} + \frac{1-\cos\varepsilon_0 t}{\varepsilon_0}\right] \quad (3.16)$$

which when inverted gives,

$$Y(x,t) = \frac{2}{L}\sum_{i=1}^{j}\frac{MgL}{H_{i1}(i,k)\mu i\pi}\left[\frac{\cos\Omega_i t - \cos\varepsilon_0 t}{\varepsilon_0^2 - \Omega_i^2} + \frac{1-\cos\varepsilon_0 t}{\varepsilon_0}\right] \times \frac{\sin i\pi x}{L} \quad (3.17)$$

which represents the displacement response to moving distributed force of simply supported Bernoulli-Euler beam resting on constant bi-parametric elastic foundation.

Next, it is pertinent to seek solution to the moving distributed mass of the problem. If Γ_0 is not equal to zero in equation (3.9), it means that the inertia term is retained and it is evident that an exact solution to the equation (3.9) is not possible. A modification of Strubles technique extensively discussed in [10] is used to obtain the modified frequency. To this end, equation (3.9) is written in the form

$$\begin{aligned}
&\left[1 + \Gamma_0\left(\frac{L^2}{\pi^2(i+k)^2} - \frac{L^2}{\pi^2(i-k)^2}\right) + \left(\frac{8ikL}{\pi^2\left[(n-k)^2-m^2\right]\left[(n+k)^2-m^2\right]}\sum_{n=1}^{\infty}\frac{\cos n\pi ct}{L}\right) + \left(\frac{L^2c_o}{2}\right)\right]\ddot{W}_i(t) \\
&+\Gamma_0\left[2cL + \frac{4i^2\pi(n^2+k^2-i^2)}{\pi^2\left[(n+k)^2-m^2\right]\left[(n-k)^2-m^2\right]} - \frac{4n^2c_oL}{k^2-n^2}\right]\dot{W}_i(t) + \left(\varepsilon_0^2 + \Gamma_0\left[c^2n^2L\left(\frac{1}{(n+k)^2} - \frac{1}{(n+k)^2}\right)\right.\right. \\
&\left.\left.+\frac{8ikL}{\pi^2\left[(n-k)^2-m^2\right]\left[(n+k)^2-m^2\right]} + \frac{c^2\pi^2n^2c_o}{2}\right]\right)W_i(t) == \frac{MgL}{\mu\pi i}\left[\cos\frac{\pi ict}{L} - \cos\pi i\right] \quad (3.18)
\end{aligned}$$

Further re-arrangements give

$$\ddot{W}_i(t)+\Gamma_1\left(\left[2cL+\frac{4i^2\pi(n^2+k^2-i^2)}{\pi^2\left[(n+k)^2-m^2\right]\left[(n-k)^2-m^2\right]}-\frac{4n^2c_oL}{k^2-n^2}\right]\right)\dot{W}_i(t)$$

$$\left[\varepsilon_0^2-\varepsilon_0^2\Gamma_1\left(\frac{L^2}{\pi^2(i+k)^2}-\frac{L^2}{\pi^2(i-k)^2}+\frac{8ikL}{\pi^2\left[(n-k)^2-m^2\right]\left[(n+k)^2-m^2\right]}\sum_{n=1}^{\infty}\frac{\cos n\pi ct}{L}\right)\right]$$

$$+\Gamma_1\left(c^2n^2L\left(\frac{1}{(n+k)^2}-\frac{1}{(n+k)^2}\right)+\left(\frac{8ikL}{\pi^2\left[(n-k)^2-m^2\right]\left[(n+k)^2-m^2\right]}\right)+\left(\frac{c^2\pi^2n^2c_o}{2}\right)\right)\Bigg]W_i(t)$$

$$=\frac{MgL}{\mu\pi i}\left[\cos\frac{\pi ict}{L}-\cos\pi i\right] \tag{3.19}$$

when Γ_1 ,the homogenous part of equation (3.19) can be written as

$$W_i(t)=\gamma_i(t)\cos\left[\varepsilon_0 t-\phi_i\right]+\Gamma_1 W_{1i}(t)+0\left(\Gamma_1^2\right) \tag{3.20}$$

where $\gamma_i(t)$ and ϕ_i are slowly varying functions or equivalently.

By Struble's method, one obtains

$$2\varepsilon_0\dot{Y}_i(t)+\Gamma_1 2c\varepsilon_0 L Y_i(t)-\Gamma_1\frac{4i^2\pi^2+k^2-i^2}{n\left[(n+k)^2-m^2\right]\left[(n-k)^2-m^2\right]}Y_i(t)+\frac{\Gamma_1 4c_o\varepsilon_0 n^2 L}{k^2-n^2}Y_i(t)=0 \tag{3.21}$$

and

$$Y_i(t)\varepsilon_0\dot{\phi}_i-\Gamma_1\frac{L^2\varepsilon_0^2c_o}{2}Y_i(t)=0 \tag{3.22}$$

which when solved gives

$$\gamma_i(t)=C_{mm}\ell\frac{\Gamma_1 B_{mm}}{2\varepsilon_0} \tag{3.23}$$

and

$$\phi_i(t)=\left(\Gamma_1\varepsilon_0\frac{L^2c_o}{2}\right)t+\phi_{mm} \tag{3.24}$$

where ϕ_{mm} is a constant.

Substituting (3.23) and (3.24) into equation (3.20), one obtains

$$W_i(t)=C_{mm}\frac{\Gamma_1 B_{mm}L}{2\varepsilon_0}\cos\left[\varepsilon_m t-\phi_{mm}\right] \tag{3.25}$$

Therefore when the mass effect of the particle is considered, the first approximation to the homogenous system is given as

$$W_i(t)=\gamma_i(t)\cos\left[\varepsilon_m t-\phi_{mm}\right] \tag{3.26}$$

where

$$\varepsilon_m = \varepsilon_0 \left[1 - \left(\Gamma_1 \varepsilon_0 \frac{L^2 c_o}{2} \right) \right] \tag{3.27}$$

is the modified frequency corresponding the frequency of the free system due to the presence of the moving distributed mass. Thus,

$$\ddot{W}_i(t) + \varepsilon_m^2 W_i(t) = \frac{MgL}{\mu \pi_i} \left[\cos \frac{i\pi ct}{L} - \cos i\pi \right] \tag{3.28}$$

Equation (3.28) is a prototype of equation (3.10) and following similar arguments, one obtains

$$\dot{W}_i(t) = \frac{MgL}{\mu \pi_i} \left[\frac{\cos \Omega_i t - \cos \varepsilon_m t}{\varepsilon_m^2 - \Omega_i^2} + 1 - \frac{\cos \varepsilon_m t}{\varepsilon_m} \right] \tag{3.29}$$

which when inverted gives,

$$Y_i(x,t) = \frac{2}{L} \sum_{i=1}^{j} \frac{MgL}{H_{i1}(i,k) \mu i\pi} \left[\frac{\cos \Omega_i t - \cos \varepsilon_0 t}{\varepsilon_0^2 - \Omega_i^2} + \frac{1 - \cos \varepsilon_0 t}{\varepsilon_0} \right] \times \sin \frac{i\pi x}{L} \tag{3.30}$$

which represents the displacement response to moving distributed mass of simply supported Bernoulli-Euler beam resting on constant elastic foundation.

IV. REMARKS ON ANALYTICAL SOLUTION

4.1 Effect of Resonance

When an undamped system such as this is considered, it is pertinent to examine the resonance condition of the structure. Following [10], and from equation (3.17), the Bernoulli- Euler beam traversed by a moving distributed force will be in a state resonance when

$$\varepsilon_0 = \frac{i\pi c}{L} \tag{4.1}$$

while equation (3.30) shows that the same Bernoulli- Euler beam reaches resonance effect at

$$\varepsilon_m = \frac{i\pi c}{L} \tag{4.2}$$

where

$$\varepsilon_m = \varepsilon_0 - \left(\Gamma_1 \varepsilon_0^2 L^2 C^0 \right) \tag{4.3}$$

Thus,

$$\varepsilon_m = 2\varepsilon_0 - {\Gamma_1 \varepsilon_0^2 L^2 C^0}\big/{2} = \frac{i\pi c}{L} \tag{4.4}$$

Clearly, $1 - \frac{1}{2}\left[\Gamma_1 \varepsilon_0^2 L^2 C^0 \right] < 1 \forall_i$

V. NUMERICAL RESULTS

From the analytical solutions, calculations of practical interests in structural engineering and physics are presented in this section. The simply supported Bernoulli-Euler beam of length L 12.123m, velocity c=8.12m/s, flexural rigidity $EJ = 6.068 \times 10^{18} N/m^2$, and for the shear modulus K_m, the values are varied between $0 N/m^3$ and $5 \times 10^5 N/m^2$, for foundation stiffness G_m varies between 0N/ m^3 and $3 \times 10^6 N/m^5$, axial force Nm values varied between $0 N/m^3$ and $\times 10^5 N/m^2$ and the mass per unit length of the structure is 4501.537g/m. The results are shown on the various curves below for the simply supported Bernoulli-Euler beam on constant bi-parametric elastic foundation.

Figure 1and 2 depict the flexural deflections of the beam resting on constant bi-parametric elastic foundation at constant velocity for both moving distributed force and moving distributed mass. It is clearly seen that for fixed values of the shear modulus Km and foundation stiffness Gm, the displacement response of the beam decreases as the values of the prestress function increases.

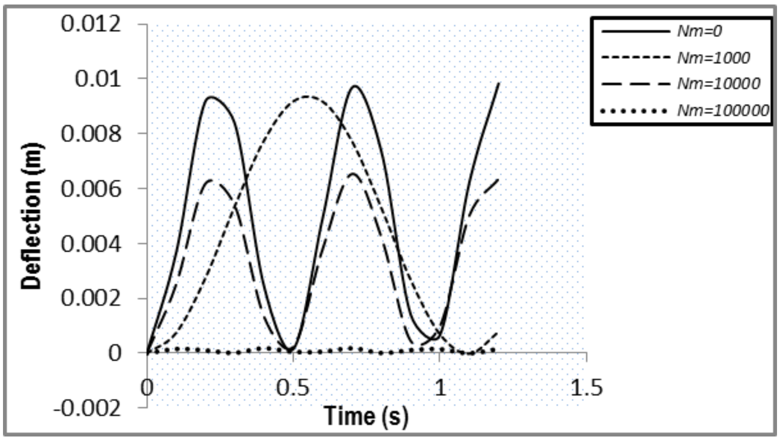

Fig.1: Displacement response of simply supported Bernoulli-Euler beam for moving distributed force for various values of axial force Nm and fixed values of shear modulus and foundation stiffness.

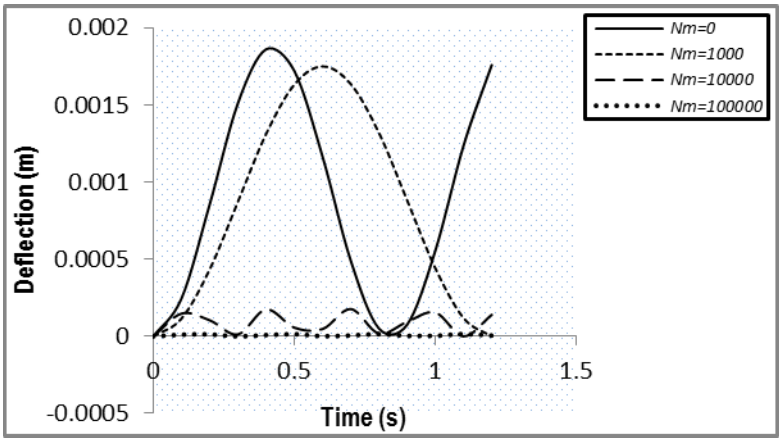

Fig.2: Displacement response of simply supported Bernoulli-Euler beam for moving distributed mass for various values of axial force Nm and fixed values of shear modulus and foundation stiffness.

Figure 3 and 4 displays the deflection profile of the simply supported Bernoulli-Euler beam resting on constant bi-parametric elastic foundation at constant velocity for both moving distributed force and moving distributed mass respectively. It is found that the dynamic deflections of the structure decreases as the values of the shear modulus Km increases for fixed values of the prestress function Nm and foundation stiffness Gm.

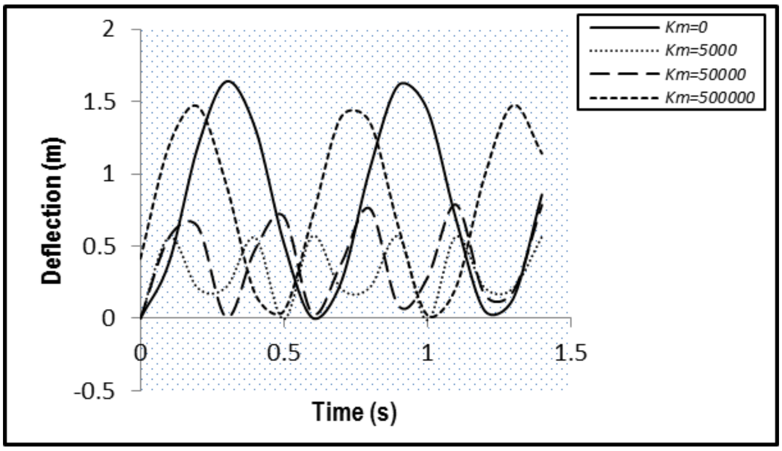

Fig.3: Deflection profile of simply supported Bernoulli-Euler beam for moving distributed force for various values of shear modulus Km and fixed values of axial force and foundation stiffness.

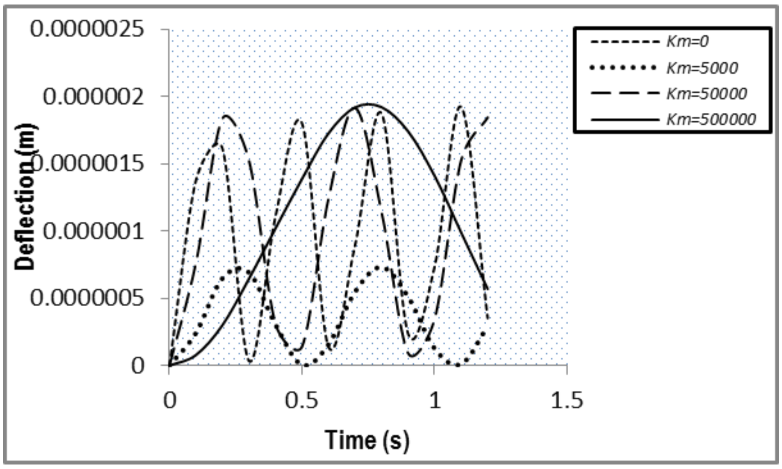

Fig.4: Deflection profile of simply supported Bernoulli-Euler beam for moving distributed mass for various values of shear modulus Km and fixed values of axial force and foundation stiffness.

Similarly, figure 3 and 4 displays the dynamic deflection of the structure resting on constant bi-parametric elastic foundation at constant velocity for both moving distributed force and moving distributed mass. For fixed values of prestress Nm, shear force Km and various values of foundation modulus Gm, it is found that the dynamic deflections of the beam decreases as the values of the foundation stiffness Gm increases.

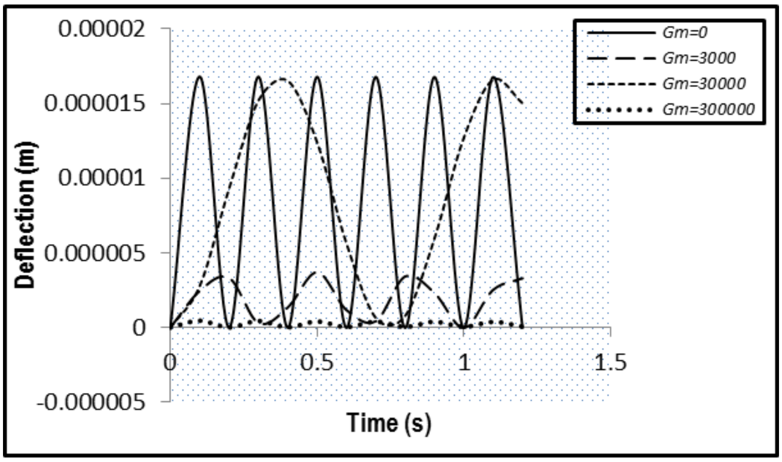

Fig.5: Deflection profile of simply supported Bernoulli-Euler beam for moving distributed force for various values of foundation stiffness and fixed values of axial force and shear modulus.

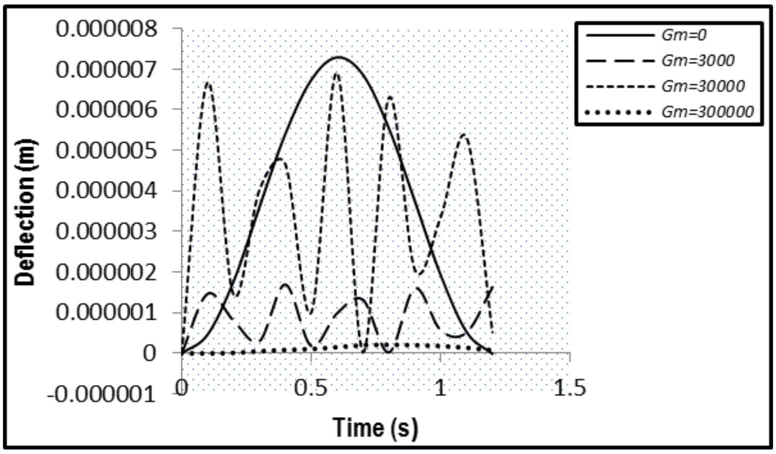

Fig.6: Deflection profile of simply supported Bernoulli-Euler beam for moving distributed mass for various values of foundation stiffness and fixed values of axial force and shear modulus.

The comparison of the displacement response of the simply supported Bernoulli-Euler beam resting on constant bi-parametric elastic foundation at constant velocity for moving distributed force and moving distributed mass. It is observed that the moving distributed force solution is not an upper bound for moving distributed mass solution as shown in the figure below

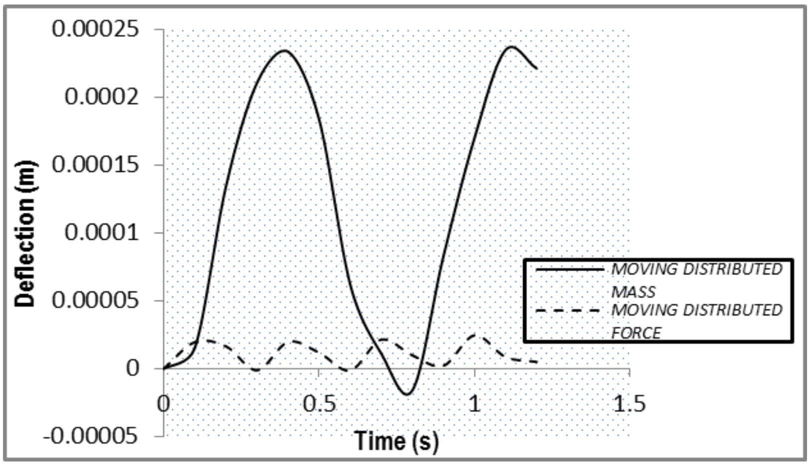

Fig.7: Comparison of the displacement response of simply supported Bernoulli-Euler beam resting on bi-parametric elastic foundation for fixed values of foundation stiffness, axial force and shear modulus.

VI. CONCLUSION

The problem of dynamic analysis under a moving distributed load of a simply supported Bernoulli-Euler beam on constant bi-parametric elastic foundation has been solved. And in view of the condition of resonance established in section VI, it is deduced that for the same natural frequency, the critical speed for the moving distributed force problem is greater than that of the moving distributed mass problem. Hence, for the same natural frequency, resonance is reached earlier in the moving distributed mass problem than in the moving distributed force.

REFERENCES

[1] L. Fryba, *Vibration of solids and structures under moving loads* (Groninggen: Noordhoof, (196), 1972).

[2] M. R. Shandnam, F. R Rofooei, M. Mofid, and B. Mehri, Periodicity in the response of non–linear moving Mass, *Thin-walled structures, 40,* 2002, 283-295.

[3] S.Timoshenko, On the correction for shear of the differential equation for transverse vibration of prismatic bars, *Phil. Mag*. S, *6(41),* l921, 744-776.

[4] G. Muscolino and A. Palmeri, Response of beams resting on viscoelastically damped foundation to moving Oscillators, *International Journal of Solids and Structures, 44(5),* 2007, 1317-1336.

[5] K. Achawakorn and T. Jearsiripongkul, Vibration analysis of Exponential Cross-Section Beam Using Galerkin's Method, *International Journal of Applied Science and Technology, 2(6),* 2012.

[6] S .T. Oni, Response of a non-uniform beam resting on an elastic foundation to several masses, *ABACUS, Journal of Mathematical Association of Nigeria, 24(2),*1996.

[7] B. Omolofe, S. T. Oni and J. M. Tolorunshagba, On the Transverse Motions of Non-prismatic Deep beam under the actions of variable magnitude moving loads, *Latin American Journal of Solid and Structures, (6)*, 2009, 153-167.

[8] S. Sadiku and H. H. E. Leipholz, On the Dynamics of elastic systems with moving Concentrated masses, *Ingenieur Archive, (57)*, 1981, 223-242.

[9] S.T. Oni and T.O. Awodola, Dynamic response to moving concentrated masses of uniform Rayleigh beams resting on variable Winkler elastic foundation, *Journal of the Nigerian Association of Mathematical Physics. (9)*, 2005, 151-162.

[10] S. T. Oni and S. N. Ogunyebi, Dynamical Analysis of finite prestressed Bernoulli-Euler beams with general Boundary conditions under travelling distributed loads, *Journal of the Nigerian Association of mathematical Physics,(12)*, 2008, 87-102.

[11] H. Tanahashi, characteristics of rigid foundations on Pasternak model (in case of two-dimensional plane Strain condition), *Summaries of Technical Papers of Annual Meeting, AIJ* (in Japanese), 2001, 519-520.

[12] P.L Pasternak, *On a new method of analysis of an elastic foundation by means of two foundation constants*, Gosudarstvennoe Izdatelstvo LIteraturi Po Stroitelstuve in Arkhitekture, Moscow (in Russian) 1954.

[13] M.A. De Rosa, Free Vibrations of Timoshenko beams on Two-Parameter Elastic Foundation, *Computer and Structures, 57(1)*, 1995, 151-156.

[14] S.H. Farghaly and K.M.Zeid, An exact frequency Equation For an Axially loaded Beam-mass-spring System Resting on a Winkler Elastic Foundation, *Journal Of Sound and Vibration, 185(2)*, 1995, 357-363.

[15] A.G Razaqpur, and K.R Shah, Exact analysis of Beams on Two-Parameter Elastic Foundations, *International Journal of Solids Structures,27(4)*, 1991, 435-454.

[16] B.Omolofe, Dynamic response under a moving load of an elastically supported non-prismatic Bernoulli-Euler beam on variable elastic foundation, *Latin American Journal of Solid and Structures,7*, 2010, 3-20.

American Journal of Engineering Research (AJER)
e-ISSN : 2320-0847 p-ISSN : 2320-0936
Volume-03, Issue-10, pp-121-129
www.ajer.org

Research Paper Open Access

THE FOSTER CHILD?...

*(A New theory on "**PARADISE**")*

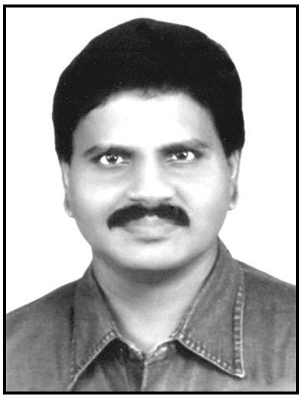

M.Arulmani, B.E.
(Engineer)

V.R.Hema Latha, M.A., M.Sc.,
M.Phil. (Biologist)

ABSTRACT: AM I FOSTER CHILD?...YES...YES...YES. Not only me everyone of the world is the **Foster Child** (Natural child) before the "**LAW OF SUPERNATURE**".

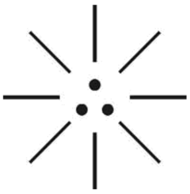

(LAW OF SUPERNATURE)

This scientific research article focus that "**VIRGIN MOTHER**" lived in "**WHITE PLANET**" (White Mars) in the early universe shall be considered as "**MOTHER OF UNIVERSE**". The white planet shall also be called as "**J-GARDEN**" (or) "**PARADISE**". The J-GARDEN consider as the absolutely pure environment of '**WIND**' (**THENDRAL**) which composed of only ions of **photon, electron, proton** and free from **Hydrogen, Carbon, Nitrogen, Ozone, Oxygen**.

J

(WHITE PLANET LOGO)

The '**Infants**' of virgin mother shall be considered as "**Natural child**". The Virgin Father, Virgin Mother shall be considered as the '**Natural Parent**' (or) '**Foster Parent**' before the '**law of supernature**'

During the course of Expanding Universe due to varied environmental condition the white planet populations consider descended to '**EARTH PLANET**' and started breathing **Ozone, Oxygen, Oxygen allotrope** such as Oxygen ion, Oxygen di-molecule etc in different phases with varied genetic structure.

*"None is "**ORPHAN**" in the world. Everyone is the **Foster child** of Natural parent. Foster child means **natural child**; adopted child means "**Legally valid child**".*

- M. Arulmani, Tamil based Indian

1. Key Words:

a) Philosophy of "**J-CODE**"?...
b) Philosophy of "**GODLY CHILD**"?...
c) Philosophy of "**FOSTER CHILD**"?...
d) Philosophy of "**ADOPTED CHILD**"?...
e) Philosophy of "**JAIL**"?...
f) Philosophy of "**JAMIN (bail)**"?...
g) Philosophy of "**PARADISE**"?...
h) Philosophy of "**MOTILAL**"?...

I. INTRODUCTION:

It is focused that global level killing of Female baby in the uterus is going on especially in **INDIA** without knowing the philosophy of female baby which is the precious gift of supernature.

i) What does mean "**Human Embryo**"?...
ii) What does mean "**Godly child**"?...
iii) What does mean "**Foster child**"?...
iv) What does mean "**Adopted child**"?...

It is focused by the author that **Human Embryo, Godly child, foster child, adopted child** have distinguished meaning before the court of "**INTERNATIONAL LAW**". It is the humble submission of author to the International courts for transparent definition for error free judgements for the benefit of future **global level populations** for promoting "**PEACE**".

*"**PEACE**" shall alternatively mean "**FOSTER CARE**"*

… Author

II. HYPOTHESIS AND NARRATION

a) Philosophy of Adopted child?...

Case study shows that the practice of Adoption of child exist since Ancient history of world in **Egyptian, Roman history**. Due to consistent controversies in adoption, the adoption terminology was under evolution and various language of adoption was formulated such as "**POSITIVE ADOPTION LANGUAGE (PAL)**", "**HONEST ADOPTION LANGUAGE (HAL)**".

HAL conveys **birth parents** are real parents (who do not need the birth prefix to express their relationship to their child), that the process of having ones child be adopted, is not always freely made and that the mother does not reliably have agency within the adoption process.

*"**GOD** is a father who graciously **adopts** believer in the **CHRIST** into his spiritual family and grants them all privileges of **Heirship**".*

…Biblical Study

It is hypothesized that the Philosophy of **Godly child** (Natural child), **Foster child, Adopted child** have distinguished meaning before International courts of law. The distinction shall be described as below.

(i)

GODLY CHILD
(Natural Process)

(ii)

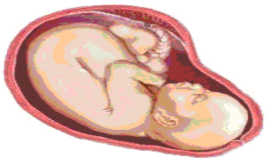

FOSTER CHILD
(Transformation Process)

(iii)

ADOPTED CHILD
(Legal Jack Fruit)

b) Philosophy of 'Human soul'?...

Case study shows that **medical science** could not claim so far **where from the first heart beat is derived?...** Scientists could not confirm "**How a small droplet of "Embryo" becomes beautiful child like "Jack Fruit" in three Trimester?...**

It is hypothesized that "**Embryo**" shall be considered as derived from "**SOUL**" (Law of Supernature) composed of **three-in one** fundamental ions of **photon, Electron proton** as described below.

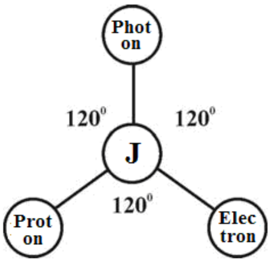

(HUMAN SOUL)

i) Proton is like "**DNA**" (Functional part)
ii) Electron is like "**HORMONE**" (structural part)
iii) Photon is like "**RNA**" (Sequential control part)
iv) J-Radiation is like "**LAW**" (Soul)

It is further hypothesized that "**J-Code**" shall be considered as the "**Universal code of Human**".

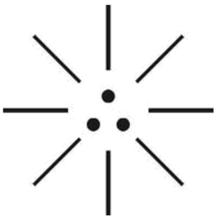

(J-CODE)

i) Right dot is like Right Nipple (**DNA**)
ii) Left dot is like Left Nipple (**HORMONE**)
iii) Centre dot is like Navel (Stem) (**RNA**)

*"The '**xx**' chromosome and '**xy**' chromosome shall be considered as the product of natural law"*

… Author

c) Philosophy of HEAVEN?...

It is hypothesized that "**Mother's womb**" on the Earth planet shall be considered as **JAIL** (Holy home). The etymology of word Jail might be derived from the proto Indo Europe roof "**CHEI ILLAM**". CHEI shall mean **INFANT**; ILLAM shall mean **HOUSE**. "**JAMIN**" (Bail) shall mean Transformation process for making "**PEACE**".

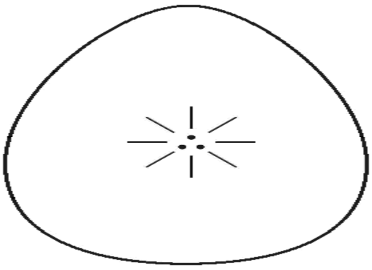

HEAVEN
(Mother's Womb)

d) Philosophy of "VIRGIN MOTHER'?...

It is hypothesized that '**Virgin mother**' shall be considered as belong to '**Angel family**' lived in white planet in the early universe. Virgin mother shall be considered as '**Supreme mother**' or **natural parent**. All children of universe shall be considered as "**FOSTER CHILDREN** or **NATURAL CHILDREN**. Earthly parents shall be considered as "**Legal birth parents**" or Legal adoptive parents. All earthly expenses have to be borne by '**Legal birth parents**'.

VIRGIN MOTHER
(FOSTER PARENT)

e) Case study on International mother's day?...

Case study shows that mother's day is being celebrated all over nations most commonly in the month of March or May to honour motherhood, maternal bonds and influence of mothers in the society. In India mother's day is being celebrated every year during second Sunday of May.

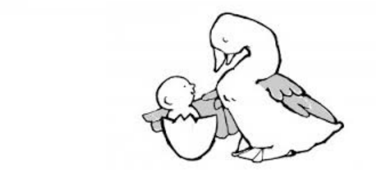

MOM THANKS FOR CARING!...
(Adopted Child)

f) Case study on Gandhiji?...

It is focused that Gandhiji is adopted by Indian Nationals as '**FATHER OF NATION**'. **If so Gandhiji is foster parent?... (or) Adoptive parent?...**

It is hypothesized that all the Indians shall be considered as the "**Foster children**" of Gandhiji. All earthly expenses have to be borne by "**legal birth parents**". However "**GANDHIAN LOAN**" shall be considered as financial assistance made to "**Poor children**" which is payable by **installments** (or) sometime **Non-payable**. It is further focused that Gandhiji shall alternatively be called as "MOTILAL". Motilal shall mean "**FOSTER PARENT**" rather than **masculine and pearl.**

OCTOBER, 2nd

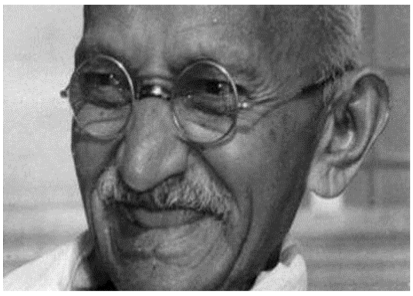

MOTILAL
(FOSTER PARENT)

*“**GANDHIJI**” does not have any account with “**SWISS BANK**”*

- Case study

It is the question of Gandhiji from his subconscious mind that everyone has ambition to become engineer, doctor, lawer, IAS, MLA, MP, Communal leader, Religious leader. But after reaching the status is it required to open account in **SWISS BANK**?... why not in **INDIAN BANK**?...

g) Case Study on INTERNATIONAL LEVEL “FOSTER CARE” SYSTEM

Case Study shows that Foster child means parental support and protection placed with a person or family to be cared for usually by **local welfare services or by court order.**

Foster Care is the term used for a system in which **MINOR** has been placed into a ward, group home or private home of **State certified** care giver referred to as a **“Foster Parent”.** The placement of child is usually arranged through **Government** or a social service agency. The Institution, a Group Home or foster parent is compensated for expenses.

In India foster care system first initiated in **1960** by the Central Government. The first non-institutional scheme was introduced in Maharashtra in **1972.** The scheme was later revised in 2005 as the **“BAL SANGOPAL SCHEME”** non-institutional services. Further the Centre for **Law and Policy Research”, Bangalore** in collaboration with **Foster Care India,** a registered organization in Rajasthan, has published a comprehensive brief on **Foster Care India** as it presently exist. Besides India has so many other schemes for **Cradle Baby, Garbage Baby** for protection of Orphan Babies and other schemes like **AMMA DRINKING WATER, AMMA FOOD, AMMA MEDICINE, AMMA SALT, AMMA SCHEME FOR TRAINING & EMPLOYMENT** for foster babies which being appreciated by world nations like **EGYPT, US, CANADA.**

Am I Garbage Baby?...

In **United States** and **United Kingdom Foster Care System** has been considered as service to the street Children and orphans. In United States **Foster Care System** started as a result of efforts of **Charles Loring Brace".** The Brace took the Children off the streets and placed them with families in most states in the country. According to U.S. Department of Health and Human Services Children's bureau, there are about **4,08,425** children in **Foster Care System** in 2010.

Searching for Voice of "AMMA"

Children of the United Kingdom's Child Migration Programme - many of whom were placed in foster care in Australia

In **Western Australia** first adoption legalization was passed in 1896. In Canada **Foster Care** is in existence and according to Canada Census 2011, majority of foster children about **29,590** of whom 62% were **"aged 14 and under".**

> *Foster Parent is like **"Godly Person".** Foster Children should take care and upright the **"Foster parents"** and should not send them to the **"old age home"** by **INIQUITY ACTIONS**.*
>
> ***- M. ARULMANI, Tamil based Indian***

III. CONCLUSION:

It is focused that '**Earth Planet**' shall be considered as **MEGA JAIL** and everyone consider living in **different cell** in different region. The Philosophy of "**Human death**" shall be considered as "**JAMIN**" (bail) to depart Earth planet and ultimately reach "**White planet**" which shall be called as Superheaven (or) **PARADISE** (J-GARDEN).

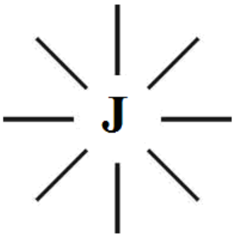

(PARADISE LOGO)

2. Previous Publication:

The philosophy of origin of first life and human, the philosophy of model Cosmo Universe, the philosophy of fundamental neutrino particles have already been published in various international journals mentioned below. Hence this article shall be considered as **extended version** of the previous articles already published by the same author.

[1] Cosmo Super Star – IJSRP, April issue, 2013
[2] Super Scientist of Climate control – IJSER, May issue, 2013
[3] AKKIE MARS CODE – IJSER, June issue, 2013
[4] KARITHIRI (Dark flame) The Centromere of Cosmo Universe – IJIRD, May issue, 2013
[5] MA-AYYAN of MARS – IJIRD, June issue, 2013
[6] MARS TRIBE – IJSER, June issue, 2013
[7] MARS MATHEMATICS – IJERD, June issue, 2013
[8] MARS (EZHEM) The mother of All Planets – IJSER, June issue, 2013
[9] The Mystery of Crop Circle – IJOART, May issue, 2013
[10] Origin of First Language – IJIRD, June issue, 2013
[11] MARS TRISOMY HUMAN – IJOART, June issue, 2013
[12] MARS ANGEL – IJSTR, June issue, 2013
[13] Three principles of Akkie Management (AJIBM, August issue, 2013)
[14] Prehistoric Triphthong Alphabet (IJIRD, July issue, 2013)
[15] Prehistoric Akkie Music (IJST, July issue, 2013)
[16] Barack Obama is Tamil Based Indian? (IJSER, August issue, 2013)
[17] Philosophy of MARS Radiation (IJSER, August 2013)
[18] Etymology of word **“J”** (IJSER, September 2013)
[19] NOAH is Dravidian? (IJOART, August 2013)
[20] Philosophy of Dark Cell (Soul)? (IJSER, September 2013)
[21] Darwin Sir is Wrong?! (IJSER, October issue, 2013)
[22] Prehistoric Pyramids are RF Antenna?!... (IJSER, October issue, 2013)
[23] HUMAN IS A ROAM FREE CELL PHONE?!... (IJIRD, September issue, 2013)
[24] NEUTRINOS EXIST IN EARTH ATMOSPHERE?!... (IJERD, October issue, 2013)
[25] EARLY UNIVERSE WAS HIGHLY FROZEN?!... (IJOART, October issue, 2013)
[26] UNIVERSE IS LIKE SPACE SHIP?!... (AJER, October issue, 2013)
[27] ANCIENT EGYPT IS DRAVIDA NAD?!... (IJSER, November issue, 2013)
[28] ROSETTA STONE IS PREHISTORIC “THAMEE STONE” ?!... (IJSER, November issue, 2013)
[29] The Supernatural “CNO” HUMAN?... (IJOART, December issue, 2013)
[30] 3G HUMAN ANCESTOR?... (AJER, December issue, 2013)
[31] 3G Evolution?... (IJIRD, December issue, 2013)
[32] God Created Human?... (IJERD, December issue, 2013)
[33] Prehistoric “J” – Element?... (IJSER, January issue, 2014)
[34] 3G Mobile phone Induces Cancer?... (IJERD, December issue, 2013)
[35] “J” Shall Mean “JOULE”?... (IRJES, December issue, 2013)
[36] “J”- HOUSE IS A HEAVEN?... (IJIRD, January issue, 2014)
[37] The Supersonic JET FLIGHT-2014?... (IJSER, January issue, 2014)
[38] “J”-RADIATION IS MOTHER OF HYDROGEN?... (AJER, January issue, 2014)
[39] PEACE BEGINS WITH “J”?... (IJERD, January issue, 2014)
[40] THE VIRGIN LIGHT?... (IJCRAR, January issue 2014)
[41] THE VEILED MOTHER?... (IJERD, January issue 2014)
[42] GOD HAS NO LUNGS?... (IJERD, February issue 2014)
[43] Matters are made of Light or Atom?!... (IJERD, February issue 2014)
[44] THE NUCLEAR “MUKKULAM”?... (IJSER, February issue 2014)
[45] WHITE REVOLUTION 2014-15?... (IJERD, February issue 2014)
[46] STAR TWINKLES!?... (IJERD, March issue 2014)
[47] “E-LANKA” THE TAMIL CONTINENT?... (IJERD, March issue 2014)
[48] HELLO NAMESTE?... (IJSER, March issue 2014)
[49] MOTHERHOOD MEANS DELIVERING CHILD?... (AJER, March issue 2014)
[50] E–ACHI, IAS?... (AJER, March issue 2014)
[51] THE ALTERNATIVE MEDICINE?... (AJER, April issue 2014)
[52] GANJA IS ILLEGAL PLANT?... (IJERD, April issue 2014)
[53] THE ENDOS?... (IJERD, April issue 2014)
[54] THE “TRI-TRONIC” UNIVERSE?... (AJER, May issue 2014)
[55] Varied Plasma Level have impact on “GENETIC VALUE”?... (AJER, May issue 2014)
[56] JALLIKATTU IS DRAVIDIAN VETERAN SPORT?... (AJER, May issue 2014)
[57] Human Equivalent of Cosmo?... (IJSER, May issue 2014)
[58] THAI-e ETHIA!... (AJER, May issue 2014)
[59] THE PHILOSOPHY OF “DALIT”?... (AJER, June issue 2014)

[60] THE IMPACT OF HIGHER QUALIFICATION?... (AJER, June issue 2014)
[61] THE CRYSTAL UNIVERSE?... (AJER July 2014 issue)
[62] THE GLOBAL POLITICS?... (AJER July 2014 issue)
[63] THE KACHCHA THEEVU?... (AJER July 2014 issue)
[64] THE RADIANT MANAGER?... (AJER July 2014 issue)
[65] THE UNIVERSAL LAMP?... (IJOART July 2014 issue)
[66] THE MUSIC RAIN?... (IJERD July 2014 issue)
[67] THIRI KURAL?... (AJER August 2014 issue)
[68] THE SIXTH SENSE OF HUMAN?... (AJER August 2014 issue)
[69] THEE… DARK BOMB?... (IJSER August 2014 issue)
[70] RAKSHA BANDHAN CULTURE?... (IJERD August 2014 issue)
[71] THE WHITE BLOOD ANCESTOR?... (AJER August 2014 issue)
[72] THE PHILOSOPHY OF “ZERO HOUR”?... (IJERD August 2014 issue)
[73] RAMAR PALAM?... (AJER September 2014 issue)
[74] THE UNIVERSAL TERRORIST?... (AJER September 2014 issue)
[75] THE “J-CLOCK”!... (AJER September 2014 issue)
[76] “STUDENTS” AND “POLITICS”?... (IJERD October 2014 issue)
[77] THE PREGNANT MAN?... (AJER September 2014 issue)
[78] PERIAR IS ATHEIST?... (IJSER September 2014 issue)
[79] A JOURNEY TO "WHITE PLANET”?... (AJER October 2014 issue)
[80] Coming Soon!... (AJER October 2014 issue)
[81] THE PREJUDICED JUSTICE?... (IJERD October 2014 issue)
[82] BRITISH INDIA?... (IJSER October 2014 issue)
[83] THE PHILOSOPHY OF “HUMAN RIGHTS”?... (IJERD October 2014 issue)

REFERENCE

a) Intensive Internet “e-book” study through, Google search and wikipedia
b) M.Arulmani, “3G Akkanna Man”, Annai Publications, Cholapuram, 2011
c) M. Arulmani; V.R. Hemalatha, “Tamil the Law of Universe”, Annai Publications, Cholapuram, 2012
d) Harold Koontz, Heinz Weihriah, “Essentials of management”, Tata McGraw-Hill publications, 2005
e) M. Arulmani; V.R. Hemalatha, “First Music and First Music Alphabet”, Annai Publications, Cholapuram, 2012
f) King James Version, “Holy Bible”
g) S.A. Perumal, “Human Evolution History”
h) “English Dictionary”, Oxford Publications
i) Sho. Devaneyapavanar, “Tamil first mother language”, Chennai, 2009
j) Tamilannal, “Tholkoppiar”, Chennai, 2007
k) “Tamil to English Dictionary”, Suravin Publication, 2009
l) “Text Material for E5 to E6 upgradaton”, BSNL Publication, 2012
m) A. Nakkiran, “Dravidian mother”, Chennai, 2007
n) Dr. M. Karunanidhi, “Thirukkural Translation”, 2010
o) “Manorama Tell me why periodicals”, M.M. Publication Ltd., Kottayam, 2009
p) V.R. Hemalatha, “A Global level peace tourism to Veilankanni”, Annai Publications, Cholapuram, 2007
q) Prof. Ganapathi Pillai, “Sri Lankan Tamil History”, 2004
r) Dr. K.K. Pillai, “South Indian History”, 2006
s) M. Varadharajan, “Language History”, Chennai, 2009
t) Fr. Y.S. Yagoo, “Western Sun”, 2008
u) Gopal Chettiar, “Adi Dravidian Origin History”, 2004
v) M. Arulmani; V.R. Hemalatha, “Ezhem Nadu My Dream” - (2 Parts), Annai Publications, Cholapuram, 2010
w) M. Arulmani; V.R. Hemalatha, “The Super Scientist of Climate Control”, Annai Publications, Cholapuram, 2013, pp 1-3

American Journal of Engineering Research (AJER)
e-ISSN : 2320-0847 p-ISSN : 2320-0936
Volume-03, Issue-10, pp-130-137
www.ajer.org

Research Paper Open Access

Extraction, physico-chemical, corrosion and exhaust analysis of transesterified neem *(Azadirachta indica)* oil blends in compression ignition (ci) engine.

Abdulkadir, L.N[1], Adisa, A.B[1], Kyauta E .E[1], Balogun, S[2].

[1]Abdulkadir, L.N, Mechanical Engineering Programme, Abubakar Tafawa Balewa University, Bauchi
[1]Adisa, A.B, Mechanical Engineering Programme, Abubakar Tafawa Balewa University, Bauchi
[1]Kyauta .E. E, Mechanical Engineering Programme, Abubakar Tafawa Balewa University, Bauchi
[2] Balogun, S, Mechanical Engineering Technology Federal Polytechnic Bauchi,

ABSTRACT: *In this work, Neem oil was extracted from its kernel, corrosive ability and physico-chemical properties of the oil were determined. The emission characteristics of a single cylinder, four stroke air-cooled diesel engine when fuelled with diesel and Neem-diesel blends at various loads were evaluated. The results showed that the fuel properties of Neem biodiesel were within the set standards for B100 and comparable with the conventional diesel. The corrosion rate of Neem biodiesel and diesel were both tested in copper and mild steel respectively. The test revealed that Neem biodiesel corrodes both test samples more than diesel. Air-fuel ratio values of Neem oil biodiesel blends are less than diesel, except for B25 and B30 NOME-Diesel fuel blends. Exhaust heat lost and exhaust temperature were lower in diesel than all blends. However, there is an appreciable decrease in HC and CO emissions while the decrease in CO is least for B20.*

Keywords: *Azadirachta indica, renewable fuel, extraction, physico-chemical analysis, exhaust emission.*

I. INTRODUCTION

Conventional energy sources, such as coal, oil and natural gas, have limited reserves that are expected not to last for an extended period. As world reserves of fossil fuels and raw materials are limited, it has stimulated active research interest in nonpetroleum, renewable, and non-polluting fuels. Biodiesel have received significant attention both as a possible renewable alternative fuel and as an additive to the existing petroleum-based fuels. Edible oils are much more valuable as a cooking fuel and as such, our concentration is going to be on development of biodiesel from non-edible oils only. Biodiesel has been defined as the monoalkyl esters of long-chain fatty acids derived from renewable feedstocks, such as vegetable oils or animal fats, for use in compression ignition (diesel) engines (Krawczyk., 1996). Transesterfication also called alcoholysis, is the displacement of alcohol from an ester by another alcohol in a process similar to hydrolysis, except that alcohol is used instead of water.

Straight vegetable oils (SVOs) have their fair share of problems in unmodified CI engines. These problems include: cold-weather starting; plugging and gumming of filters lines; excessive engine wear; and deterioration of engine lubricating oil. Vegetable oils decrease power output and thermal efficiency while leaving carbon deposits inside the cylinder. Most of these problems with vegetable oil are due to high viscosity, low cetane number, low flash point, and resulting incomplete combustion. To avoid some of these problems, vegetable oils have been converted via a chemical process (transesterification) to result in a fuel more like fossil diesel. The resulting fuel is biodiesel, a biodegradable and nontoxic renewable fuel. Furthermore, biodiesels have reduced molecular weights (in relation to triglycerides), reduced viscosity, and improved volatility when compared to ordinary vegetable oils.

As far as environmental considerations are concerned, unlike hydrocarbon-based fuels, the sulphur content of vegetable oils is close to zero and hence, the environmental damage caused by sulphuric acid is reduced. Moreover, vegetable oils take away more carbon dioxide from the atmosphere during their production than is added to it by their later combustion. Therefore, it alleviates the increasing carbon dioxide content of the atmosphere.

Neem (Azadirachta indica) which belongs to the family Meliaceae, originated from South Asia, but grows widely in India, Pakistan and other tropical and sub-tropical parts of the world (Bokhari and Aslam, 1985;Von Maydell, 1986). The tree was introduced in Nigeria from Ghana, and it was first grown from the seeds in Maiduguri, in the then Bornu Province (now Borno State), Nigeria, in 1928 (National Research Council, 1992; Nwoeabia, 1994).

The Neem tree is significant in Nigerian forestry because it constitutes the largest population of trees, especially in the Northern States. It was nicknamed ‘Dogon Yaro’ after the first caretaker of the Neem tree Nursery in Maiduguri. It is a large evergreen tree usually 12–18m high, and grows on almost all kinds of soil. It thrives well in arid and semi-arid climate with maximum shade temperature as high as 49^{o}C and the rainfall is as low as 250 mm (Bringi 1987, Narain and Satyavir 2002). A Neem tree can produce many thousands of flowers, and in one flowering cycle, a mature tree may produce a large number of seeds. The fruits are yellowish green when ripe and have a sweetish pulp containing one seed. Neem trees start bearing harvestable seeds within 3–5 years, and full production may be reached in 10 years, and this will continue up to 150 – 200 years of age. A mature neem tree may produce 30–50 kg of fruit each year. Neem seeds yield 40–60% oil (Narwal et al., 1997).

II. MATERIALS AND METHODS

100g of pounded neem seed was wrapped up in a filter paper which was placed in an extraction thimble of a soxhlet apparatus. The extraction flask was then fitted with 250ml of petroleum ether using an electric heating mantle, the petroleum ether was gently heated. The filter paper was removed, dried and its content weighed to determine the change in mass. The Percentage yield of the oil was calculated thus:

$$\%\ Oil\ yield = \frac{Wieght\ of\ oil}{Wieght\ of\ sample} \times 100$$

Physico-chemical properties such as; saponification value (S.V), iodine value (I.V), free fatty acid (FFA), acid value (A.V) where determined. Fatty Acid Methyl Ester (FAMES) of Neem was prepared by preheating 280g of oil to 45- 50^{o}C and adding 192g of methanol in a plastic container to maintain 6:1 alcohol to oil molar ratio. 2.8 g of KOH was also weighed on a digital beam balance and dissolved in a beaker containing 100ml of distilled water (H_2O) to give 1% of KOH solution based on weight of crude Neem oil. 1% of KOH solution was then introduced into the methanol in the plastic container and gently swirled. The preheated Neem oil was then added and stirred for 5 -10 minutes, and then heated to a temperature of 60^{o}C - 80^{o}C in a water bath to initiate the transesterification reaction (Lele, 2009; Belsor and Hedlund, 2007). The mixture was then poured into a separating funnel and allowed to settle for about 7-8 hours for the complete separation of glycerol from Neem oil methyl ester (NOME). About 10ml of 50^{o}C distilled water was added to the crude product and swirled slowly and left for some time to stand, the lower layer was then run off. This washing process was repeated until the product was clear. A small quantity of anhydrous magnesium sulphate was added and stirred for 5 minutes and the magnesium sulphate was allowed to settle. The biodiesel was later filtered using a filter paper to separate the biodiesel from the hydrated magnesium sulphate. The yield of the biodiesel was calculated thus:

$$\%\ yield\ of\ biodiesel = \frac{Volume\ of\ biodiesel}{Volume\ of\ oil}$$

Biodiesel blends of B10, B15, B20, B25 and B30 were respectively prepared and fuel qualities such as flash point, pour point, cloud point, kinematic viscosity, calorific value and corrosion tests were all tested.

Armfield corrosion test kit was used to test for the corrosive tendency of the produced Neem oil biodiesel using milled steel and copper strips as coupons. The test kit was set at normal environmental conditions away from direct sun light and test duration of four (4) weeks. The initial mass of the samples at the beginning of the test and that at the end of the test were taken to determine the change in mass of the samples. Average weight loss, Corrosion Penetration Rate (CPR) and Corrosion Ratio (CR) of biodiesel and diesel samples were calculated.

Surface area of coupons = $2\{T \times L + L \times W + W \times T\} - \frac{2\pi}{4}D^2$

Where T = Thickness
L = length
W = Width
D = Diameter of hole drilled on coupons = 0.5cm

Thickness of copper coupons = $T_c = 0.3$ cm
Length of copper coupons = $L_c = 5.9$ cm
Weight of copper coupons = $W_c = 2.2$ cm

$$\therefore \text{Area copper coupons} = 2\,(0.3 \times 5.9 + 0.3 \times 2.2 + 5.9 \times 2.2) - \frac{2 \times \pi \times 0.5^2}{4}$$

$$A_{CC} = \mathbf{30.43cm^2}$$

Thickness of milled steel coupons = $T_m = 0.3$cm
Length of milled steel coupons = $L_m = 4$cm
Width of milled steel coupons = $W = 2.0$cm

$$\therefore \text{Area milled steel coupons} = 2\,(0.3 \times 4 + 2 \times 4 + 0.3 \times 2) - \frac{2 \times \pi \times 0.5^2}{4}$$

$$A_{MSC} = \mathbf{19.21cm^2}$$

Average weight loss = $\frac{\Sigma \text{ of change in mass for the weeks}}{\text{number of weeks}}$

Corrosion penetration rate (CPR) = $\frac{W}{\rho A T}$

Where W = weight loss
T = Time in days
$A_{CC} = 30.43cm^2$
$A_{MSC} = 19.21cm^2$
$\rho_{CC} = 8.92g/cm^3$
$\rho_{MSC} = 7.88g/cm^3$

Corrosion Ratio (CR) = $\frac{\text{CPR for a coupon type in biodiesel}}{\text{CPR for the same coupon type in diesel}}$

AVL DiGas 4000 gas analyser was used to measure concentration of gaseous emissions [Unburned hydrocarbon (UHC), carbon monoxide (CO)] to evaluate and compute the behavior of the diesel engine at constant speed of 1500 rev/min and varying load of between 500g – 3000g. The results obtained from performance analyses was tabulated and necessary graphs plotted. Technical detail of the engine is given in table 1. A hydraulic dynamometer was coupled to the engine for torque measurement.

Table 1: Technical specifications of engine test rig

Type	Single cylinder, four stroke, air-cooled
Bore * Stroke	65 mm x 70 mm
Brake power	2.43kW
Rated speed	1500rpm
Starting method	Manual cranking
Compression ratio	20.5:1
Net weight	45Kg
Manufacturer	TQ Educational Training Ltd

III. RESULTS AND DISCUSSION

Percentage oil yield: The oil yield of Neem was found to be 58.3% this compares favourably with 40–60% oil yield by Narwal et al (1997). The high oil yield of Neem seed is an indication that Neem is a good source of oil. Yield of biodiesel from different non-edible oils (Jatropha curcas, Pongamia pinnata, Madhuca Indica and Azadirachta Indica) which are commonly available in India were examined and the results recommended the biodiesel production from Azadirachta Indica oil on the basis of high yield and quality of biodiesel (Mathiyazhagan et al., 2011). The economic evaluation has also shown that biodiesel production from Neem is very profitable (Mathiyazhagan et al., 2011).

Physico-chemical Properties: The physico-chemical properties of Neem oil, Neem methyl ester, Neem blends and conventional diesel (D2 or No2) are presented in Table 2 The physico-chemical properties of Neem biodiesel were within the limits and comparable with the conventional diesel. Except calorific value, all other properties of Neem biodiesel and its blends were found to be higher as compared to diesel.

Table 2: Summary of the properties of tested samples

Fuel Property	**Diesel**	**Neem Oil**	**B100 (NOME)**	**B10**	**B15**	**B20**	**B25**	**B30**
Density at 15°C (kg/m^3)	830	920	872	845	849	854	860	865
Kinematic Viscosity at 40°C (mm^2/s)	4.0	35.52	5.5	4.4	4.45	4.5	4.55	4.6
Flash Point (°C)	65	212	136	72	79	87	94	101
Pour Point (°C)	-16	10	2	-11	-10	-8	-7	-5
Coud Point (°C)	-12	19	9	-7	-6	-5	-4	-3
Saponification Value (mgKOH/g)	-	188.1	-	-	-	-	-	-
Acid Value (mgKOH/g)	-	6.77	-	-	-	-	-	-
Iodine Value (mgI/g)	-	64	-	-	-	-	-	-
Specific gravity	0.830	0.920	0.872	0.845	0.849	0.854	0.860	0.865
Cetane Number	45-55	31-51	48-53	-	-	-	-	-
Calorific Value (MJ/kg)	44.76	34.10	36.70	43.80	43.30	42.80	42.40	41.90
FFA Value wt %	-	3.40	-	-	-	-	-	-

Corrosion value: The corrosion rate of Neem biodiesel and diesel were both tested in copper and mild steel respectively. The test revealed that Neem biodiesel corrodes both test samples more than diesel (Table 3). Biodiesel is believed to contain residual water because of transesterification; this could be responsible for higher rate of corrosion. Many of the parts in the diesel fuel injection system are made of high carbon steels; thus, they are prone to corrosion when in contact with water. Water damage is a leading cause of premature failure of fuel injection systems. The water content of petroleum diesel is usually quite low since hydrocarbons are generally hydrophobic. Fatty acid esters, on the other hand, are hygroscopic and will contain high water content by merely being exposed to moist air during storage. Water will cause corrosion of vital fuel system components fuel pumps, injector pumps, fuel tubes, etc (Ayhan, 2009). Also the higher the acid value of biodiesel the more it corrodes. Neem biodiesel has an appreciably high acid value above the benchmark standards given by both ASTM and DIN V 51606.

Table 3: Corrosion test of biodiesel using armfield corrosion test kit

Sample immersion	**Metal coupons**	***W***	**CPR**
Samples immersed in biodiesel	Milled steel	0.015	1.416 × 10^{-5} cm / day
	Copper	0.0525	2.763 × 10^{-5} cm / day
Samples immersed in petroleum diesel	Milled steel	0.0125	1.180 × 10^{-5} cm / day
	Copper	0.0225	1.184 × 10^{-5} cm / day

Corrosion Ratio (CR)

CR for Copper coupons = $\frac{2.763 \times 10^{-5}}{1.184 \times 10^{-5}} = 2.334$

CR for Milled steel coupons = $\frac{1.416 \times 10^{-5}}{1.180 \times 10^{-5}} = 1.2$

Exhaust Temperature: Figure 1 shows the variation of exhaust gas temperature with load for various blends and diesel. The results showed that exhaust gas temperature increases with increase in load for all blends. At all loads, diesel was found to have the lowest temperature and the temperatures for various blends showed an upward trend with increasing concentration of NOME in the blends . This increase in exhaust gas temperature with load is obvious from the simple fact that more amount of fuel is required in the engine to generate that extra power needed to take up the additional loading. Biodiesel contains oxygen, which enables the combustion process; hence the exhaust gas temperatures are higher. Moreover, the engine being air-cooled runs hotter, this resulted in higher exhaust gas temperatures. The heat release may occur in the later part of the power stroke this may result in lower time for heat dissipation and higher exhaust gas temperatures. The increased exhaust gas temperature of the engine with the use of biodiesel blends may be caused by the rise in peak cylinder pressure resulting in higher peak combustion temperature as reported by Ecklud, (1984).

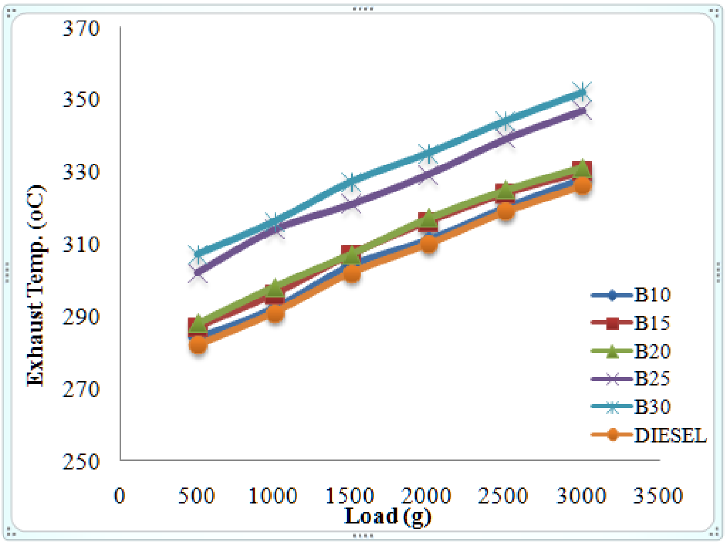

Figure 1: *Variation of Exhaust Temp. For all samples with increase in load*

Air/Fuel ratio(AFR): Figure 2 shows the variation of air-fuel ratio with load for all tested samples. In C.I engines at a given speed the air flow do not vary with load, it is the fuel flow that varies directly with load. As seen from the figure below, as percentage blend increases the air fuel ratio decreases but increases with increase in load. Air-fuel ratio values of neem oil biodiesel blends are less than diesel. Except for B25 and B30 NOME-Diesel fuel blends, which demonstrated average difference of 6.18% and 9.4% from the AFR of diesel fuel, B10, B15 and B20 NOME-Diesel fuel are 1.78%, 2.24% and 2.81% lower than diesel fuel benchmark respectively. The observation made from this finding is that all tested fuel samples reached maximum power output and torque at higher than the stoichiometric AFR values (i.e. 18-25) for compression ignition engines. In this case, maximum power output is achieved at lean mixture, therefore causing the engine to run at higher engine temperature. The bound oxygen on the biodiesel molecule may also play a role in creating a leaner air-fuel ratio, which in turn leads to high air-fuel ratio higher than the stoichiometric AFR values for all the samples tested.

According to Goering (1992), the stoichiometric AFR values of engines running on biodiesel are usually lower than diesel fuel because more oxygen presence is evident in biodiesel due to the methanolysis of sheanut oil, and it enabled SHOME blended fuel samples to burn much richer than diesel fuel.

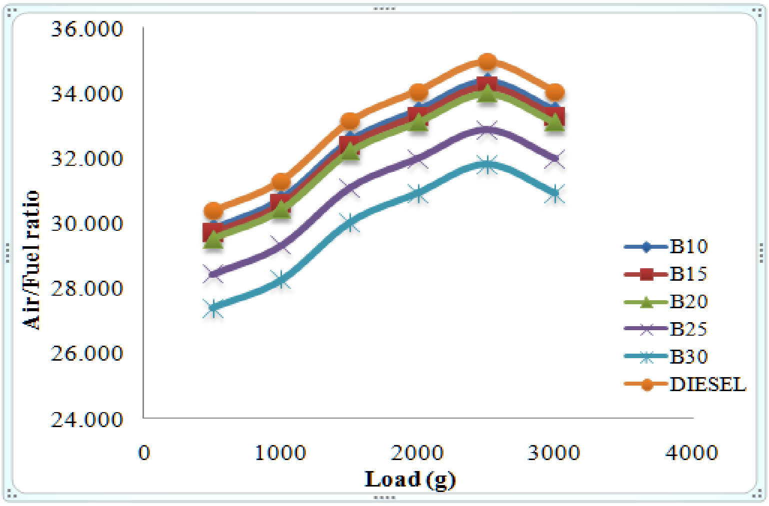

Figure 2: *Variation of Air/Fuel ratio for all samples with increase in load*

Percentage heat loss

From figure 3, all NOME-Diesel blends show evidence of higher heat losses in engines than diesel fuel by average values of 0.65% for B10, 2.90% for B15, 3.86% for B20, 6.29% for B25 and 5.65% for B30 respectively. The higher heat loss recorded could be explained in terms of lower calorific (heating) valve, increase in fuel density, the difference between the exhaust and ambient temperatures and the size of the engine. The temperature difference existing between the fuel blends and diesel fuel benchmark in figure 3 also presented a proportional increase in the heat carried away by the exhaust. However, for heat unaccounted for by losses is partly a function of the engine size, because for smaller engines, considerable conductive and radiative heat losses are usually caused by inefficient combustion (Plint and Partners, 1984). High exhaust gas temperature and reduction in thermal efficiency with increase in blend is an evidence of increase in heat loss. The mean exhaust gas temperature of B20, B40, B60 and B100 were 7%, 9% 10% and 12%, respectively, higher than the mean exhaust gas temperature of diesel. This could be due to the increased heat loss of the higher blends, which are also evident from, their lower brake thermal efficiencies as compared to diesel (Sharanappa et al., 2009).

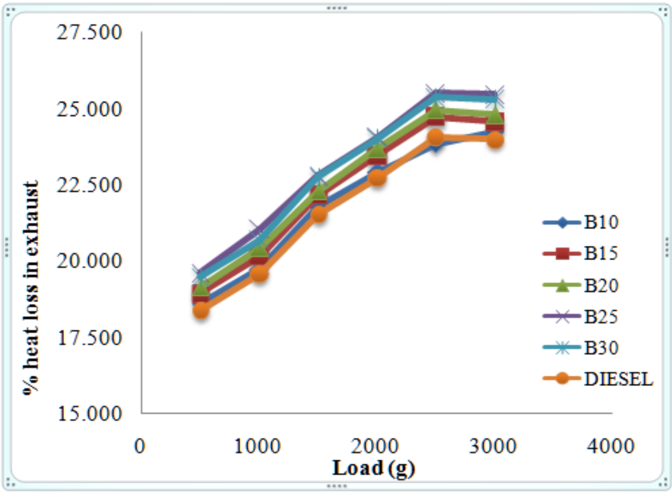

Figure 3: *Variation of % heat loss for all samples with increase in load*

CO Emission of diesel and Neem biodiesel blends: The variation of CO emission with load is shown in figure 4. It was observed that the engine emits more CO for diesel at all load conditions when compared to the blends. However, as the proportion of NOME in the blend increases the percentage emission decreases due to higher oxygen content and lower carbon to hydrogen ratio in biodiesel compared to diesel. The percentage variation of carbon monoxide for all the blends when compared with base line diesel is very much less. These lower CO emissions of biodiesel blends may be due to their more complete oxidation as compared to diesel. Some of the CO produced during combustion of biodiesel might have converted to CO_2 by taking up the extra oxygen molecule present in the biodiesel chain (Biodiesel has up to 11% oxygen content :Ragit et al, 2010) and thus reduced CO formation. It can be observed from figure 4 that the CO initially decreased with load and latter increased at higher load. This trend was observed for all the fuel blends tested. At lower biodiesel concentration, the oxygen present in the biodiesel aids for complete combustion. However as the biodiesel concentration increases, the negative effect due to high viscosity and small increase in specific gravity suppresses the complete combustion process, which produces small amount of CO (Sureshkumar and Veltra., 2007). Last et al. (1995) fuelled a heavy-duty engine with 10%, 20%, 30%, 50% and 100% soybean-oil biodiesel. All the blends reduced CO emissions with respect to the diesel fuel, but such decreases did not depend on the biodiesel percentage (10%, 8%, 18%, 6% and 14% reductions, respectively). Also, Rakopoulos et al. (2004) reported lower CO concentration in the exhaust line when oxygen in the combustion chamber was increased either with oxygenated fuels or oxygen-enriched air.

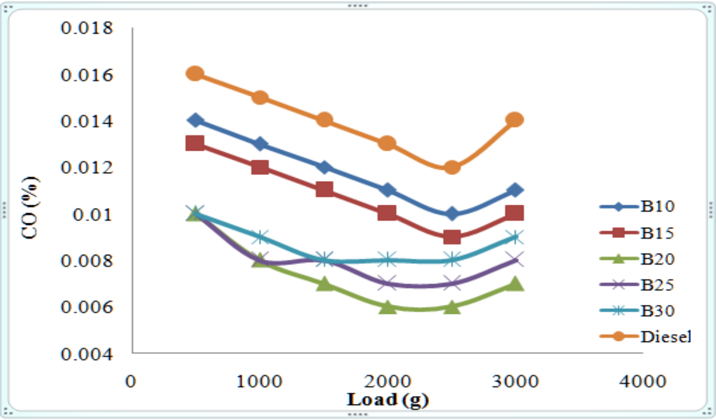

Figure 4: *Emission of CO for all samples with increase in load*

HC Emission of diesel and neem biodiesel blends: The HC emission variation for different blends is indicated in figure 5. All blends have lower values than diesel owing to higher combustion chamber temperature, which helps in cracking and faster burning. It was observed that the HC emission decreased up to a load of 2500g and then increased slightly with further increase in load for all the samples. The HC emission for the blends also followed a similar trend but comparatively the values were lower. The presence of oxygen in the Neem blends aids combustion and hence the hydrocarbon emission reduced. It was suggested that the short ignition delay when using biodiesel could also attribute to lower HC emissions (Lapueta et al., 2008). Rakopoulos et al. (2004) concluded in to their review that HC emissions decreased as the oxygen in the combustion chamber increased, either with oxygenated fuels or oxygen-enriched air. Sahoo et al. (2009) reported that the reduction of HC was of the order of 32.28%, 18.19% and 20.73% for JB20, JB50, JB100, respectively.

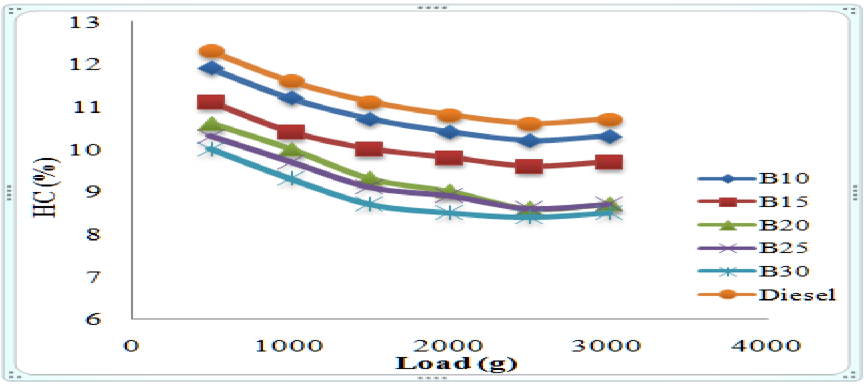

Figure 28: *Emission of HC for all tested samples with increase in load*

IV. CONCLUSION

The physico-chemical properties of Neem biodiesel were within the set standards for B100 and comparable with the conventional diesel. Except calorific value, all other physico-chemical properties of Neem biodiesel were found to be higher as compared to diesel. Exhaust gas temperature emission increases with increase in percentage blend and load for all the cases. The engine being air-cooled the exhaust gas temperatures are higher. As percentage blend increases the Air-fuel ratio decreases but increases with increase in load. Air-fuel ratio values of Neem oil biodiesel blends are less than diesel. B30 gave the best and least ratio. The lean mixture of the engine was observed to be responsible for the high temperature operation which is also linked to the increased heat loss. Percentage heat loss in exhaust increases with increase in blend and load. Diesel showed the best performance as regards heat loss while B10 showed the closest value to it amongst all the blends. It was observed that all samples showed a close relation in heat loss. The engine emits more CO for diesel at all load conditions when compared to the blends, however, as the proportion of NOME in the blend increases the percentage emission decreases. HC emission was lower in blends than diesel and decreases with increase in load. The lowest value obtained for CO emission was with B20 blend. Hydrocarbon emission decreased with increase in percentage NOME in the blend and decreased with increase load until 2500g load where it showed an increase value. HC emission in all blends are lower than that of diesel and the least value was obtained with B30 blend.

REFRENCES

[1]. ASTM 1982. ASTM Standard parts 17 and 18. *American Society of Testing and Materials.* Philadelphia, Pennsylvania.

[2]. Ayhan Demirbas. (2009). Progress and recent trends in biodiesel fuels. *Journal of Energy Conversion and Management. 50,* 14–34.

[3]. Belsor, E. & Hedlund, N. (2004). Synergy of the Americas.: a model for biodiesel production. *CU Biodiesel publication.* 9-10.

[4]. Bokhari, M. H. and Aslam, K. M. (1985). Neem (*Melia Azadirachta* A. Juss). A useful tree in Northern Nigeria. *Annals of Borno* II: 83 – 86.

[5]. Bringi, N. V. (1987). Non- traditional oilseeds and oils of India. New Delhi: Oxford & IBH Publishing Co. Pvt. Ltd.

[6]. Ecklund, E. (1984). Alcohols in diesel engine: A review SAE paper no. 840119. *Society of Automotive Engineers.* 28 (1):70-74

[7]. Goering, C.F. (1992). Engine Tractor Power. Copyright Edition. American Society of Agricultural Engineers Publications, Michigan: 358 – 362.

[8]. Krawczyk, T. (1996). Biodiesel-alternative fuel makes inroads but hurdles remain. *INFORM 7. (8),* 800±15.

[9]. Lapuerta, M., Herreros, J. M., Lyons, L. L., Garcia-Contreras, R. and Briceno, Y. (2008). Effect of the alcohol type used in the production of waste cooking oil biodiesel on diesel performance and emissions. *Fuel. 87,* 3161–3169.

[10]. Lapuerta, M., Octavio, A. and Jose´, R. (2008). Effect of biodiesel fuels on diesel engine emissions. *Progress in Energy and Combustion Science. 34,*198–223.

[11]. Last, R. J., Kru¨ ger, M. and Du¨ rnholz, M. (1995). Emissions and performance characteristics of a 4-stroke, direct injected diesel engine fueled with blends of biodiesel and low sulfur diesel fuel. *Society of Automotive Engineers paper 950054.*

[12]. Lele S (2009) Biodiesel in India. Publication of Indian Biodiesel Awareness Centre. Retrieved May 2, 2009, from: http://www.svlele.com

[13]. Mathiyazhagan, M., Ganapathi, A, Jaganath, B,, Renganayaki, N. and Sasireka, N. (2011). Production of biodiesel from non-edible plant oils having high FFA content. *Int J Chem Environ Eng; 2(2),*119–22.

[14]. Narain P. Satyavir. (2002, November 27-30). Neem in India: present status and future thrust. *In: Proceeding of world neem conference, Mumbai. 1,* 10–20.

[15]. Narwal, S. S,, Tauro, P. and Bisla, S. S. (1997). Neem in sustainable agriculture. Jodhpur, India: Scientific Publishers.

[16]. National Research Council (1992). *Neem: a tree for solving global problems.* National Academy Press, Washington, DC. Pp.115.

[17]. Nwoekeabia, O.D. (1994). Annual Report, Federal Department of Forestry, Federal Ministry of Agriculture, Abuja, Nigeria. Pp 45.

[18]. Plint and Partners (1984): Shell- Plint Engine Test Bed Manual. Plint and Partners Publications, England , Pp 8-14 .

[19]. Ragit, S.S., Mohapatra, S. K. and Kundu, K. (2010). Performance and emission evaluation of a diesel engine fuelled with methyl ester of neem oil and filtered neem oil. *J Sci Ind Res. 69,* 62–6.

[20]. Rakopoulos, C. D., Hountalas, D. T., Zannis, T. C. and Levendis, Y. A. (2004). Operational and environmental evaluation of diesel engines burning oxygen-enriched intake air or oxygen-enriched fuels: a review. *Society of Automotive Engineers paper -01-2924.*

[21]. Sahoo, P. K., Das, L. M., Babu, M. K. G., Arora, P., Singh, V. P., Kumar, N. R, *et al*. (2009). Comparative evaluation of performance and emission characteristics of jatropha, karanja and polanga based biodiesel as fuel in a tractor engine. *Fuel. 88:*1698–707.

[22]. Sharanappa, G., Suryanarayana, M. C. H. & Rana, P. R. (2009). 6BTA 5.9 G2-1 Cummins engine performance and emission tests using methyl ester mahua (Madhuca indica) oil/diesel blends. *Renewable Energy 34:* 2172–2177.

[23]. Sureshkumar, K. and Velra, R. (2007). Performance and Characteristics Study of the Use of Environment Friendly Pongamia Pinnata Methyl Ester in C. I. Engines. *Journal of Energy & Environment, 5:* 60-71.

[24]. Von Maydell, H. J. (1986). *Trees and shrubs of the Sahel, their characteristics and uses*. Eschborn Germany. 173-175.

American Journal of Engineering Research (AJER)
e-ISSN : 2320-0847 p-ISSN : 2320-0936
Volume-03, Issue-10, pp-138-144
www.ajer.org

Research Paper Open Access

Important Pitot Static System in Aircraft Control System

Er. Naser.F.AB.Elmajdub[1], Dr.A.K. Bharadwaj[2]
[1, 2] (Department, of Electrical Engineering, SHIATS Allahabad, India)

ABSTRACT : In order to safely fly any aircraft, a pilot must understand how to interpret and operate the flight instruments. The pilot also needs to be able to recognize associated errors and malfunctions of these instruments. When a pilot understands how each instrument works and recognizes when an instrument is malfunctioning, he or she can safely utilize the instruments to their fullest potential. The pitot-static system is a combined system that utilizes the static air pressure, and the dynamic pressure due to the motion of the aircraft through the air. These combined pressures are utilized for the peration of the airspeed indicator (ASI), altimeter, and vertical speed indicator (VSI)

I. INTRODUCTION

Impact Pressure Chamber and Lines

The pitot tube is utilized to measure the total combined pressures that are present when an aircraft moves through the air. Static pressure, also known as ambient ressure, is always present whether an aircraft is moving or at rest. It is simply the barometric pressure in the local area. Dynamic pressure is present only when an aircraft is in motion; therefore, it can be thought of as a pressure due to motion. Wind also generates dynamic pressure. It does not matter if the aircraft is moving through still air at 70 knots or if the aircraft is facing a wind with a speed of 70 knots, the same dynamic pressure is generated.When the wind blows from an angle less than 90° off the nose of the aircraft, dynamic pressure can be depicted on the ASI. The wind moving across the airfoil at 20 knots is the same as the aircraft moving through calm air at 20 knots. The pitot tube captures the dynamic pressure, as well as the static pressure that is always present. The pitot tube has a small opening at the front which allows the total pressure to enter the pressure chamber. The total pressure is made up of dynamic pressure plus static pressure. In addition to the larger hole in the front of the pitot tube, there is a small hole in the back of the chamber which allows moisture to drain from the system should the aircraft enter precipitation. Both openings in the pitot tube need to be checked prior to flight to insure that neither is blocked. Many aircraft have pitot tube covers installed when they sit for extended periods of time. This helps to keep bugs and other objects from becoming lodged in the opening of the pitot tube.The one instrument that utilizes the pitot tube is the ASI. The total pressure is transmitted to the ASI from the pitot tube's pressure chamber via a small tube. The static pressure is also delivered to the opposite side of the ASI which serves to cancel out the two static pressures, thereby leaving the dynamic pressure to be indicated on the instrument. When the dynamic pressure changes, the ASI shows either increase or decrease, corresponding to the direction of change. The two remaining instruments (altimeter and VSI) utilize only the static pressure which is derived from the static port.Static

Pressure Chamber and Lines

The static chamber is vented through small holes to the free undisturbed air on the side(s) of the aircraft. As the atmospheric pressure changes, the pressure is able to move freely in and out of the instruments through the small lines which connect the instruments into the static system. An alternate static source is provided in some aircraft to provide static pressure should the primary static source become blocked. The alternate static source is normally found inside of the flight deck. Due to the venturi effect of the air flowing around the fuselage, the air pressure inside the flight deck is lower than the exterior pressure.

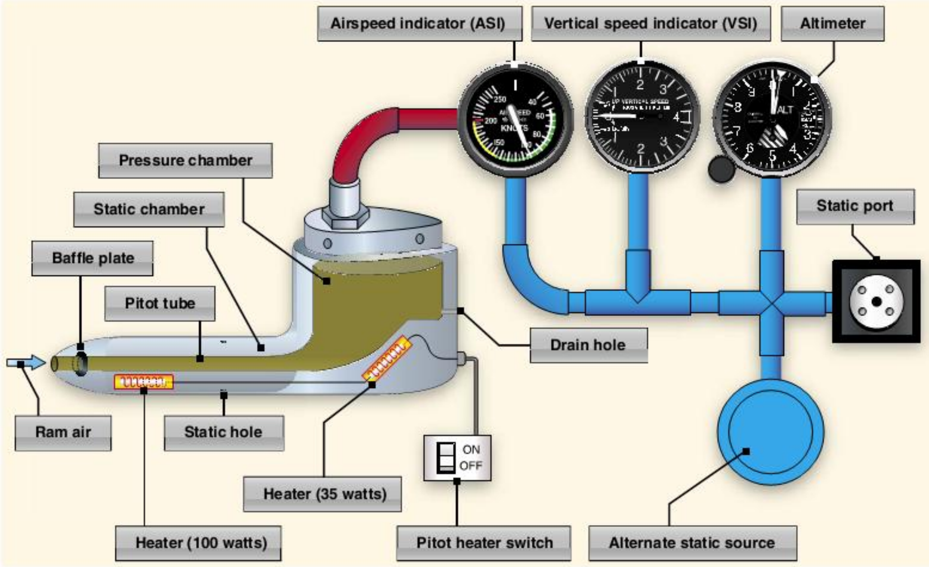

Figure 1. Pitot-static system and instruments

II. MATERIAL & METHODS

Altimeter

The altimeter is an instrument that measures the height of an aircraft above a given pressure level. Pressure levels are discussed later in detail. Since the altimeter is the only instrument that is capable of indicating altitude, this is one of the most vital instruments installed in the aircraft. To use the altimeter effectively, the pilot must understand the operation of the instrument, as well as the errors associated with the altimeter and how each effect the indication.A stack of sealed aneroid wafers comprise the main component of the altimeter. An aneroid wafer is a sealed wafer that is evacuated to an internal pressure of 29.92 inches of mercury (29.92 "Hg). These wafers are free to expand and contract with changes to the static pressure. A higher static pressure presses down on the wafers and causes them to collapse. A lower static pressure (less than 29.92 "Hg) allows the wafers to expand. A mechanical linkage connects the wafer movement to the needles on the indicator face, which translates compression of the wafers into a decrease in altitude and translates an expansion of the wafers into an increase in altitude.Notice how the static pressure is introduced into the rear of the sealed altimeter case. The altimeter's outer chamber is sealed, which allows the static pressure to surround the aneroid wafers. If the static pressure is higher than the pressure in the aneroid wafers (29.92 "Hg), then the wafers are compressed until the pressure inside the wafers is equal to the surrounding static pressure. Conversely, if the static pressure is less than the pressure inside of the wafers, the wafers are able to expand which increases the volume. The expansion and contraction of the wafers moves the mechanical linkage, which drives the needles on the face of the ASI.

Principle of Operation

The pressure altimeter is an aneroid barometer that measures the pressure of the atmosphere at the level where the altimeter is located, and presents an altitude indication in feet. The altimeter uses static pressure as its source of operation. Air is denser at sea level than aloft—as altitude increases, atmospheric pressure decreases. This difference in pressure at various levels causes the altimeter to indicate changes in altitude.The presentation of altitude varies considerably between different types of altimeters. Some have one pointer while others have two or more. Only the multipointer type is discussed in this handbook. The dial of a typical altimeter is graduated with numerals arranged clockwise from zero to nine. Movement of the aneroid element is transmitted through gears to the three hands that indicate altitude. The shortest hand indicates altitude in tens of thousands of feet, the intermediate hand in thousands of feet, and the longest hand in hundreds of feet.

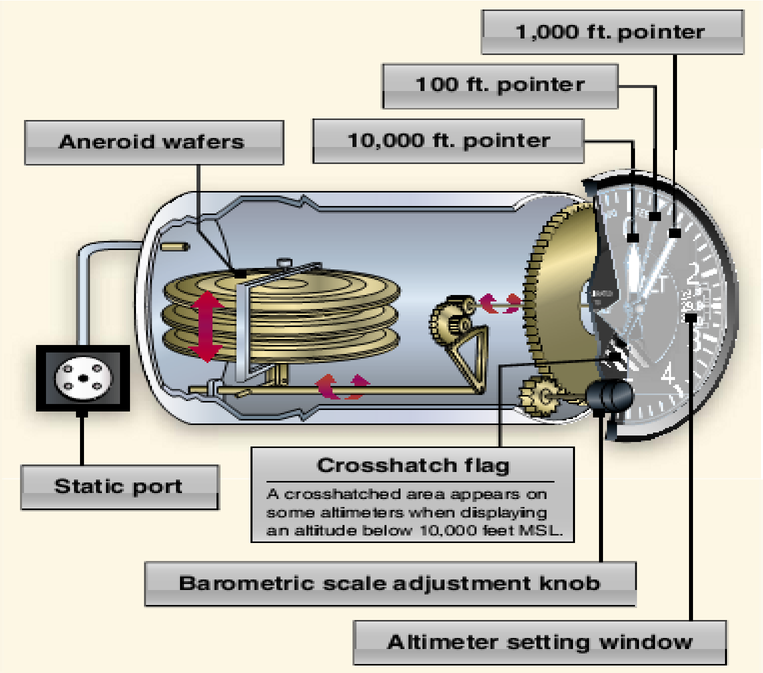

A crosshatched area appears on some altimeters when displaying an altitude below 10,000 feet MSL.

Figure 2. Altimeter

Vertical Speed Indicator (VSI)

The VSI, which is sometimes called a vertical velocity indicator (VVI), indicates whether the aircraft is climbing, descending, or in level flight. The rate of climb or descent is indicated in feet per minute (fpm). If properly calibrated, the VSI indicates zero in level flight.

Principle of Operation

Although the VSI operates solely from static pressure, it is a differential pressure instrument. It contains a diaphragm with connecting linkage and gearing to the indicator pointer inside an airtight case. The inside of the diaphragm is connected directly to the static line of the pitot-static system. The area outside the diaphragm, which is inside the instrument case, is also connected to the static line, but through a restricted orifice (calibrated leak).Both the diaphragm and the case receive air from the static line at existing atmospheric pressure. The diaphragm receives unrestricted air while the case receives the static pressure via the metered leak. When the aircraft is on the ground or in level flight, the pressures inside the diaphragm and the instrument case are equal and the pointer is at the zero indication. When the aircraft climbs or descends, the pressure inside the diaphragm changes immediately, but due to the metering action of the restricted passage, the case pressure remains higher or lower for a short time, causing the diaphragm to contract or expand. This causes a pressure differential that is indicated on the instrument needle as a climb or descent.

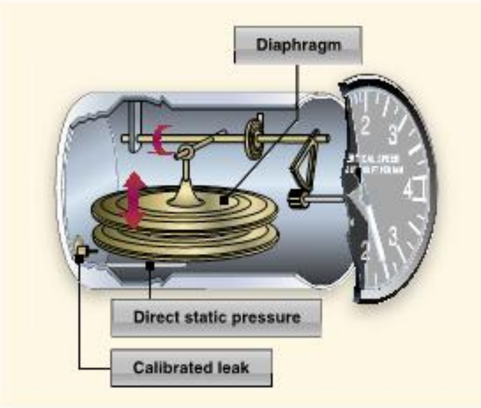

Figure 3. Vertical speed indicator (VSI)

Airspeed Indicator (ASI)

The ASI is a sensitive, differential pressure gauge which measures and promptly indicates the difference between pitot (impact/dynamic pressure) and static pressure. These two pressures are equal when the aircraft is parked on the ground in calm air. When the aircraft moves through the air, the pressure on the pitot line becomes greater than the pressure in the static lines. This difference in pressure is registered by the airspeed pointer on the face of the instrument, which is calibrated in miles per hour, knots (nautical miles per hour), or both. The ASI is the one instrument that utilizes both the pitot, as well as the static system. The ASI introduces the static pressure into the airspeed case while the pitot pressure (dynamic) is introduced into the diaphragm. The dynamic pressure expands or contracts one side of the diaphragm, which is attached to an indicating system. The system drives the mechanical linkage and the airspeed needle.Just as in altitudes, there are multiple types of airspeeds. Pilots need to be very familiar with each type.

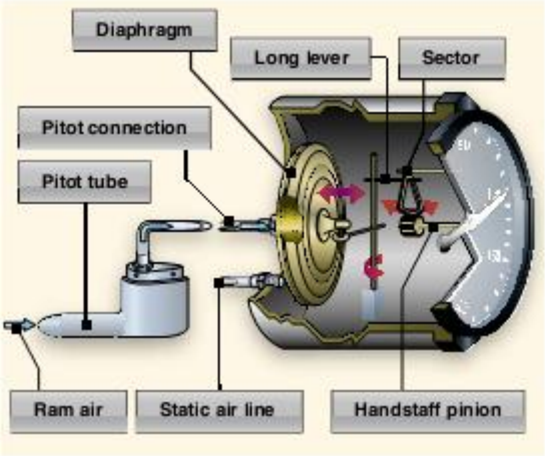

Figure 4. Airspeed indicator (ASI).

I. RESULT & DISCUSSION

Effect of Nonstandard Pressure and Temperature

It is easy to maintain a consistent height above ground if the barometric pressure and temperature remain constant, but this is rarely the case. The pressure temperature can change between takeoff and landing even on a local flight. If these changes are not taken into consideration, flight becomes dangerous.If altimeters could not be adjusted for nonstandard pressure, a hazardous situation could occur. For example, if an aircraft is flown from a high pressure area to a low pressure area without adjusting the altimeter, a constant altitude will be displayed, but the actual height of the aircraft above the ground would be lower then the indicated altitude. There is an old aviation axiom: “GOING FROM A HIGH TO A LOW, LOOK OUT BELOW.” Conversely, if an aircraft is flown from a low pressure area to a high pressure area without an adjustment of the altimeter, the actual altitude of the aircraft is higher than the indicated altitude. Once in flight, it is important to frequently obtain current altimeter settings en route to ensure terrain and obstruction clearance.Many altimeters do not have an accurate means of being adjusted for barometric pressures in excess of 31.00 inches of mercury ("Hg). When the altimeter cannot be set to the higher pressure setting, the aircraft actual altitude will be higher than the altimeter indicates. When low barometric pressure conditions occur (below 28.00), flight operations by aircraft unable to set the actual altimeter setting are not recommended. Adjustments to compensate for nonstandard pressure do not compensate for nonstandard emperature. Since cold air is denser than warm air, when operating in temperatures that are colder than standard, the altitude is lower than the altimeter indication. It is the magnitude of this “difference” that determines the magnitude of the error. It is the difference due to colder temperatures that concerns the pilot. When flying into a cooler air mass while maintaining a constant indicated altitude, true altitude is lower. If terrain or obstacle clearance is a factor in selecting a cruising altitude, particularly in mountainous terrain, remember to anticipate that a colder-than-standard temperature places the aircraft lower than the altimeter indicates. Therefore, a higher indicated altitude may be required to provide adequate terrain clearance. A variation of the memory aid used for pressure can be employed: “FROM HOT TO COLD, LOOK OUT BELOW.” When the air is warmer than standard, the aircraft is higher than the altimeter indicates. Altitude corrections for temperature can be computed on the navigation computer.

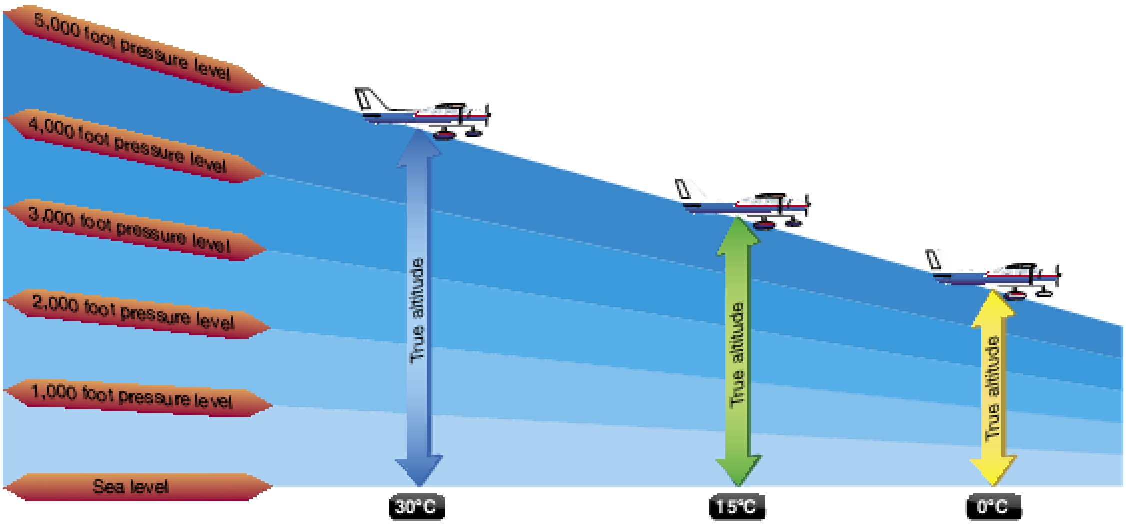

Figure 5. Effects of nonstandard temperature on an altimeter.

Blocked Pitot System

The pitot system can become blocked completely or only partially if the pitot tube drain hole remains open. If the pitot tube becomes blocked and its associated drain hole remains clear, ram air no longer is able to enter the pitot system. Air already in the system vents through the drain hole, and the remaining pressure drops to ambient (outside) air pressure. Under these circumstances, the ASI reading decreases to zero, because the ASI senses no difference between ram and static air pressure. The ASI no longer operates since dynamic pressure can not enter the pitot tube opening. Static pressure is able to equalize on both sides since the pitot drain hole is still open. The apparent loss of airspeed is not usually instantaneous but happens very quickly. If both the pitot tube opening and the drain hole should become clogged simultaneously, then the pressure in the pitot tube is trapped. No change is noted on the airspeed indication should the airspeed increase or decrease. If the static port is unblocked and the aircraft should change altitude, then a change is noted on the ASI. The change is not related to a change in airspeed but a change in static pressure. The total pressure in the pitot tube does not change due to the blockage; however, the static pressure will change.Because airspeed indications rely upon both static and dynamic pressure together, the blockage of either of these systems affects the ASI reading. Remember that the ASI has a diaphragm in which dynamic air pressure is entered. Behind this diaphragm is a reference pressure called static pressure that comes from the static ports. The diaphragm pressurizes against this static pressure and as a result changes the airspeed indication via levers and indicators

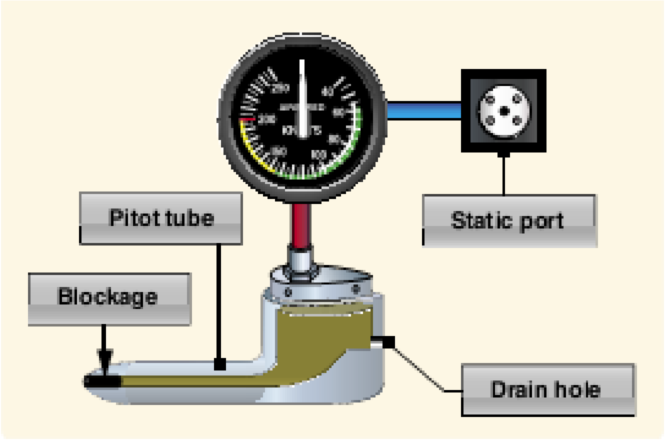

Figure 6. A blocked pitot tube, but clear drain hole

Blocked Static System

If the static system becomes blocked but the pitot tube remains clear, the ASI continues to operate; however, it is inaccurate. The airspeed indicates lower than the actual airspeed when the aircraft is operated above the altitude where the static ports became blocked, because the trapped static pressure is higher than normal for that altitude. When operating at a lower altitude, a faster than actual airspeed is displayed due to the relatively low static pressure trapped in the system. Revisiting the ratios that were used to explain a blocked pitot tube, the same principle applies for a blocked static port. If the aircraft descends, the static pressure increases on the pitot side showing an increase on the ASI. This assumes that the aircraft does not actually increase its speed. The increase in static pressure on the pitot side is equivalent to an increase in dynamic pressure since the pressure can not change on the static side. If an aircraft begins to climb after a static port becomes blocked, the airspeed begins to show a decrease as the aircraft continues to climb. This is due to the decrease in static pressure on the pitot side, while the pressure on the static side is held constant.A blockage of the static system also affects the altimeter and VSI. Trapped static pressure causes the altimeter to freeze at the altitude where the blockage occurred. In the case of the VSI, a blocked static system produces a continuous zero indication

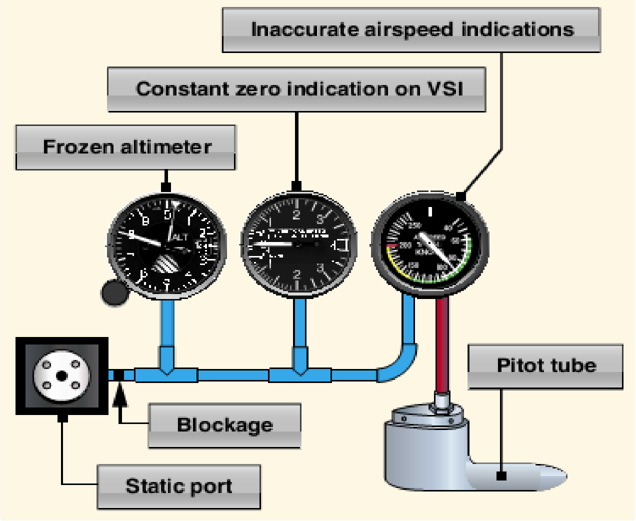

Figure 7. Blocked static system.

II. CONCLUSION

- As part of a preflight check, proper operation of the VSI must be established. Make sure the VSI indicates near zero prior to leaving the ramp area and again just before takeoff. If the VSI indicates anything other than zero, that indication can be referenced as the zero mark. Normally, if the needle is not exactly zero, it is only slightly above or below the zero line. After takeoff, the VSI should trend upward to indicate a positive rate of climb and then, once a stabilized climb is established, a rate of climb can be referenced.
- Instrument Check Prior to takeoff, the ASI should read zero. However, if there is a strong wind blowing directly into the pitot tube, the ASI may read higher than zero. When beginning the takeoff, make sure the airspeed is increasing at an appropriate rate.
- Blockage of the Pitot-Static SystemErrors almost always indicate blockage of the pitot tube, the static port(s), or both. Blockage may be caused by moisture (including ice), dirt, or even insects. ring preflight, make sure the pitot tube cover is removed. Then, check the pitot and static port openings. A blocked pitot tube affects the accuracy of the ASI, but, a blockage of the static port not only affects the ASI, but also causes errors in the altimeter and VSI.

III. SUMMARY

Flight instruments enable an aircraft to be operated with maximum performance and enhanced safety, especially when flying long distances. Manufacturers provide the necessary flight instruments, but to use them effectively, pilots need to understand how they operate. As a pilot, it is important to become very familiar with the operational aspects of the pitot-static system and associated instruments.

REFERENCES

[1]. Willits, Pat, ed. (2004) [1997]. *Guided Flight Discovery - Private Pilot*. Abbot, Mike Kailey, Liz. Jeppesen Sanderson. pp. 2–48–2–53. ISBN 0-88487-333-1.

[2]. "Pitot Static System Performance" flighttest.navair.navy.mil. Retrieved 2008-04-25.

[3]. Evans, David (1 May 2004). "Safety: Maintenance Snafu with Static Ports". Avionics Magazine. Retrieved 2008-04-25.

[4]. "Pitot-Static Instruments - Level 3 - Pitot-Static Instruments". allstar.fiu.edu. Retrieved 2007-01-07.

[5]. "Pilot Handbook - Chapters 6 through 9" . FAA. Archived from the original on 2007-01-06. Retrieved 2007-01-07.

BIOGRAPHY

Er. Naser.F.AB.Elmajdub

This Work Supported by Electric Engineering Department,
Sam Higginbottom Institute of Agriculture, Technology & Science
Allahabad india
Er. Naser.F.AB.Elmajdub “Phd student
Btech from Technology College of Civil Aviation & Meterology
In year 1995 Tripoli –Libya
M.tech from Sam Higginbottom Institute of Agriculture,
Technology & Science in year 2012

Dr. A.K. Bhardwaj

Dr. A.K. Bhardwaj is working as “Associate Professor” in

the Department of Electrical and Electronics Engineering,
Faculty of Engineering and Technology of
Sam Higginbottom Institute of Agriculture,
Technology & Sciences (Formerly AAI-DU)
Allahabad, India from last 7 years after obtaining
M. Tech. degree from Indian Institute of Technology Delhi,
India in 2005. He has competed his Ph.D. degree from
Sam Higginbottom Institute of Agriculture, Technology
& Sciences (Formerly AAI-DU) Allahabad, India in July 2010.
Earlier he was “Assistant Professor” in department of Electrical
and Electronics Engineering, IMS Engineering College Ghaziabad (U.P.)

India in the year 2005. He also worked for 6 years as faculty with IIT Ghaziabad (U.P.) India.
He is also having practical experience with top class multinational companies during 1985-1998. His research interest includes, power management, energy management, reactive power control in electrical distribution system.

American Journal of Engineering Research (AJER)
e-ISSN : 2320-0847 p-ISSN : 2320-0936
Volume-03, Issue-10, pp-145-150
www.ajer.org

Research Paper Open Access

Cylinder Block Fixture for Mistake Proofing.

L.B.Raut[1], V.S.Jakukore[2]
[1]*(M.E.Coordinator, SVERI College of Engineering/ Solapur, India)*
[2]*(P.G.Student, SVERI College of Engineering / Solapur, India)*

ABSTRACT **:** *The project idea basically developed from trunnion tables which are one type of fixture having ability to rotate about its axis and able to fix the component at any angle, so there is no requirement of angle plate and sine plates, drilling process is also computer controlled so no guide bush is required, So robust design for extra rigidity, flexibility and simple to use. In this project task is difficult as design rotary cage type fixture for component like cylinder block, which is heavy of 76 kg. it is not possible to rotate or handle component manually and proceed on them to make this process accident proof and automated for this purpose we are designing a rotary cage which rotate 360 degree and allow indexing to process on the component. Processes are to be operated on the component are drilling tapping and air blow washing ,Since drilling don't need clamping here components self weight will enough to carry drilling force and tapping force coming through power tools. Therefore, rotary cage type fixture is critical importance.*

Keywords - *Poka-yoke, Mistake proofing, AISI304, UHMW*

I. INTRODUCTION

Poka-yoke (poh-kah yoh-keh) is a quality improvement concept, coined by Shigeo Shingo in Japan during the 1960s who was one of the Industrial Engineers at Toyota. The initial term was baka-yoke, which means fool proofing. Poka-yoke helps people and processes work right the first time. Poka-yoke refers to techniques that make it impossible to make mistakes. These techniques can drive defects out of products and processes and substantially improve quality and reliability. The use of simple Pokayoke ideas and methods in product and process design can eliminate both human and mechanical errors. Thus, Poka Yoke is central to the concept of Lean thinking, which aims to reduce waste and make sure that everything and every process is as efficient as possible. The concept of stopping defects or mistakes from happening is central to Poka Yoke thinking. It is not about rectifying mistakes or defects; it is about ensuring that they simply do not happen.

The Poka-Yoke entrance is promoted in the manufacturing industry as a way of improving productivity by reducing errors using often very simple modification. This research gives that, as Poka-Yoke are designed to make process mistake proof quality control. This research provides a study demonstrating the use of the Poka-Yoke approach in assembly of rotary cage fixture process highlighting how they served to improve accessibility to work by fulfilling Universal Design principles**.**

a. Poka-Yoke example from manufacturing industry

Fig 1: Sample example Poka-Yoke

A good example of Poka-Yoke design from manufacturing industry – SIM card slot in cell phones is designed in such a way that user is allowed to insert SIM card in correct way only.

b. Poka-Yoke is required to implement for cylinder block machining fixture

Fixturing is an important manufacturing activity, but there are very few hard and fast engineering principles involved in the fixture design process. Even the available limited analytical rules are not so flexible enough for the correct fixture design. Further, more, there is no exact definition as to what constitutes a good fixture design. A skilled tool designer learns his trade through apprenticeship training and many years of experience. With the current decline in the number of skilled machinists, tool and die workers, there is a clear need for an increase in the level of fixture automation. The present project describes Computer Aided Fixture Design system using the 3-2-1 Method for the design of a fixture to hold Cylinder Head components during processing on SPM. The fixturing modules, allows the user to model the component in terms of meaningful operation features and help in the selection of correct location points. The mechanical analysis of the component, which has been carried out in the project, will suggest the holding details.

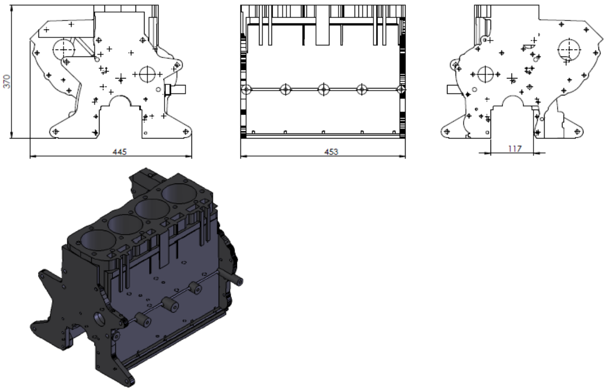

Fig 2 : Component four cylinder head

II. MATERIALS USED FOR FIXTURE

a. AISI 304 stainless steel

It is having Better corrosion resistance than Type 302. High ductility, excellent drawing, forming, and spinning properties. Stainless steels can absorb considerable impact without fracturing due to their excellent ductility and their strain-hardening characteristics. Essentially non-magnetic, becomes slightly magnetic when cold worked. Low carbon content means less carbide precipitation in the heat-affected zone during welding and a lower susceptibility to inter granular corrosion.

Grade	**Tensile strength, Yield (N/mm^2)**	**Ultimate tensile strength (N/mm^2)**	**Young's Modulus (N/mm^2)**	**Elongation (%)**
Stainless steel				
304 (1.4301)	210	520	200000	45

Table a: Material Properties

- **Applications**

Welded and bolted fixture design, Beer kegs, bellows, chemical equipment, coal hopper linings, cooking equipment, cooling coils, cryogenic vessels, dairy equipment, evaporators, flatware utensils, feed water tubing, flexible metal hose, food processing equipment, hospital surgical equipment, hypodermic needles, kitchen sinks, marine equipment and fasteners, nuclear vessels, oil well filter screens, refrigeration equipment, paper industry, pots and pans, pressure vessels, sanitary fittings, valves, shipping drums, spinning, still tubes, textile dyeing equipment, tubing.

b. Ultra-high-molecular-weight-polyethylene

(UHMWPE, UHMW) is a subset of the thermoplastic polyethylene. Also known as high-modulus polyethylene, (HMPE), or high-performance polyethylene (HPPE), it has extremely long chains, with a molecular mass usually between 2 and 6 million u. The longer chain serves to transfer load more effectively to the polymer backbone by strengthening intermolecular interactions. This result in a very tough material, with the highest impact strength of any thermoplastic presently made.

UHMWPE is odour less, tasteless, and nontoxic. It is highly resistant to corrosive chemicals except oxidizing acids; has extremely low moisture absorption and a very low coefficient of friction; is self-lubricating; and is highly resistant to abrasion, in some forms being 15 times more resistant to abrasion than carbon steel. Its coefficient of friction is significantly lower than that of nylon and acetal, and is comparable to that of polytetrafluoroethylene used for making lock pad.

III. PROBLEM DEFINITION

Trunnion tables are used for drilling facing operation on cylinder block but it is having problem of fixing the component manually it require 3 to 4 workers for one machine. Lifting of heavy weight and locate it in correct position is time-consuming process. It also create back pain in spinal cord of the workers It is also dangerous if cylinder block fall down on worker.

IV. OBSERVATION

It is essential to have proper position of cylinder block particular machining operation. The main types of error found in trunnion tables were mis-location, and wrong insert of cylinder block. Some possible causes for these problems are workers not able to follow or are not following the standard operation procedure, from observations it was observed that human error is a major issue in this production. Since human cause is the major factor in this problem, as well as method and machine factor, Poka Yoke or a mistake proofing Problem identification technique implemented by following activities

Documents of company such as Operation standards, process flow layout, worker complaint, customer complaint, process flow chart, procedure documentation etc observed.

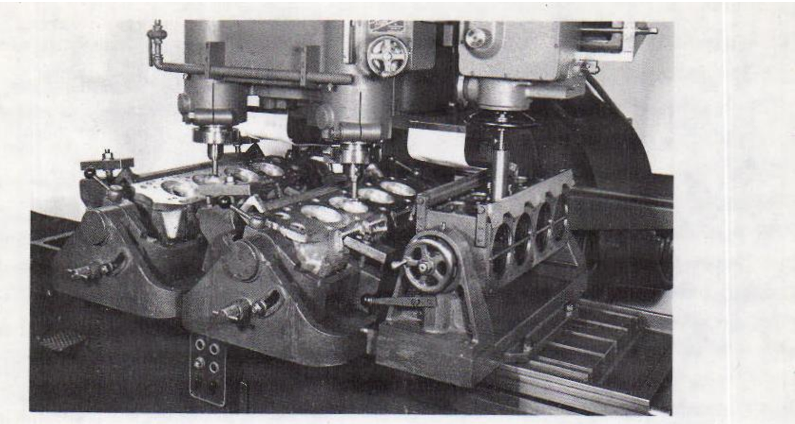

Courtesy of Cincinnati Milacron Inc.

Milling fixtures and template bracket for profile milling cylinder heads. Fixtures and template are trunnion mounted.

Fig 3: Trunnion tables

V. DESIGNS OF ROTARY CAGE FIXTURE FOR MISTAKE PROOFING

Poka yoke system is designed in such a way that the cylinder block insert only in correct orientation on to the trolley in direction locator pins and lock pad and it restrict the motion of cylinder block in ,+- X and + -Y axis.

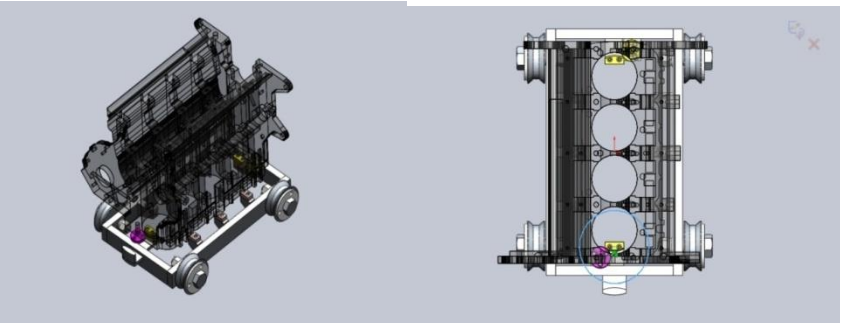

Fig 4: Transparent isometric and top view of trolley and cylinder block

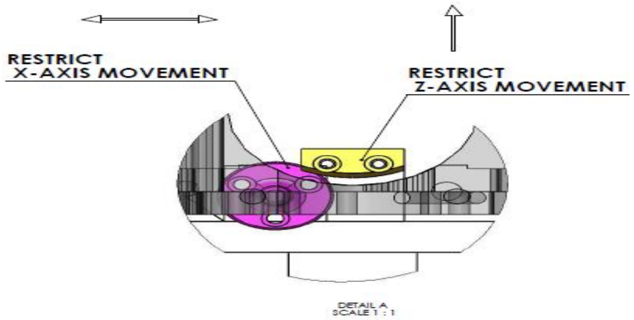

Fig 5: Transparent zoom top view of pink locator and yellow lock pad

Trolley will pass in standard defined direction into the cage for that assembly has been designed in such way that pipe is connected to the rotary cage joining plate shown in figure 7 and slots are provided on cylinder block on the in go side shown in figure 6. It allows trolley and cylinder block in only one direction as shown in figure 8. This device is mounted on conveyor before the station if off standard cylinder block along with trolley comes, it does not pass through the rotary cage fixture. Schematic views with its part names have been shown in following figure.

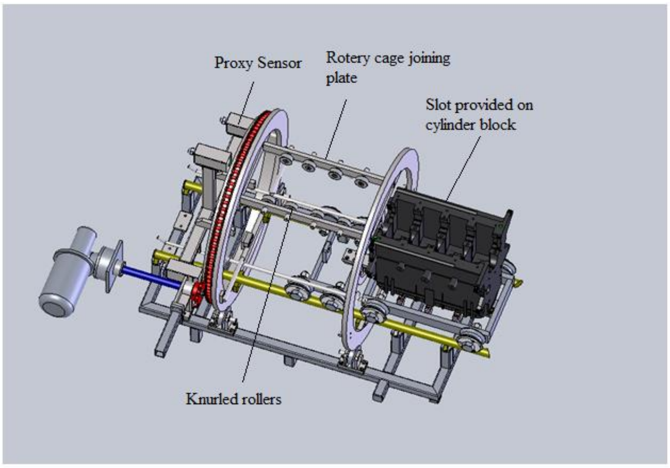

Fig 6: Isometric view showing slot on cylinder block

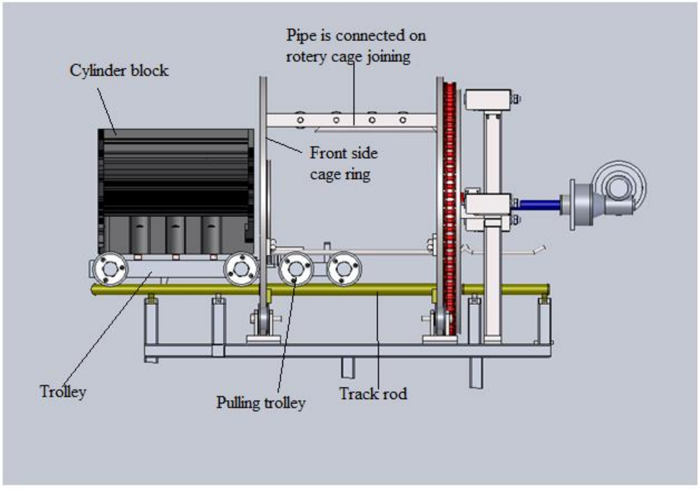

Fig 7: Front view showing pipe is connected to rotary cage joining plate

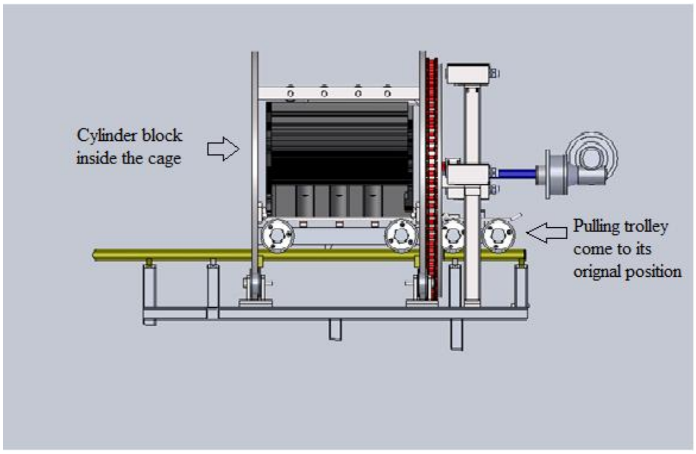

Fig 8: Front view showing complete assembly

a. Pulling trolley and its function

Pulling trolley powered by pneumatic cylinder, initially pulling trolley rest near to the loading and unloading station. When cylinder block is loaded on trolley the pulling trolley pulls the cylinder block inside the cage by pneumatic cylinder. The following figure show connection between pulling and cylinder block trolley some parts are intentionally make transparent to visualization of all the thing.

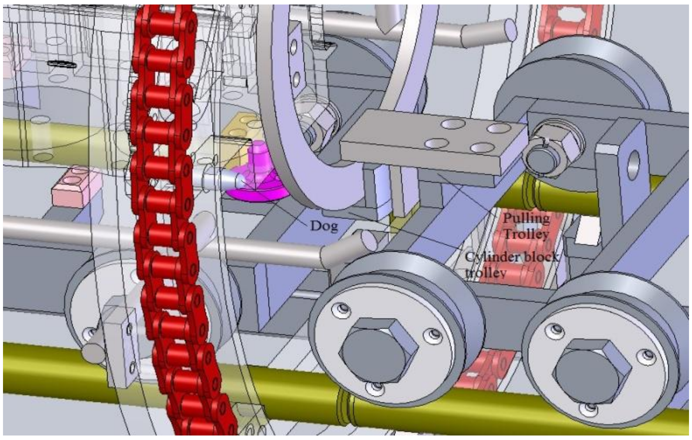

Fig 9: Pulling trolley pulls the cylinder block trolley magnified transparent view

b. Proxy sensor and dog fixed on cage:

As soon as the cylinder block and trolley come in to the cage according to the machining opera ration cage start rotating through 0, 90, 180, 360-degree cage rotation. For this purpose three proxy sensor and one dog is placed on back side of cage ring ,proxy sensor and dog comes in to the line mother control the sprocket and chain through plc circuits. Figure b shows the magnified view of proxy sensor and dog.

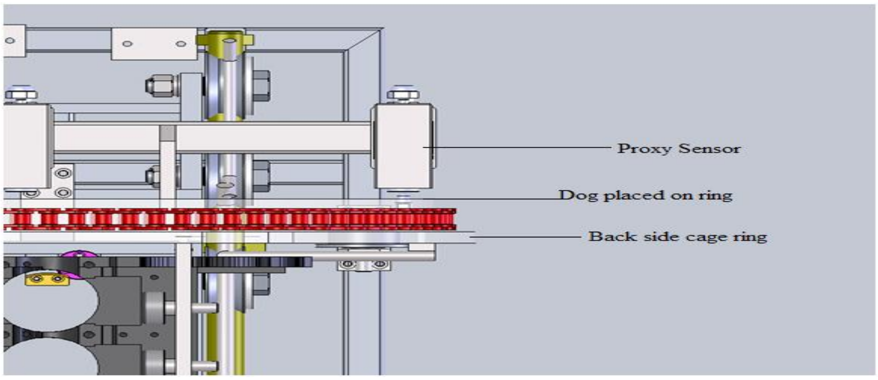

Figure 10: Transparent top view of backside cage ring

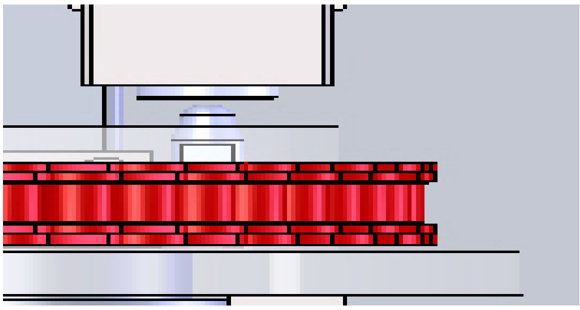

Fig 11: Magnified transparent top view of backside cage ring, Dog, and proxy Sensor

In this way system is made mistake proof and cylinder block getting hold by 3-2-1 principle. Due to mistake proof system there will be no error in system, production cost decreases and quality of product increase.

c. Fixture assembly

Figure shows actual manufactured rotary cage fixture used to hold the cylinder block. It helps for distributed load to be applied on the track rod and when it rotate load act on cage joining plate. The front side assembly photograph shown in figure.

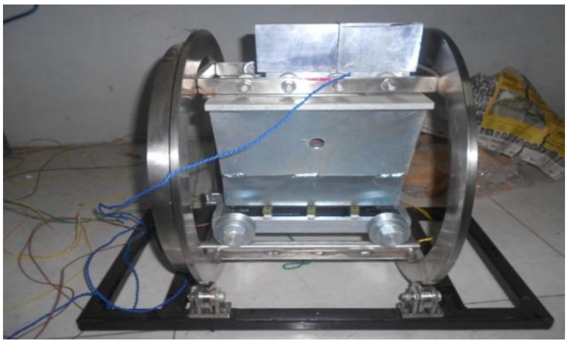

Fig 12: Actual setup manufactured for proto type cylinder block

VI. CONCLUSION

After manufacturing of rotary cage fixture, observed that it is possible to operate cage fixture successfully and scaling of model used for experimentation.

System is made mistake proof and cylinder block getting hold by 3-2-1 principle. Due to mistake proof system there will be no error in system, production cost decreases and quality of product increase.

From results and discussion, we concluded that though there are continuous changes in product design, we could arrest the defect by implementing Poka-Yokes.

We did automation to detect wrong assembly therefore any kind of operator can work to do assembly supervision.

REFERENCES

[1]. H.P.Luo,B. Zhang, Z.X. Zhou “A rotary flexural bearing for micro manufacturing”, *CIRP Annals – Manufacturing Technology*, 57 (2008) ,179–182.

[2]. Sudharsan.S, S.Bhaskar,“ Reducing Electrical Faults in Pumps Using Pokayoke ”, *International Journal of Emerging Trends in Engineering and Development Issue 3*,. Vol.2 (May 2013).

[3]. Nirav P. Maniar1, D. P.Vakharia, A. B. Andhare, Chetan M. Patel “Design of 28 Operations, 4 Axis – 360^0 Indexing Milling Fixture for CNC”, *International Journal of Recent Trends in Engineering, Vol. 1*, No. 5, May 2009.

[4]. Gerald R.Molitor, Holland; Richard G.Bidigare, Hamilton, “Cylinder bore finishing bore apparatus “, *United States patent [19] Patent Number* 4, 907,372.

Books:

[5]. V. B. Bhandari, *Design of Machine Elements*, (TATA Mc-Graw-Hill Publications, second edition, 2007).

[6]. Erik K. Henriksen ,” *Jig and Fixture Design Manual*” ,(Industrial press inc. New York, 1902) .

American Journal of Engineering Research (AJER)
e-ISSN : 2320-0847 p-ISSN : 2320-0936
Volume-03, Issue-10, pp-151-159
www.ajer.org

Research Paper Open Access

Effect of Homogenization &Quenching Media on the Mechanical Properties of Sintered Hot Forged AISI 9250 P/MSteel Preforms

S. Aamani[1], Dr. S. K. Pandey[2], Dr. R. Nagalakshmi[3],Dr. K. S. Pandey[4]

[1]Former M. Tech. Student, Dept. of Metallurgical and Materials Engineering, National Institute of Technology, Tiruchirappalli-620015, Tamil Nadu, India, Presently PhD. Research Scholar, Dept. of Materials Science and Metallurgical Engineering, Indian Institute of Technology, Hyderabad, Telangana, India.
[2]Director, National Institute of Technology, Puducherry, Karaikal 609605, India.
[3]Manager, Welding Research Institute, Bharat Heavy Electricals Limited, Tiruchirappalli 620014, Tamil Nadu, India,
[4]Former Professor, Dept. of Metallurgical and Materials Engineering, National Institute of Technology, Tiruchirappalli-620015, Tamil Nadu, India,

ABSTRACT: *Present investigation is an attempt to generate experimental data in order to establish the influence of homogenization and cooling media on the mechanical properties of hot forged AISI 9250 sintered P/M steel to square cross-section bars produced using elemental powders. The elemental powders corresponding to final AISI 9250 composition ofFe-0.5%C-0.75%Mn-2.0%Si were taken in an appropriate proportion and blended in a pot mill for a period of 32 hours while maintaining the powder to ball ratio by weight as 1.1:1. Compacts of 28mm diameter and 36mm height were prepared on a 1.0 MN capacity Universal Testing Machine (UTM) and using suitable die, punch and bottom insert assembly in the density range of 85±1 percent of theoretical by applying the pressure in the range of 550±10 MPa and by taking pre-weighed powder blend. In all 36 compacts were prepared. These green compacts were coated using the indigenously developed ceramic coating and the same was allowed to dry under the ambient conditions for a period of 14-16 hours. These ceramic coated compacts were re-coated 90° to the previous coating and re-dried under the aforementioned conditions for the same length of time. Ceramic coated compacts were sintered in an electric muffle furnace at 1120±10°C for a period of 120 minutes and subsequently hot forged to square cross-section bars of approximate dimensions of 14mm X 14mm X 95-100mm on a friction screw press of 1.00MN capacity at the sintering temperature itself. Nine forged specimens were oil quenched and remaining 27 forged bars were homogenized at the sintering temperature for a period of 60 minutes followed by quenching nine of them in oil, nine specimens in air and remaining nine were cooled in the furnace itself. Standard tensile specimens were prepared from each set and tested for evaluation of mechanical properties followed by SEM Fractography on the fractured specimen surfaces. Tensile tests results have established that the homogenization step followed by cooling them in different media has improved the values of toughness as the per cent elongation and per cent area reduction, both, have gone up though the strength values have gone down.*

Key Words: Bars, Ceramic, Coated, Compacts, Density, Forged, Fractographs, Generate, Properties, Tensile.

I. INTRODUCTION

It is interesting to note that the period falling between late 1970s and the early 1980s have gone through a significant metallurgical break - through in the recognition of powder metallurgy (P/M)techniques principally in the form of the production of P/Mtools and P/Mforgings [1-14]. However, in the present scenario, the commercial powder metallurgy spans the density spectrum from highly porous metal filters through self-lubricating bearings and the P/Mparts with controlled density to fully dense P/Mwrought metal stems. But, today's P/M has crossed many hurdles and has become a very rapid, economical and high volume production methods for making precision components from elemental or alloy powders or elemental powder blends with or without the addition of carbide, ceramic, oxides, borides or nitrides etc. The technology of powder forging has established itself for fabricating powders into precise engineering parts which have properties comparable or even superior to those of conventional forgings [15-30]. The strength and the toughness of a forged metal assures a greater safety, whenever, the forged products are subjected to excessive loads and the internal stresses from the loads during actual service conditions [4, 5, and 15]. Apart from all these, the powder forging is an attractive manufacturing route for many components because of the fact that the material utilization is better than what is in conventional forgings. Further, the details and tolerances obtainable lead to the elimination of much, if not all finish machining and also induce tight tolerance in the as forged condition. The process technically sounds economical on the ground that lower forging temperatures are anticipated which would result in better surface finish and that would enhance the fatigue strengths [6, 28]. In addition to this, powder forging requires one or two blows instead of three or many more that are necessarily required in the conventional forging of bar stocks. Single quality of iron powder can be used to produce wide variety of steels of any desired composition. Reduced die wear and simplified die configuration accompanied by the expected properties that can be successfully tailored to the required applications. Basically, these factors govern the economics of the process, favouring ultimately the use of powder preform forgings [31-42], therefore, every forging operation must have definite requirements or engineering specifications with the intended applications. The mechanical properties of these forgings are normally determined from the test pieces that are taken from the forgings themselves or other from locations well within the body of the forgings or full size prolongations provided for this purpose [7,8,11-15,18,19,27]. However, technically, the forging of sintered P/Mpreforms whether it is cold, warm or hot, involves three main stages of deformations, namely, upsetting, plane - strain and hydrostatic as reported elsewhere [43-46]. In the above stages, the densification as well as shape changes do occur simultaneously, and, therefore, it is, fundamentally essential to assess the mechanical properties such as the tensile strength, the fracture strength, the hardness, the per cent elongation and the per cent area reduction of the final product. The present investigation is also aimed to assess the mode of fracture during tensile testing of specimens subjected to different heat treatments along with the tensile properties evaluations. Thus, it is obvious that the mechanical properties of the product must depend upon the modefollowed to achieve the complete densification as well as the shape change. Obviously, the densification must precede the shape change or otherwise the component would remain porous. This effect is anticipated to be detrimental to the expected mechanical properties of the P/M forged parts. However, for clarity to be demonstrated, fig. 1 shows the influence of porosity on mechanical properties of the P/M parts. Fig. 1 very clearly shows that as the porosity content in P/M parts are increased, all tensile and impact properties are abruptly dropped. Therefore, in the present investigation attempt is made to ensure that the production of fully dense products and their properties are assessed in clear terms. Thus, from this fig. 1, it is very clear that if the P/Mproduct is to be developed for high load carrying capacity in the stressed conditions, it is, therefore, imperative to reduce the porosity content to almost nil level. It has been reported that the porosity levels can be brought down to almost zero level by means of applying adequate pressures at elevated temperatures [29, 30]. It is also reported [47] that at sometimes an additional impact load is required so as to create sound metallurgical bond across the collapsing pore surfaces. Tensile properties of P/M parts can be referred elsewhere [7,11,13-15,17-19,31,35,38,39,41,42,47]. Literature reporting mechanical properties of P/Mforged parts such as fatigue and impact can be referred elsewhere [4- 6, 26, 28]. However, the properties such as ring rupture strengths can be found elsewhere [48-50]. Now, therefore, in the present investigation, an attempt is made to develop an AISI 9250 grade of sintered hot forged P/Msteel using elemental powders.

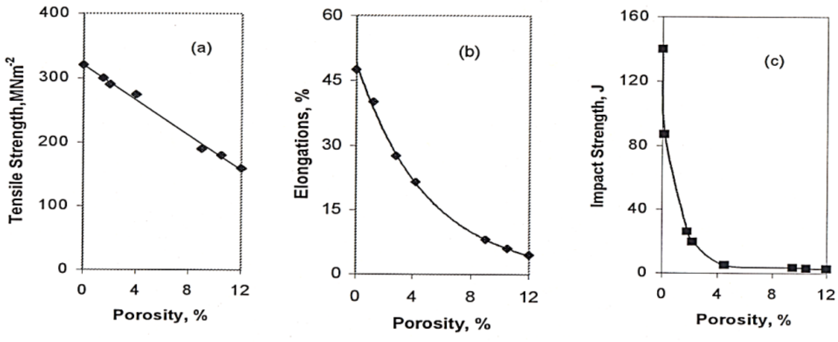

Figure 1 Mechanical Properties of Powder Metallurgy Components against Porosity

II. EXPERIMENTAL DETAILS

Atomized iron powder of -180 ×µm with the chemical purity of 99.63 per cent was procured from the M/s.Sundaram Fasteners, Hyderabad, A.P., and India. This powder contained 0.37 percent insoluble impurities. Manganese and Silicon powders were obtained from the M/s. The Ghrishma Specialty Powders, Mumbai, Maharashtra, India. All these powders were of the particle size below 37µ. However, the graphite powder of 2-5 µm was supplied by the M/s. Asbury Graphite Mills, Inc., Warren County, New Jersey, U.S.A. The basic characteristic features of the iron powder and powder blend prepared to yield the composition of AISI 9250 P/M steel are given in Table I and Table II respectively.

Table I Basic Characteristic Features of Iron Powder and AISI 9250 Steel Blend

Sl. No.	Property	Iron Powder	AISI 9250 Blend
1.	Apparent Density, g/cc	2.93	3.24
2.	Flow rate by Hall Flow Meter, Sec./50g	24.10	23.64
3.	Compressibility, g/cc at a pressure of 410±10 MPa	6.4	6.37

Table II Sieve Size Analysis of Iron Powder

Sieve Size, µm	% Weight Retained	Cum. Wt.% Retained
-180 + 150	3.61	3.61
-150 + 125	3.62	7.23
-125 + 106	2.48	9.71
-106 + 90	0.70	10.41
-90 + 75	8.33	9.20
-75 + 63	9.20	27.94
-63 + 53	16.68	44.62
-53 + 45	15.83	60.45
-45 + 37	3.60	64.05
- 37	35.89	99.94

II.1 Powder Blend Preparation

Required amounts of iron powders of size -180 µm, manganese (-37µm), silicon (-37µm) and graphite (2-5µm) were accurately weighed and mixed in a stainless steel pot with a powder mix weight to porcelain balls (12-19mm diameters) weight in the ratio of 1.1: 1 and the pot lid was securely tightened. The blending operation was carried out on a pot mill for a period of 32 hours. Uniformity in blending was tested as per the procedure described elsewhere [36-39]. Once the blending operation was completed, the porcelain balls were removed manually from the powder blend and the blend was available for preparing the green compacts of suitable initial aspect ratios with desired initial preform geometries and the densities.

II.2 Compact Preparation

Green compacts (28 mm diameter and 35 mm height) of powder blend corresponding to AISI 9250 steel were prepared on a 1.0 MN capacity Universal Testing Machineusing a suitable die, punch and the bottom insert along with top and bottom die plates. During compaction graphite powder paste with acetone was used as a lubricant to minimize friction between the inner die walls, punch and bottom insert surfaces coming in contactwith the powder blend charge in order to minimize the friction between the powder blend charge and the die, punch and the bottom insert surfaces. Further, in order to maintain the constant aspect ratio (height to diameter ratio), a pressure in the range of 540±10 MPa was employed while taking the accurately pre-weighed powder blend. Thus, the initial compact density was maintained in the range of 85±1 per cent of theoretical. Fig. 2 shows the die, punch, thebottom insert and the powder blend compaction assembly.

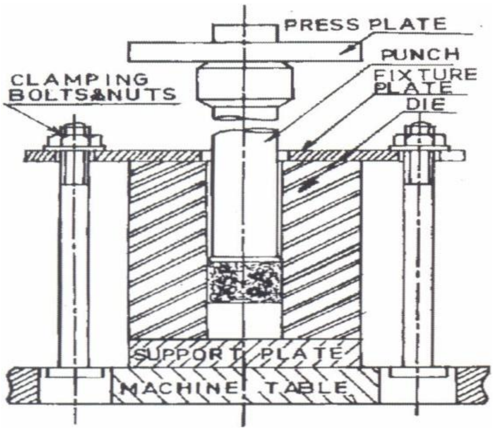

Figure 2Die, Punch and the Bottom Insert Compaction Assembly along with the Powder Blend.

II.3 Application of Indigenously Developed Ceramic Coating

Indigenously developed ceramic coating [51] was applied over the entire surfaces of the green compacts and then the coating was allowed to dry under the ambient conditions for a period of 16 hours. Immediately after the drying of this applied ceramic coating, all these compacts were recoated 90° to the previous coating and the same were allowed todry once again under the aforementioned conditions. The ceramic coating, thus, applied protects the compacts from oxidation and subsequent loss of carbon. The ceramic coating employed in the present investigation was tested up to 1250 ± 10 °C. It was found that this coating had successfully protected the compacts during the sintering operation.

II.4 Sintering and Hot Forging to Square Cross-Section Bars

Indigenously developed ceramic coated compacts were sintered in an electric muffle furnace at 1150 ± 10^0C for a period of 120 minutes. Once the sintering schedule was completed, the sintered compacts were hot forged to square cross-section bars of approximate dimensions of 14mm x 14mm x 95-l00 mm. During forging operation care was taken to avoid excessive drop in the forging temperature by reheating the partially upset forged preforms to the sintering temperature and retaining them at this temperature at least for 30 minutes before re-forging them. This provided the quality forged products. In addition to the above, the upset die set assembly was pre-heated in the temperature range of 350 ±10°C to avoid excessive die chilling. The hot forging operation was carried out on a friction screw press of 1.0 MN capacity. Once the forging operation was completed, nine forged square cross-section bar specimens were oil quenched and the remaining twenty seven forged bars were homogenized in the furnace itself for a period of 1 hour at 1150 ± 10^0C. Immediately after the completion of homogenizing schedule, nine bars were oil quenched, six specimens were air cooled and the remaining nine bars were cooled in the furnace itself. Thus, four groups of specimens were categorized such as: (A) Sintered - Forged and Oil Quenched (SFOQ); (B) Sintered - Forged - Homogenized and Oil Quenched (SFHOQ); (C) Sintered - Forged - Homogenized andAir Cooled (SFHAC) and (D) Sintered-Forged-Homogenized and Furnace Cooled (SFHFC) for tensile testing. Tensile Testing. Five of thenine bars of each groups A, B, C and D were machined to a standard tensile test specimens for carrying out tensile testing.The tensile tests were carried out following the procedure described elsewhere [52]. Properties, such as tensile strength, the fracture strength, the percent elongation and the percent area reduction were calculated for all the specimens and the average values were taken in each group as the final. However, before carrying out the tensile tests, the density measurements were carried out for all the specimens. Density for each specimen was found to be virtually 100%.

III. RESULTS AND DISCUSSION

III.1 Tensile Properties Assessment

Table III shows the mechanical properties of sintered - hot forged and heat treated under different conditions for AISI 9250 P/Msteel prepared from the elemental powders and hot forged to square cross-section bars. The properties reported in this table include tensile strength, the fracture strength, the percentage elongation, the percentage area reduction, and the hardness values. It is, observed from this table that the sintered forged and oil quenched specimens have shown the maximum tensile strength of 1455 MPa. But, if this table is examined w.r.t. the processing such as (A) SFOQ, (B) SFHOQ, (C) SFHAC and (D) SFHFC, it is noticed that the ultimate tensile strength has dropped and the true fracture strength values have gone up. Except in the case SFHOQ condition where there is a little drop in the value In general, the percent elongation and the per cent area reduction have shown an increasing trend in order of consideration, i.e., (A), (B), (C) and (D) respectively. The hardness values have also dropped in the same sequence.

Table III Mechanical Properties of AISI 9250 Sintered - Hot Forged and Heat Treated P/M Steel

Condition	UTS, MPa	True Fracture Stress, MPa	Engineering Fracture Stress, MPa	% El.	%A.R.	Hardness Vickers, HV.
SFOQ	**1455**	**1480**	**1457.8**	**4.80**	**l.50**	**445**
SFHOQ	**968**	**1050**	**952.88**	**16.60**	**9.25**	**311**
SFHAC	**952**	**1093**	**982.39**	**17.04**	**10.12**	**309**
SFHFC	**728**	**1137**	**907.21**	**20.21**	**14.34**	**290**

III.2 Relative Tensile Test Results of AISI 9250 Forged P/M Steel

Fig. 3 shows the stress versus per cent elongation curves (only a relative magnitude, not the actual units) for the sintered hot forged AISI 9250 P/Msteels heat treated under the conditions described by the abbreviations SFOQ,SFHOQ, SFHAC and SFHFC respectively. None of these curves have exhibited distinct yield points (either lower orupper).It is further observed that the AISI 9250 steel under SFOQ condition has

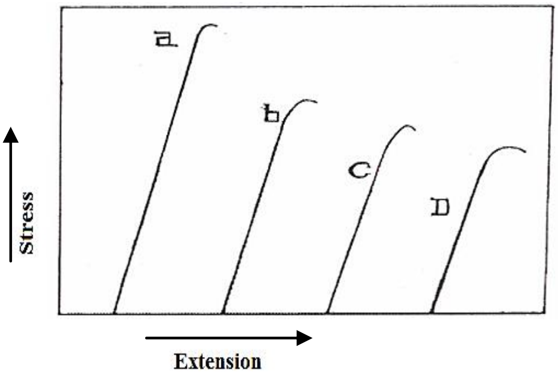

Figure 3Relative Plots Between Stress and Percentage Elongation for the specimens

(a) SFOQ = SinteredForged & Oil Quenched(A);(b) SFHOQ = Sintered Forged Homogenized for 1 hour at 1150± 10°C and Oil Quenched (B); (c) SFHAC = SinteredForged Homogenized for 1 hour at 1150± 10°C and Air Cooled (C) and (d) SFHFC = Sintered Forged Homogenized for I hour at 1150± 10°C and Furnace Cooled (D)

exhibited highest UTS and highest true fracture strength values, but, with the least values of percent elongation and the percent area reduction. The relative appearance of the stress versus percentage elongation curves for each heat treatment condition corresponded very well to the calculated values that are shown in Table III.

III.3 Evaluations of SEM Fractographs

III.3.1 SEM Fractograph of Tension Tested AISI 9250 Steel under SFOQ and SFHOQ Conditions

Fig.4 shows the scanning electron fractograph of tension tested specimen corresponding to sintered and hot forged but oil quenched condition. The fractograph shows the failure occurring in a typical way resembling to a quasi- cleavage fracture. The structure also shows few micro-cracks and presence of porosity. Therefore, the fracture mode is associated to be highly brittle with a negligible degree of ductile failure. Few dimples do indicate the fracture to be partially associated to be ductile. Hence, it is established that the failure was truly brittle and insignificantly ductile. Fig. 5 demonstrates the SEM fractograph of tension tested specimen of AISI 9250 sintered - hot forged homogenized at 1150±10^0 C for a period of 1 hour and oil quenched. At 1000X magnification, fine dimples are seen throughout the fractographand at couple of places well grown voids do indicate that there had been a clear case of coalescence of pores into a fully blown voids - resulting into failure of the specimen. Thus, the fracture mode is characterized by mainly ductile and partly brittle which can be further called as mixed mode.

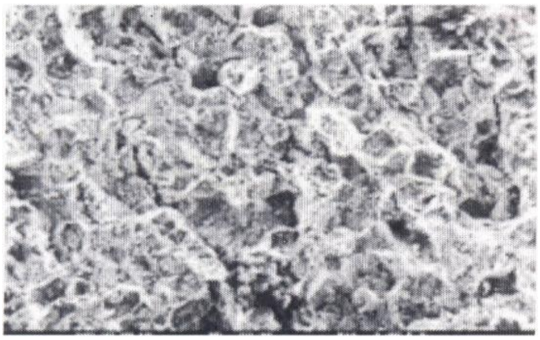

Figure 4 Fractograph of AISI 9250 P/MSteel under SFOQ

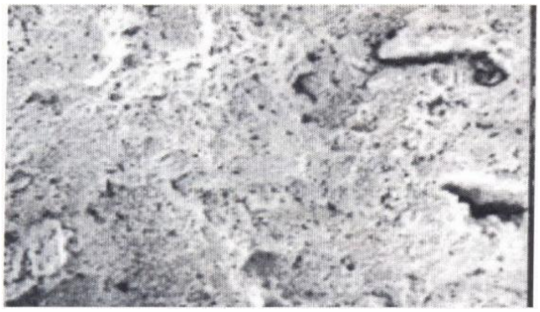

Figure 5 Fractograph of AISI 9250 P/MSteel under SFHOQ

III.3.2 SEM Fractograph of Tension Tested AISI 9250 Steel under SFHACand SFHFC Conditions

Fig. 6 shows the SEM fractograph of tensile fractured specimen of hot forged - homogenized at 1150±10° C for a period of 1 hour and cooled in still air. This fractograph exhibits fairly distributed fine dimples and at places a coalescence of pores while the fracture proceeded. At places, a sign of tearing is also evident. The fractograph has shown an overall picture of being fairly ductile and partially brittle. This is in close conformity with the experimentalresults of tensile testing showing over 17 per cent elongation and over 10 per cent area reduction. Thus, the failure mode is characterized to be extensively ductile and partially brittle. This is a mixed mode of failure. Incidental presence of porosity in the structure is virtually absent.

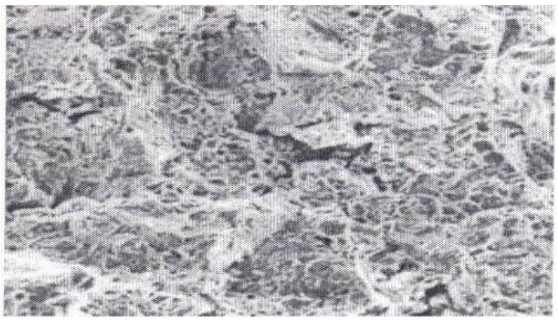

Figure 6Fractograph of AISI 9250 P/Steel under SFHAC

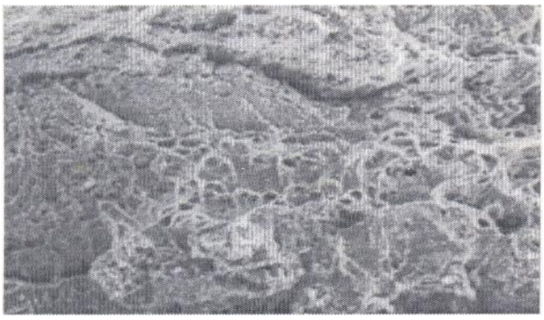

Figure 7 Fractograph of AISI 9250P/MSteel under SFHFC

Fig. 7 shows the fractograph obtained through the scanning electron microscope from the fractured surface of tensile tested specimen which was machined from the sintered - hot forged square cross-section and the same was homogenized for 1 hour at 1150±10°C and subsequently cooled inside the furnace itself. The fractograph is taken at 1000X magnification. This fractograph predominantly exhibits the large number of dimples and also at places coalescence of pores while the structure started showing failure. The mode of failure is highly ductile which is in tune with the percent elongation of 20.21 and percentage area reduction of 14.34 respectively.

IV. CONCLUSION

Based on the critical analysis of the experimental data and the calculated parameters, along with the analysis of the Fractographs of the tensile tested specimens under all the conditions of heat treatments, the following salient features as major findings emerged out from the present investigation and they are as beneath:

1. Mechanical properties such as UTS and True F.S. have been found to be maximum under SFOQ condition and minimum under SFHFC condition of heat treatment. However, the percentage elongation and the percentage area reduction followed the increasing trend in a sequence such as SFOQ, SFHOQ, SFHAC and SFHFC respectively. It is also established that the UTS and true FS values were found to decrease in the same order of sequence, i.e., SFOQ, SFHOQ, SFHAC and SFHFC,
2. The failure mode established during tension testing under SFOQ condition to be highly brittle and virtually no trace is noticed to establish that this failure mode to be ductile. Hence, the failure mode ispredominantly characterized as brittle mode of failure,
3. The failure mode during tensile testing under SFHOQ is characterized to be mainly ductile and partly brittle,
4. Failure modes under SFHAC and SFHFC conditions have been established to be predominantly ductile. However, traces are also present in the structure to associate the failure to be mildly brittle and predominantly ductile.

Summing up, it is concluded that the heat treatment schedules such as homogenizing the forged bars at 1150± 10°C for a period of 1 hour followed by quenching them in oil or in still air or cooling in the furnace itself has resulted in a substantial drop in ultimate tensile and fracture strength values coupled with the enhancement in per cent elongation and per cent area reduction, i.e., an increasing trend in toughness. Thus, the present investigation has established the feasibility of producing successfully an AISI 9250 P/Msteel by using elemental powders for structural applications. Many more such AISI grade of P/M steel can be successfully produced by using elemental powders which may possess strong potential for structural applications.

REFERENCES

[1] Anon, “Where Powder Metallurgy is Growing Applications and outlook for forging *PIM* preforms," Metal Progress, Vol. 99, No.4, 1971, pp. 54- 60.

[2] J. S. Hirschhorn and R. B. Bargainnier, "The forging of Powder metallurgy Preforms," Jl. of Metals, Vo1.22, No.9, 1970, pp. 21-29.

[3] S. Mocarski, L. E. De Angelis and L. A. Winquist, "Influence of Controlled Atmosphere on the magnetic Properties of Forged Powder Metal Preforms", Proc. of 1970, Int. Powder Met. Conf., Sponsored by MPIF and APMI, Ed. By H. H. Hausner, Vol. A, Processes, Plenum Press, 1971, pp.167-189.

[4] K. H. Moyer, "The Effect of Preform Density on the Impact Properties of Atomized Iron P/MForgings", Fall Powder Met. Conf., Detroit, Mich. Sponsored by MPIF, APMI &ASM, 1971, pp. 53-63.

[5] K. H. Moyer, "The Effect of Flow on the Impact Properties of Hot Forged Iron Powder reforms", National Powder Metallurgy, Conf. Proc. Ed by Allan S. Bufford, MPIF, New York, 1972, pp. 6-40.

[6] T. W. Pietrocini and D.A. Gustafson, "Fatigue and Toughness of Hot Formed Cr-Ni-Mo and Ni-Mo Pre-alloyed Steel Powders", Int. J1. Of Powder Metallurgy, Vo1.6, No. A, 1970, pp. 19-25.

[7] R. E. Westerman and K. R. Sump, "Properties of Pre-alloyed Steel Powder Metallurgy Products", Battelle Mem. Inst. Pacific Northwest Labs., ADA 727 660, AMSWERE- 71-22 May 1971 - A Report.

[8] W. V. Knopp, "Properties of Hot Forged *PIM* Steels", Fall Powder Metallurgy Conf. Proc., Oct. 14-16, 1969, Philadelphia, Pa. Sponsored by MPIF and APMI, Published by MPIF, NY, 1970, pp.11-24.

[9] E. E. Carlson, "New High Strength Ferrous P/MMaterials", Progress in Powder Metallurgy, Vol. 125, 1969, pp.63-69.

[10] S. Mocarski et.al, "Properties of Magnetically Soft Parts Made by Hot Forging of P/M Preforms", Modem Dev. In Powder Metallurgy, Proc., 1970, Int. Powder Met. Conf. Sponsored by MPIF and APMI, Ed. By H. H. Hausner, Vol. A, Processes, Plenum Press, 1971, pp. 451-462.

[11] Y. Ishimaru, eta1, "On the Properties of Forged P/M Alloys", ibid, pp. 441-449.

[12] T. Kawakita eta1, "Properties of Forged Super-High Density Sintered Steel", New Perspectives in Powder Metallurgy, Ed. By H.H. Hausner et.al, Published by MPIF, 1973, pp.349-356.

[13] S. M. Kaufman and S. Mocarski, "The Effect of Small Amounts of Residual Porosity on the Mechanical Properties of *PIM* Forgings", Int. JI. of Powder Metallurgy, vo1.7, No.3, 1971, pp.19-30.

[14] S. Mocarski, "Influence of Process Variables on the Properties of Modified 8600 and Manganese Nickel - Molybdenum Low Alloy Steels", Mod. Dev. In P/M,Ed. By H. H. Hausner and Walter E. Smith, Vo1.7, P/MForging and Copper P/M Proc.1973, Int. P/M Conf. MPIF, 1974, 303-321.

[15] C. G. Goetzel, "Tensile Properties of Titanium alloy Forgings made from Spark-Sintered Preforms", ASM Metals Eng. Quart., Vo1.11, No.2, 1971, pp.53-61.

[16] Anon, "Powder Metallurgy - A Sleeping Giant", Iron Age, Vo1.208, No.15, 1971, pp.63-67.

[17] H. W. Antes and P. L. Stockl, "The Effect of Deformation on Tensile and Impact Properties of Hot Forged P/MForged Nickel Molybdenum Steels", Powder Metallurgy, VoLl7, No.33, 1974, pp. 178-192.

[18] D. S. Ma Clean, W.E. Campbell and RJ. Dower, "An Insight into the Mechanical Properties of Powder Metal Forgings as a Function of Processing Ro ute", Powder Metallurgy International, Vol.7, No.3, 1975, pp.1l8-120.

[19] R. T. Cundil, E. Marsh and K. A. Ridal, "Mechanical Properties of Sinter *I* Forged Low Alloy Steels", Forging of Powder Metallurgy Preforms New Perspectives in P/M, Vol.6, Ed. By H.H. Hausner et.al. Published by MPIF, NY, U.S.A., 1973, pp.175-204.

[20] D. A. Gustafon, "High Density P/MHigh Density via P/MTechniques", Metal Progress, VoLl01, No.4, 1972, pp.44-45 and 48-49.

[21] P. de Sablet and A. Accary, "Comparison between Powder Metallurgy and Competitive Processes for the Mass Production of Structural Parts", Powder Metallurgy International, Vo1.9, No.3, 1977, pp.127-130.

[22] N.P. Jarret and P.K. Jones, "The Powder Forging Process and Its Potentialities", Engineers Digest, Vo1.34, No.3, 1973, pp.41-43.

[23] L. Alves, "Powder Forging Techniques and Physical Properties", Fall Powder Metallurgy Conf. Proc., Oct.20-21, 1970, Cleveland Ohio, Sponsored by MPIF and APMI, published by MPIF, 1971, pp.135-165.

[24] J. A. Vaccari, "P/MForgings A Rapidly Emerging Technology", Mater. Eng., Vo1.78, No.3, 1973, pp.20-27.

[25] G.T. Brown, "Properties of Structural Powder - Metal Parts - Over rated or Under Estimated?" Powder Metallurgy, VoLl7, No.33, 1974, pp. 103-125.

[26] K. H. Moyer, "The Effect of Density on Impact Properties of Iron Forgings", Metals Engineering Quarterly, 972, pp.34-38.

[27] T. Kawakita and Y. Nagasaki, "Properties of Hot Forged Super High Density Sintered steel", New Perspectives in Powder Metallurgy, Ed. By H. H. Hausner, et.a1. , 1973, pp.349-356.

[28] G. Bockstiegel and C. A. Blande, "The Influence of Slag inclusions and Pores on Impact Strength and Fatigue Strength of Powder Forged Iron and Steel", Powder Metallurgy International, Vo1.8, 1976, pp.155-160.

[29] Darrel W. Smith, "Calculation of Pore-Free Density of P/MSteels: Role of Microstructure and Composition", Int. Jl. of Powder Metallurgy, Vo1.28, No.3, 1992, pp.259-269.

[30] Darrel W. Smith and Stephen J. Mashl, "Pore-Free Density of Powder Forged Steel: Comparison of Measured and Calculated Values", Int. Jl of Powder Metallurgy, Vo1.28, No.3, 1992, pp. 271-278.

[31] K. S. Pandey, P. S. Mishra and M. L. Mehta, "Effect of Carbon Content on the Mechanical Properties of Upset Forged Iron Powder Preforms to Square Cross-section Bars", Quart. Int. J1. OfP/MSci. &Tech., Vol.2, No.1, 1990, pp.36-44.

[32] K.S. Pandey, "Some Characteristics of Sinta-Forging of Iron and Hyper Eutectoid Steel Through Partially Open Step Down Cylindrical Die Cavity at 1400K", Quart. Int. J1. Of P/MSci., & Tech., Vol. 3, No.1, 1992, pp.25-34.

[33] K. S. Pandey, P. S. Mishra and M. L. Mehta, "Effect of Forging Temperature and Cracking Behaviour of Iron Powder Preforms - Hot Upset Forged", Trans. of PMAI, VoLl5, 1988, pp.9-14.

[34] J. Arrivudainambi and K. S. Pandey, "Densification Behaviour of Iron and AISI 4340 Powder Preform during Hot Upsetting", Engineering Today, Vol. l, No. 11, 1999, pp. 2-4.

[35] J. Arrivudainambi and K. S. Pandey, "Assessment of Mechanical Properties of Hot Forging AISI 4340 P/MSteel", Engineering Today, Vol. 1, No.12, 1999, pp.19-21.

[36] P. Aravindan and K. S. Pandey, "Characteristics Features of Hot Forgings of Sintered Iron and Iron- 0.5% Carbon Steel P/MPreforms", Engineering Today, Vol. III, No.10, 2001, pp. 10-13.

[37] K. S. Pandey and P. Aravindan, "Densification Behaviour of Sintered Eutectoid *P/M* Steel Containing 1.5% Molybdenum m Hot Forging", Engineering Today, Vo1.III, No.10, 2001, pp.53-56.

[38] V. Samuel, K.S. Pandey and P. Aravindan, "Processing of Carbon-Molybdenum Sintered *P/M* Steels for Structural Applications", Engineering Today, Vol. IV, No.1, 2002, pp.8-11.

[39] J. V. Samuel, K. S. Pandey and P. Aravindan, "Significance of Adding Small Amount of Molybdenum in Sintered Eutectoid P/MSteel Hot Forged at 1150°C", Engineering Today, Vol. IV, No.1, 2002, pp.26-27.

[40] R. Bindu, K. S. Pandey and P. Aravindan, "Some Aspects of High Temperature Forging of Sintered Low Alloy Carbon-Manganese-Nickel *P/M* Steels", Engineering Today, Vol. IV, No.1, 2002, pp.31-32.

[41] Siddhartha Pandey, R. Chandramouli and K. S. Pandey, "Densification Behaviour and Mechanical Properties of Sintered Hot Forged Iron-Carbon- Titanium Carbide Composites", Proc. of the National Conf. On Recent Trends in Manufacturing Technology &Management at ACE, Hosur, Jan.28-29, 2003, pp.134-141.

[42] P. K. P. Rupa and K. S. Pandey, "Densification Behaviour and Mechanical Properties of Heat Resistant P/MSteels Sintered and Hot Forged at 1150±10°C", Proc. of the Conf. On Processing of Metals at PSG College of Tech., Coimbatore, Jan.31-Feb.l, 2002, pp.362-369.

[43] H.W. Antes, "Cold and Hot Forging of P/MPreforms", SME lnt. Meeting, Philadelphia, April 1971, published as a special report, EMR 71-01, 1971.

[44] H. F. Fischmeister, B. Arjen and K. E. Easterling, "Deformation and Densification of Porous Preforms in Hot Forging", Powder Metallurgy, VoLl4, No. A, 1971, pp.144 - 163.

[45] H. A. Kuhn, "Material Behaviour in Powder Forging", J1. Of Engineering Materials and Tech., Vol. 46,1973, pp. 41-46. .

[46] H. A. Kuhn and C. L. Downey, "Deformation Characteristics and Plasticity Theory of Sintered Powder Materials", Int. J1. of P/M, Vol.7, No.1, 1971, pp.15-25

[47] K. S. Pandey, "Salient Characteristics of High Temperature Forging of Ferrous Powder Preforms", Key Eng. Mater., Vo1.29-31, 1989, pp.46S-486.

[48] A. Bose and P. G. Mukunda, "Influence of Rate of Testing on Radial Crushing Strengths of P/M Bearings", Int. J1. Of Powder Metallurgy, Vo1.17, No.3, 1981, pp.223-236.

[49] S. Thiagarajan, R.Narayanasamy, K. S. Pandey and K. Mathrubootham, "Relationship Between Ring Fracture Strength and Porosity for Cold Deformed Aluminium and Al-4%Cu Alloy Powder Preforms", Trans. of PMAI, Vol. 15, 1988, pp.59-64.

[50] P. Aravindan and K. S. Pandey, "Relationship Between Radial Crushing Strengths and Porosity for Annular Rings Machined from Hot Upset Forged P/MSteels", Presented in an Int. Conf., Silver Jubilee & Annual Technical Meeting on Advances in P/M Maters., Processing in Nuclear, Space, Defense and other sectors between March 23-25, 1999, Hyderabad, Andhra Pradesh,India.

[51] K. S. Pandey, "Special High Temperature Ceramic Coating Indigenously Developed to Protect Against Oxidation during Sintering", 1986, Regional Engineering College, Tiruchirappalli - 620 015, T.N., India.

[52] Instruction Manual for Hounsfield Tensometer (Type -'W') Monsanto, Regd. No.291962.

American Journal of Engineering Research (AJER)
e-ISSN : 2320-0847 p-ISSN : 2320-0936
Volume-03, Issue-10, pp-160-168
www.ajer.org

Research Paper Open Access

Design of UWB Filter with Notch Band for WLAN (5.3-5.8 GHz) Signal Interference Rejection

Vinay Kumar Sharma[1], Mithilesh Kumar[2]
[1, 2,] *(Electronics Engg. Department, University College of Engineering, Rajasthan Technical University, India)*

ABSTRACT : *In this letter, a design of Compact Ultra-Wideband (UWB) bandpass filter with a switchable notch band for WLAN (5.3-5.9GHz) interference rejection is proposed. As 5.3-5.9GHz wireless local area network (WLAN) is existed in UWB spectrum range (3.1 -10.6GHz) and may interfere with UWB system operation. The UWB bandpass filter is implemented using a basic multiple mode resonator (MMR) structure feed by interdigital coupled lines for achieving higher degree of coupling. The notch band is obtained using a etched slot on main microstrip line. The centre frequency and bandwidth of notch band is optimized. The filter is compact in size with dimension 37.4 X 25 mm^2.The electromagnetic simulation software, Computer Simulation Technology Microwave Studio (CST MWS) is used for the simulation and analysis of the designed structure. For fabrication of this structure Rogers RT5880 substrate of thickness 0.4 mm* and dielectric constant 2.2 is used. Measured and simulated results show good agreement.

Keywords *- WLAN, Microstrip, MMR, UWB*

I. INTRODUCTION

The tremendous progress in **U**ltra wideband (3.1–10.6 GHz) radio technology is reported now days. The researchers' interest rose dramatically in developing UWB devices due to its potential application in modern short distance defense and commercial communication systems. Ultra wideband (UWB) band pass filter (BPF) is an important part of and UWB communication system[1-2]. There are various types of UWB bandpass filters are reported In recent years[3-13]. To achieve low cost and easy integration, these filters are usually implemented in a microstrip or coplanar waveguide technology.

The 5.2-5.8 GHz wireless local area network (WLAN) signal is interfered with UWB system operations in the UWB in-door specification (3.1 - 10.6 GHz) standardized by U.S. (FCC). There are many designs are reported for rejecting these WLAN signals. Most of these designs used stepped impedance resonators [14], defective ground structure (DGS) [15]. The DGS structure has a serious drawback of packaging, because there is an absence of ground plane and EM field is leaked so we cannot use it for commercial fabrication purpose. Whereas stepped impedance resonators create structure too bulky and required additional space.

In this letter, A compact UWB bandpass filter is proposed using a multiple mode resonator (MMR) structure. The stop band selectivity is improved by achieving higher degree of coupling using interdigital coupled lines. The notch band for WLAN interference rejection is realized by etching a slot in the main microstrip line in MMR structure. In this design notch band is realized on the main structure itself so the design space is reduced. The switching feature is added here by using diode D1, so we can switch the notch band ON/OFF in our UWB passband according to our need. Fig. 1 shows the proposed filter structure. All dimensions of this filter are presented in TABLE I.

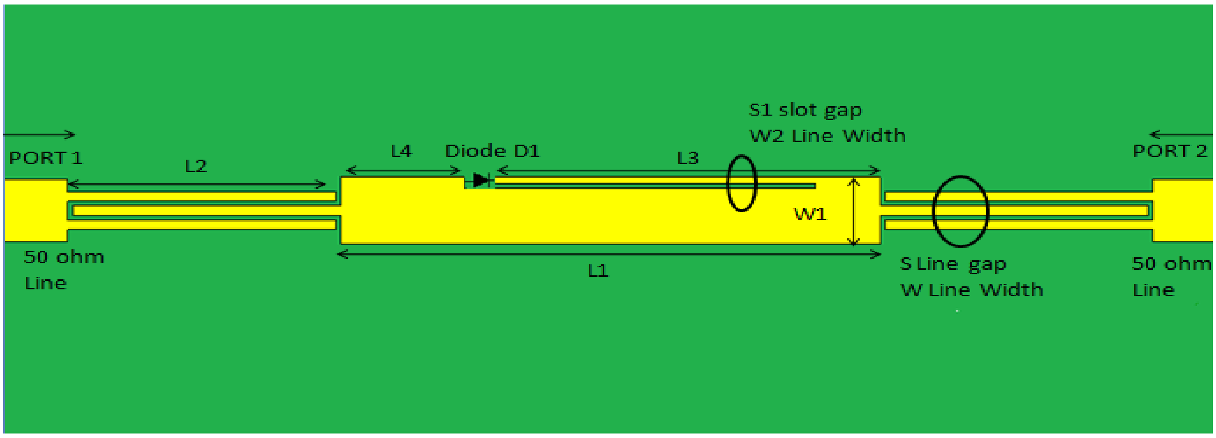

Fig. 1 Layout of the proposed UWB bandpass filter with notch band

TABLE I. Dimension of proposed filter

Filter parameter	Value	Filter parameter	Value
L_1	**16.6mm**	**S_1**	**0.15mm**
L_2	**8.25mm**	**W**	**0.3mm**
L_3	**12.2mm**	**W_1**	**2.1mm**
L_4	**3.8mm**	**W_2**	**0.2mm**
S	**0.15mm**		

II. FILTER DESIGN

The basic UWB band pass filter is designed using a MMR structure based on stepped impedance resonator discussed in chapter three. At the central frequency of the UWB passband, i.e., 6.85 GHz, the MMR structure composed of one half wavelength λ/2 low-impedance line section in the center and two identical λ/4 high-impedance line sections at the two sides. The low impedance section is 59.42 Ω and high impedance section of the MMR is 138 Ω resulting in an impedance ratio of 2.32. Impedance ratio greater than 1 is utilised to design UWB filters. In this design we use Interdigital coupled lines as a I/O feed lines. The width of feed lines W is 0.3 mm and spacing S which is optimized at 0.15 mm for proper response. When giving energy to the MMR coupling energy of interdigital coupling is high compared with the single line parallel coupling.

Many designs are reported based on defective ground structure for creating notch band in a UWB passband. But due to the various drawbacks of DGS structure including the commercial packaging and fabrication problem, here we proposed a etched slot in the main microstripline in MMR structure to create a notch band. It does not require any additional structure as reduced the overall dimension.

Fig. 2 shows the etched slot structure in the main microstrip line. The stub length L3 and slot gap S1 and line width W2 is optimized at 12.2 mm, 0.15 mm and 0.2 mm respectively for notch band of center frequency 5.6 GHz and bandwidth 5.3-5.8 GHz (0.5GHz). The center frequency and bandwidth of notch band varies with the parameters L3, S1 and W2.

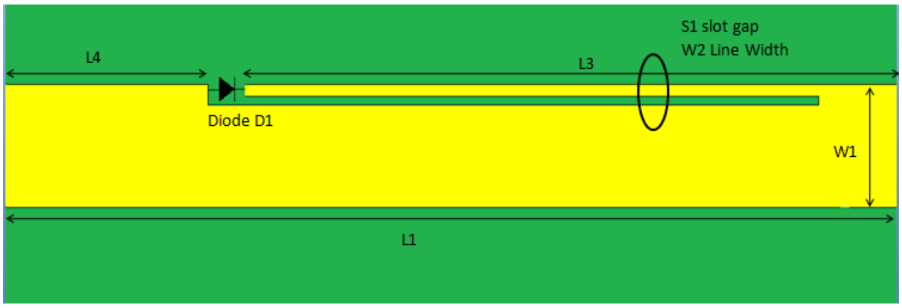

Fig. 2 Etched slot structure for notch band realization

The centre frequency of notch band varies with the length L3. The length of open stub transmission line is such that quarter- wave- length at the desired notched frequencies. The variation of centre frequency with length L3 is presented in TABLE II. Fig. 3 shows the variation of centre frequency of notch band with stub length L3 keeping S1 and W2 constant.

TABLE II. Variation of centre frequency with stub length L3

Stub Length L3	Centre frequency of notch band
7.2 mm	7.7 GHz
8.2 mm	6.85 GHz
9.2 mm	6.2 GHz
10.2 mm	5.5 GHz
11.2 mm	5 GHz
11.8 mm	4.8 GHz

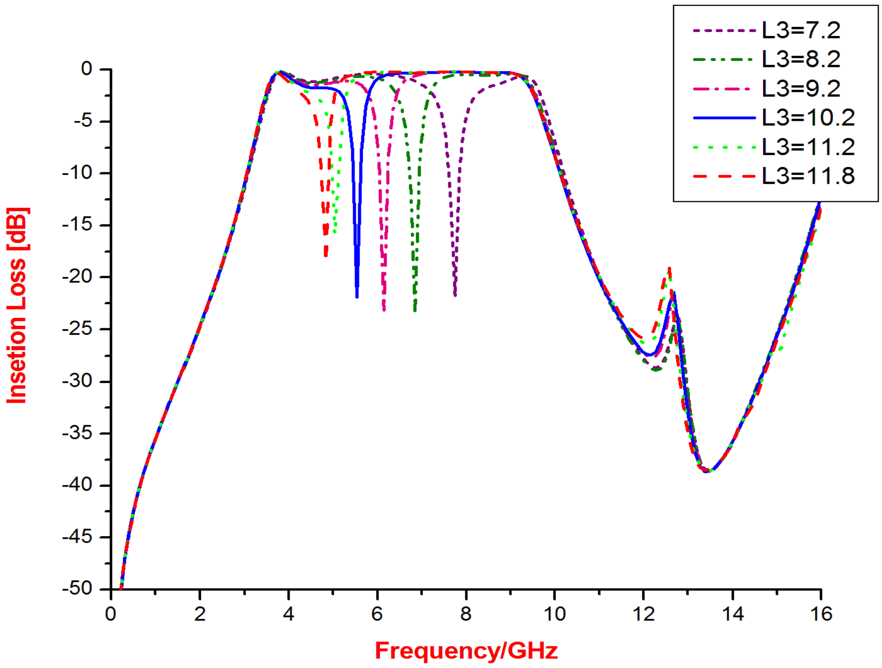

Fig. 3 Variation of centre frequency with stub length L3

The bandwidth of notch band varies with the slot gap S1. The variation of bandwidth of notch band with slot gap S1 is presented in TABLE III and shown in Fig. 4 keeping L3 and W2 constant.

TABLE III. Variation of bandwidth of notch band with slot gap S1

Line Width W2	Bandwidth of notch band
0.1 mm	0.3 GHz (5.4-5.73 GHz)
0.15 mm	0.5 GHz (5.3-5.8 GHz)
0.2 mm	0.7 GHz (5.1-5.8 GHz)
0.25 mm	0.8 GHz (5.0-5.8 GHz)
0.3 mm	1.0 GHz (4.8-5.8 GHz)
0.35 mm	1.2 GHz (4.6-5.8 GHz)

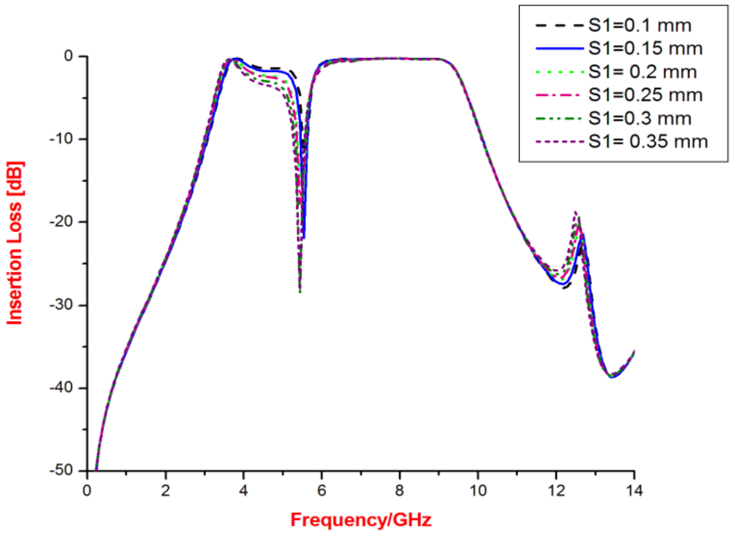

Fig. 4 Variation of bandwidth of notch band with slot gap S1

The bandwidth of notch band also varies with the line width W2. The variation of bandwidth of notch band with line width S1 is presented in TABLE IV and shown in Fig. 4 keeping S1 and L3 constant.

TABLE IV. Variation of bandwidth of notch band with line width W2

Line Width W2	**Bandwidth of notch band**
0.1 mm	**0.4 GHz (5.3-5.7 GHz)**
0.15 mm	**0.5 GHz (5.25-5.75 GHz)**
0.2 mm	**0.7 GHz (5.1-5.8 GHz)**
0.25 mm	**0.8 GHz (5.05-5.85 GHz)**
0.3 mm	**1 GHz (4.9-5.9 GHz)**
0.35 mm	**1.1 GHz (4.85-5.95 GHz)**

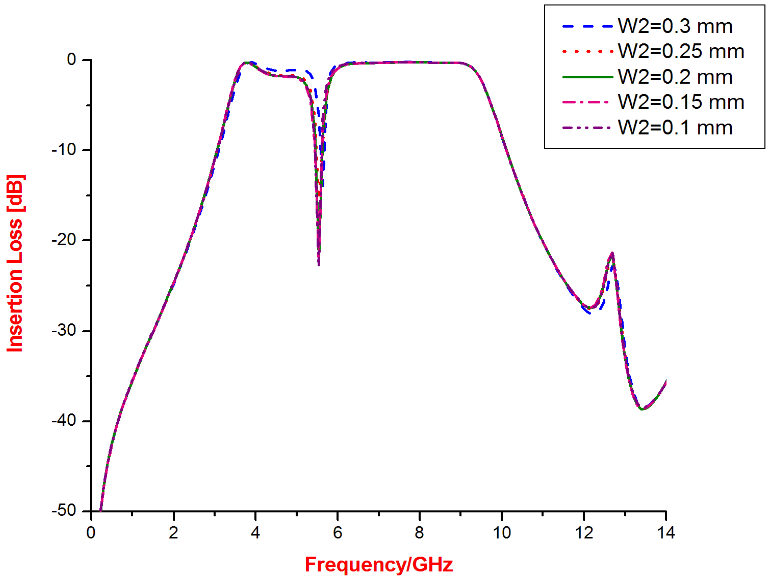

Fig. 5 Variation of bandwidth of notch band with line width W2

The switching scheme is achieved by introduction of Diode D1 in the etched slot. When diode is in forward bias (ON) state we get the UWB passband from 3.3 to 11 GHz without notch band. When diode is in reverse bias (OFF) state we get a notch band from 5.3 to 5.9 GHz for WLAN interference rejection. So by this scheme we provide additional swichable notch band feature in this design.

III. SIMULATED AND MEASURED RESULTS OF PROPOSED FILTER

The EM simulated frequency response and fabricated measured result of propose UWB bandpass filter with a switchable notch band for WLAN signal interference rejection is discussed here. The electromagnetic simulation software, Computer Simulation Technology Microwave Studio (CST MWS) is used for the simulation and analysis of the designed structure. The return loss S11, insertion loss S21and group delay is discussed in this section.

Based on the design analysis presented above, the UWB BPF is realized by MMR feed by interdigital coupled lines. Notch band for WLAN interference rejection is implemented using etched slot structure. Switchable notch band characteristics is achieved using Diode D1.The substrate used is Rogers RT5880 with a relative dielectric constant of 2.2 and a thickness of 0.4 mm. Fig. 6 shows the photograph of the fabricated UWB BPF.

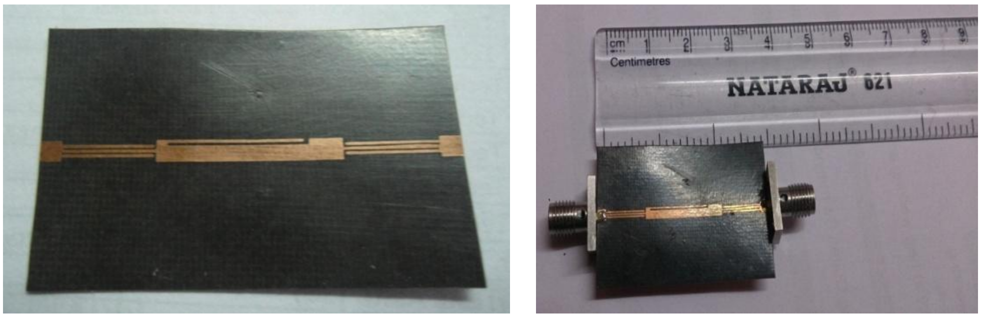

Fig. 6 Photograph of the fabricated UWB filter with WLAN notch

There are only simulated result of switching is presented here because switch based on lumped element could not be implemented easily in this design. When the Diode D1 is in forward bias (ON) state the EM simulated frequency response of proposed filter is shown in Fig. 7(a). The filter has the passband from 3.3 to 10.6 GHz. The passband is almost flat with attenuation around 0.3 dB in the whole passband. The return loss S11 is almost less than -10 dB in the whole passband. Group delay of proposed filter when diode D1 is ON is around 0.2 ns and overall linear in the whole pass band.

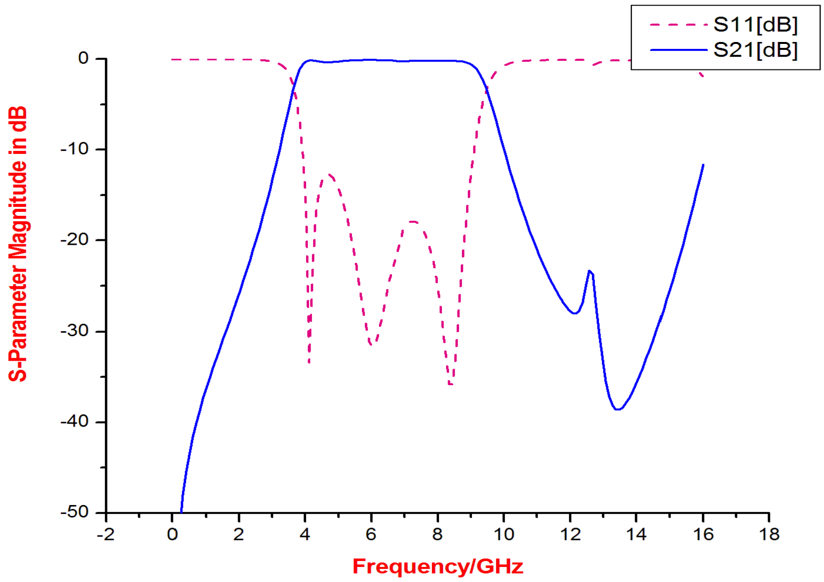

(a)

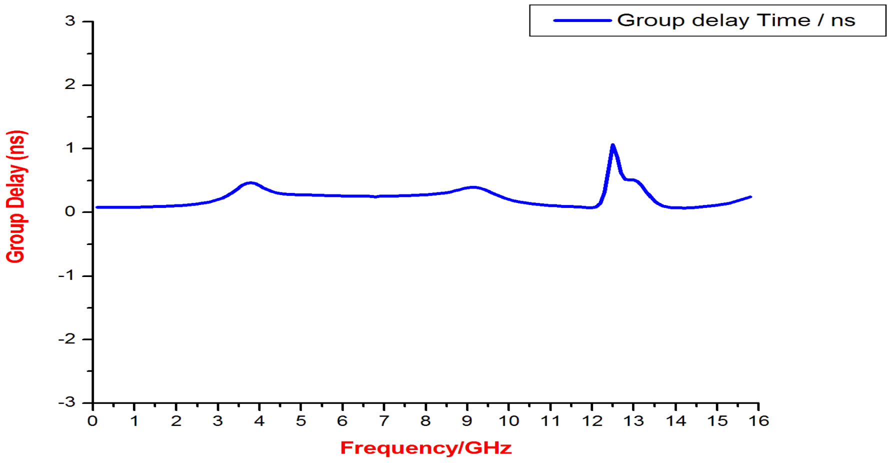

(b)

Fig. 7 Simulated result of proposed UWB BPF when diode D1 is ON state (a) Frequency response (b) group delay result

Fig. 8 (a) shows the EM simulated frequency response of proposed filter when Diode D1 is in reverse bias (OFF) state. In the OFF state we get the high selective notch band to suppress the undesired WLAN signal interference starts from 5.3 GHz to 5.8 GHz with attenuation around 25 dB. Group delay of proposed filter with notch band is around 0.2 ns and overall linear in the whole pass band as shown in Fig. 8 (b).

The fabricated measured results of the proposed UWB BPF with WLAN notch is presented in Fig. 5.9. The comparison of simulated and measured result is presented in Fig. 5.10, good agreement between simulated and measured results is observed. There are slight discrepancy may be due to the unexpected tolerance of fabrication and implement. In addition, the group delay within the UWB passband is between 0.56–0.85 ns, showing a good linearity.

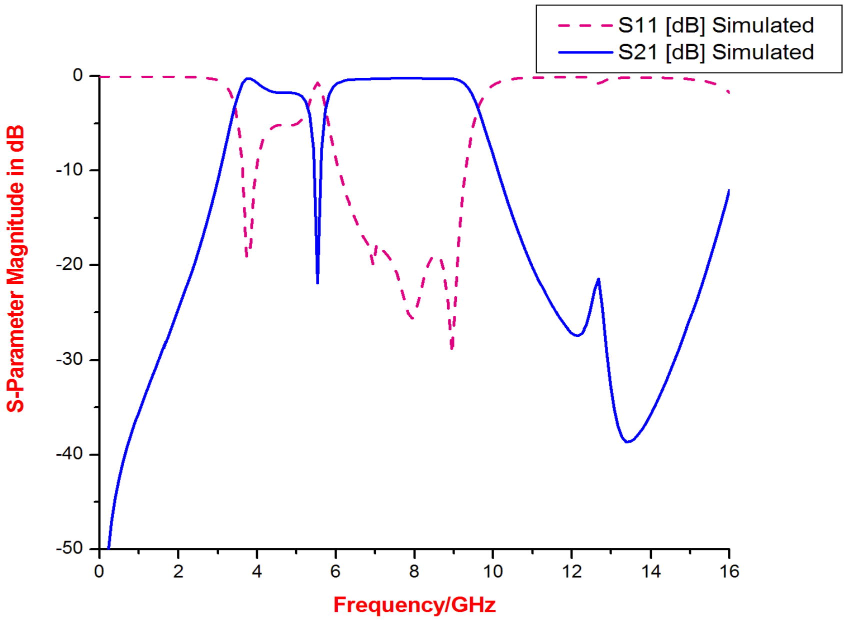

(a)

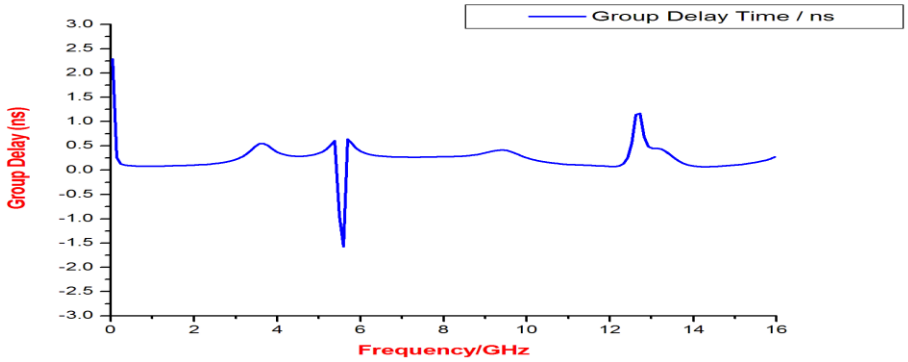

(b)

Fig. 8 Simulated result of proposed UWB BPF when diode D1 is OFF state (a) Frequency response (b) group delay result

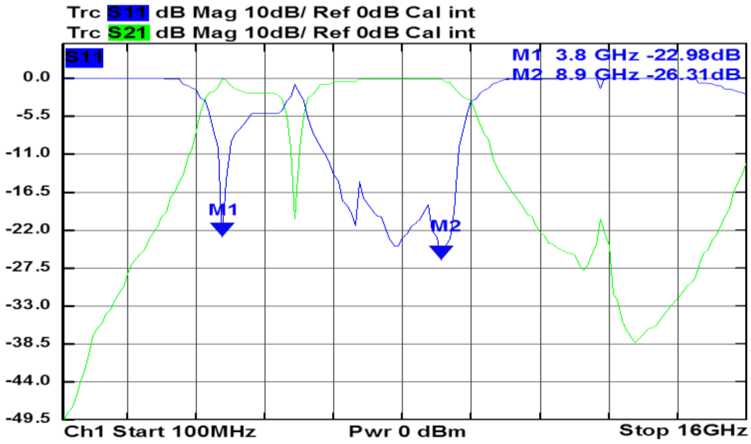

(a)

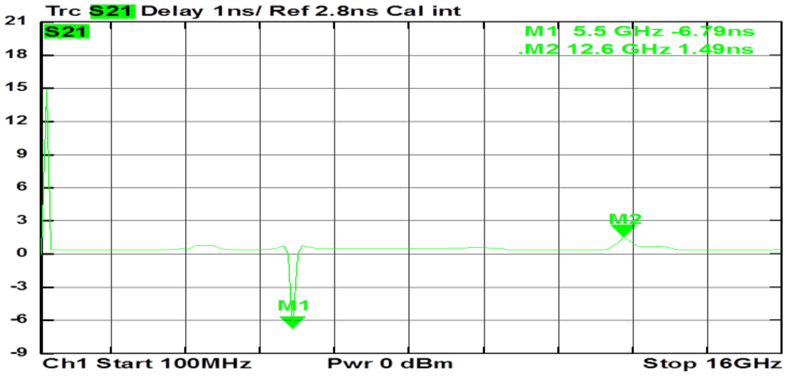

(b)

Fig. 9 Fabricated measured result of proposed UWB BPF with WLAN notch (a) Frequency response (b) group delay result

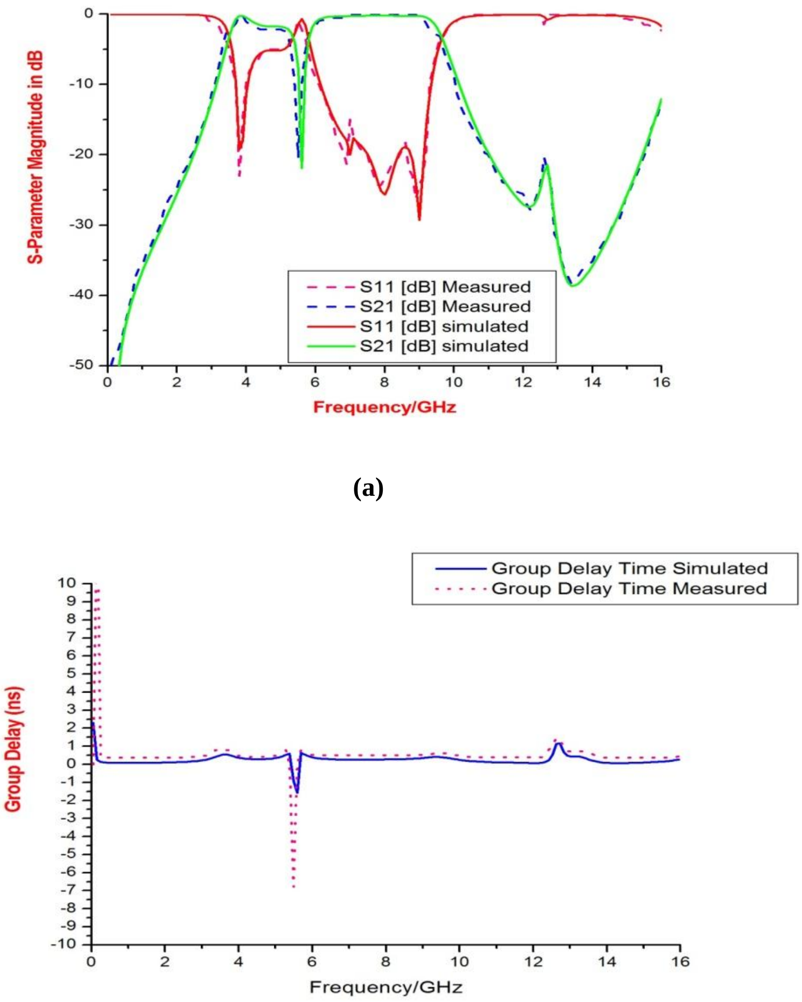

(a)

Fig. 10 Comparision of simulated and fabricated measured result of proposed UWB BPF with WLAN notch (a) Frequency response (b) group delay result

IV. CONCLUSION

In this letter, a design of UWB bandpass filter with notch band for WLAN interference rejection is proposed. Here we implement a notch band in the same structure by etching out the slot in the main structure, which reduce the size because no extra circuitry is required for band stop filter. There is also switchable feature introduced using a diode. So due to its compact size 37.4 X 25 $mm^2$and satisfactory passband and stopband performance, the filter can be useful for commercial UWB wireless communication systems.

REFERENCES

[1] S. Sun and L. Zhu, “Multimode resonator based band pass filters,” *IEEE Microw. Mag.*, vol. 10, no. 2, pp. 88–98, Apr. 2009.
[2] Z.-C. Hao and J.-S. Hong, “Ultrawideband filter technologies,” *IEEE Microw. Mag.*, vol. 11, no. 4, pp. 56–68, Jun. 2010.
[3] L. Zhu, S. Sun, andW. Menzel, “Ultra-wideband (UWB) bandpass filters using multiple-mode resonator,” *IEEE Microw. Wireless Compon. Lett.*, vol. 15, no. 11, pp. 796–798, Nov. 2005.
[4] H.Wang, L. Zhu, andW.Menzel, “Ultra-wideband bandpass filter with hybrid microstrip/CPW structure,” *IEEE Microw. Wireless Compon. Lett.*, vol. 15, no. 12, pp. 844–846, Dec. 2005.
[5] B. Yao,Y. Zho, Q.Cao, andY. Chen, “Compact UWB band pass filter with improved upper-stopband performance,” *IEEE Microw. Wireless Compon. Lett.*, vol. 19, no. 1, pp. 27–29, Jan. 2009.
[6] S. W. Wong and L. Zhu, “Quadruple-mode UWB bandpass filter with improved out-of-band rejection,” *IEEE Microw. Wireless Compon. .Lett.*, vol. 19, no. 3, pp. 152–154, Mar. 2009.

[7] J. Garcia-Garcia, J. Bonache, and F. Martin, “Application of Electromagnetic Bandgap to the Design of Ultra-Wide Bandpass Filters with Good Out of Band performance,” *IEEE Trans. Microw. Theory Tech.*, vol. 54, no. 12, pp. 4136–4140, Dec. 2006.

[8] S. W. Wong and L. Zhu, “EBG embedded multiumode resonator for UWB bandpas filter with improved upper stopband performance,” *IEEE Microw. Wireless Compon. .Lett.*, vol. 17, no. 6, pp. 421–423, Jun. 2007.

[9] M.-H.Weng, C.-T. Liauh,H.-W.Wu, andS.R.Vargas, “An ultra wideband bandpass filter with an embedded open-circuited stub structure to improve in-band performance,” *IEEE Microw. Wireless Compon. .Lett.*, vol. 19, no. 3, pp. 146–148, Mar. 2009.

[10] G.-M. Yang, R. Jin, C. Vittoria, V. G. Harrisand, and N.X. Sun, “Small ultra wideband (UWB) band pass filter with notch band,” *IEEE Microw. Wireless Compon. Lett.*, vol. 18, no. 3, pp. 176–178, Mar. 2008.

[11] S. Pirani, J. Nourinia, and C. Ghobadi, “Small ultra wideband (UWB) band pass filter with notch band,” *IEEE Microw. Wireless Compon. Lett.*, vol. 20, no. 8, pp. 444–446, Aug. 2010.

[12] C. H. KimandK. Chang, “Ultra-wideband (UWB) ring resonator bandpass filter with a notched band,” *IEEE Microw.Wireless Compon. Lett.*, vol. 21, no. 4, pp. 206–208, Apr. 2011.

[13] R. Ghatak, P. Sarkar, R. K. Mishra, and D. R. Poddar, “A compact UWB bandpass filter with embedded SIR as band notch structure,” *IEEE Microw. Wireless Compon. Lett.*, vol. 21, no. 5, pp. 261–263, May2011.

[14] Fu-Chang Chen And Quing-Xin Chu, “Design of compact triband bandpass filter using assembled resonator” IEEE Transaction on Microwave Theory and Techniches, vol.57, no.1,pp.165-171, January 2009.

[15] Adel Z. El Dein, Adel B. Abdel-Rahman, Raafat E. Fat- Helbary, and A. M. Montaser, “Tunable-compact bandstop defected ground structure (DGS) with lumped element,” 7th International Multi Conference on Systems, Signals and Devices, pp. 1-3, June 2010.

American Journal of Engineering Research (AJER)
e-ISSN : 2320-0847 p-ISSN : 2320-0936
Volume-03, Issue-10, pp-169-177
www.ajer.org

Research Paper Open Access

Design of Microstrip UWB bandpass Filter using Multiple Mode Resonator

Vinay Kumar Sharma[1], Mithilesh Kumar[2]
[1, 2] *(Electronics Engg. Department, University College of Engineering, Rajasthan Technical University, India)*

ABSTRACT : *In this letter, we present a design of microstrip ultrawideband (UWB) bandpass filter (BPF) for the use in UWB wireless communication application set by Federal Communications Commission (FCC). The UWB filter is realized with a Basic MMR (Multiple Mode Resonators) structure feed by interdigital coupled lines for achieving higher degree of coupling. The structure is optimized for high selectivity, inband and stopband performance. Finally for fabrication of this structure Rogers RT5880 substrate of thickness 0.4mm with Dielectric constant 2.2 is used. The electromagnetic simulation software, Computer Simulation Technology Microwave Studio (CST MWS) is used for the simulation and analysis of the designed structure. The comparison between simulated and fabricated measured result shows good agreement. The insertion loss of proposed filter is greater then 0.2 dB at 6.8 GHz and very flat over whole pass band also returns loss is less then -12db.*

Keywords - *Interdigital coupled lines, Microstrip, MMR, UWB*

I. INTRODUCTION

Ultra wideband (3.1–10.6 GHz) radio technology has tremendous progress now a days, and found potential application in medical imaging systems, pulse communication and ground penetration radar. One of the key components in the ultrawideband (UWB) communication system is the band pass filter (BPF) [1-2]. In recent years various UWB bandpass filters are reported based on numerous design techniques[3-13]. These are mainly ring resonator structure; hybrid microstrip/coplanar-waveguide (CPW) structure; multiple mode resonator structure. To achieve low cost and easy integration, these filters are usually implemented in a microstrip or coplanar waveguide technology.

We have to fulfill few requirements for designing a full band ultra wideband bandpass filter which are as:

- ✓ Ultra bandwidth like from 3.1 GHz to 10.6 GHz.
- ✓ Low insertion loss up to -1db.
- ✓ Low and flat group delay.
- ✓ Out-band performance (strongly required to meet the regulation such as the FCC's spectrum mask) [14].

In this paper, The MMR(Multiple Mode Resonator) structure is used to achieve a wide bandwidth. The position of first three resonant modes are optimized to locate in the UWB passband at the equal distance, and the fourth resonant mode is placed much above the upper stopband to achieve wide upperstopband. The MMR is feed by interdigital coupled lines gives higher degree of coupling and hence improve selectivity of the filter. The layout of proposed filter is shown in Fig.1 and its dimensions are presented in TABLE I.

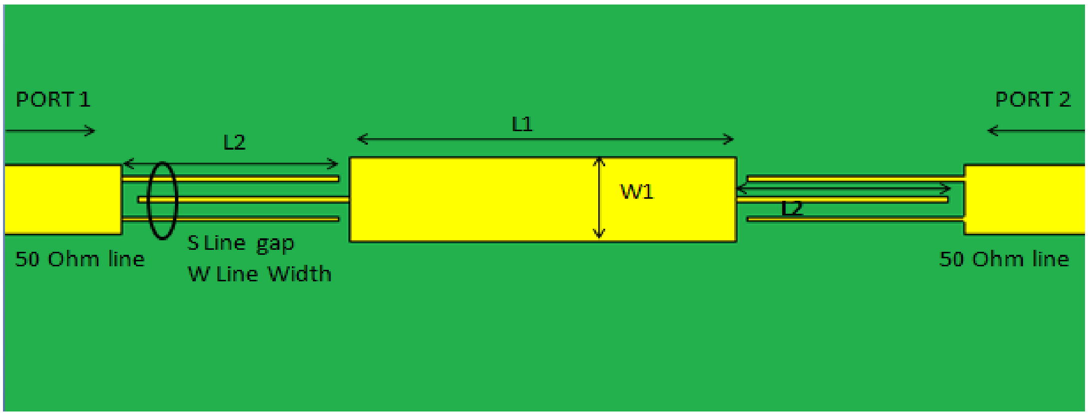

Fig 1. Layout of the proposed UWB bandpass filter

TABLE I. DIMENSION OF OPTIMIZED PROPOSED FILTER

Filter parameter	**Value**	**Filter parameter**	**Value**
L_1	7.5mm	**W_1**	1.6mm
L_2	4.2mm	**W**	0.1mm
S	1.2mm		

In the next section we will discuss the simulated design and optimization of UWB band pass filter. The different resonant modes of MMR and locating these modes for our objectives are discussed in this section. The comparison of simulated and fabricated measured result is discussed in third section. Fabricated result shows quite similarity with the result simulated on EM simulation software. At the end we conclude the optimized design and its application.

II. FILTER DESIGN

Fig.1presents the geometry of the proposed UWB bandpass filter on Microstripline which consists of an open ended multiple mode resonator (MMR) and interdigital coupled lines. This MMR has one low-impedance section in middle and two high impedance sections in two sides. The high impedance sections are edge-coupled with the interdigital geometry to the I/P signal line. To get a UWB passband, the first three resonant modes are allocated near the lower-end, center, and high-end of the targeted UWB frequencies, and the quarter-wave interdigital coupled line excite two additional poles below and above the UWB's center or 6.85GHz.

Fig 2(a) depicts the open-ended Microstrip stepped impedance MMR. It is composed of three distinctive sections, one low-impedance section in the middle and two identical high-impedance sections insides. Fig 2(b) is its equivalent transmission line network model. This Microstrip MMR aims to make effective use of its lowest multiple resonant modes for wideband filter design. This MMR resonator is very similar to SIR in geometry and equilvalent topology, but it should be emphasized here that the so-called SIR only uses the lowest or dominant resonant mode in the design of narrow band filters with widened upper stopband.

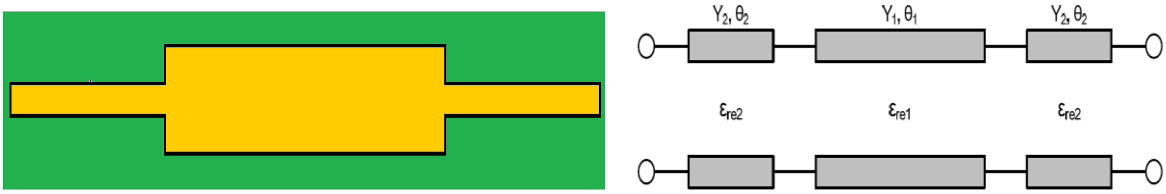

(a) (b)

Fig 2. (a) Geometry and (b) equivalent circuit network of the multiplemode resonator (MMR).

The input admittance (Yin) at the left open-end, looking into the right side, as indicated in Fig 2(b).

$$Y_{in} = jY_2 \times \frac{2(K\tan\theta_1 + \tan\theta_2)(K - \tan\theta_1\tan\theta_2)}{K(1-\tan^2\theta_1)(1-\tan^2\theta_2) - 2(1+K^2)\tan\theta_1\tan\theta_2} \qquad (1)$$

Where $K=Y_1/Y_2$ is the admittance ratio of two dissimilar sections in this MMR. At the resonance, $Y_{in}=0$ is valid. From Eq. 1, a set of algebraic equations are established to solve all the resonant to solve all the resonant frequencies, including the three lowest ones of interest, i.e. f_1, f_2, and f_3. In this design, electrical lengths of these two sections are selected as $\theta_1 \approx \theta_2 = \theta$ such that the three separate closed-form equations are deduced to individually determine f_1, f_2, and f_3. Eq. (2) and (4) presents the lower and higher frequencies, $f1$ and $f3$, are mainly controlled by K, while the center $f2$ relies on the selected actual lengths of the three sections in this MMR.

$$\theta(f_1) = \tan^{-1}\sqrt{K} \qquad (2)$$

$$\theta(f_2) = \frac{\pi}{2} \qquad (3)$$

$$\theta(f_3) = \pi - \tan^{-1}\sqrt{K} \qquad (4)$$

By de-tuning, the resonant frequencies can be observed and three resonant frequencies can be observed within UWB band. In the MMR the impedance ratio $K=Y_1/Y_2$ of low impedance line to high impedance line plays an important role for locating the resonant frequencies f_1, f_2, and f_3. The variation of resonant modes with varying impedance ratio K is presented in TABLE II. It is clear from the presented data that when we decrease the impedance ratio from 3.32 to 1.80, the resonant mode f_1 shifted from 4.3GHz to 3.8GHz and f_3 shifted from 8.5 GHz to 9.2 GHz, which shows that the distance of f_1 and f_2 from center resonant mode f_2 gets increased. The resonant mode f_4 is placed much above the upper stopband to achieve wide upper stopband. The S_{21}[dB] response under weak coupling of MMR with different impedence ratio K is shown in Fig. 3. Comparision of simulated detuned resonant frequencies with variation in impedance ratio is shown in Fig. 4.

TABLE II. VARIATION OF RESONANT MODES WITH IMPEDANCE RATIO K

Impedance Ratio(K)	**Resonant Frequencies(GHz)**			
	f_1	f_2	f_3	f_4
3.32	**4.3GHz**	**6.4GHz**	**8.5GHz**	**12.5GHz**
3	4.2GHz	6.4GHz	8.6GHz	12.6GHz
2.7	4.1GHz	6.4GHz	8.7GHz	12.7GHz
2.4	4.0GHz	6.45GHz	8.8GHz	12.7GHz
2.1	3.9GHz	6.45GHz	9GHz	12.77GHz
1.80	3.8GHz	6.5GHz	9.2GHz	12.9GHz

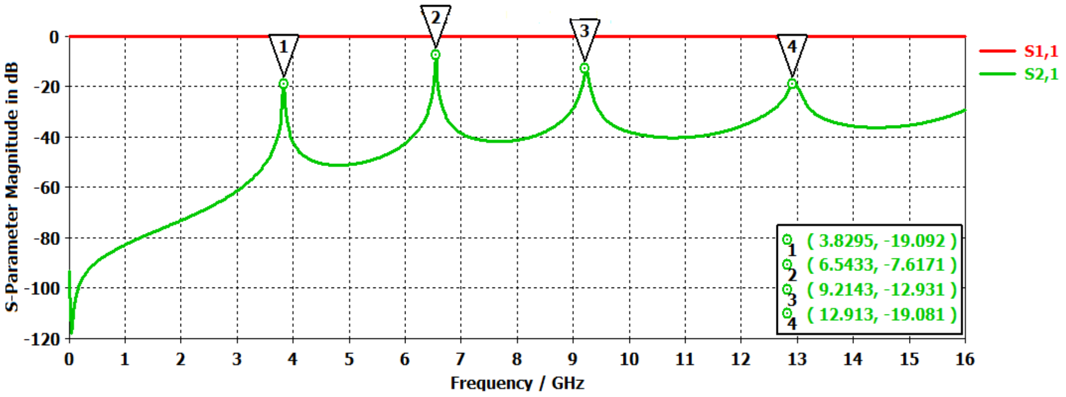

(a)

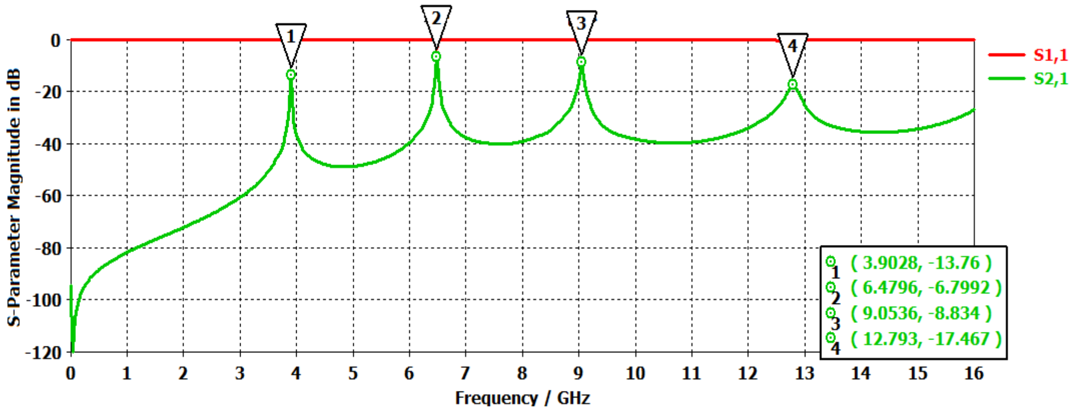
S-Parameter Magnitude in dB
Frequency / GHz
S1,1
S2,1
1
2
3
4
(3.9028, -13.76)
(6.4796, -6.7992)
(9.0536, -8.834)
(12.793, -17.467)

(b)

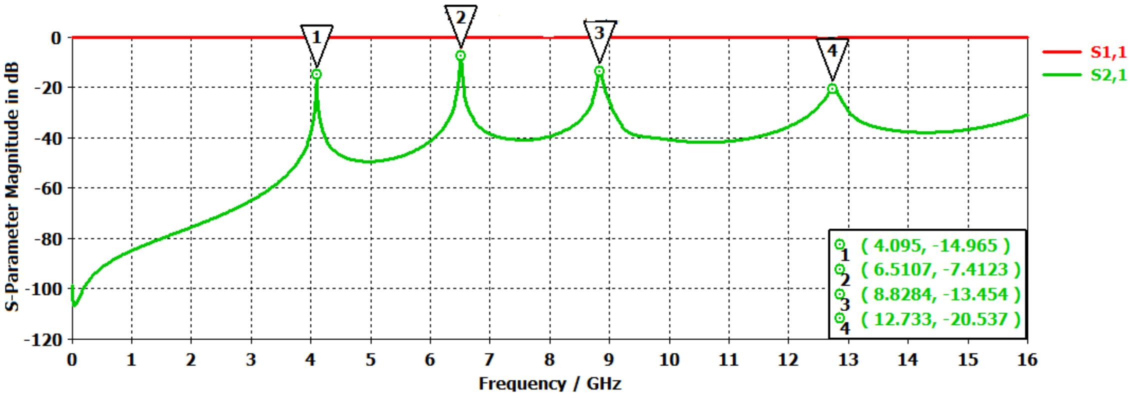
S-Parameter Magnitude in dB
Frequency / GHz
S1,1
S2,1
1
2
3
4
(4.095, -14.965)
(6.5107, -7.4123)
(8.8284, -13.454)
(12.733, -20.537)

(c)

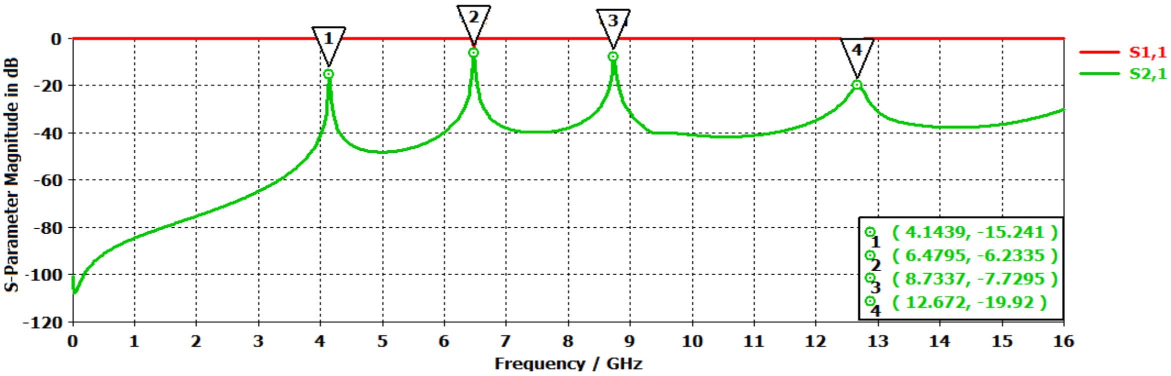
S-Parameter Magnitude in dB
Frequency / GHz
S1,1
S2,1
1
2
3
4
(4.1439, -15.241)
(6.4795, -6.2335)
(8.7337, -7.7295)
(12.672, -19.92)

(d)

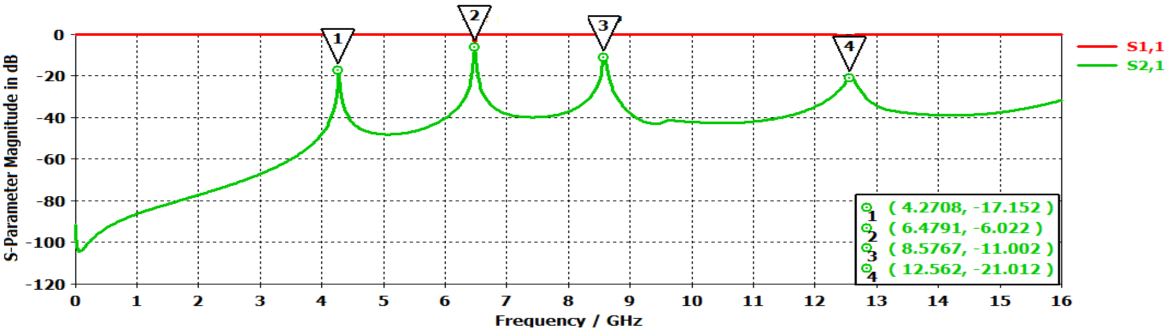
S-Parameter Magnitude in dB
Frequency / GHz
S1,1
S2,1
1
2
3
4
(4.2708, -17.152)
(6.4791, -6.022)
(8.5767, -11.002)
(12.562, -21.012)

(e)

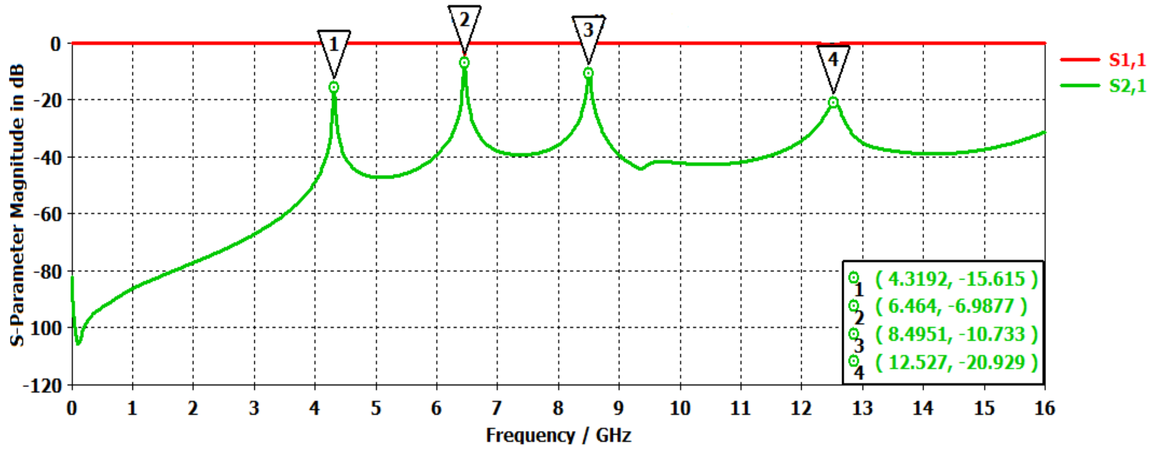

(f)

Fig. 3 Simulated detuned resonant frequencies with impedance ratio (a) K=1.80 (b) K=2.1 (c) K=2.4 (d) K=2.7 (e) K=3 (f) K=3.32

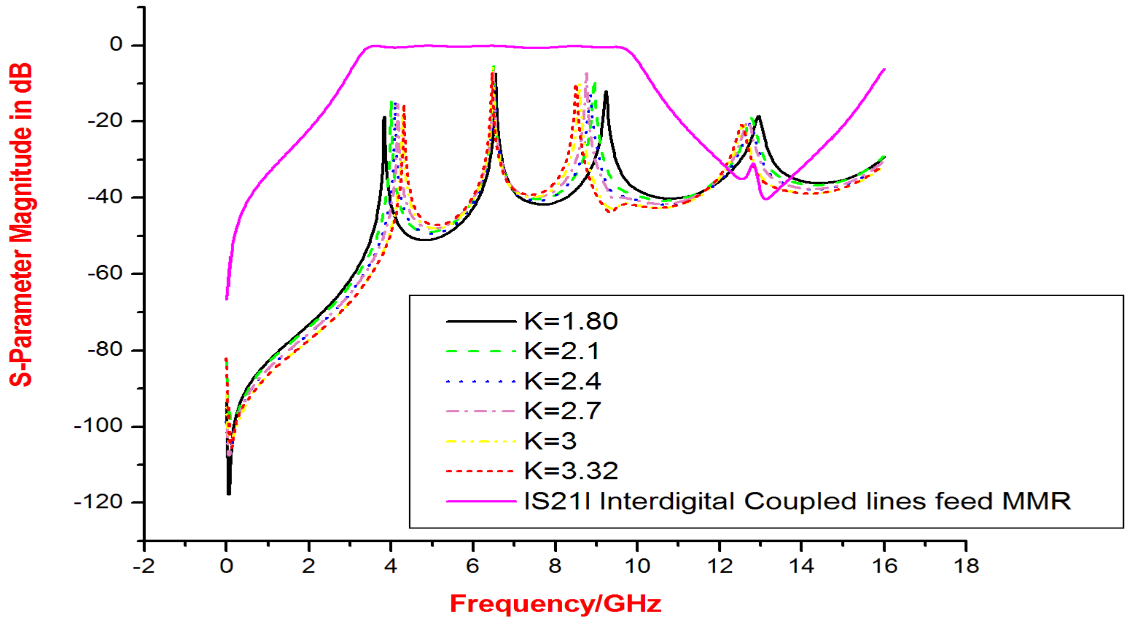

Fig. 4 Comparision of simulated detuned resonant frequencies with variation in impedance ratio (a) K=1.80 (b) K=2.1 (c) K=2.4 (d) K=2.7 (e) K=3 (f) K=3.32 and S_{21}[dB] of tuned MMR feed by interdigital coupled lines

Impedance ratio greater than 1 is utilised to design UWB filters. At the central frequency of the UWB passband, i.e., 6.85 GHz, the MMR structure is consist of one half wavelength λ/2 low-impedance line section in the center and two identical λ/4 high-impedance line sections at the two sides. So the MMR structure is optimized to cover all UWB passband such that the low impedance section is 51.65 Ω and high impedance section of the MMR is 140.93 Ω resulting in an impedance ratio of 2.72.

In this design we use Interdigital coupled lines as a I/O feed lines instead of single parallel line coupling. When giving energy to the MMR coupling energy of interdigital coupling is high compared with the single line parallel coupling. The current density result is shown in Fig. 3.4. The maximum current density of single line is 3.80 Amps/Meter and of double line it is 4.80 Amps/meter.

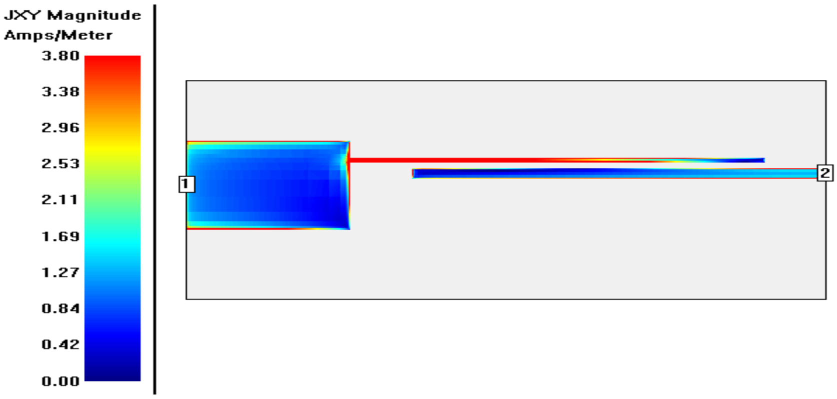

(a)

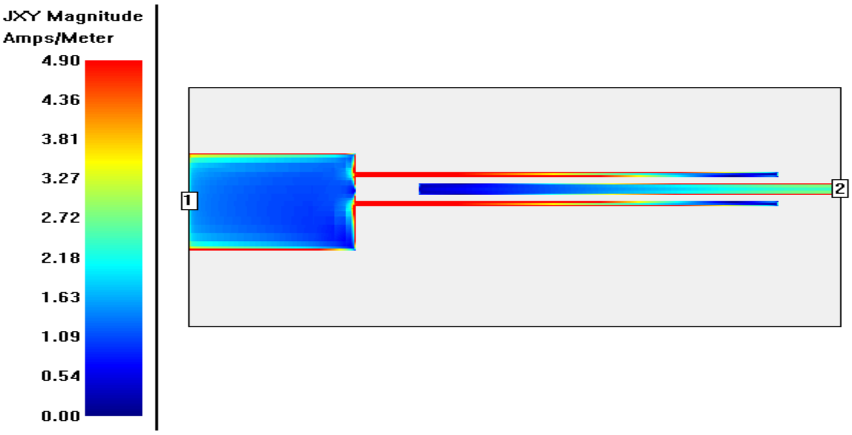

(b)

Fig. 5 (a) Current density distribution under single parallel line coupling. (b)Current density distribution under interdigital coupling.

III. SIMULATED AND MEASURED RESULTS OF PROPOSED FILTER

Here the simulated and fabricated measured result of proposed ultra wide band bandpass filter structure is presented. The proposed filter is simulated by the help of the Electromagnetic (EM) simulation software. The return loss S11, insertion loss S21and group delay is discussed in this section.

Based on the design analysis presented above, the UWB BPF is realized by applying strong interdigital coupled feed lines to the presented MMR as shown in Fig. 1. The substrate used in this paper is *Rogers RT5880* with a relative dielectric constant of 2.2 and a thickness of 0.4 mm. Fig. 6 shows the photograph of the fabricated UWB BPF. The simulated and measured results are presented in TABLE III.

TABLE III. Simulated and Measured Results of Proposed UWB BPF

Parameter	**Simulated**	**Measured**
Center frequency (GHz)	6.85 GHz	6.8 GHz
Return loss S_{11}, S_{22} (dB)	Better than -12.3 dB in passband	Better than -13 dB in passband
Insertion loss S_{21}, S_{12} (dB)	About 0.2dB in the whole passband	About 0.4 dB in whole passband
Group delay	Less than 0.55 ns Linear in whole passband	Less than 0.57ns Linear in whole pass band

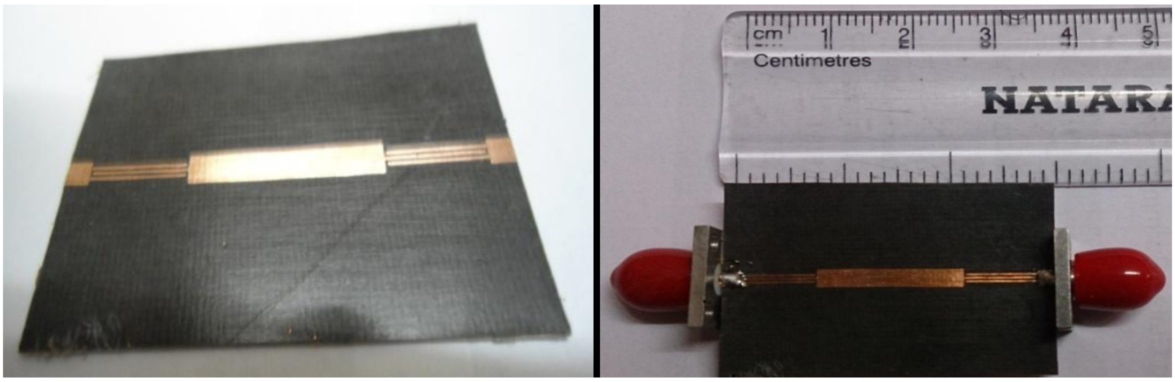

(a) **(b)**

Fig. 6. Photograph of the fabricated UWB filter

The simulated and measured results of the proposed UWB BPF are presented in Fig. 7 and Fig. 8 respectively. The comparison of simulated and measured result is presented in Fig. 9, good agreement between simulated and measured results is observed. As seen in Fig. 7, the 3 dB passband covers the range of 3.3–10.6GHz and it has a fractional bandwidth of 107%. The measured return loss is better than 12 dB within the UWB passband, and owing to the two transmission zeros in the lower and upper cut-off frequencies, sharp selectivity is observed. The measured upper stopband with 20 dB attenuation level is extended to 16 GHz. There are slight discrepancy may be due to the unexpected tolerance of fabrication and implement. In addition, the group delay within the UWB passband is between 0.56–0.85 ns, showing a good linearity as shown in Fig 9.

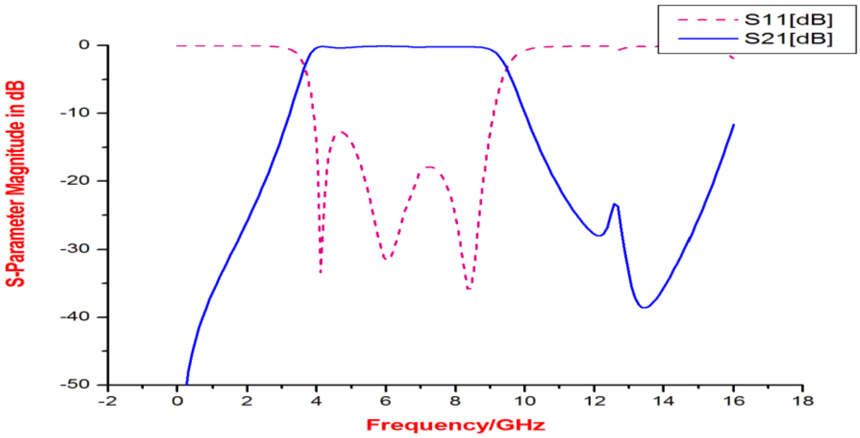

Fig. 7 Simulated result of proposed UWB BPF

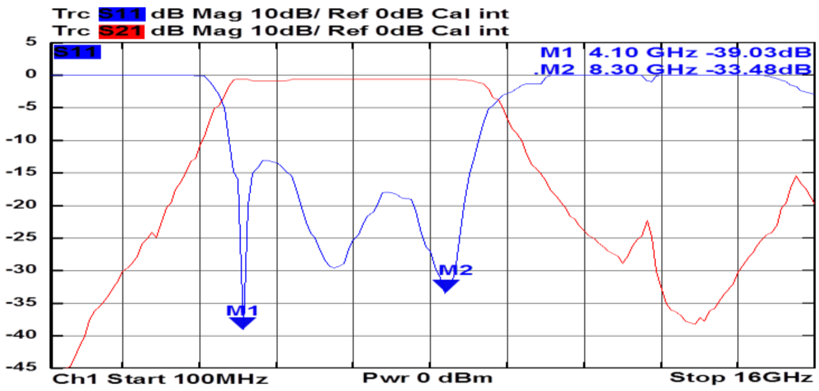

Fig. 8 Fabricated measured result of proposed UWB BPF

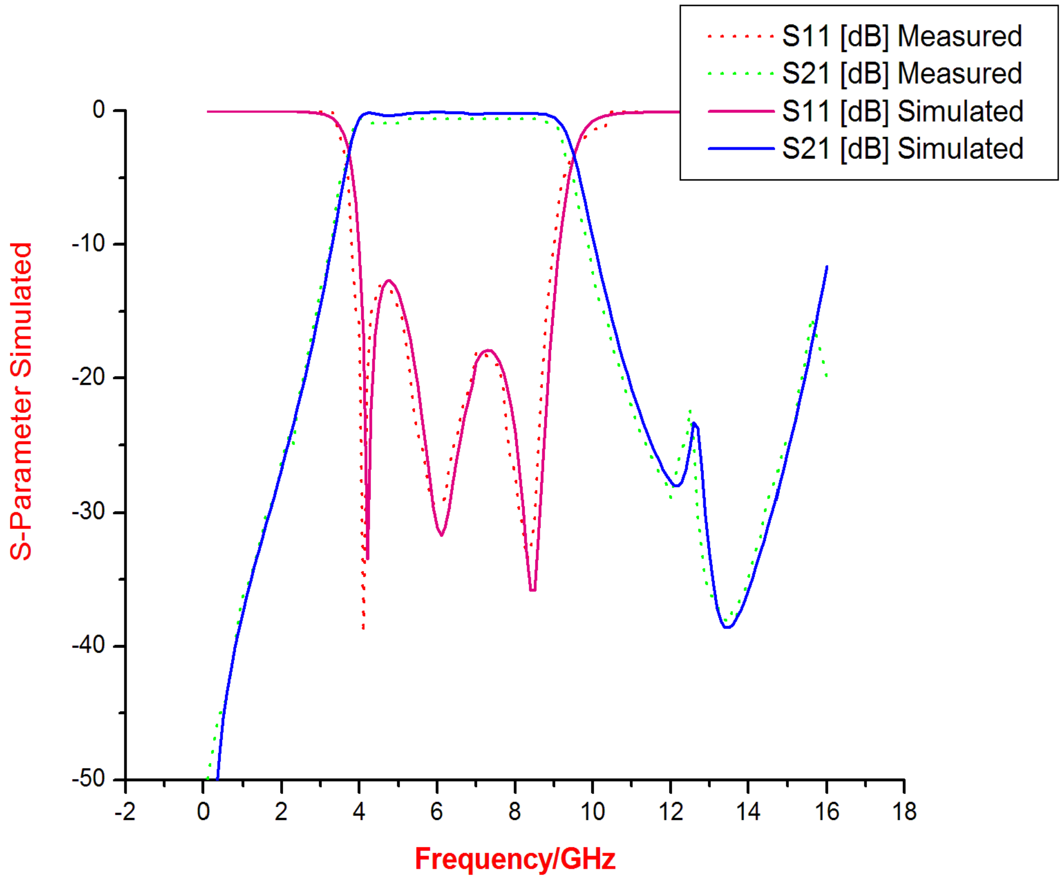

Fig. 9 Comparison of fabricated measured and simulated Result of proposed UWB BPF.

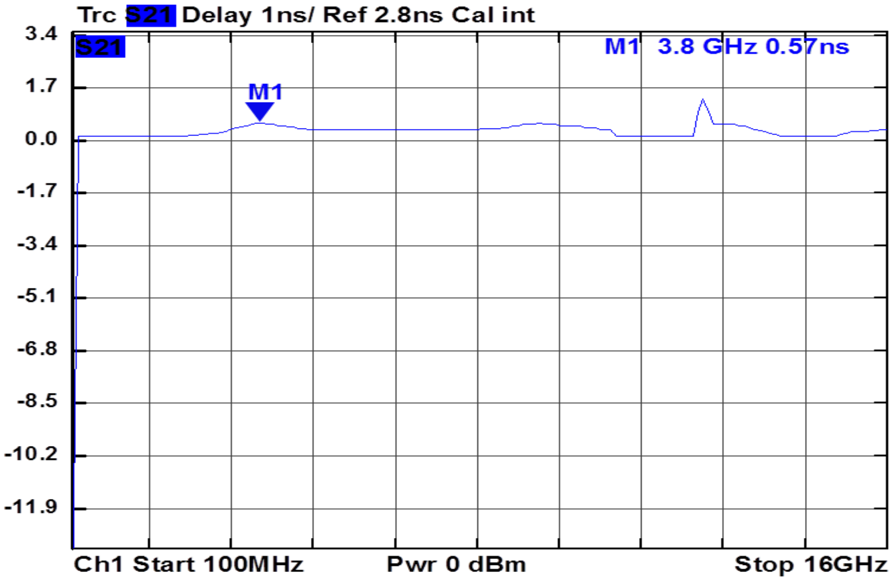

Fig. 10 Fabricated measured group delay result of proposed UWB BPF.

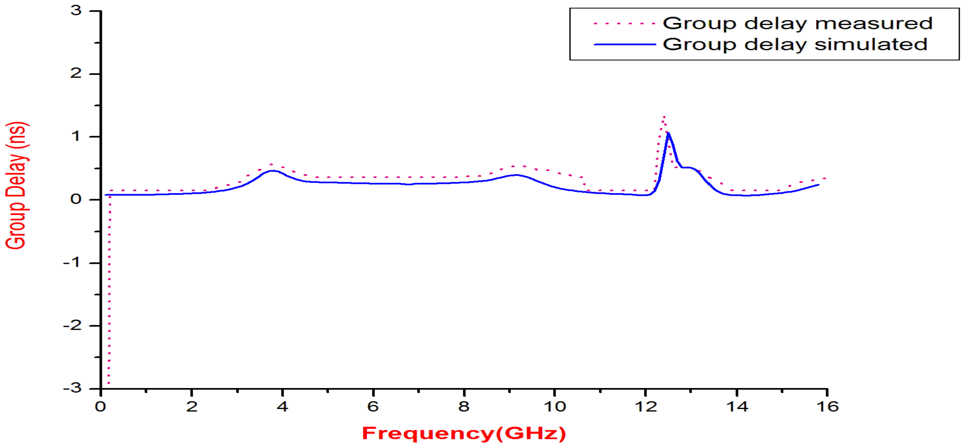

Fig. 11 Comparison of group delay result of proposed UWB BPF.

IV. CONCLUSION

In this letter, a compact UWB bandpass filter using MMR (multiple mode resonator) is discussed. As UWB filter is a part of UWB communication systems so it is always desirable to reduce the size of components. The MMR is constructed by one low-impedance section in middle and two high impedance sections in two sides. There are first three resonant modes of MMR are located in the UWB passband and fourth mode is placed much above the passband. The high impedance sections are edge-coupled with the interdigital geometry to the I/P signal line. By using MMR structure with I/O feed by double side coupled interdigital lines we can design compact filters even for wider bands. As earlier for increasing bandwidth and sharpness of a filter we have to increase the order of filter but that would make our filter bulky. MMR structure based designs give a perfect solution for this problem. The overall performance and Characteristic of designed filter is excellent and can be useful for any modern wireless device.

REFERENCES

[1] Qi Li, Chang-Hong Liang, *Senior Member IEEE*, Hai-Bin Wen, Guo-Chun Wu "Compact Planar Ultra-Wideband (UWB) Bandpass Filter with Notched Band" IEEE 2009.

[2] Sheng Sun, Student Member, IEEE, and Lei Zhu, Senior Member, IEEE "Capacitive-Ended Interdigital Coupled Lines for UWB Bandpass Filters With Improved Out-of-Band Performances" IEEE Microwave and Wireless components letters, vol. 16, no. 8, august 2006.

[3] Lei Zhu,Sheng Sun and Wolfgang Menzel, "Ultra-Wideband (UWB) Bandpass Filters Using Multiple-Mode Resonator", *IEEE Microwave and Wireless Components Letters*, Vol. 15, no. 11, pp. 796-798, NOV 2005.

[4] Hang Wang, Lei Zhu and Wolfgang Menzel, "Ultra-Wideband Bandpass Filter With Hybrid Microstrip/CPW Structure", *IEEE Microwave and Wireless Components Letters*, Vol. 15, NO. 12, pp. 844-846, DEC. 2005

[5] Qing-Xin Chu, Xiao-Hu Wu, and Xu-Kun Tian, "Novel UWB Bandpass Filter Using Stub-Loaded Multiple-Mode Resonator", *IEEE Microwave and Wireless Components Letters*, Vol. 21, No. 8, pp. 403-405, AUG. 2011.

[6] Xiao-Hu Wu, Qing-Xin Chu, Xu-Kun Tian, and Xiao Ouyang, "Quintuple-Mode UWB Bandpass Filter With Sharp Roll-Off and Super-Wide Upper Stopband" *IEEE Microw. Wireless Compon. Lett.*, vol. 21, no. 12, pp. 661--663, Dec. 2011.

[7] Zhebin Wang, Fathi Nasri, and Chan-Wang Park "Compact Tri-band Notched UWB Bandpass Filter Based on Interdigital Hairpin Finger Structure" 2011 Crown

[8] Xiu Yin Zhang, Yao-Wen Zhang and Quan Xue, "Compact Band Notched UWB Filter Using Parallel Resonators With a Dielectric Overlay", Microwave and Wireless Components Letters, Vol. 23, No. 5, pp. -252-254, May 2013.

[9] H. Zhu, Q.-X. Chu & X.-K. Tian, "Compact UWB bandpass filter using folded-T-shaped resonator with a notch-band", *Journal of Electromagnetic Waves and Applications*, Vol. 26, No. 10, pp. 1366–1373, July 2012.

[10] Min-Hang Weng, Chihng-Tsung Liauh, Hung-Wei Wu and Steve Ramrez Vargas, "An Ultra-Wideband Bandpass Filter With an Embedded Open-Circuited Stub Structure to Improve In-Band Performance" *IEEE Microwave and Wireless Components Letters*, Vol. 19, NO. 3, pp. 146-148, March 2009.

[11] Chan Ho Kim and Kai Chang, "Ultra-Wideband (UWB) Ring Resonator Bandpass Filter With a Notched Band", *IEEE Microwave and Wireless Components Letters*, Vol. 21, No. 4, pp. 206-208, April 2011.

[12] Pankaj Sarkar, Rowdra Ghatak, Manimala Pal, and D. R. Poddar, "Compact UWB Bandpass Filter With Dual Notch Bands Using Open Circuited Stubs" *IEEE Microwave and Wireless Components Letters*, vol. 22, no. 9, pp. 453-455, September -2012.

[13] M. Makimoto and S. Yamashita, *Microwave resonators and Filters for Wireless Communication*, Springer, 2003.

[14] J.S. Hong and M.J. Lancaster, *Microstrip Filters for RF/Microwave Applications*, New York; Wiley, 2001.

American Journal of Engineering Research (AJER)
e-ISSN : 2320-0847 p-ISSN : 2320-0936
Volume-03, Issue-10, pp-178-187
www.ajer.org

Research Paper Open Access

Developing a highly reliable cae analysis model of the mechanisms that cause bolt loosening in automobiles

Ken Hashimoto[1], TakehiroOnodera[2], Kakuro Amasaka[3]
[1](Graduate School of Science and Engineering/ Aoyama Gakuin University, Japan)
[2](Graduate School of Science and Engineering/ Aoyama Gakuin University, Japan)
[3](School of Science and Engineering/ Aoyama Gakuin University, Japan)

ABSTRACT : *In this study, we developed a highly reliable CAE analysis model of the mechanisms that cause loosening of bolt fasteners, which has been a bottleneck in automobile development and design, using a technical element model for highly accurate CAE that we had previously developed, and verified its validity. Specifically, drawing on knowledge gained from our clarification of the mechanisms that cause loosening of bolt fasteners using actual machine tests, we conducted an accelerated bench test consisting of a three-dimensional vibration load test of the loosening of bolt fasteners used in mounts and rear suspension arms, where interviews with personnel at an automaker indicated loosening was most pronounced, and reproduced actual machine tests with CAE analysis based on a technical element model for highly accurate CAE analysis. Based on these results, we were able to reproduce dynamic behavior in which larger screw pitches (lead angles) lead to greater non-uniformity of surface pressure, particularly around the nut seating surface, causing loosening to occur in areas with the lowest surface pressure. Furthermore, we implemented highly accurate CAE analysis with no error (gap) compared to actual machine tests.*

Keywords -*CAE, Bolt fastener, Reliable*

I. INTRODUCTION

Japan’s automotive industry enjoys a position of international prominence. However, since the industry began to address the problem of recalls following greater social awareness of the issue in recent years, there has been a trend toward increases in both the number of recalls and the number of vehicles involved. Serious quality problems such as this threaten the very social status of the companies involved and could end up compromising the status of the Japanese manufacturing industry as a whole, which has traditionally competed successfully with counterparts in other countries. Consequently, it has become a key for companies to pursue measures to address quality defects and to establish systems for preventing such defects.

Moreover, recent diversification of consumer needs is driving the industry toward a super-fast development and design cycle, and it will be difficult for automakers to survive as companies if they are unable to outcompete their rivals, both domestically and overseas. For these reasons, automakers are seeking to put in place development and design systems that deliver high quality and short lead times and using computer-aided engineering (CAE) to pursue concurrent engineering. In recent years, the industry has sought highly accurate CAE analysis that yields results that do not diverge from actual machine test results, but the state of the art in such analysis has stopped at relative evaluation, which does not allow companies to perform predictive evaluation. The reason for this impediment lies in differences in how companies developing CAE analysis software and their customers in the manufacturing industry use that software.

Against this backdrop, this paper develops a highly reliable CAE analysis model that facilitates a predictive evaluation-oriented CAE design system. We conducted a two-dimensional CAE analysis to determine test characteristics values for actual machine tests and to set three-dimensional CAE analysis parameters drawing on information gained from previous research[1-8]. Next, we conducted actual machine tests and a three-dimensional CAE analysis. By applying this model so that we could conduct a three-dimensional analysis after setting only a minimum number of test parameters, we were able to boost the accuracy of the prediction and evaluation processes.

To verify the validity of this model, and to provide an example application, we conducted a bolt loosening vibration test using actual vehicle parts and a CAE analysis, focusing on clarifying the mechanisms that cause loosening of bolts. Specifically, we focused on comparing bolts and nuts with different pitches and studied the causes that lead to bolt loosening by comparing the drop in axial force during bolt fastening and assessing the stress distribution at areas of contact on the nut seating surface [9].

II. HIGHLY ACCURATE CAE ANALYSIS MODEL

In this section, we will focus on the loosening of bolt fasteners and offer a five-step approach to implementing highly accurate CAE analysis in the development and design process, as summarized inFig.1.

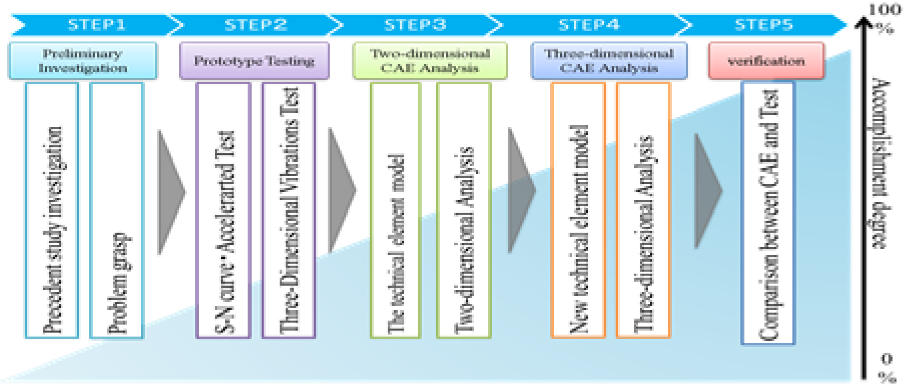

Fig.1Highly Accurate CAE Analysis Model

2.1 Preliminary Investigation

In order to solve the technical problems that lie behind market complaints (cases where manufacturers are unable to reduce the incidence of functional failures, which is an area of concern in automobile development and design) by determining, for example, why failures occur and the mechanisms that are responsible for them, it is important that step 1 be to engage in cooperative creative activities that bring together the knowledge of in-house and outside experts. It is also important to use the latest techniques of statistical science to investigate and analyze convergent causal relationships and conduct a detailed analysis of the phenomenon in question in order to deduce the failure mechanism in step 1.

2.2 Prototype Testing

In order to visualize the phenomenon in question, it is necessary to visualize the dynamic behavior that accompanies the occurrence of the problem using actual machines and tests. In this step 2, we search for latent factors that have remained unknown or overlooked using techniques such as N7 (new seven QC tools), SQC (Statistical Quality Control), RE (a reliability technique), MA (multivariate analysis), and DE (experimental design) to analyze the failure and its principal causes in a precise manner.

In this way, the failure mechanism is verified by means of a logical thought process. We also analyze the mechanism based on the phenomena that were visualized through actual machine tests. Then by conducting other tests, we identify issues that could not be fully understood by means of the visualization tests. These issues are identified through the three-dimensional CAE analysis carried out in Step 3.

2.3 Two-dimensional CAE Analysis

In this step 3, we carry out two-dimensional CAE analysis by modeling the phenomenon being studied using CAD based on the parameters obtained during the actual machine tests. The objective is to assess characteristics values and boundary conditions for the three-dimensional CAE analysis and to predict its results.

2.4 Three-dimensional CAE Analysis

Based on the two-dimensional CAE analysis, we then establish a technical element model for three-dimensional CAE analysis and devise an analysis model. In particular, we develop a three-dimensional model that achieves consistency at a qualitative level by using three-dimensional CAD. At this step 4, it will be necessary to conduct actual machine tests that model (qualitatively) the causal relationship characterizing the unexplained mechanism, and it becomes important to select precise calculation techniques, analysis models, and algorithms in order to clearly identify boundary conditions and contact states and conduct a highly accurate numerical simulation.

In addition, we create a technical element model, which is the most important approach model in order to explicate technical problems. Through this process, it is extremely important to shrink the gap by absolute value evaluation of actual machine and tests and CAE results.

In highly reliable CAE analysis, a thorough battery of actual machine tests is performed based on the information gained from the logical thought process described above in order to adequately clarify implicit knowledge about the failure mechanism. Then we integrate the information gained from these work processes to conduct a highly reliable numerical simulation (quantitative modeling) enabling prediction and control of absolute values.

2.5 Verification

In this step 5, we conduct a comparative verification and evaluation of actual machine test results and three-dimensional CAE analysis results. The benefits of this approach model are apparent in its ability to deliver enough accuracy to keep the error within 3%. Additionally, by using a model that increases the accuracy of the analysis, it is possible to transition from relative evaluation to absolute evaluation in the use of analysis results in development. We believe that this transition will lead to the establishment of a prediction- and evaluation-based design system.

III. EXAMPLE APPLICATION-ANALYSIS OF THE MECHANISMS THAT CAUSE BOLT FASTENER LOOSENING IN BOLT-FASTENED PARTS IN MOUNTS AND REAR SUSPENSION ARMS-

Our purpose was to clarify behavior in terms of stress distribution on nut seating surfaces, which is an important problem when using bolt fastening, and to search for behavior consisting of a reduction in axial force caused by simultaneous vibration from the three axial directions. We focused our tests on the mount and rear suspension arms, both of which are automotive components, and set out to visualize the mechanisms that cause bolt loosening in those parts. To do so, we used fatigue testing (three-dimensional vibration testing) of bolt fasteners to assess the stress distribution on the nut seating surface and the behavior of axial force reduction using time sequences of data.

3.1 Bolts and Nuts Used

We chose M12 10T flanged hexagonal bolts and nuts with three different pitches (0.50 mm, 1.25 mm, 1.75 mm) for testing. Since the bolts and nuts would be used in the rear suspension, we used the largest and smallest pitches of 0.50 mm (Fig. 2) and 1.75 mm (Fig. 4) that could be manufactured in compliance with the JIS standard for bolts and nuts with a pitch of 1.25 mm (Fig. 3).

Fig.2 Pitch 0.50mm

Fig.3 Pitch 1.25mm

Fig.4 Pitch 1.75mm

3.2 Used Equipment

Concerning the equipment used in our tests (Fig. 5), we reproduced a working chassis designed to simulate bench testing of an actual vehicle. Furthermore, the mount and suspension arm shown in Fig. 6 and Fig. 7 were the automotive parts most prone to loosening according to interviews at YaeiAutomobileMaintenance Factory. We combined these parts to conduct tests to subject the bolt fasteners to vibrations in three dimensions.

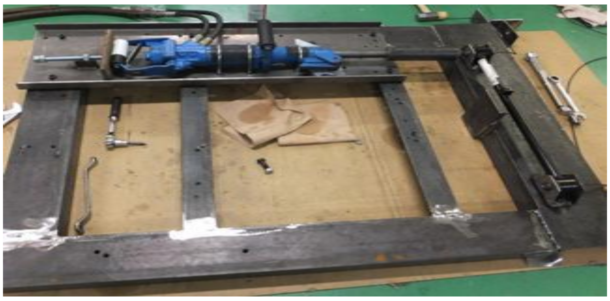

Fig. 5Vibration-Testing Machine

Fig. 6Rigid Part

Fig. 7 Rear Suspension

3.3 Bolt Fastening Test

Our objective in actual machine tests was to ascertain the axial force extraction fastening load at which sliding of the seating surface occurs and to identify the mechanisms that cause bolt loosening due to three-dimensional vibration. First, we determined the stress amplitude value to use in accelerated testing. Furthermore, we identified the loosening mechanism by applying that value to the bolts, nuts, equipment, and parts being used.

3.3.1 Accelerated Test

We used an accelerated test as the first actual machine test. In an accelerated test, it is possible to trigger a failure in a shorter amount of time (smaller number of cycles) than usual by applying a large stress amplitude. Our accelerated stress procedure consisted of creating an S-N curve based on the results of past tests conducted by the Amasaka-Laboratory and then using Miner's rule to calculate the acceleration coefficient [3, 6, 7]. We then conducted the accelerated test.

(a)S-N Curve

Fig. 8 illustrates the results of plotting a curve consisting of the number of vibration cycles (N) at which bolt loosening occurred in past tests versus the stress amplitude (S) at that point in time.

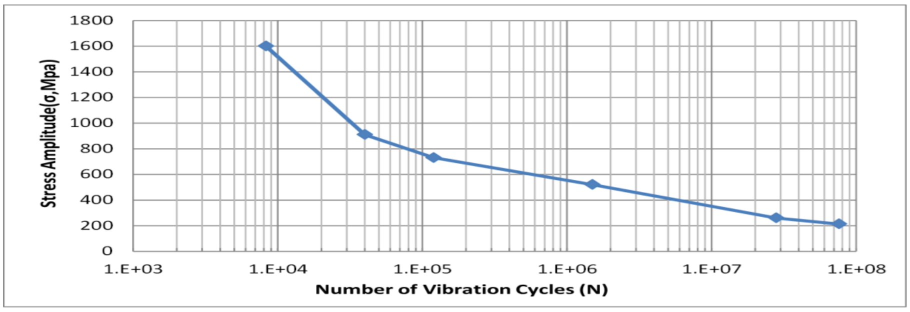

Fig. 8S-N Curve

(b) Miner's rule

$$\sum_{n=1}^{\infty}\left(\frac{n_i}{N_i}\right)=1 \qquad (1)$$

$$N_i * S^{\alpha} = \beta \qquad (2)$$

The approach of Miner's rule can be expressed by (1) above. The stress amplitude (S), repeat cycles (N), and stress cycles (n) at the maximum and minimum value points from the S-N curve calculated in (a) are substituted into (2) to calculate the acceleration coefficient (α). Then the damage-specific coefficient (β) is calculated from the calculated acceleration coefficient (α) and (2), and as a result the stress amplitude (S) is calculated. The stress amplitude value calculated here was used as the stress amplitude in this paper's actual machine tests.

(c)Determining the amplitude output device

Next, we study vibration generators capable of outputting the stress amplitude value calculated using the S-N curve in (a) and Miner's rule in (b). We looked at vibration motors and jackhammers manufactured by EXEN Corp. and Maruzen Co., Ltd., and ultimately chose to use the BH-16 (Fig. 9) as the vibration output device for our actual machine tests.

Fig. 9Jackhammer Manufactured by Maruzen Co., Ltd.

3.3.2 Three-Dimensional Vibrations Test

First, to estimate the vibration load to use in the vibration test, we applied a fastening load of 12 kN to the bolt fasteners in a static test to measure the tester load at which sliding of the seating surface increased abruptly. Specifically, we applied a series of varying three-dimensional vibrations to the fixture holding the mount and rear suspension arm in place (Fig. 5).

Then, we applied vibrations to the tester at a vibration load equivalent to ±20% of the static extraction load. At this point, we ascertained the phenomenon by which bolt loosening occurs due to repeated sliding of the seating surface. In this test, we measured the displacement between the bolt and tester and the trend in the bolt axial force extraction load relative to the number of repetitions. The results are summarized in Fig. 10 and Fig. 11 below.

In both figures, the 1.25 mm pitch bolts are subjected to vibrations under the same test conditions, but only the suspension arm (Fig. 12) is fastened at both ends by two bolts. The line graph shows the mount results in yellow, the area of the suspension to which external stress was applied (red circle) in red, and the fixed part on the opposite side (blue circle) in blue. Both show a reduction in axial force, but we found that for the suspension arm, the area shown by the red circle loosened first, and then the area shown by the blue circle loosened in response.

Based on the large reduction in axial force at the mount, we also found a link with suspension arm hazard and the manner in which the bolts loosen.

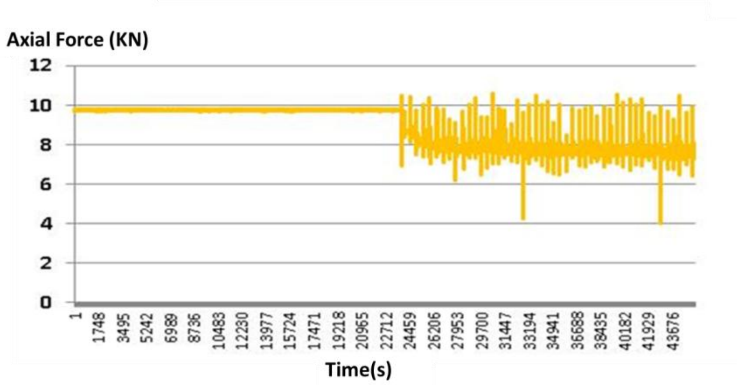

Fig. 10Result of Rigid Par

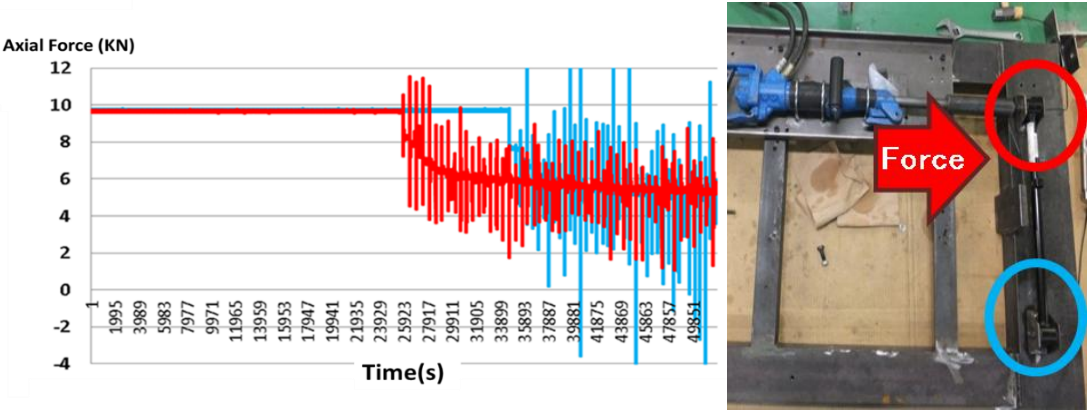

Fig. 11Result of Rear Suspension

3.4 Two-Dimensional Analysis

In this section, we describe how we created a technical element model expressing the elements shown in Fig. 12 below in order to ascertain the stress behavior inside the bolt and to improve the accuracy of our three-dimensional CAE analysis. To achieve those objectives, it is necessary to carry out a highly accurate CAE analysis without any inadequacies in terms of modeling, algorithms, theory, or computer technology.

In modeling, the model’s material properties must be uniquely selected in the form of a material constitutive model. These properties are then assigned as quantitative values for the constitutive model that defines the material.

In terms of theory, the coefficients of friction serve as important elements. In this case, we assigned the coefficients of friction for the thread and seating surface as quantitative values based on test results. In terms of the calculation technique, we opted to use the penalty method based on consideration of the balance between calculation time and accuracy.

Based on the above considerations, we conducted a finite element analysis using a two-dimensional model taking into account the thread’s helical structure and contact.

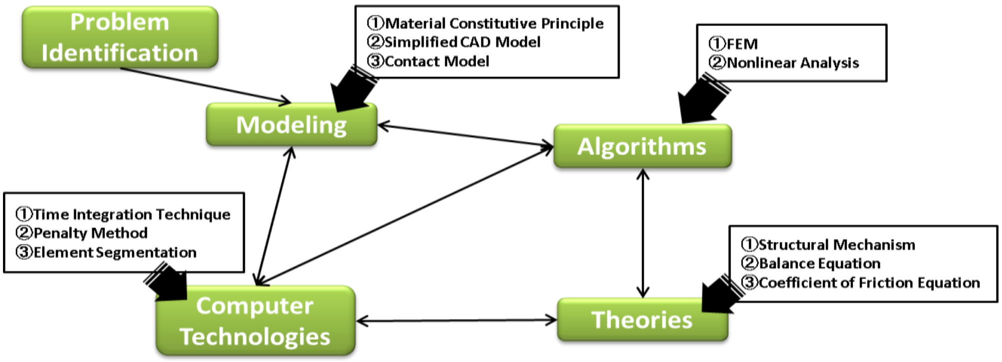

Fig. 12Two-Dimensional Technical Element Model

3.4.1 Result of Two-dimensional Analysis

Fig. 13 and Fig. 14 illustrate the results of a numerical simulation that applied external force from the left side of thefigures to the 0.50 mm and 1.75 mm pitch bolts, respectively, using the same boundary conditions as the actual machine tests. The contours indicate stress, with stress values increasing as the colors change from blue to red. These figures indicate that while the stress spread throughout the bolt with the short 0.50 mm pitch, it was concentrated in the area indicated by the red circle in the bolt with the longer 1.75 mm pitch.

Furthermore, based on the numerical stress distribution, it can be predicted that the 1.75 mm pitch bolt would loosen more readily due to the high load on the thread helix and nut seating surface. Based on this analysis, we were able to estimate such information as the coefficient of friction for each pitch, the element segmentation method, and contact condition, as detailed in Table 1. We then conducted a three-dimensional analysis using the conditions and characteristics values obtained in this step.

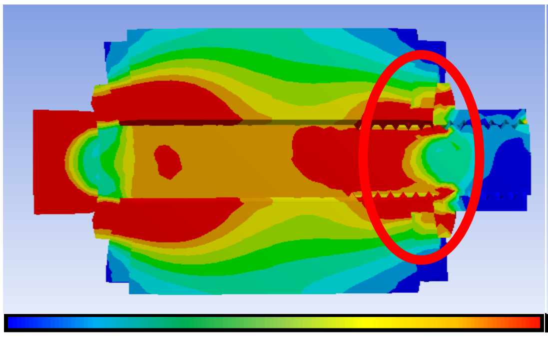

Fig. 13 Result of 0.50mm Pitch

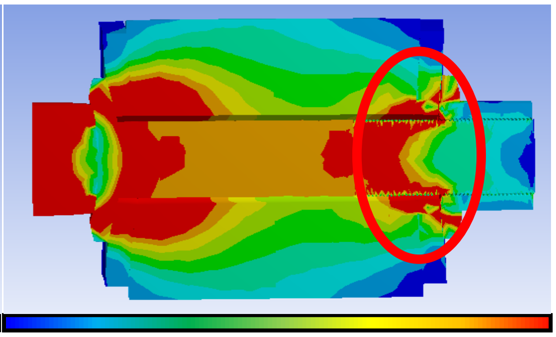

Fig. 14 Result of 1.75mm Pitch

Table 1Information Gained from the Two-dimensional Analysis

Pitch	COF	Element Model	Contact Condition	MAX Stress(Mpa)
0.50mm	0.08691	Equilateral Triangle	Lagrange Multipliers Method	84
1.25mm	0.19398	Equilateral Triangle	Lagrange Multipliers Method	106
1.75mm	0.30420	Equilateral Triangle	Lagrange Multipliers Method	146

3.5 Three-Dimensional Analysis

We created a new technical element model, illustrated in Fig. 15, in order to facilitate a highly accurate three-dimensional analysis. Our objectives with this model were to (1) ascertain the contact surface pressure on the nut seating surface and (2) assess the phenomenon of reduced axial force. To achieve these objectives, highly accurate CAE analysis can be performed by implementing modeling, algorithms, theory, and computer technology without any inadequacies. The model diagram expresses the relationships between the elemental technologies of (1) problem identification, (2) modeling, (3) algorithms, (4) theory, and (5) computer technology.

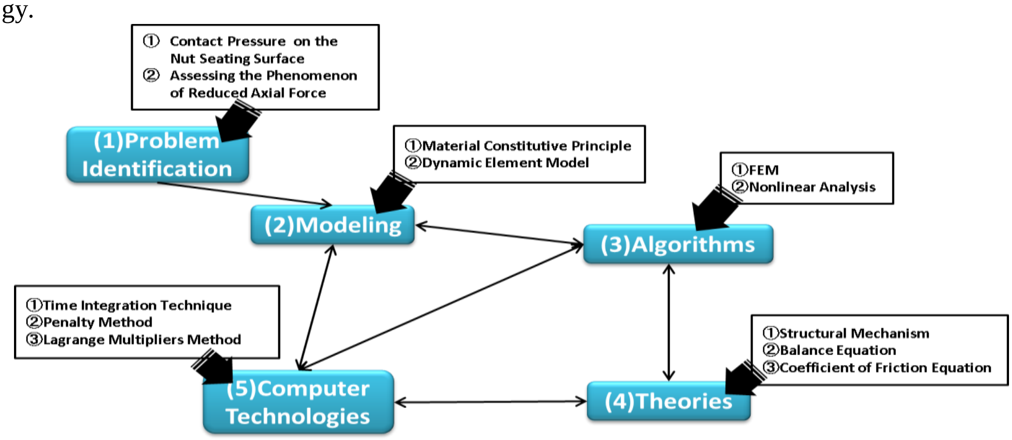

Fig. 15Three-Dimensional Technical Element Model

3.5.1 Problem Identification

We identified the problem as ascertaining the contact pressure on the nut seating surface, as indicated by the example application addressed by this paper, and assessing the phenomenon of reduced axial force.

3.5.2 Modeling

In this section, we model the problem in the form of a mathematical formula. Our dynamic element model used a calculation process that involved applying control to a shape model that reproduced the target objects using CAD [10]. The material constitutive principle is necessary in order to numerically assess the target object's material composition values in order to reproduce the results of actual machine tests.

3.5.3 Algorithms

We used the finite method because it serves as a convenient algorithm. Since it was necessary for us to visualize the contact surface pressure on the nut seating surface in this paper, this approach allowed us to calculate highly accurate results by performing calculations on the level of minute elements. Additionally, we used nonlinear analysis (the Newton-Raphson method) to increase the level of calculation accuracy and set up iterative processing for use when repeatedly calculating, revising, and recalculating solutions [11,12].

3.5.4 Theories

We used the finite element method because it serves as a convenient algorithm. Since it was necessary for us to visualize the contact surface pressure on the nut seating surface in this paper, this approach allowed us to calculate highly accurate results by performing calculations on the level of minute elements. Additionally, we used nonlinear analysis (the Newton-Raphson method) to increase the level of calculation accuracy and set up iterative processing for use when repeatedly calculating, revising, and recalculating solutions.

3.5.5 Computer Technology

Accurate computer technology is the key to a successful CAE analysis. First, we divided the analysis into steps using the time integration method and performed the necessary calculations. Then we used the penalty method to treat the analysis of the contact surface pressure on the nut seating surface of the bolt fasteners, a nonlinear property, as a linear problem. Additionally, we used the Lagrange multiplier method as a substitute for the penalty method at locations at which we wished to perform particularly highly accurate calculations. However, because that approach requires a higher level of calculation speed than the penalty method, it was necessary to consider the give-and-take between quality and delivery timeframe.

3.5.6 Three-Dimensional Analysis Contents

We then performed our analysis using the algorithms of the technical element model for three-dimensional CAE analysis. This process involves choosing various numerical data and analysis methods. For the CAE model, we uniquely determined the material properties in the form of a material constitutive principle model. Additionally, we assigned properties as quantitative values for the constitutive model that defines the material.

In terms of theory, the coefficients of friction serve as important elements. In this case, we assigned the coefficients of friction for the thread and seating surface as quantitative values based on test results. In terms of the calculation technique, we opted to use the penalty method based on consideration of the balance between calculation time and accuracy.

Based on the above considerations, we conducted a finite element analysis using a three-dimensional model taking into account the thread's helical structure and contact.

3.5.7 Result of Three-Dimensional Analysis

Fig.16 and Fig. 17 illustrate the results of an analysis of the contact surface pressure on the nut seating surface immediately after sliding of the seating surface occurred as external force was applied from the bolt part of the bolt fasteners, using the same guidelines as the actual machine test. Both figures show the non-uniformity of stress on the nut seating surface, and it is clear that a high level of stress occurred locally at the beginning of the nut's helical structure. Looking at differences between the two pitches in the area indicated by the red circle, which identifies the beginning of the nut thread's helix, a large amount of stress is distributed across the 0.50 mm pitch nut. In the 1.75 mm pitch nut, the nut has completely loosened and the stress distribution is non-uniform, but there is a high level of stress at the beginning of the thread helix.

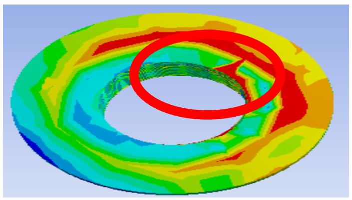

Fig. 16 Result of 0.50mm Pitch

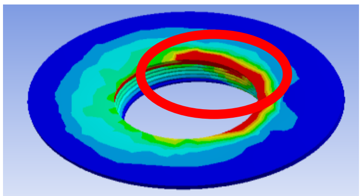

Fig. 17 Result of 1.75mm Pitch

Fig. 18 provides a relationship diagram illustrating the maximum and minimum stress levels observed in the results of the analysis based on the pitch differences (at the nut seating surface). The larger the pitch, the higher the level of stress, and the minimum stress shows a declining trend. Considering the stress amplitude (average of the maximum and minimum stress values), the amplitude increases with the pitch. The results of our analysis showed that the bolt loosens more easily as the stress amplitude increases.

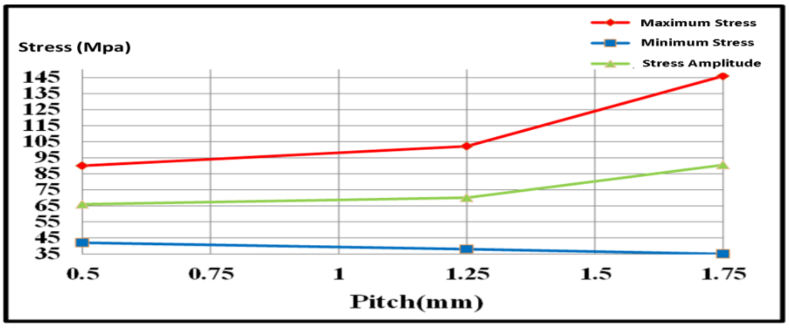

Fig. 18Comparison of Maximum and Minimum Stress on the Nut Seating Surface

3.6 Conclusion of Three-Dimensional Analysis

At this stage, we verified the actual machine tests and CAE analysis results by comparing them from the dual standpoints of time sequence and accuracy. As in the time sequence comparison in Fig. 19 axial force is shown on the vertical axis, and number of vibration cycles on the horizontal axis. Actual machine test results are shown in blue, and CAE values in green. The figure reveals that we achieved an analysis with a good level of accuracy in terms of both the timing at which the bolt loosened and in the extent of the decline in axial force. Furthermore, to verify accuracy, we plotted axial force on the vertical axis versus the start and end points on the horizontal axis in Fig. 20. The broken lines delineate an error of 3% around the test values; since the CAE analysis results fall within those lines, we can conclude that we were able to conduct a highly accurate CAE analysis.

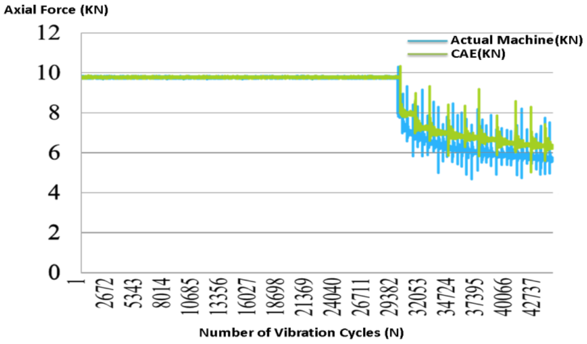

Fig. 19Comparison of Actual Machine and CAE Results (Time Sequence)

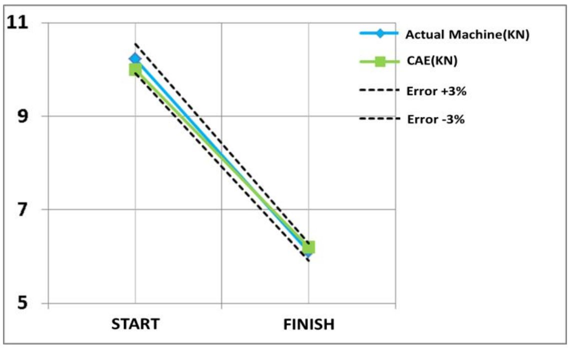

Fig. 20Comparison of Actual Machine and CAE Results (Axial Force)

IV. CONCLUSION

In this paper, we developed a highly reliable CAE analysis approach model to help shorten the development and design stage for various manufactured products. We verified the validity of this model by applying it to an analysis of the nut seating surface in automotive bolts and obtained the expected results by conducting a detailed simulation of stress distribution on the nut seating surface.

REFERENCES

[1] K. Amasaka, Proposal and Effectiveness of a High Quality Assurance CAE Analysis Model: Innovation of Design and Development in Automotive Industry, Current Development in Theory and Applications of Computer Science, *Engineering and Technoogy, 2(1/2)*, 2010, 23-48.

[2] K. Amasaka and M. Yamaji, CAE Analysis Technology for Development Design Utilizing Statistical Sciences, *The Open Industrial and Manufacturing Engineering Journal, 1*, 2008, 1-8.

[3] K. Amasaka and T. Onodera, Developing a Higher-cycled Product Design CAE Model: The Evolution of Automotive Product Design and CAE, *International Journal of Technical Research and Applications, 2(1)*, 2012, 17-28.

[4] K. Hashimoto and K. Amasaka, Researching Technical Prevention Measures for Development and Design Utilizing Highly-Accurate CAE Analysis: Automotive Nut loosening Mechanism, *IOSR Journal of Mechanical and Civil Engineering, 11(4)*, 2013, 24-27.

[5] T. Onodera and K. Amasaka,Automotive Bolts Tightening Analysis using Contact Stress Simulation: Developing An Optimal CAE Design Approach Model, *Journal ofBusiness Research Mechanical, 10(7)*, 2012, 435-442.

[6] T. Onodera T. Kozaki ,and K. Amasaka, Applying a Highly Precise CAE Technology Component Model: Automotive Bolt-Loosening Mechanism, *China-USA Business Review, 12(6)*, 2013, 597-607.

[7] T. Ueno, M. Yamaji, H. Tsubaki, andK. Amasaka, Establishment of Bolt Tightening Simulation System for Automotive Industry Application of the Highly Reliable CAE Model, *International Business & Economics Research Journal, 8(5)*, 2009, 57-67.

[8] H. Yamada and K.Amasaka, Highly-Reliable CAE Analysis Approach-Application in Automotive Bolt Analysis, *China-USA Business Review, 10(3)*, 2011, 199-205.

[9] S. Kasei, W. Yoshida, H. Ishibashi, and M. Okada, Bearing Surface Slip and Self-loosening of Threaded Fasteners, *Proc. JSME Annual Meeting*, Japan, 2003(4), 67-68.

[10] M. Zhang and Y. Jiang, Finite Element Modeling of Self-Loosening of Bolted Joints, Analysis of Bolted Joints, *ASME Journals of Mechanical Design, 478*, 2004, 19-27.

[11] E. Alba, *A New Class of Algorithms*(Parallel Metaheuristics, London: Addison Wihey, 2005).

[12] R. C. Whaley, A. Petitet, and J.J. Dongarra, Automated Empirical Optimization of Software and the ATLAS Project, *Parallel Computing, 27(1-2)*, 2001, 3-7.

American Journal of Engineering Research (AJER)
e-ISSN : 2320-0847 p-ISSN : 2320-0936
Volume-03, Issue-10, pp-188-202
www.ajer.org

Research Paper Open Access

Study the Effective of Shear Wall on Behavior of Beam in Frame Structure

Dr, Hadihosseini[1], Mahdi hosseini[2], Ahmad hosseini[3]
[1,] Aerospace Engineering , working in International Earthquake Research Center of America (IERCA)
[2,] Master of Technology in Structural Engineering, Dept. of Civil Engineering, Jawaharlal Nehru Technological University Hyderabad (JNTUH), Hyderabad, Telengana , India
[3,] Under Graduate Student in Mechanical Engineering, Dept. of Mechanical Engineering,Kakatiya University Warangal, Telengana, India

---

ABSTRACT:*Shear walls are a type of structural system that provides lateral resistance to a building or structure. They resist in-plane loads that are applied along its height. The applied load is generally transferred to the wall by a diaphragm or collector or drag member. The performance of the framed buildings depends on the structural system adopted for the structure The term structural system or structural frame in structural engineering refers to load-resisting sub-system of a structure. The structural system transfers loads through interconnected structural components or members. These structural systems need to be chosen based on its height and loads and need to be carried out, etc. The selection of appropriate structural systems for building must satisfy both strength and stiffness requirements. The structural system must be adequate to resist lateral and gravity loads that cause horizontal shear deformation and overturning deformation. Other important issues that must be considered in planning the structural schemes and layouts are the requirements for architectural details, building services like vertical transportation and fire safety among others. Each of the structural system will be having its own prospects and considerations. The efficiency of a structural system is measured in terms of their ability to resist lateral load, which increases with the height of the frame. A building can be considered as tall when the effect of lateral loads is reflected in the design. Lateral deflections of framed buildings should be limited to prevent damage to both structural and nonstructural elements. In the present study, the structural performance of the framed building with shear wall will be analysis. The importance of the shear wall in resist the wind and earthquake load are study, the effect of the shear walls on the conventional frame system. The improvement in the structural performance of the building with frame system by using shear wall is study.*

Key words:Shear walls, Wind Load, Earthquake Load, frame system

---

I. INTRODUCTION

What Causes Lateral Loads?

Lateral loads result from wind or earthquake actions and both can cause a collapse of improperly braced building. The way that wind or earthquake loads act on a building is completely different, but they have the same general effect. These two sources of lateral load are discussed below.

Wind Load

Wind load is really the result of wind pressures acting on the building surfaces during a wind event. This wind pressure is primarily a function of the wind speed because the pressure or load increases with the square of the wind velocity (i.e., doubling of wind speed results in a four-fold increase in wind load or pressure). Wind load during a hurricane can last hours and a building experiences sustained wind load and short wind impacts (gusts). While the wind pressures are treated as a “static” (do not vary with time) or constant load for purposes of design, the real loads actually fluctuate dramatically with gustiness of wind as well as wind direction. Two fundamental wind effects are of a concern: (1)localized “spikes” in wind pressure that act on small areas of a building to cause damage to items such as roof panels or siding (known as components and cladding wind loads in engineering terms) and (2)averaged wind loads that act on larger areas of the building which the entire structure must resist(known in engineering terms as main wind force resisting system loads).

Earthquake Load

Earthquake forces experienced by a building result from ground motions (accelerations) which are also fluctuating or dynamic in nature, in fact they reverse direction some what chaotically. The magnitude of an earthquake force depends on the magnitude of an earthquake, distance from the earthquake source(epicenter), local ground conditions that may amplify ground shaking (or dampen it), the weight(or mass) of the structure, and the type of structural system and its ability to with stand abusive cyclic loading. In theory and practice, the lateral force that a building experiences from an earthquake increases in direct proportion with the acceleration of ground motion at the building site and the mass of the building (i.e., a doubling in ground motion acceleration or building mass will double the load).This theory rests on the simplicity and validity of Newton's law of physics: F = m x a, where 'F' represents force, 'm' represents mass or weight, and 'a' represents acceleration. For example, as a car accelerates forward, a force is imparted to the driver through the seat to push him forward with the car(this force is equivalent to the weight of the driver multiplied by the acceleration or rate of change in speed of the car). As the brake is applied, the car is decelerated and a force is imparted to the driver by the seat-belt to push him back toward the seat. Similarly, as the ground accelerates back and forth during an earthquake it imparts back-and-forth(cyclic) forces to a building through its foundation which is forced to move with the ground. One can imagine a very light structure such as fabric tent that will be undamaged in almost anyearthquake but it will not survive high wind. The reason is the low mass (weight) of the tent. Therefore, residential buildings generally perform reasonably well in earthquakes but are more vulnerable in high-wind load prone areas. Regardless, the proper amount of bracing is required in both cases.

Why Are Buildings With Shear Walls Preferred In Seismic Zones?

Reinforced concrete (RC) buildings often have vertical plate-like RC walls called Shear Walls in addition to slabs, beams and columns. These walls generally start at foundation level and are continuous throughout the building height. Their thickness can be as low as 150mm, or as high as 400mm in high rise buildings. Shear walls are usually provided along both length and width of buildings. Shear walls are like vertically-oriented wide beams that carry earthquake loads downwards to the foundation.

"We cannot afford to build concrete buildings meant to resist severe earthquakes without shear walls." Mark Fintel, a noted consulting engineer in USA Shear walls in high seismic regions requires special detailing. However, in past earthquakes, even buildings with sufficient amount of walls that were not specially detailed for seismic performance (but had enough well-distributed reinforcement) were saved from collapse. Shear wall buildings are a popular choice in many earthquake prone countries, like Chile, New Zealand and USA. Shear walls are easy to construct, because reinforcement detailing of walls is relatively straight-forward and therefore easily implemented at site. Shear walls are efficient; both in terms of construction cost properly designed and detailed buildings with Shear walls have shown very good performance in past earthquakes. The overwhelming success of buildings with shear walls in resisting strong earthquakes is summarized in the quote: And effectiveness in minimizing earthquake damage in structural and non- Structural elements (like glass windows and building contents).

When a building is subjected to wind or earthquake load, various types of failure must be prevented:

- slipping off the foundation (sliding)
- overturning and uplift (anchorage failure)
- shear distortion (drift or racking deflection)
- collapse (excessive racking deflection)

The first three types of failure are schematically shown in the Figure 1: Clearly, the entire system must be tied together to prevent building collapse or significant deformation.

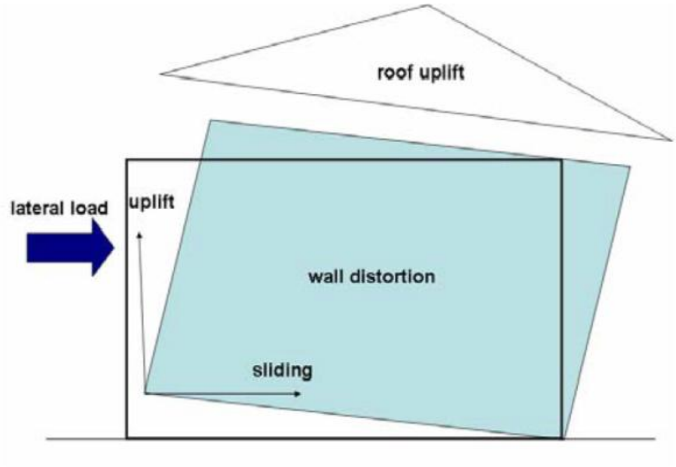

Fig 1: Schematic of the deformations of the structure due to the lateral loads

II. METHODOLOGY

Earthquake motion causes vibration of the structure leading to inertia forces. Thus a structure must be able to safely transmit the horizontal and the vertical inertia forces generated in the super structure through the foundation to the ground. Hence, for most of the ordinary structures, earthquake-resistant design requires ensuring that the structure has adequate lateral load carrying capacity. Seismic codes will guide a designer to safely design the structure for its intended purpose.

Quite a few methods are available for the earthquake analysis of buildings; two of them are presented here:

1- Equivalent Static Lateral Force Method (pseudo static method).
2- Dynamic analysis.
I. Response spectrum method.
II. Time history method.

Equivalent lateral Force (Seismic Coefficient) Method

This method of finding lateral forces is also known as the static method or the equivalent static method or the seismic coefficient method. The static method is the simplest one and it requires less computational effort and is based on formulae given in the code of practice.

In all the methods of analyzing a multi storey buildings recommended in the code, the structure is treated as discrete system having concentrated masses at floor levels which include the weight of columns and walls in any storey should be equally distributed to the floors above and below the storey. In addition, the appropriate amount of imposed load at this floor is also lumped with it. It is also assumed that the structure flexible and will deflect with respect to the position of foundation the lumped mass system reduces to the solution of a system of second order differential equations. These equations are formed by distribution, of mass and stiffness in a structure, together with its damping characteristics of the ground motion.

Dynamic Analysis

Dynamic analysis shall be performed to obtain the design seismic force, and its distribution in different levels along the height of the building, and in the various lateral load resisting element, for the following buildings:

Regular buildings**:** Those greater than 40m in height in zones IV and V, those greater than 90m in height in zone II and III.

Irregular buildings**:** All framed buildings higher than 12m in zones IV and V, and those greater than 40m in height in zones II and III.

The analysis of model for dynamic analysis of buildings with unusual configuration should be such that it adequately models the types of irregularities present in the building configuration. Buildings with plan irregularities, as defined in Table 4 of IS code: 1893-2002 cannot be modeled for dynamic analysis.

Dynamic analysis may be performed either by the TIME HISTORY METHOD or by the RESPONSE SPECTRUM METHOD

Time History Method

The usage of this method shall be on an appropriate ground motion and shall be performed using accepted principles of dynamics. In this method, the mathematical model of the building is subjected to accelerations from earthquake records that represent the expected earthquake at the base of the structure.

Response Spectrum Method

The word spectrum in engineering conveys the idea that the response of buildings having a broad range of periods is summarized in a single graph. This method shall be performed using the design spectrum specified in code or by a site-specific design spectrum for a structure prepared at a project site. The values of damping for building may be taken as 2 and 5 percent of the critical, for the purposes of dynamic of steel and reinforce concrete buildings, respectively. For most buildings, inelastic response can be expected to occur during a major earthquake, implying that an inelastic analysis is more proper for design. However, in spite of the availability of nonlinear inelastic programs, they are not used in typical design practice because:

1- Their proper use requires knowledge of their inner workings and theories. design criteria, and
2- Result produced are difficult to interpret and apply to traditional design criteria , and
3- The necessary computations are expensive.

Therefore, analysis in practice typically use linear elastic procedures based on the response spectrum method. The response spectrum analysis is the preferred method because it is easier to use.

III. NUMERICAL ANALYSES

STRUCTURE

G+19 earthquake resistant structure with shear walls

Problems In The Building Due To Earthquake

Main problems that would be arising due to earthquake in the structure are story drift and deflection of the building due to its large height and also torsion and others, so if the structure is proved to be safe in all the above mentioned problems than the structure would be safe in all cases in respect earthquake.

Geometrical Properties

1.No.of stories of the Building model=20
2.Column size=500 mm x 500 mm
3.Beam size= 700 mm x 500 mm
4.Slab thickness=200mm

Loads

1.Live Load=3KN/m2
2.Wall Load=12.4KN/m
3.Floor Finishing =1KN/m2
4. Wind load
Wind coefficients
(i) Wind Speed=50m/s
(ii)Terrain Category =2
(iii) Structure Class=B
(iv) Risk Coefficient(k1)=1
(v)Topography(k3)=1
Seismic loading
(i) Seismic zone factor(Z)=0.36
(ii) Soil Type= Medium(II)
(iii) Response Reduction factor(R) =5%
(iv) Story Range=Base to 20
(v) Important factor(I)=1

Material Properties

Table I The materials used in structure and their general properties are

Material	Unit weight	Elastic Modulus	Shear Modulus	Poisson Ratio	Thermal expansion coefficient
Text	KN/m3	KN/m2	KN/m2	Unit less	1/C
Concrete	23.563	24855578.28	10356490.95	0.2	0.0000099
Rebar steel	76.973	199947978.8	76903068.77	0.3	0.0000117
Bar steel	76.9730	199947978.8	769030068.77	0.3	0.0000117

Load Combinations

Load combination is the foremost important criteria for designing any structure and more important is the distribution of those loads on to various components of the structure like beams, columns, slabs and in our case shears walls and concrete core wall too. There are many kinds of loads existing depending on the location of the where the structure is to be constructed for example in a place where wind is frequent there we have to consider the wind loads and places where rains are heavy rain loads are included and same way all the other loads such as snow loads, earthquake load and etc. are included however DEAD LOADS, LIVE LOADS AND IMPOSEDLOADS are always included. Dead loads are all common depending onthe structural components and specific gravity of the structure, to get the self weight of the structural component volume or area of the component is multiplied by the specific gravity of the component. Live loads depend on the purpose we are constructing the building. Imposed loads depend on the seismic loads, dead loads and according to are 1893 part 1 percentage of those values is finally considered.

The following Load Combinations have been considered for the design

1. 1.5(DL+ LL)
2. 1.5(DL ± EQXTP)
3. 1.5(DL ± EQYTP)
4. 1.5(DL ± EQXTN)
5. 1.5(DL ± EQYTN)
6. 1.2(DL + LL ± EQXTP)
7. 1.2(DL + LL ± EQYTP)
8. 1.2(DL + LL ± EQXTN)
9. 1.2(DL + LL ± EQYTN)
10. 1.5(DL ± WLX)
11. 1.5(DL ± WLY)
12. 1.2(DL + LL ± WLX)
13. 1.2(DL + LL ± WLY)

DL – Dead Load

LL – Live Load

EQTP–Earthquake load

With torsion positive

EQTN–Earthquake load

With torsion negative

WL- Wind load

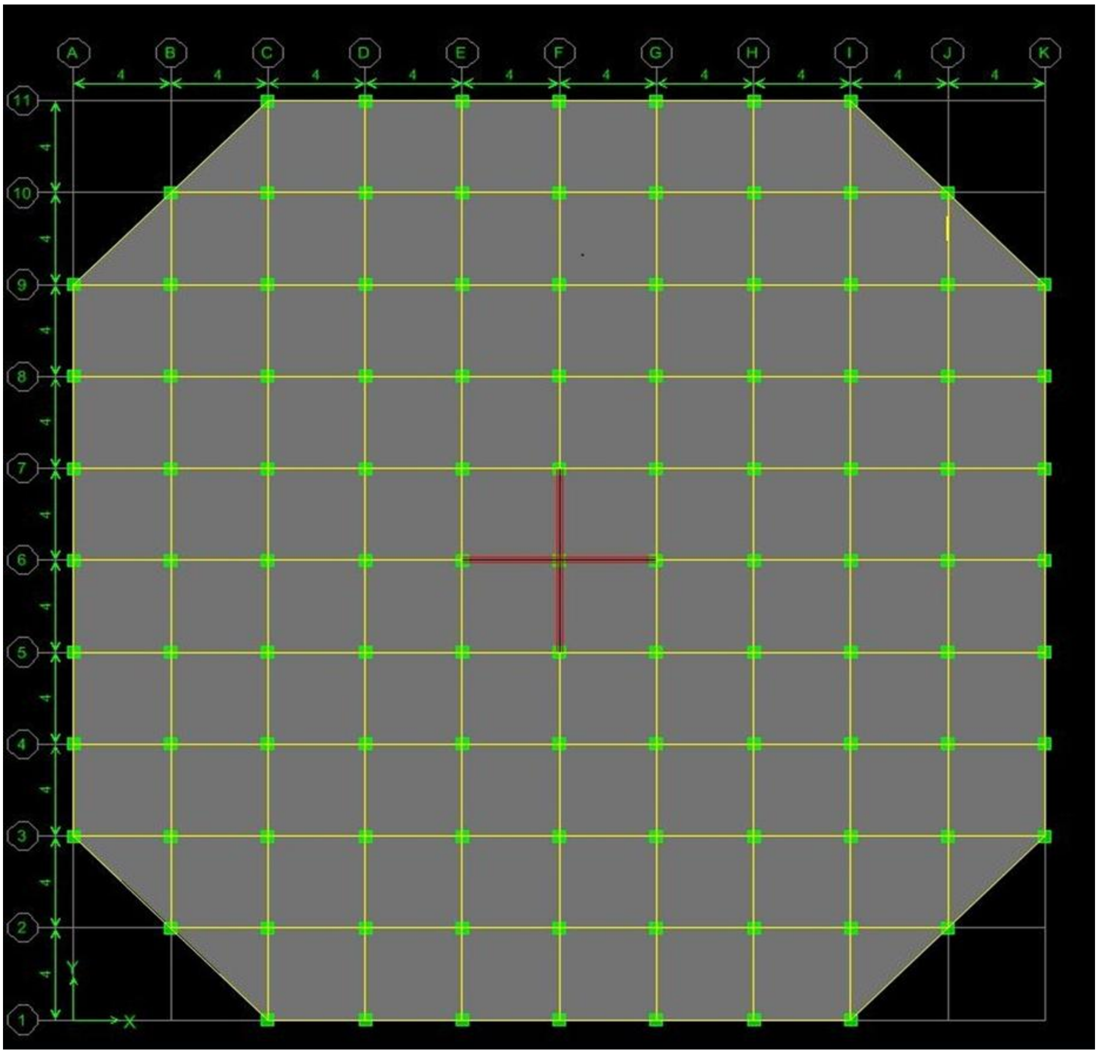

Figure2: Basic Plan of The Building

Table II: Shear Force, Torsion and Moment for Beam B1

Story	Beam	Load	Loc	AXIAL FORCE	SHEAR FORCE	TORSION	MOMENT
STORY1	B1	1.2DLLLWLX	2.25	0	-1.53	-0.372	24.927
STORY2	B1	1.2DLLLWLX	2.25	0	4.28	-0.893	23.077
STORY3	B1	1.2DLLLWLX	2.25	0	8.83	-1.261	22.389
STORY4	B1	1.2DLLLWLX	2.25	0	13.15	-1.617	21.487
STORY5	B1	1.2DLLLWLX	2.25	0	17.1	-1.932	20.602
STORY6	B1	1.2DLLLWLX	2.25	0	20.69	-2.214	19.736
STORY7	B1	1.2DLLLWLX	2.25	0	23.92	-2.463	18.908
STORY8	B1	1.2DLLLWLX	2.25	0	26.84	-2.683	18.126
STORY9	B1	1.2DLLLWLX	2.25	0	29.47	-2.878	17.39
STORY10	B1	1.2DLLLWLX	2.25	0	31.84	-3.049	16.702
STORY11	B1	1.2DLLLWLX	2.25	0	33.99	-3.2	16.058
STORY12	B1	1.2DLLLWLX	2.25	0	35.93	-3.334	15.457
STORY13	B1	1.2DLLLWLX	2.25	0	37.71	-3.452	14.897
STORY14	B1	1.2DLLLWLX	2.25	0	39.33	-3.556	14.374
STORY15	B1	1.2DLLLWLX	2.25	0	40.82	-3.65	13.886
STORY16	B1	1.2DLLLWLX	2.25	0	42.2	-3.732	13.438
STORY17	B1	1.2DLLLWLX	2.25	0	43.49	-3.811	12.995
STORY18	B1	1.2DLLLWLX	2.25	0	44.42	-3.849	12.841
STORY19	B1	1.2DLLLWLX	2.25	0	47.46	-3.996	10.936
STORY20	B1	1.2DLLLWLX	2.25	0	29.08	-4.471	22.397

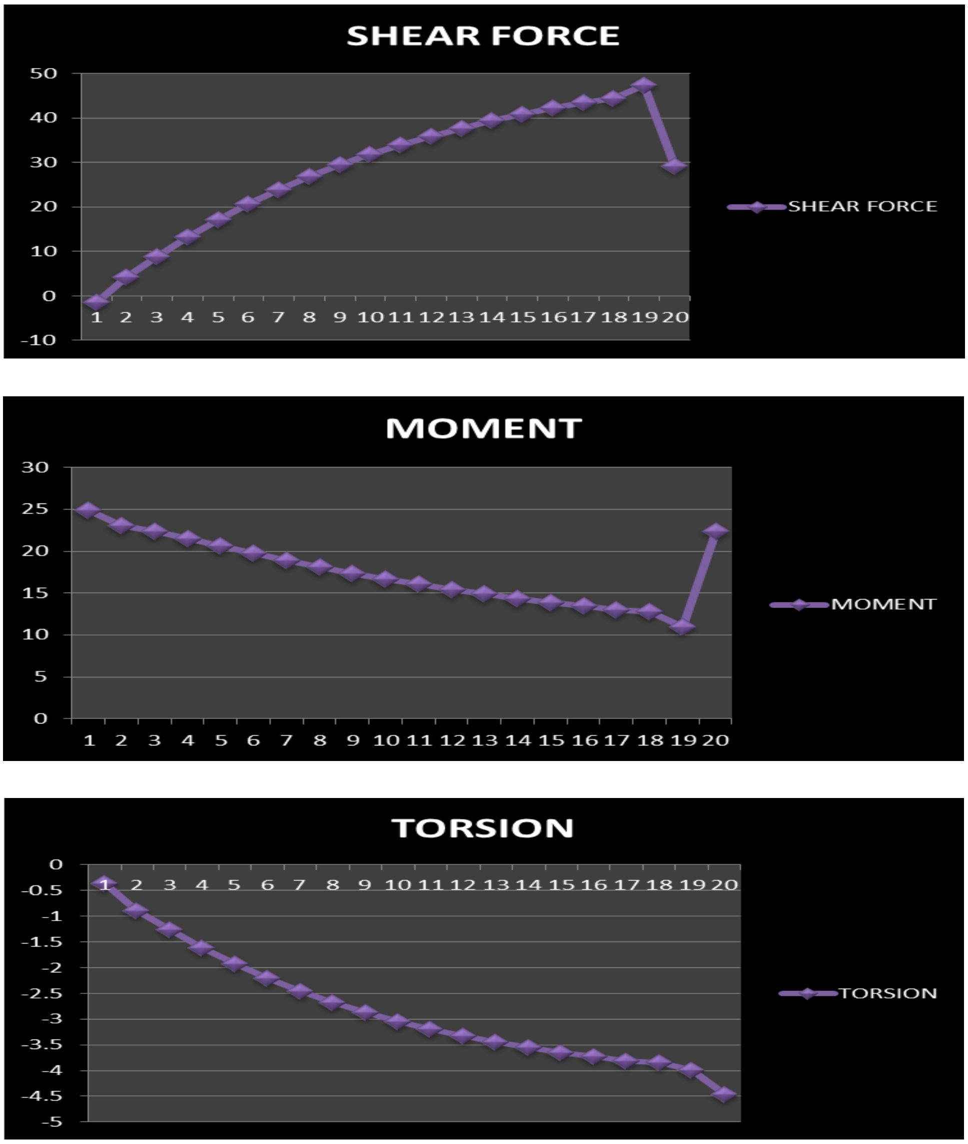

Figure 3: Shear Force, Torsion and Moment for Beam B1

Table III :Shear Force, Torsion and Moment for Beam B10

Story	Beam	Load	Loc	AXIAL FORCE	SHEAR FORCE	TORSION	MOMENT
STORY1	B10	12DLLLWLX	2.25	0	6.26	-0.014	15.691
STORY2	B10	12DLLLWLX	2.25	0	6.32	-0.023	15.645
STORY3	B10	12DLLLWLX	2.25	0	6.36	-0.035	15.601
STORY4	B10	12DLLLWLX	2.25	0	6.4	-0.046	15.559
STORY5	B10	12DLLLWLX	2.25	0	6.44	-0.057	15.517
STORY6	B10	12DLLLWLX	2.25	0	6.47	-0.068	15.476
STORY7	B10	12DLLLWLX	2.25	0	6.5	-0.078	15.437
STORY8	B10	12DLLLWLX	2.25	0	6.53	-0.088	15.4
STORY9	B10	12DLLLWLX	2.25	0	6.56	-0.098	15.364
STORY10	B10	12DLLLWLX	2.25	0	6.59	-0.107	15.331
STORY11	B10	12DLLLWLX	2.25	0	6.61	-0.115	15.299
STORY12	B10	12DLLLWLX	2.25	0	6.63	-0.123	15.271
STORY13	B10	12DLLLWLX	2.25	0	6.65	-0.131	15.245
STORY14	B10	12DLLLWLX	2.25	0	6.66	-0.137	15.223
STORY15	B10	12DLLLWLX	2.25	0	6.68	-0.143	15.204
STORY16	B10	12DLLLWLX	2.25	0	6.69	-0.148	15.188
STORY17	B10	12DLLLWLX	2.25	0	6.7	-0.152	15.176
STORY18	B10	12DLLLWLX	2.25	0	6.7	-0.154	15.167
STORY19	B10	12DLLLWLX	2.25	0	6.73	-0.157	15.169
STORY20	B10	12DLLLWLX	2.25	0	6.48	-0.202	15.075

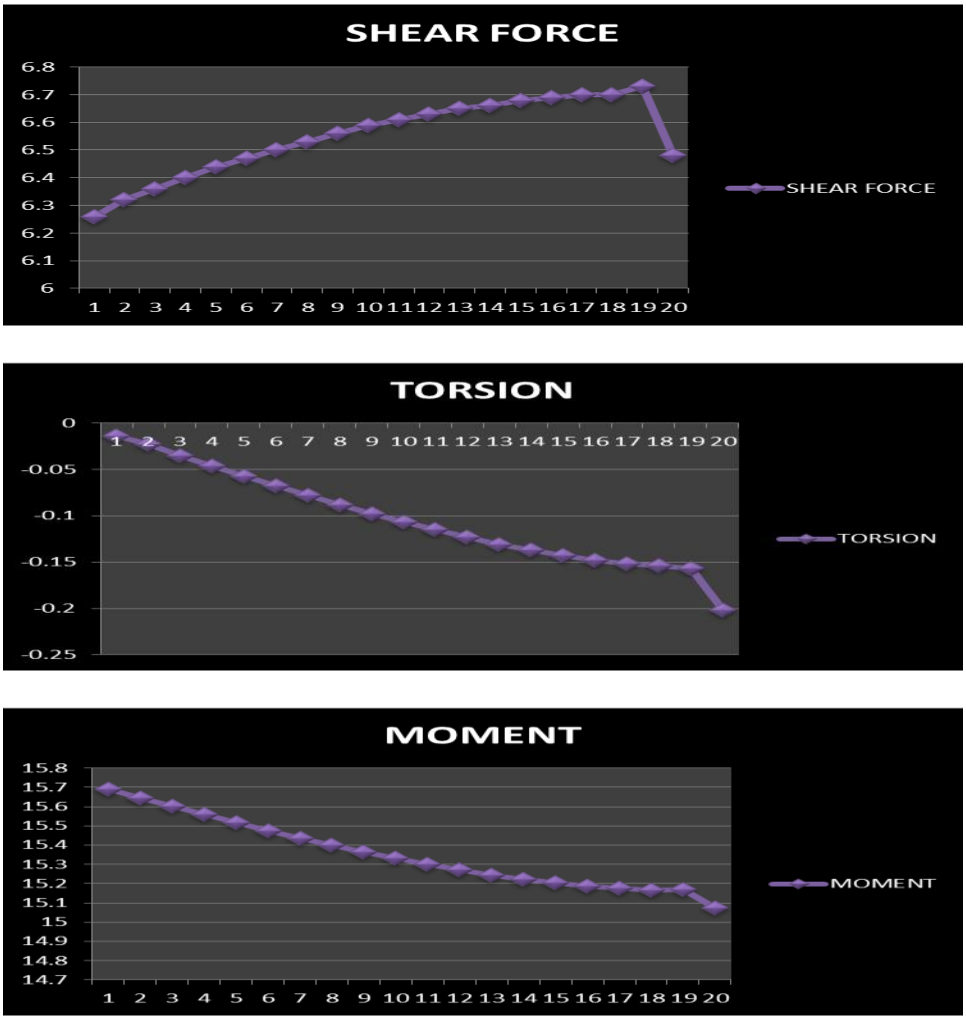

Figure 4:Shear Force, Torsion and Moment for Beam B10

Table IV: Shear Force, Torsion and Moment for Beam B20

Story	Beam	Load	Loc	AXIAL FORCE	SHEAR FORCE	TORSION	MOMENT
STORY1	B20	1.2DLLLWLX	2.25	0	5.47	2.791	14.587
STORY2	B20	1.2DLLLWLX	2.25	0	5.88	2.613	14.206
STORY3	B20	1.2DLLLWLX	2.25	0	6.26	2.709	13.834
STORY4	B20	1.2DLLLWLX	2.25	0	6.65	2.75	13.526
STORY5	B20	1.2DLLLWLX	2.25	0	7.03	2.777	13.272
STORY6	B20	1.2DLLLWLX	2.25	0	7.39	2.79	13.062
STORY7	B20	1.2DLLLWLX	2.25	0	7.72	2.795	12.889
STORY8	B20	1.2DLLLWLX	2.25	0	8.02	2.791	12.749
STORY9	B20	1.2DLLLWLX	2.25	0	8.29	2.783	12.638
STORY10	B20	1.2DLLLWLX	2.25	0	8.54	2.77	12.55
STORY11	B20	1.2DLLLWLX	2.25	0	8.76	2.755	12.482
STORY12	B20	1.2DLLLWLX	2.25	0	8.95	2.737	12.432
STORY13	B20	1.2DLLLWLX	2.25	0	9.12	2.717	12.398
STORY14	B20	1.2DLLLWLX	2.25	0	9.26	2.697	12.375
STORY15	B20	1.2DLLLWLX	2.25	0	9.39	2.676	12.363
STORY16	B20	1.2DLLLWLX	2.25	0	9.49	2.655	12.36
STORY17	B20	1.2DLLLWLX	2.25	0	9.57	2.641	12.359
STORY18	B20	1.2DLLLWLX	2.25	0	9.64	2.602	12.383
STORY19	B20	1.2DLLLWLX	2.25	0	9.73	2.663	12.333
STORY20	B20	1.2DLLLWLX	2.25	0	8.04	2.925	12.372

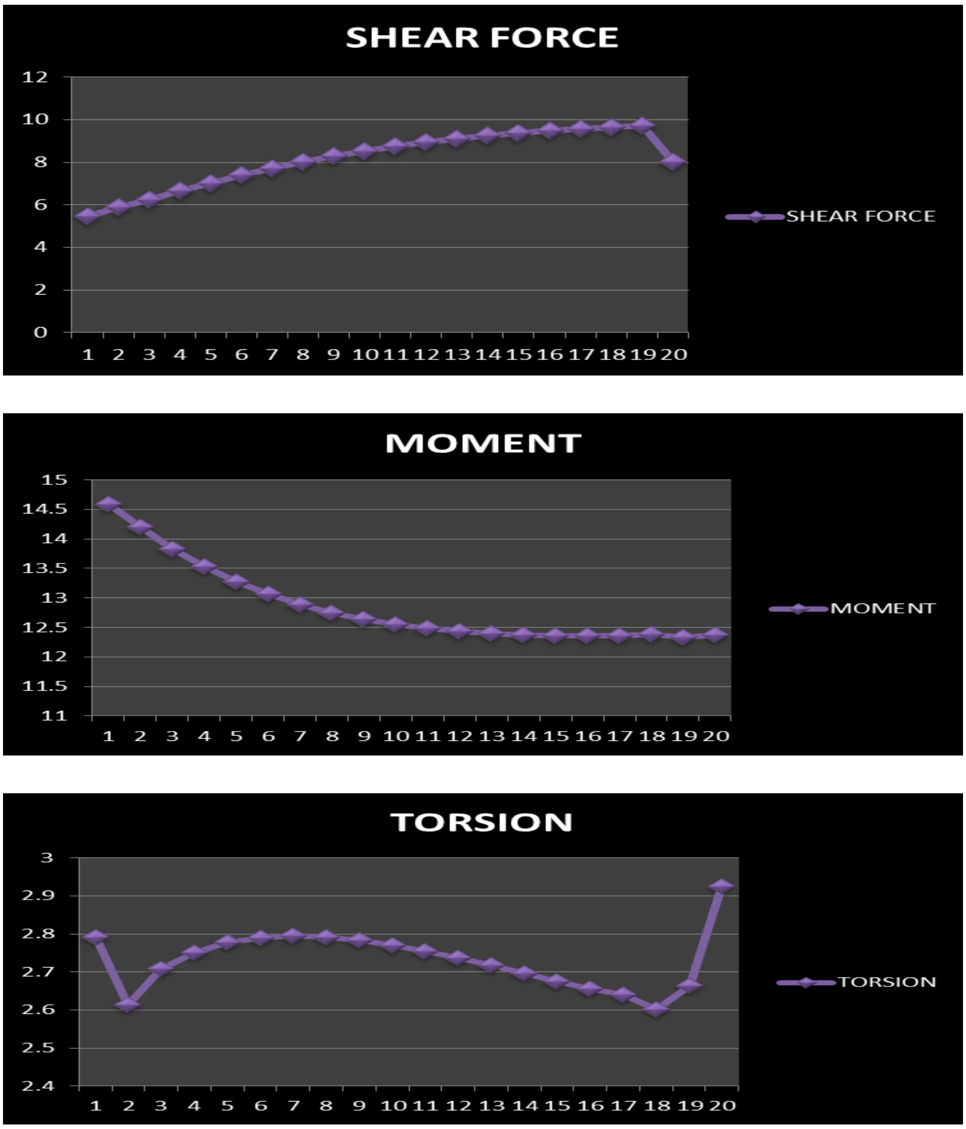

Figure 5:Shear Force, Torsion and Moment for Beam B20

Table V: Shear Force, Torsion and Moment for Beam B1

Story	Beam	Load	Loc	AXIAL FORCE	SHEAR FORCE	TORSION	MOMENT
STORY1	B1	1.2DLLLEQY	2.25	0	-1.53	-0.372	24.927
STORY2	B1	1.2DLLLEQY	2.25	0	4.28	-0.893	23.077
STORY3	B1	1.2DLLLEQY	2.25	0	8.83	-1.261	22.389
STORY4	B1	1.2DLLLEQY	2.25	0	13.15	-1.617	21.487
STORY5	B1	1.2DLLLEQY	2.25	0	17.1	-1.932	20.602
STORY6	B1	1.2DLLLEQY	2.25	0	20.69	-2.214	19.736
STORY7	B1	1.2DLLLEQY	2.25	0	23.92	-2.463	18.908
STORY8	B1	1.2DLLLEQY	2.25	0	26.84	-2.683	18.126
STORY9	B1	1.2DLLLEQY	2.25	0	29.47	-2.878	17.39
STORY10	B1	1.2DLLLEQY	2.25	0	31.84	-3.049	16.702
STORY11	B1	1.2DLLLEQY	2.25	0	33.99	-3.2	16.058
STORY12	B1	1.2DLLLEQY	2.25	0	35.93	-3.334	15.457
STORY13	B1	1.2DLLLEQY	2.25	0	37.71	-3.452	14.897
STORY14	B1	1.2DLLLEQY	2.25	0	39.33	-3.556	14.374
STORY15	B1	1.2DLLLEQY	2.25	0	40.82	-3.65	13.886
STORY16	B1	1.2DLLLEQY	2.25	0	42.2	-3.732	13.438
STORY17	B1	1.2DLLLEQY	2.25	0	43.49	-3.811	12.995
STORY18	B1	1.2DLLLEQY	2.25	0	44.42	-3.849	12.841
STORY19	B1	1.2DLLLEQY	2.25	0	47.46	-3.996	10.936
STORY20	B1	1.2DLLLEQY	2.25	0	29.08	-4.471	22.397

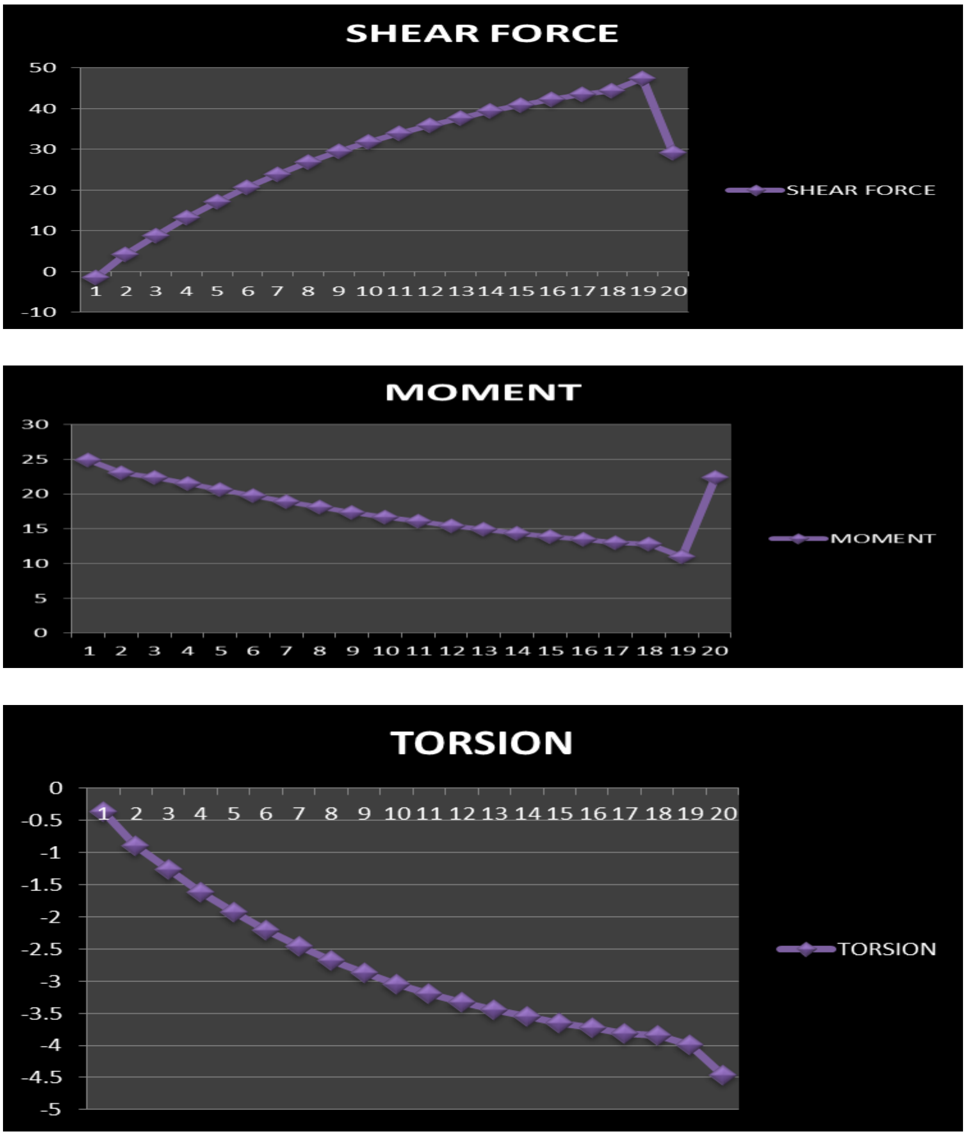

Figure 6:Shear Force, Torsion and Moment for Beam B1

Table VI: Shear Force, Torsion and Moment for Beam B10

Story	Beam	Load	Loc	AXIAL FORCE	SHEAR FORCE	TORSION	MOMENT
STORY1	B10	1.2DLLLEQY	2.25	0	6.26	-0.014	15.691
STORY2	B10	1.2DLLLEQY	2.25	0	6.32	-0.023	15.645
STORY3	B10	1.2DLLLEQY	2.25	0	6.36	-0.035	15.601
STORY4	B10	1.2DLLLEQY	2.25	0	6.4	-0.046	15.559
STORY5	B10	1.2DLLLEQY	2.25	0	6.44	-0.057	15.517
STORY6	B10	1.2DLLLEQY	2.25	0	6.47	-0.068	15.476
STORY7	B10	1.2DLLLEQY	2.25	0	6.5	-0.078	15.437
STORY8	B10	1.2DLLLEQY	2.25	0	6.53	-0.088	15.4
STORY9	B10	1.2DLLLEQY	2.25	0	6.56	-0.098	15.364
STORY10	B10	1.2DLLLEQY	2.25	0	6.59	-0.107	15.331
STORY11	B10	1.2DLLLEQY	2.25	0	6.61	-0.115	15.299
STORY12	B10	1.2DLLLEQY	2.25	0	6.63	-0.123	15.271
STORY13	B10	1.2DLLLEQY	2.25	0	6.65	-0.131	15.245
STORY14	B10	1.2DLLLEQY	2.25	0	6.66	-0.137	15.223
STORY15	B10	1.2DLLLEQY	2.25	0	6.68	-0.143	15.204
STORY16	B10	1.2DLLLEQY	2.25	0	6.69	-0.148	15.188
STORY17	B10	1.2DLLLEQY	2.25	0	6.7	-0.152	15.176
STORY18	B10	1.2DLLLEQY	2.25	0	6.7	-0.154	15.167
STORY19	B10	1.2DLLLEQY	2.25	0	6.73	-0.157	15.169
STORY20	B10	1.2DLLLEQY	2.25	0	6.48	-0.202	15.075

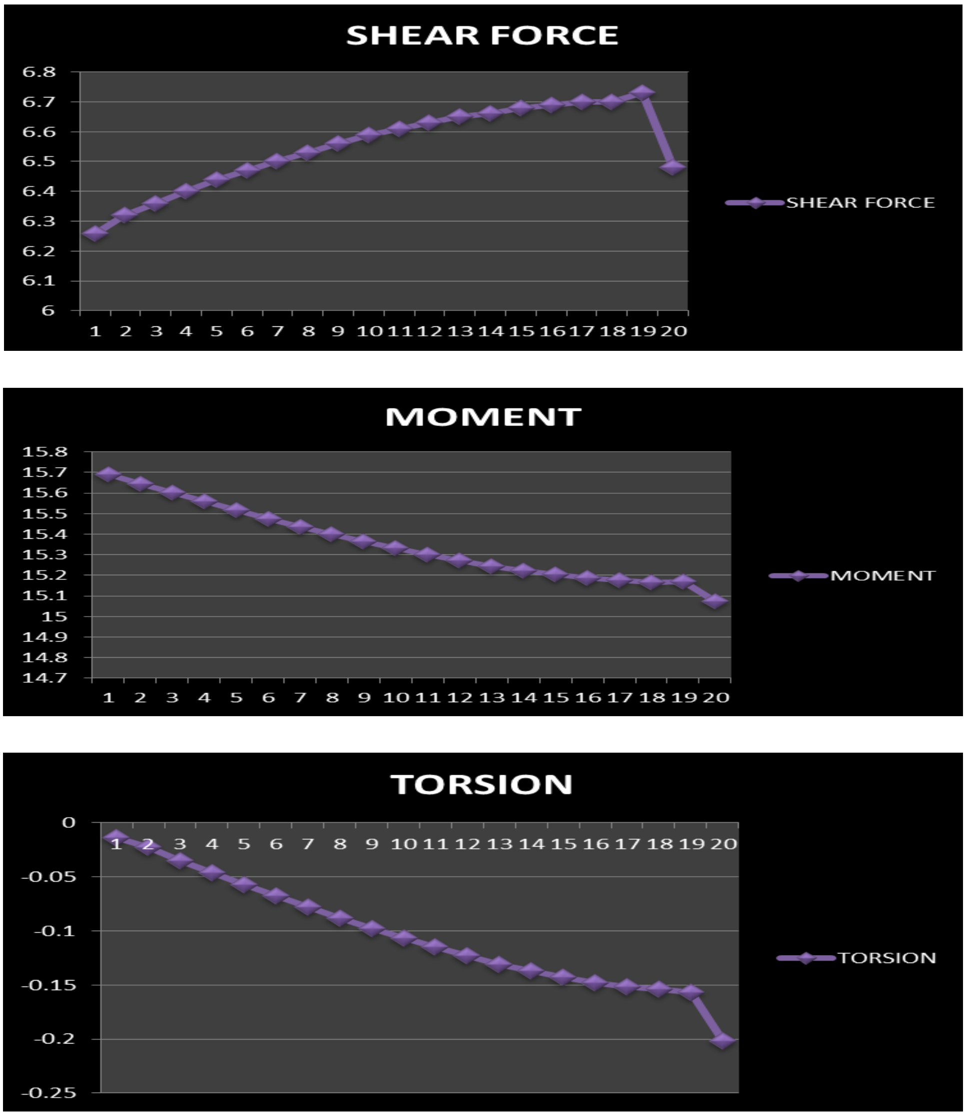

Figure 7: Shear Force, Torsion and Moment for Beam B10

Table VII: Shear Force, Torsion and Moment for Beam B20

Story	Beam	Load	Loc	AXIAL FORCE	SHEAR FORCE	TORSION	MOMENT
STORY1	B20	1.2DLLLEQY	2.25	0	5.47	2.791	14.587
STORY2	B20	1.2DLLLEQY	2.25	0	5.88	2.613	14.206
STORY3	B20	1.2DLLLEQY	2.25	0	6.26	2.709	13.834
STORY4	B20	1.2DLLLEQY	2.25	0	6.65	2.75	13.526
STORY5	B20	1.2DLLLEQY	2.25	0	7.03	2.777	13.272
STORY6	B20	1.2DLLLEQY	2.25	0	7.39	2.79	13.062
STORY7	B20	1.2DLLLEQY	2.25	0	7.72	2.795	12.889
STORY8	B20	1.2DLLLEQY	2.25	0	8.02	2.791	12.749
STORY9	B20	1.2DLLLEQY	2.25	0	8.29	2.783	12.638
STORY10	B20	1.2DLLLEQY	2.25	0	8.54	2.77	12.55
STORY11	B20	1.2DLLLEQY	2.25	0	8.76	2.755	12.482
STORY12	B20	1.2DLLLEQY	2.25	0	8.95	2.737	12.432
STORY13	B20	1.2DLLLEQY	2.25	0	9.12	2.717	12.398
STORY14	B20	1.2DLLLEQY	2.25	0	9.26	2.697	12.375
STORY15	B20	1.2DLLLEQY	2.25	0	9.39	2.676	12.363
STORY16	B20	1.2DLLLEQY	2.25	0	9.49	2.655	12.36
STORY17	B20	1.2DLLLEQY	2.25	0	9.57	2.641	12.359
STORY18	B20	1.2DLLLEQY	2.25	0	9.64	2.602	12.383
STORY19	B20	1.2DLLLEQY	2.25	0	9.73	2.663	12.333
STORY20	B20	1.2DLLEQY	2.25	0	8.04	2.925	12.372

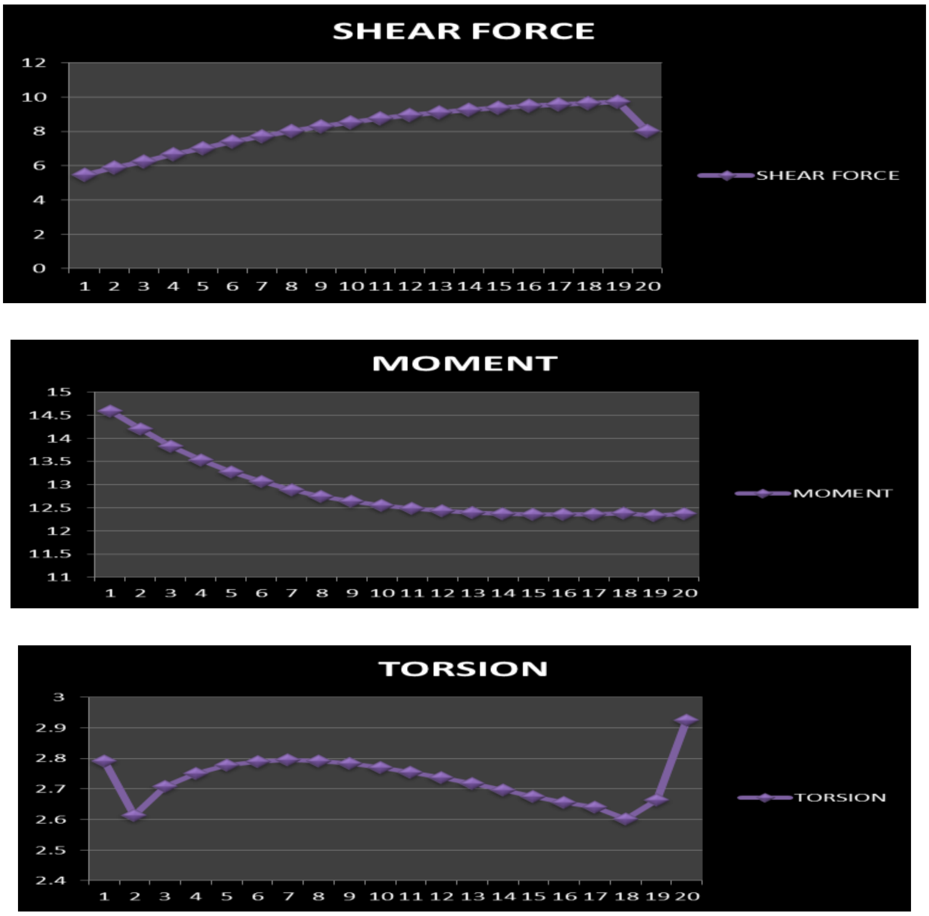

Figure 8:Shear Force, Torsion and Moment for Beam B20

Table VIII: Story Drift in X and Y Direction

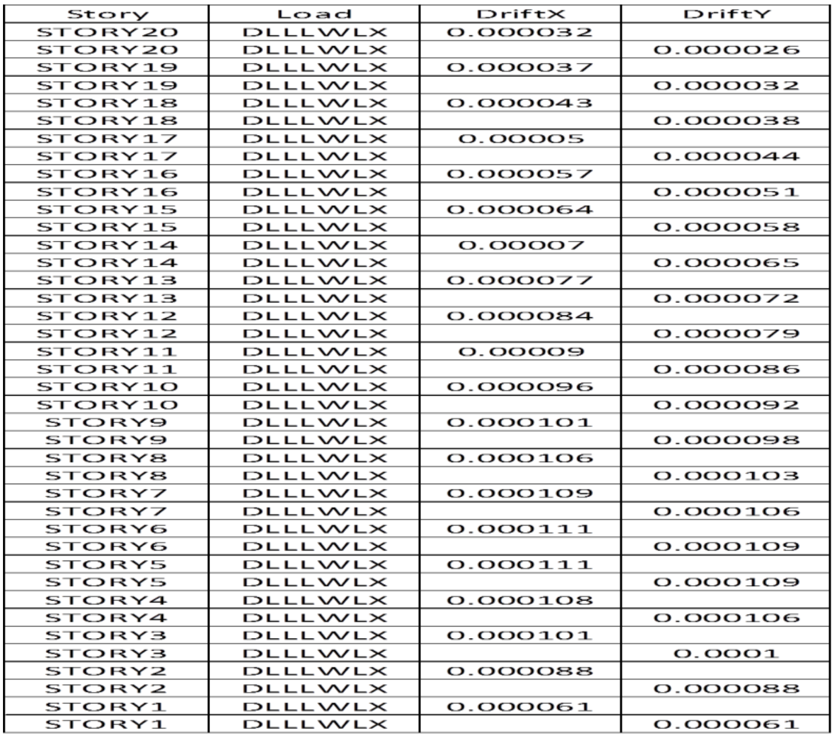

Story	Load	DriftX	DriftY
STORY20	DLLLWLX	0.000032	
STORY20	DLLLWLX		0.000026
STORY19	DLLLWLX	0.000037	
STORY19	DLLLWLX		0.000032
STORY18	DLLLWLX	0.000043	
STORY18	DLLLWLX		0.000038
STORY17	DLLLWLX	0.00005	
STORY17	DLLLWLX		0.000044
STORY16	DLLLWLX	0.000057	
STORY16	DLLLWLX		0.000051
STORY15	DLLLWLX	0.000064	
STORY15	DLLLWLX		0.000058
STORY14	DLLLWLX	0.00007	
STORY14	DLLLWLX		0.000065
STORY13	DLLLWLX	0.000077	
STORY13	DLLLWLX		0.000072
STORY12	DLLLWLX	0.000084	
STORY12	DLLLWLX		0.000079
STORY11	DLLLWLX	0.00009	
STORY11	DLLLWLX		0.000086
STORY10	DLLLWLX	0.000096	
STORY10	DLLLWLX		0.000092
STORY9	DLLLWLX	0.000101	
STORY9	DLLLWLX		0.000098
STORY8	DLLLWLX	0.000106	
STORY8	DLLLWLX		0.000103
STORY7	DLLLWLX	0.000109	
STORY7	DLLLWLX		0.000106
STORY6	DLLLWLX	0.000111	
STORY6	DLLLWLX		0.000109
STORY5	DLLLWLX	0.000111	
STORY5	DLLLWLX		0.000109
STORY4	DLLLWLX	0.000108	
STORY4	DLLLWLX		0.000106
STORY3	DLLLWLX	0.000101	
STORY3	DLLLWLX		0.0001
STORY2	DLLLWLX	0.000088	
STORY2	DLLLWLX		0.000088
STORY1	DLLLWLX	0.000061	
STORY1	DLLLWLX		0.000061

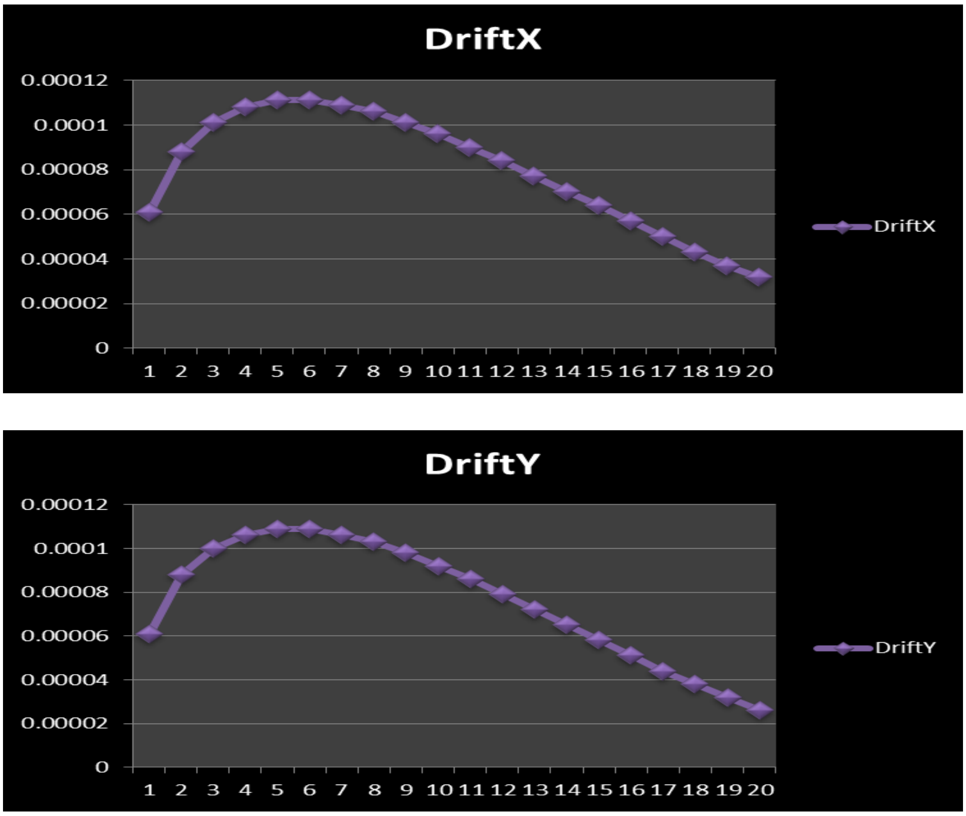

Figure 9:Story Drift in X and Y Direction

IV. DISCUSSION ON RESULTS

The structural prototype is prepared and lots of data is been collected from the prototype. All the aspects such as safety of structure in shear, moment and in story drift have been collected. So now to check whether to know whether the structure is safe with established shear walls and all construction of core wall in the center we need to compare the graphical values of structure with the shear wall and a simple rigid frame structure.

Story Drift

The tallness of a structure is relative and cannot be defined in absolute terms either in relation to height or the number of stories. The council of Tall Buildings and Urban Habitat considers building having 9 or more stories as high-rise structures. But, from a structural engineer's point of view the tall structure or multi-storied building can be defined as one that, by virtue of its height, is affected by lateral forces due to wind or earthquake or both to an extent. Lateral loads can develop high stresses, produce sway movement or cause vibration. Therefore, it is very important for the structure to have sufficient strength against vertical loads together with adequate stiffness to resist lateral forces. So lateral forces due to wind or seismic loading must be considered for tall building design along with gravity forces vertical loads. Tall and slender buildings are strongly wind sensitive and wind forces are applied to the exposed surfaces of the building, whereas seismic forces are inertial (body forces), which result from the distortion of the ground and the inertial resistance of the building. These forces cause horizontal deflection is the predicted movement of a structure under lateral loads and story drift is defined as the difference in lateral deflection between two adjacent stories. Lateral deflection and drift have three effects on a structure; the movement can affect the structural elements (such as beams and columns); the movements can affect non-structural elements (such as the windows and cladding); and the movements can affect adjacent structures. Without proper consideration during the design process, large deflections and drifts can have adverse effects on structural elements, nonstructural elements, and adjacent structures. When the initial sizes of the frame members have been selected, an approximate check on the horizontal drift of the structures can be made. The drift in the non-slender rigid frame is mainly caused by racking. This racking may be considered as comprising two components: the first is due to rotation of the joints, as allowed by the double bending of the girders, while the second is caused by double bending of the columns. If the rigid frame is slender, a contribution to drift caused by the overall bending of the frame, resulting from axial deformations of the columns, may be significant. If the frame has height width ratio less than 4:1, the contribution of overall bending to the total drift at the top of the structure is usually less than 10% of that due to racking. [2]. The following method of calculation for drift allows the separate determination of the components attributable to beam bending, and overall cantilever action. Drift problem as the horizontal displacement of all tall buildings is one of the most serious issues in tall buildingdesign, relating to the dynamic characteristics of the building during earthquakes and strong winds. Drift shall be caused by the accumulated deformations of each member, such as a beam, column and shear wall. In this study analysis is done with changing structural parameters to observe the effect on the drift (lateral deflection) of the tall building due to both wind and earthquake loading. There are three major types of structures were identified in this study, such as rigid frame, coupled shear wall and wall frame structures.

Is 1893 Part 1 CodalProvoisionsForStoreyDriftLimitations

The storey drift in any storey due to the minimum specified design lateral force, with partial load factor of 1.0, shall not exceed 0.004 times the storey height For the purposes of displacement requirements only, it is permissible to use seismic force obtained from the computed fundamental period (T) of the building without the lower bound limit on design seismic force specified in dynamic analysis.

V. CONCLUSION

- It is evident from the observing result that the shear wall are making value of torsion very low.

- The story drift for the combination load DL+LL+WLx in X&Y direction shown same performance for the building, and less value for story drift in all combinations at story 20.The value of story drift is very low because of adding shear walls to the building.
- It is evidentfrom the observing result that for combination loads 1.2 DLLLWLX&1.2DLLLEQY ,maximum value of moment at story one and minimum value of shear force also at story one . The Moment is maximum when the shear force is minimum or changes sign.
- Based on the analysis and discussion ,shear wall are very much suitable for resisting earthquake induced lateral forces in multistoried structural systems when compared to multistoried structural systems whit out shear walls. They can be made to behave in a ductile manner by adopting proper detailing techniques.
- The vertical reinforcement that is uniformly distributed in the shear wall shall not be less than the horizontal reinforcement .This provision is particularly for squat walls (i.e. Height-to-width ratio is about 1.0).However ,for walls whit height-to-width ratio less than 1.0, a major part of the shear force is resisted by the vertical reinforcement. Hence ,adequate vertical reinforcement should be provided for such walls.

VI. VI.REFRENCES

[1] *IS-456-2000-Code of Practice for Plane and Reinforced Concrete .*

[2] *IS 1893(Part 1)-2002:Eriteria for Earthquake Resistant Design of Structure .*

[3] *IS:875(Part1)-1987- Code of Practice for Design Load(other than earthquake) for Buildings andStructure –Dead loads*

[4] *IS:875(Part2)-1987- Code of Practice for Design Load(other than earthquake) for Buildings andStructure –Imposed Load*

[5] *IS:875(Part2)-1987- Code of Practice for Design Load(other than earthquake) for Buildings andStructure –Wind Load*

[6] *Mark fintel-Hand Book of Concrete Engineering. Second Edition .CBS Publishers &Distributors-New Delhi,2004*

[7] *Anil k.Chopra-Dynamics of Structure :Theory and Application to Earthquake Engineering, SecondEdition ,Pearson Education (Singapore) Pvt.Ltd 2005*

[8] *Mariopaz-Structure Dynamics : Theory and Computations,(Second Edition) , .CBS Publishers&Distributors-New Delhi,2004*

[9] *Indian Society of Earthquake Technology –Proceedings of the Sixth World Conference EarthquakeEngineering,Vol.1,Published by Sarita Prakashan,Merut,1977.*

[10] *A.r.chandrasekharan and D.s.prakashrao –a Seismic Design of Multi –Storied RCC Buildings (published in the proceeding ot the 12th symposium on earthquake engineering held iit-roorkee in dec 2002)*

[11] *Medhekar,m.s,andJain,s,k, Seismic Behavior ,Design and Detailing of RC Shear Wall,part 1:behavior and strength –an icj compilation .*

[12] *Kaustubhdasgupta ,C.v.r.murty and Shaileshk.agrawal,Seismic Shear Design of RC Structural Walls897-971.*

[13] *Crandell, J., and S. Herrenbruck. 2006.Residential wall bracing principles and design options. Journal of Building Safety. August2006*

[14] *Mahdi hosseini , Ahmed najim Abdullah alaskari, Prof.N.V.RamanaRao, International Journal of Civil Engineering and Technology (IJCIET), ISSN 0976 –6316(Online), Volume 5, Issue 8, August (2014)*

Author's Profile:

I. Dr, Hadihosseini,Aerospace Engineering , working in International Earthquake Research Center of America (IERCA)

II. Mahdi hosseini , Master of Technology in Structural Engineering, Dept. of Civil Engineering, Jawaharlal Nehru Technological University Hyderabad (JNTUH), Hyderabad, Telengana , India

Research interest: Structural Engineering, StructuralDynamics, Structural Optimization, structural design, Reinforced Concrete Structures, Finite element analysis, Earthquake Engineering

III.Ahmadhosseini, Under Graduate Student in Mechanical Engineering, Dept. of Mechanical Engineering,Kakatiya University ,Warangal, Telengana, India